Materials Engineering for Light Water Reactors

Yoshiyuki Kaji

Research Group for Radiation Materials Engineering
Fuels and Materials Engineering Unit
Nuclear Science and Engineering Directorate
Japan Atomic Energy Agency

September 26, 2013

Materials Engineering for Light Water Reactors

Preface:

Exposure to intense radiation fields, high temperatures, chemically active environments, and high pressures for long periods of time are characteristic of many materials in nuclear reactor systems. Since their satisfactory performance is vital for operation of the reactor system, the associated development, design, and maintenance are major aspects of nuclear reactor engineering. *(Ref.1)*

Materials degradation in service represents one of the major technological factors that can limit the efficiency and viability of nuclear power. Extensive experience with commercial thermal reactors has demonstrated the need for improved understanding of materials phenomena (*principally related to corrosion and irradiation*) and better analytical procedures for transferring test information to the real problem. *(Ref. 2)*

In the present lectures, we will deal with the fundamentals of materials engineering and actual material issues experienced in LWR operation.

Materials Engineering for Light Water Reactors

Contents:

Materials Engineering for Light Water Reactors

Contents (continued):

Materials Engineering for Light Water Reactors

Contents (continued):

1.1 Introduction

1.1 Introduction (1/5)

Since the beginning of the nuclear power generation age, various components of nuclear power plants (NPPs) have been suffered from the various kind of material degradation and failure.

For example, in 1980s many NPPs suffered the stress corrosion cracking (SCC) which is known as one of typical subcritical cracking failures, and it reduced NPP availability remarkably.

The intergranular SCC (IGSCC) of piping system caused by a thermally sensitization at the heat-affected-zone (HAZ). The IGSCC was overcome by the extensive material research.

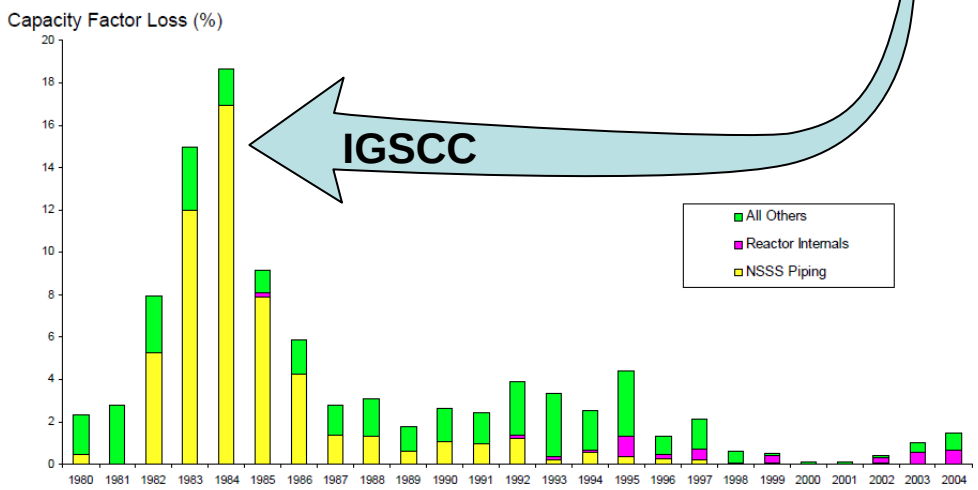

Fig.1.1.2 Capacity Factor Losses Due to Corrosion-Related Damage in BWRs (Ref.4)

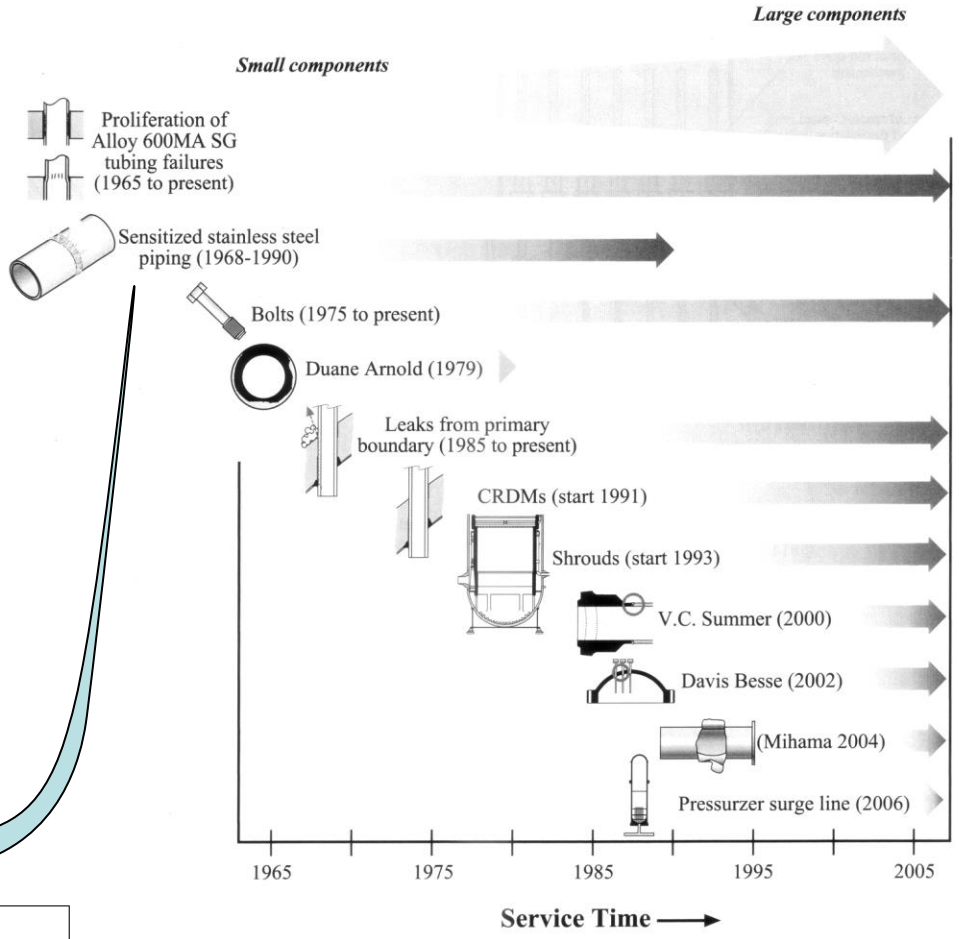

Fig.1.1.1 Chronology of some significant failures in light water nuclear plants. (Ref.3)

1.1 Introduction (2/5)

Materials selection : The steps in the process can be defined as follows:

1. *Analysis of the materials requirements.* Determine the conditions of service and environment that the product must withstand. Translate them into critical material properties.
2. *Screening of candidate materials.* Compare the needed properties (responses) with a large materials property data base to select a few materials that look promising for the application.
3. *Selection of candidate materials.* Analyze candidate materials in terms of trade-offs of product performance, cost, fabricability, and availability to select the best material for the application.
4. *Development of design data.* Determine experimentally the key material properties for the selected material to obtain statistically reliable measures of the material performance under the specific conditions expected to be encountered in service. (quoted from Ref.5)

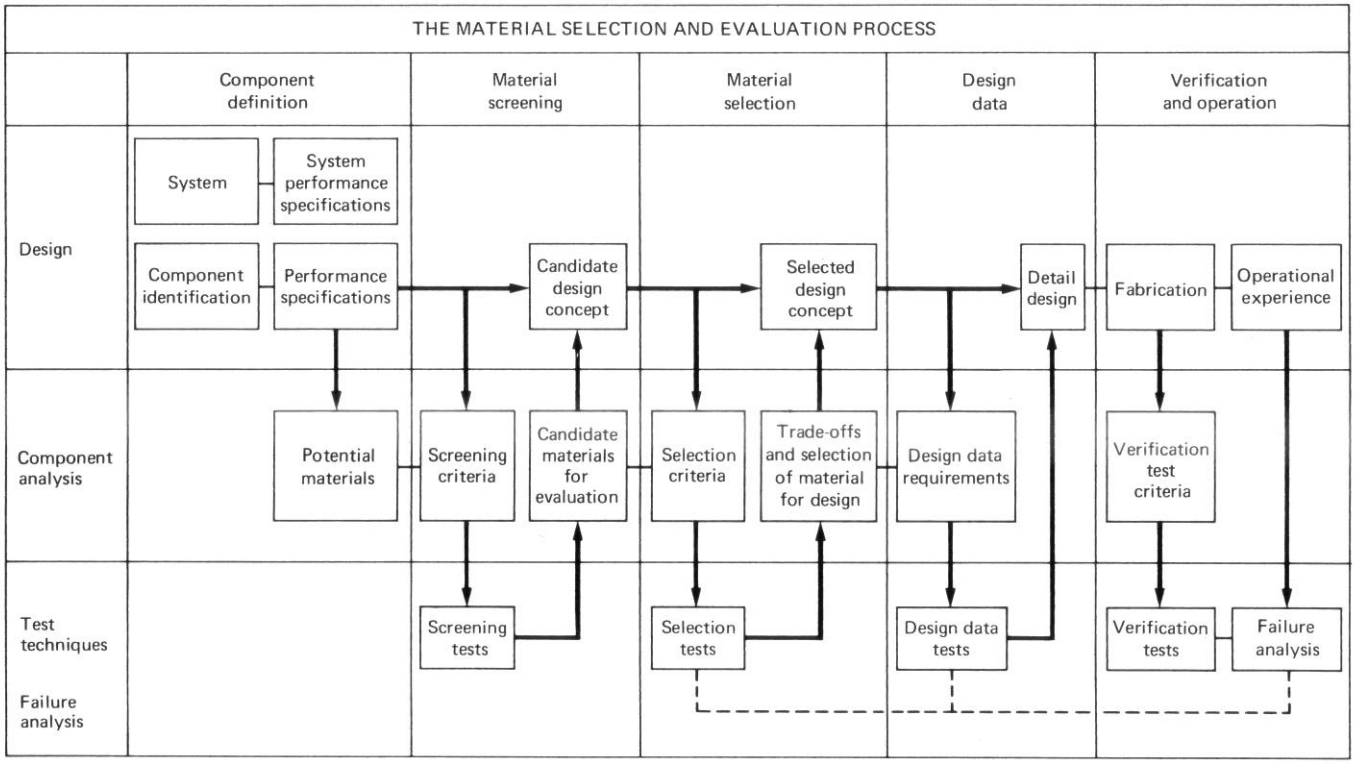

Fig.1.1.3 Materials selection and evaluation process for a complex product. (Ref.5)

1.1 Introduction (3/5)

This figure shows an example of ***diversity of materials*** of PWR components that need to be evaluated for their long term integrity.

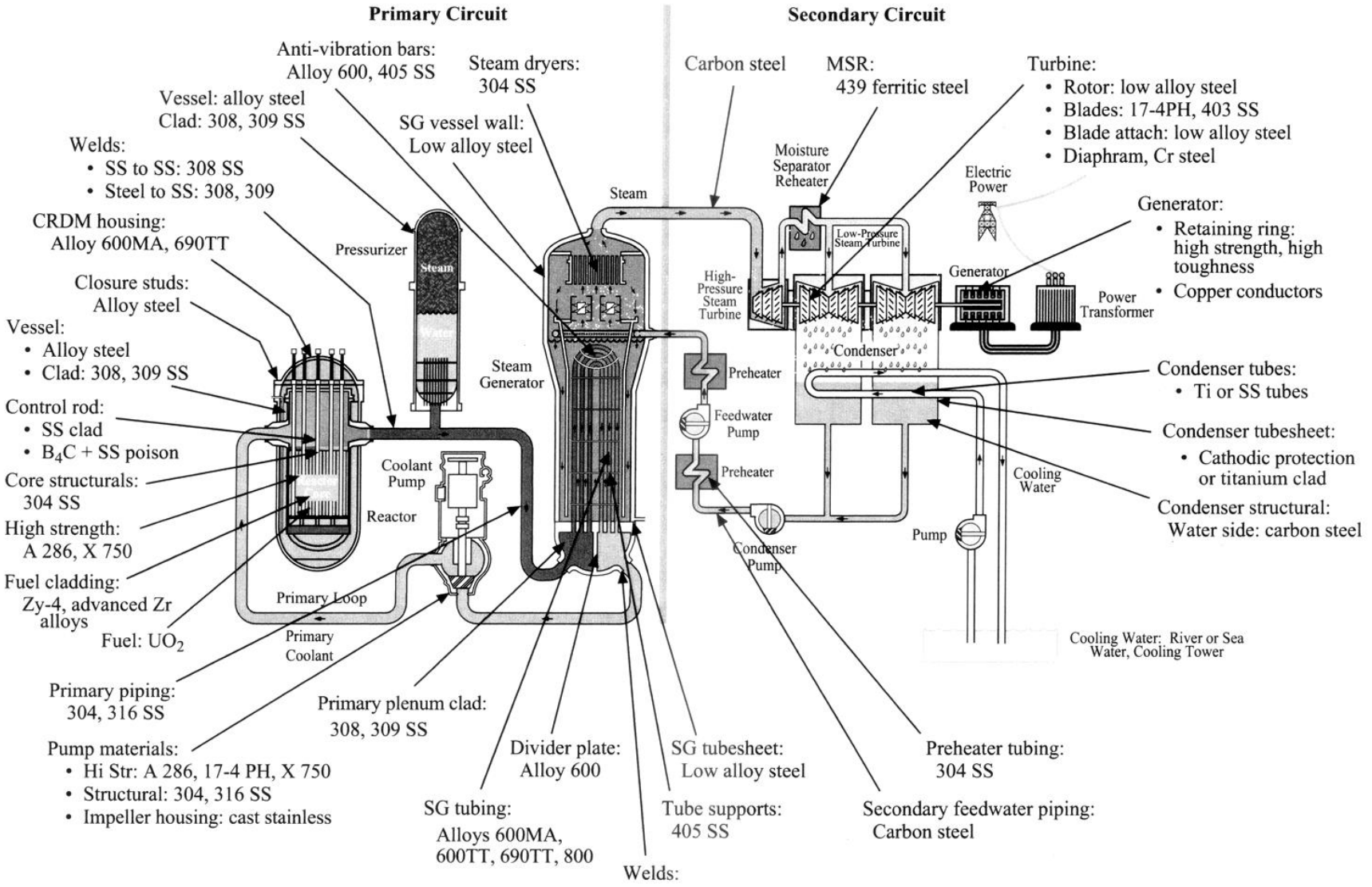

Fig.1.1.4 Overview of a PWR system showing materials used in construction. (Ref.3)

1.1 Introduction (4/5)

There is also a diversity of the chemical and radiation environment and the thermo-hydraulic conditions in NPPs.

There are many components operating at different mass flows, different temperatures, different pressures, different alloys, and different chemistries. Each of these components is prone to different kinds of failure modes with different dependencies. (Ref.3)

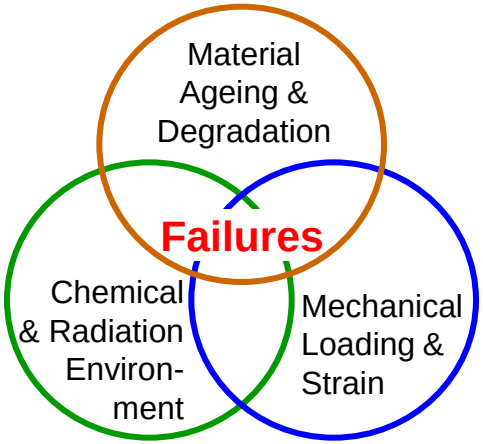

Fig.1.1.6 Factors dominating failures of structural materials

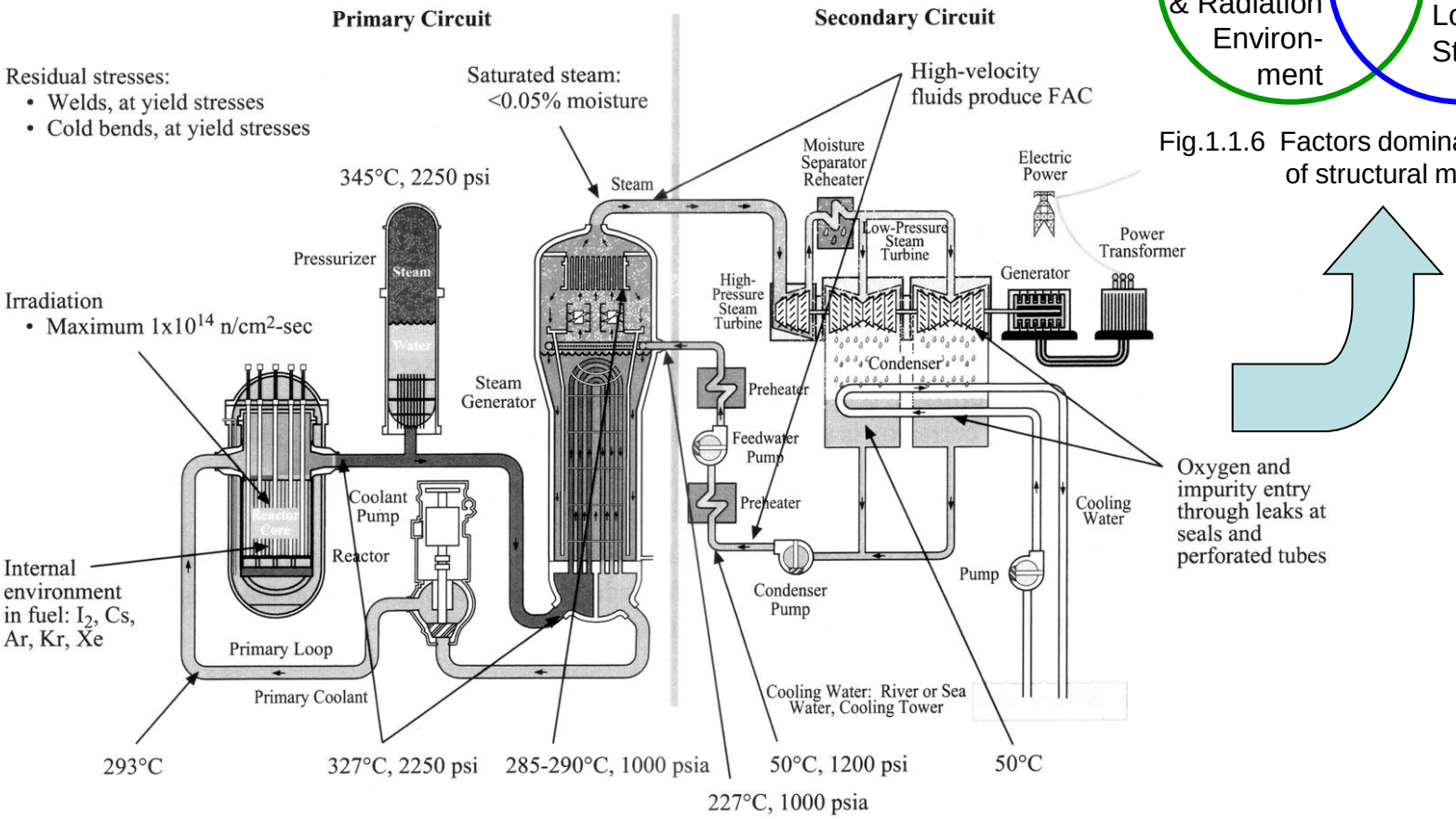

Fig.1.1.5 Overview of a PWR system showing environments to which materials are exposed. (Ref.3)

1.1 Introduction (5/5)

Most important aspect of materials engineering for LWRs is an assessment of materials integrity and degradation during an operation of NPP, because a start of the operation means a start of the degradation.

Ageing of the major components in NPPs must be effectively managed to ensure the availability of design functions throughout the plant service life. The assessment of materials integrity/degradation is a significant part involved in the component ageing management program.

The right figure shows an example of systematic ageing management process for BWR reactor vessel internal components which is adaptation of Deming's "Plan-Do-Check-Act" (PDCA) cycle [Ref.6].

Understanding ageing is the key to effective management of the ageing. Knowledge of the materials engineering is essential for this purpose.

This understanding consists of: knowledge of the materials and material properties, stresses and operating conditions; likely degradation sites and ageing mechanisms; condition indicators and data needed for assessment and management of the ageing and effects of ageing on safety margins.

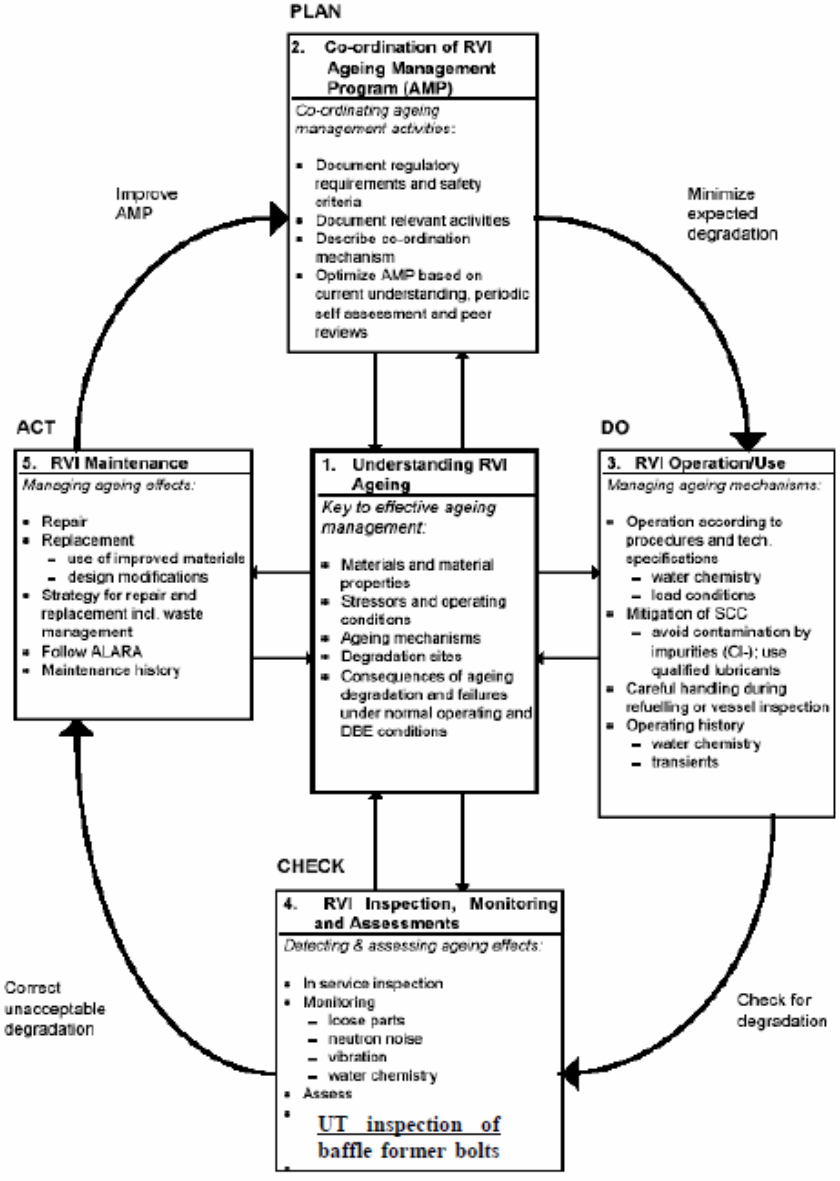

Fig.1.1.7 Key elements of PWR RPV internals ageing management program utilizing the systematic ageing management process. (Ref.6)

1.2 Major Structural Materials

In this section, Requirements of Nuclear Material Properties, Materials used in LWR Plants and as the major structural materials used in PWR/BWR; Carbon Steels, Stainless Steels, and Nickel Alloys are briefly summarized. Detail of the specifications, properties and behavior of the materials will be explained the following sections.

1.2.1 Requirements of Nuclear Material Properties

In selection of nuclear materials required, the material properties, or considerations, and the changes of material properties in an intense radiation environment must be taken into account. The requirements of material properties in nuclear reactors can be divided into two main categories:

A. **general properties**, or basic considerations

B. **special properties**, or particular considerations

The general properties are, in general, similar to the conventional engineering properties of materials, which are required in most engineering designs. The requirements of general properties for nuclear reactor materials are given in Table 1.2.1.

The special properties required for nuclear reactor materials arise from nuclear radiation, or irradiation, sources and circumstances of the reactor system. Material properties of a reactor component can have a tremendous change under severe radiation. The requirements of special properties for nuclear reactor materials are listed in Table 1.2.2.

Furthermore, the mechanical processes, heat treatments, etc., used in the production and fabrication of nuclear reactor materials can also modify their general and special properties. Some applications may not involve all those properties, or considerations, but others may require additional properties besides the general and special properties given above, such as hardness to resist wear.

Table 1.2.1 General Properties of Nuclear Reactor Materials

Mechanical strength	Heat transfer properties
Ductility	Thermal stability
Structural integrity	Compatibility
Fabricability, machinability	Availability
Corrosion resistance	Cost

Table 1.2.2 Special Properties of Nuclear Reactor Materials

Neutronic properties	Chemical interactions
Induced radioactivity	Particle interdiffusion
Irradiation stability	Ease of fuel reprocessing

(quoted from Ref.[7], see handout)

1.2.2 Materials used in LWR Plants (1/3)

Carbon steels, stainless steels and Nickel alloys are the major materials in PWR.

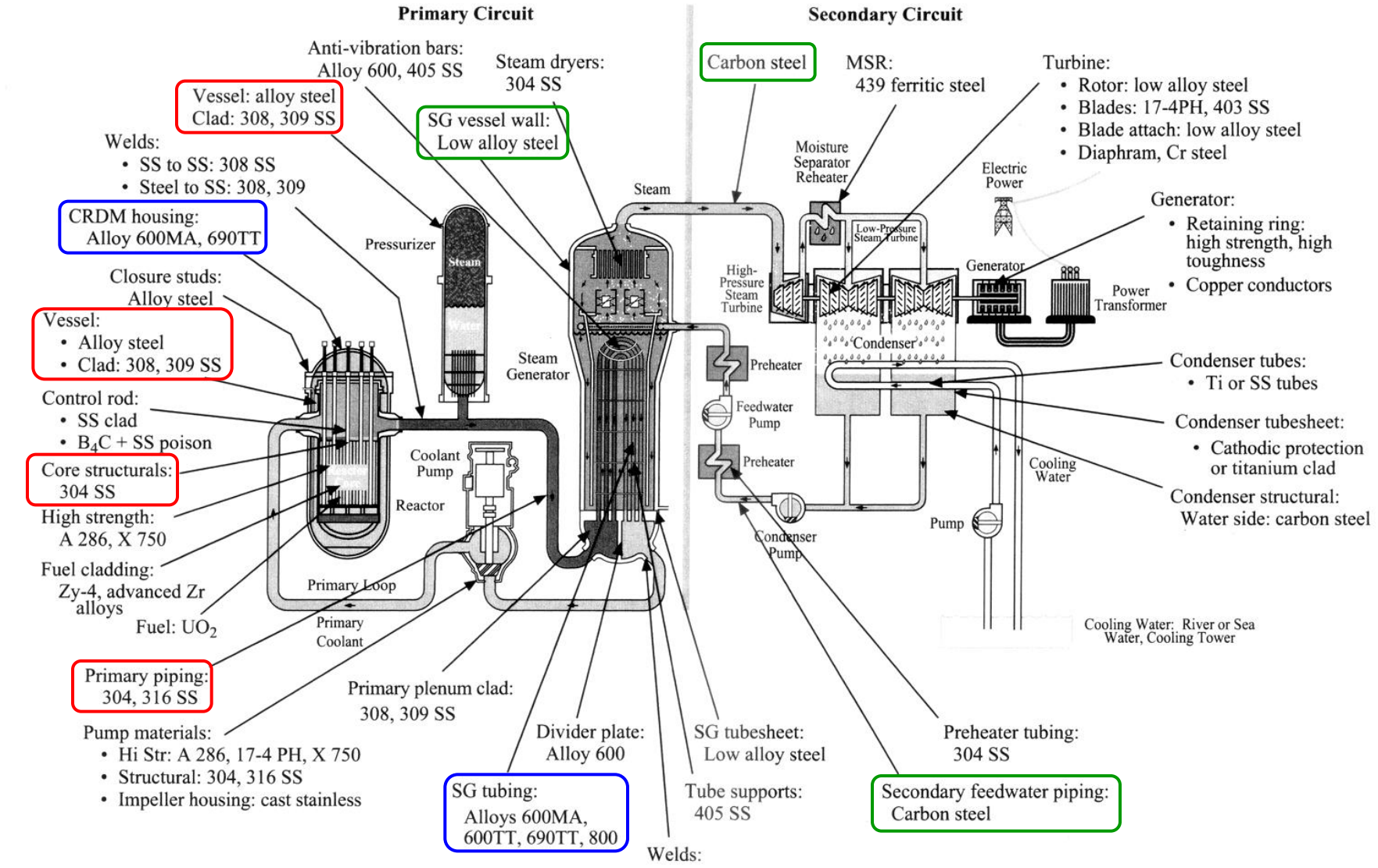

Fig.1.2.1 Overview of a PWR system showing materials used in construction. (Ref.3)

1.2.2 Materials used in LWR Plants (2/3)

Table 1.2.3 Materials used for the components of PWR/BWR.

Component	Parts	BWR	PWR
Reactor Pressure Vessel (RPV)	Vessel and Head Cladding Stud bolts	Low alloy steel: SA533 Gr.B Cl.1 SA508 Cl.2, SA508 Cl.3 Stainless steel: Type308L high-strength low alloy steel: SA540 Gr.B Cl.3	Low alloy steel: SA533 Gr.B Cl.1 SA508 Cl.2, SA508 Cl.3 Stainless steel: Type308L high-strength low alloy steel: SA540 Gr.B Cl.3
RPV Internals (RPVI)	Core support plate Shroud Core internals, etc. Support/bolt, etc.	Low carbon stainless steel: Type304L, Type316L Nickel alloy: Alloy 600, Alloy X750	Stainless steel: Type 304 Cold-worked type 316 SS Nickel alloy: Alloy X750
Fuel Assembly	Fuel cladding Channel box	Zircaly-2 Zircaly-4	Zircaloy-4 -
Steam Generator (SG)	Shell Tubesheet Tube	- - -	Low alloy steel: SA533 Gr.B Cl.2 Low alloy steel: SA508 Cl.3 Nickel alloy: Alloy 600, Alloy 690
Piping	Pipes	Low carbon stainless steel: Type304L, Type316L Carbon steel: SA106 Gr.B	Stainless steel: Type304, Type316 Carbon steel: SA516 Gr.70

1.2.2 Materials used in LWR Plants (3/3)

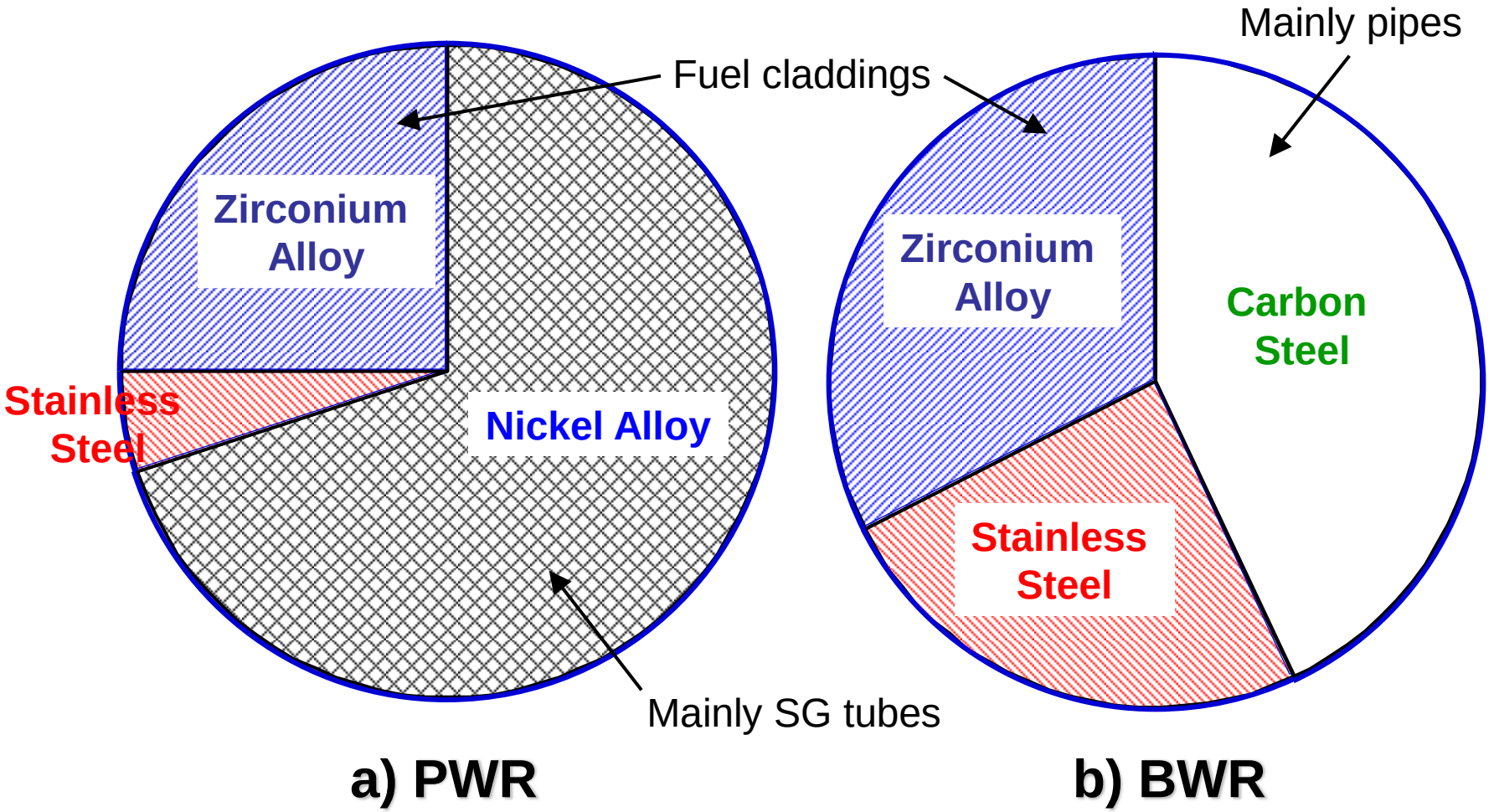

Fig. 1.2.4 Major materials in primary system shown by the ratio of their wetted surface area

By S. Uchida, JAEA

1.2.3 Carbon Steels (1/2)

Carbon steel:

The American Iron and Steel Institute (AISI) defines carbon steel as follows: Steel is considered to be carbon steel when no minimum content is specified or required for chromium, cobalt, columbium [niobium], molybdenum, nickel, titanium, tungsten, vanadium or zirconium, or any other element to be added to obtain a desired alloying effect; when the specified minimum for copper does not exceed 0.40 per cent; or when the maximum content specified for any of the following elements does not exceed the percentages noted: manganese 1.65, silicon 0.60, copper 0.60.

Low-alloy Steels:

Low-alloy steels constitute a category of ferrous materials that exhibit mechanical properties superior to plain carbon steels as the result of additions of alloying elements such as nickel, chromium, and molybdenum. Total alloy content can range from 2.07% up to levels just below that of stainless steels, which contain a minimum of 10% Cr.

For many low-alloy steels, the primary function of the alloying elements is to increase hardenability in order to optimize mechanical properties and toughness after heat treatment. In some cases, however, alloy additions are used to reduce environmental degradation under certain specified service conditions.

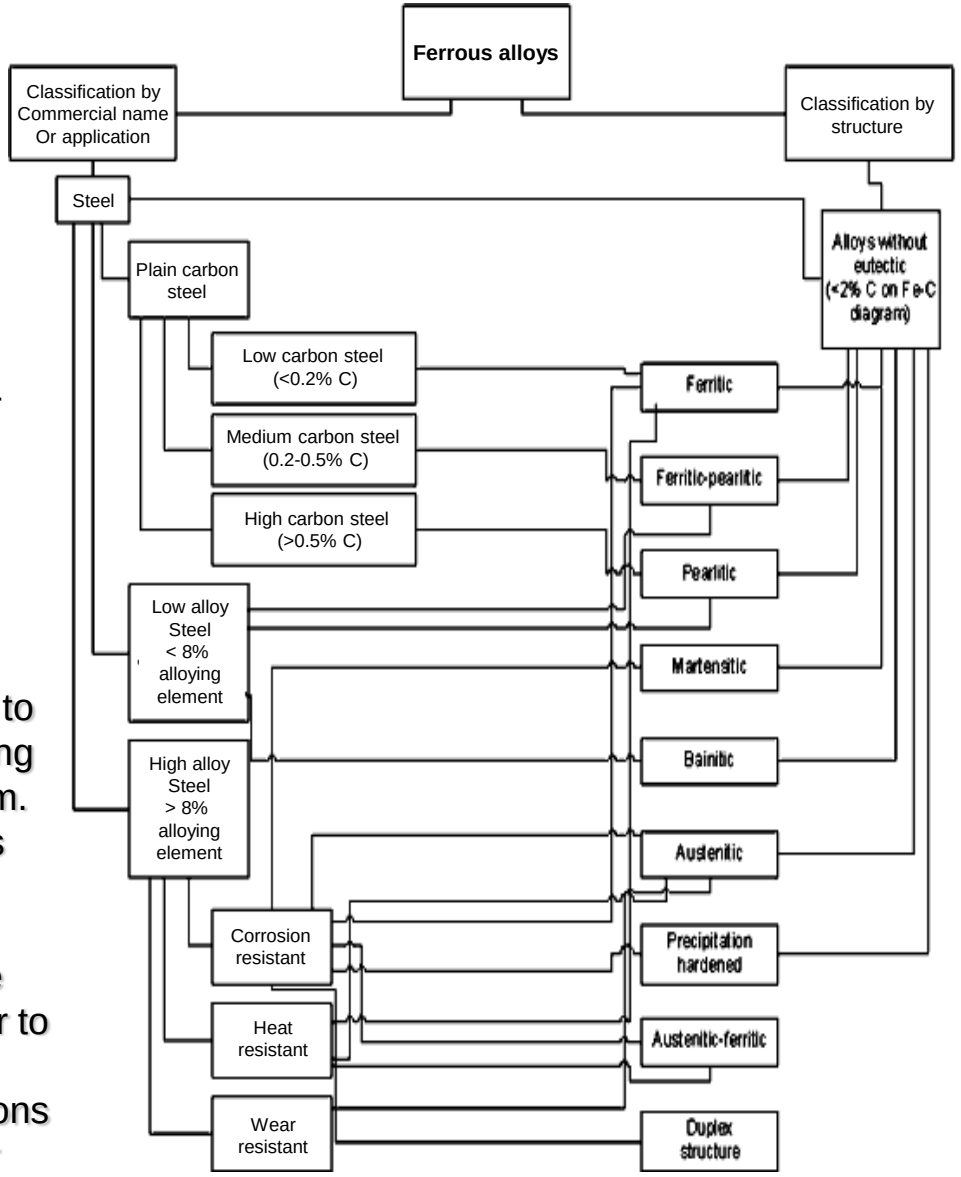

See: http://www.key-to-steel.com/Articles/Art62.htm

1.2.3 Carbon Steels (2/2)

Low-alloy carbon steel is an important reactor material for use in **pressure vessels** and miscellaneous components where the corrosion resistance of stainless steels is not required but an ability to withstand thermal stress is desirable.

Steels for thick-walled pressure vessels are specified in the ASME Code and are more accurately described as high-strength, low-alloy steels. These steels contain small amounts of alloying elements to improve mechanical properties. The composition and some properties of a typical pressure-vessel steel, ASTM A 533-B, are given in Table 1.2.4.

The effect of exposure to fast neutrons (energy>1 MeV) on the mechanical properties of ASTM A 533-B steel is shown in Fig. 1.2.5. The increase in the yield and tensile strengths and the decrease in elongation are consistent with a decrease in the ductility of the steel with increasing fluence. The loss of ductility reduces the ability of the metal to accommodate thermal stresses, but the accompanying increase in the NDT temperature may be a more serious matter for pressure vessels. Steels with higher amounts of copper exhibit a greater irradiation effect.

(quoted from Ref.1)

Table 1.2.4 Composition and Mechanical Properties of Pressure-Vessel Steel ASTM A 533-B (Ref.1)

Alloy Element	Weight Percent, Maximum
Carbon	0.25
Manganese	1.50
Phosphorus	0.035
Sulfur	0.04
Silicon	0.03
Molybdenum	0.60
Nickel	0.70
	Mechanical Properties
Tensile strength (MPa)	550 to 690
Yield strength (MPa)	345
Elongation (percent)	18

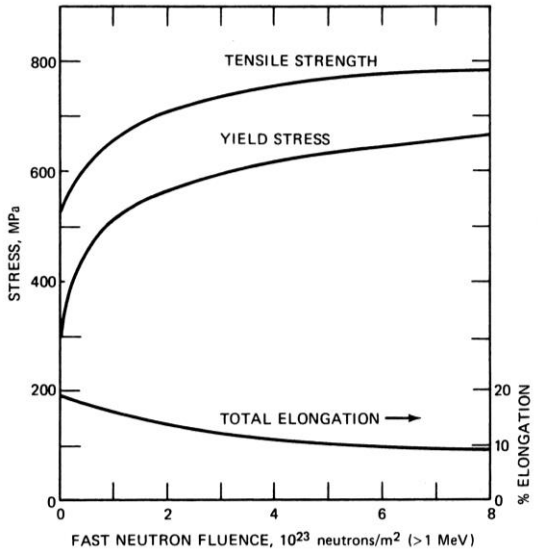

Fig. 1.2.5 Effects of fast-neutron irradiation at 260C on tensile properties of pressure vessel steel (ASTM A 533-B) (Ref.1)

1.2.4 Stainless Steels (1/4)

Stainless steels are iron alloys containing a minimum of approximately 11% chromium. This amount of chromium prevents the formation of rust in unpolluted atmospheres, as shown in Fig. 1.2.6; it is from this characteristic that their popular designation "stainless" is derived. Their corrosion resistance is provided by a very thin surface film, known as the "passive film," which is self-healing in a wide variety of environments.

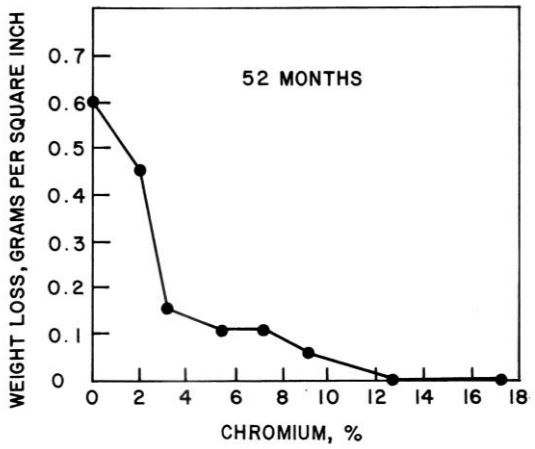

Fig. 1.2.6 Influence of Cr on the atmospheric corrosion of low-carbon steel. (Ref.8)

Table 1.2.5 Compositions of the 300 series of austenitic stainless steels (Ref.8)

UNS Number	Name	Composition[a] (%) Cr	Ni	C	Mn	Si	P	S	*Other*
S30400	304	18–20	8–10	0.08	2.0	1.0	0.045	0.030	—
S30403	304L	18–20	8–12	0.03	2.0	1.0	0.045	0.030	—
S30430	302Cu	17–19	8–10	0.08	2.0	1.0	0.045	0.030	Cu 3–4
S30451	304N	18–20	8–10.5	0.08	2.0	1.0	0.045	0.030	N 0.1–0.16
S30453	304LN	18–20	8–12	0.03	2.0	1.0	0.045	0.030	N 0.1–0.16
S30500	305	17–19	10.5–13	0.12	2.0	1.0	0.045	0.030	—
S30800	308	19–21	10–12	0.08	2.0	1.0	0.045	0.030	—
S30900	309	22–24	12–15	0.20	2.0	1.0	0.045	0.030	—
S30908	309S	22–24	12–15	0.08	2.0	1.0	0.045	0.030	—
S31000	310	24–26	19–22	0.25	2.0	1.5	0.045	0.030	—
S31008	310S	24–26	19–22	0.08	2.0	1.5	0.045	0.030	—
S31400	314	23–26	19–22	0.25	2.0	1.5–3.0	0.045	0.030	—
S31600	316	16–18	10–14	0.08	2.0	1.0	0.045	0.030	Mo 2–3
S31620	316F	16–18	10–14	0.08	2.0	1.0	0.20	0.10[c]	Mo 1.75–2.5
S31603	316L	16–18	10–14	0.03	2.0	1.0	0.045	0.030	Mo 2–3
S31651	316N	16–18	10–14	0.08	2.0	1.0	0.045	0.030	Mo 2–3, N 0.1–0.16
S31653	316LN	16–18	10–14	0.03	2.0	1.0	0.045	0.030	Mo 2–3, N 0.1–0.16
S32100	321	17–19	9–12	0.08	2.0	1.0	0.045	0.030	Ti 5 × C[b]
N08330	330	17–20	34–37	0.08	2.0	0.75–1.5	0.040	0.030	—
S34700	347	17–19	9–13	0.08	2.0	1.0	0.045	0.030	Nb + Ta 10 × C[b]
S34800	348	17–19	9–13	0.08	2.0	1.0	0.045	0.030	Nb + Ta 10 × C[b] Ta 0.1, Co 0.2
S38400	384	15–17	17–19	0.08	2.0	1.0	0.045	0.030	—

Source: Specialty Steel Industry of the United States, Washington, D. C.

[a]Balance iron. Single values are maximum value unless otherwise noted.

[b]Minimum.

[c]Optional.

1.2.4 Stainless Steels (2/4)

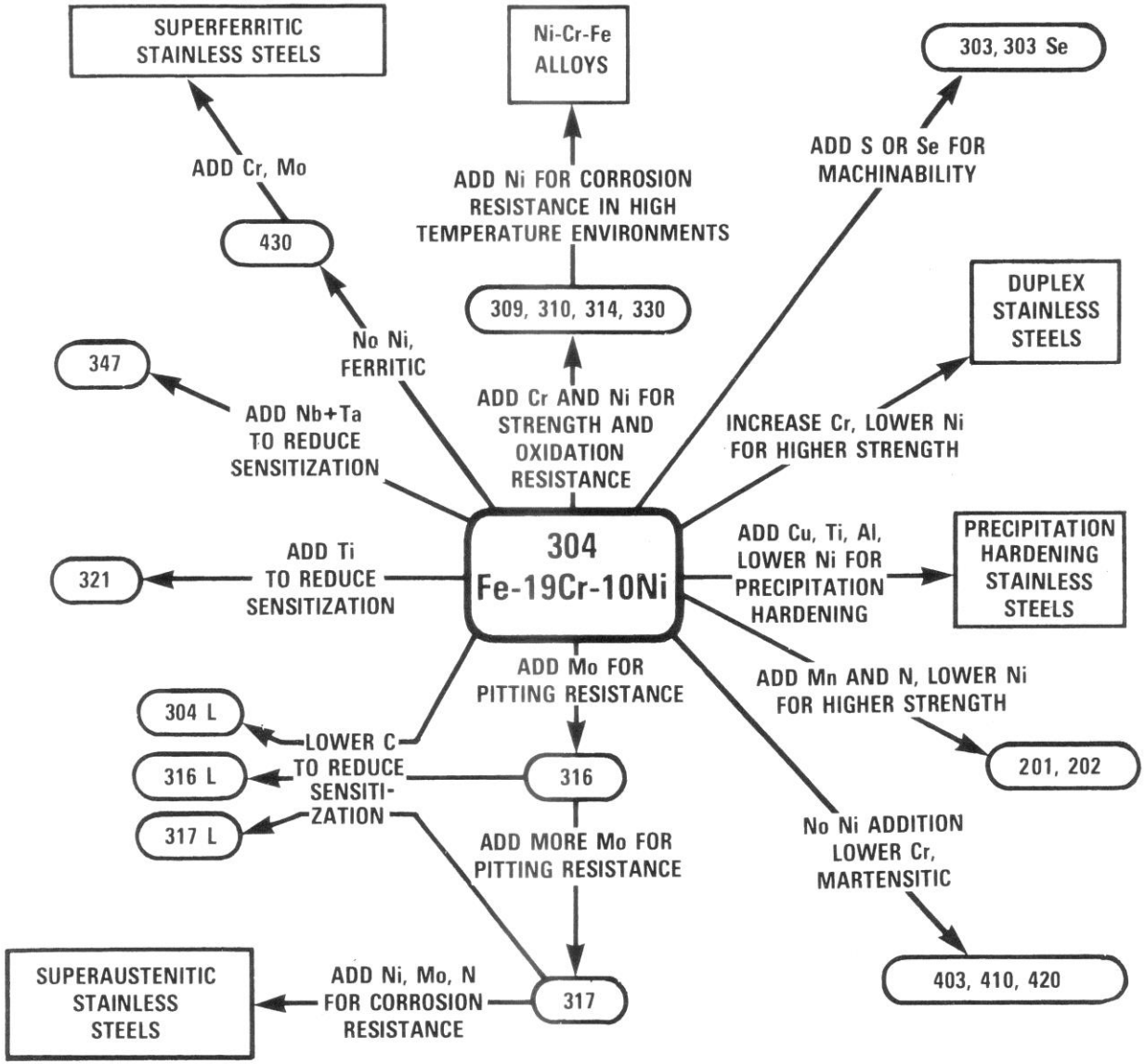

Fig. 1.2.7 Compositional and property linkages in the stainless steel family of alloys (Ref.8)

1.2.4 Stainless Steels (3/4)

Sensitization: The exposure of austenitic stainless steels to elevated temperatures for long periods of time can result in the formation of various precipitates. The formation of such precipitates is generally described in the metallurgical literature by time-temperature-precipitation (TTP) diagrams. A TTP diagram for type 316 stainless steel is shown in Figure 1.2.8, where it is seen that carbide ($M_{23}C_6$), chi, Laves phase, and sigma can be precipitated at certain elevated temperatures. This figure also shows that the precipitation of $M_{23}C_6$ carbide can occur in relatively short times or at relatively fast cooling rates compared to the other precipitates. Carbide precipitation can give rise to a phenomenon known as "**sensitization**," which can cause **intergranular corrosion** and **intergranular stress corrosion cracking (IGSCC)** in certain BWR environments. It is now widely accepted that these phenomena are related to the precipitation of carbide at the austenite grain boundaries.

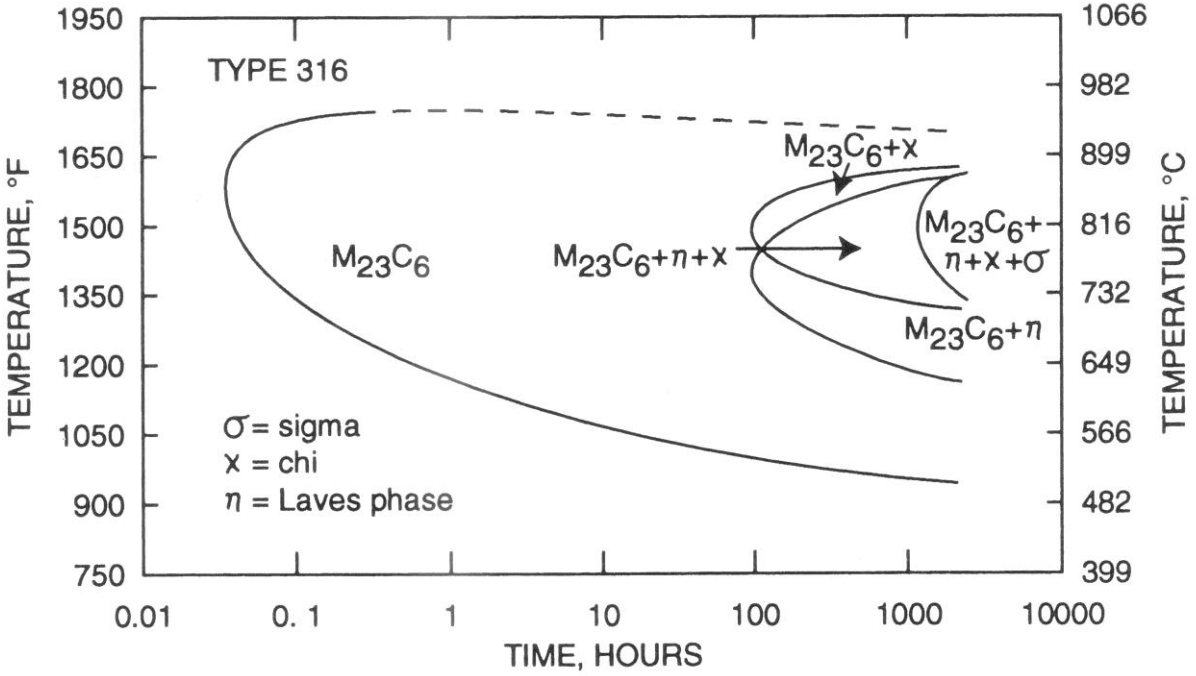

Fig. 1.2.8 Time–temperature–precipitation diagram for type 316 stainless steel containing 0.066% carbon. (After Reference 3).

1.2.4 Stainless Steels (4/4)

To understand this phenomenon in terms of microstructure, it is instructive to examine the equilibrium relation-ships and carbon solubility in the Fe-18Cr-8Ni alloy, illustrated in Figure 1.2.9. This figure shows that in alloys containing between about 0.03 and 0.7% carbon, the equilibrium structure at room temperatures should contain austenite, alpha ferrite, and carbide ($M_{23}C_6$).

In considering carbon solubility in austenite, the simplified diagram, as shown in Figure 1.2.10, is often considered as being representative of real (i.e., non-equilibrium) situations. In terms of this simplified diagram, austenite containing less than about 0.03% carbon should be stable. Austenite containing carbon in excess of 0.03% should precipitate $M_{23}C_6$ on cooling below the solubility line.

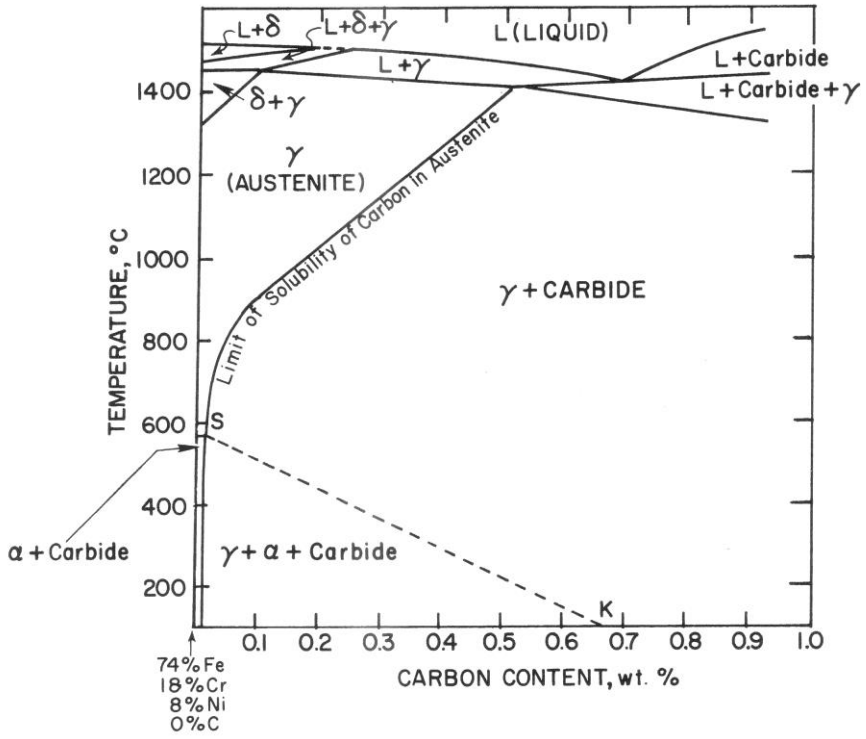

Fig. 1.2.9 Pseudo-binary phase diagram for an Fe–18%Cr–8%Ni alloy with varying carbon content. **(Ref.8)**

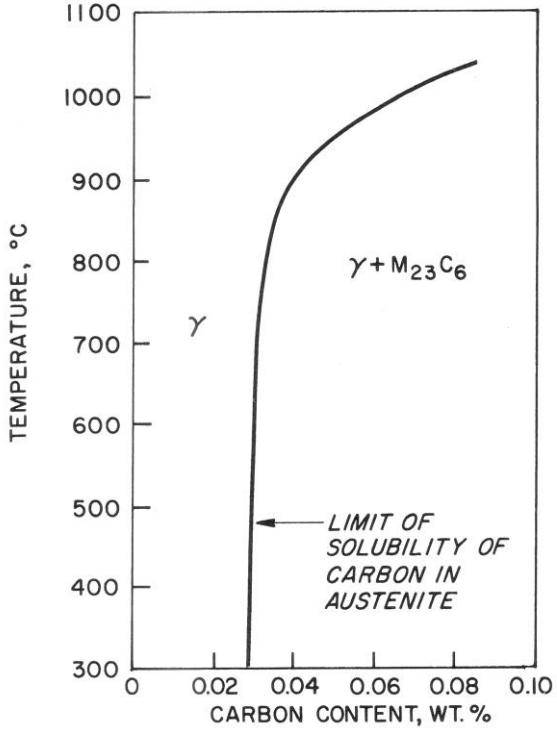

Fig. 1.2.10 Solid solubility of carbon in an Fe–18%Cr–8%Ni alloy. **(Ref.8)**

1.2.5 Nickel Alloys

Nickel-based alloys of interest in reactor systems are primarily those in the Inconel family, because of their corrosion resistance at high temperatures. However, the large thermal-neutron absorption cross section of cobalt, present as an impurity in the nickel, requires that these alloys be used outside the core, such as in heat exchangers or parts of the pressure vessel.

However, they have been used for fuel bundle spacer components. Resistance to stress corrosion cracking is an important consideration and has been found to be sensitive to microstructure and impurity content. **Inconel 600**, which contains 16 percent chromium, 7.6 percent iron, and smaller amounts of other elements, has been widely used for PWR steam generator tubing. It is also used at the ends of pressure vessel nozzles to improve weldability.

Inconel 800 (21 percent chromium) is also used in PWR steam generators. It has better high-temperature strength than Inconel 600, and is of interest for fast-reactor heat exchangers. However, both alloys have had such problems as wastage and stress-corrosion cracking.

Inconel 690, containing 30 percent chromium, has been specified for steam generator tubing in the advanced AP600 reactor because of its superior resistance to stress-corrosion cracking.

Table 1.2.6 Chemical composition of Ni alloys. (Ref.2)

Type	Ni	Cr	Fe
Inconel 600	60.5	23.0	14.1
Inconel 690	60.0	30.0	9.5
Inconel (Alloy) 800H	32.5	21.0	46.0
Inconel (Alloy) 800	34.0	21.0	43.0
PE 16	42.3 max.	16.6	34.1

Composition (wt.%)						
C	Mn	Si	Ti	Mo	S	Others
0.08	0.5	0.2	1.4	—	—	
0.03	—	—	—	—	—	
0.05	0.8	0.5	0.4	—	—	0.4 Cu
0.02	0.64	0.3	—	—	—	—
0.06	0.12	0.24	1.31	3.63	0.004	0.99 Al 0.003 P

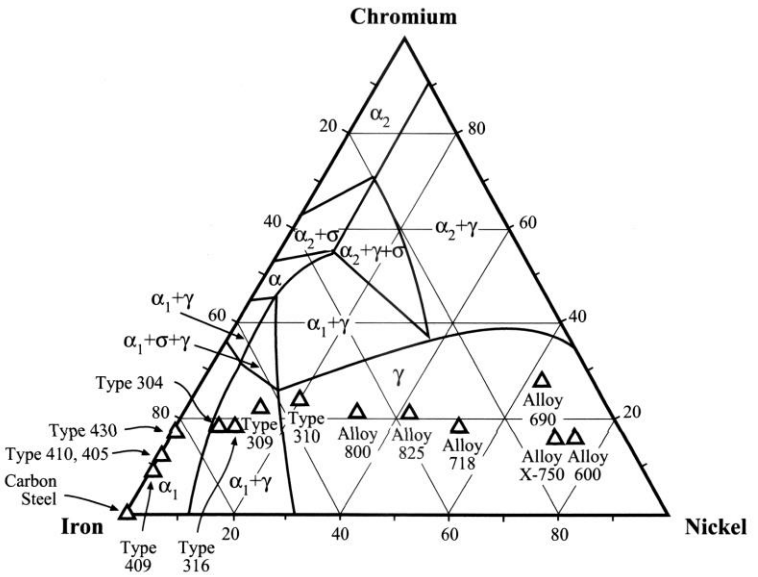

Fig. 1.2.11 Ternary Fe-Cr-Ni diagram determined at 400 C. (Ref.3)

1.3 Mechanical Properties of Materials

1.3.0 Introduction (1)

Purpose of components and structural systems is to support and resist various loads not only during long time operation but also at construction and at in-service inspection, and even at emergency and faulted conditions.

For examples;

At construction, when heavy components is transported and suspended, a load and bending moments is applied on the components at air temperature.

At over pressure test in in-service inspection, a pressure vessel and pipes made of steels are failed with brittle manner at cool air temperature.

At severe accident, such as TMI, structural materials and systems must shut and dissipate explosion energy.

Therefore, knowledge of mechanical properties and corrosion behavior complement design (including selection of materials) and protective maintenance.

1.3.0 Introduction (2)

- Requirements of nuclear material properties
  - 2 main categories: general and special properties.

General properties	Special properties
➢ Mechanical strength, Ductility ➢ Structural integrity ➢ Fabricability, Machinability ➢ Corrosion resistance ➢ Heat transfer properties ➢ Thermal stability ➢ Compatibility ➢ Cost	➢ Neutronic properties ➢ Induced radioactivity ➢ Irradiation stability ➢ Chemical interactions ➢ Particle interdiffusion ➢ Ease of fuel reprocessing

1.3.0 Introduction (3)

- When we control materials' deformation and failure, we must control stress, strain, stress concentration, stress intensity, temperature, loading modes, and environment.

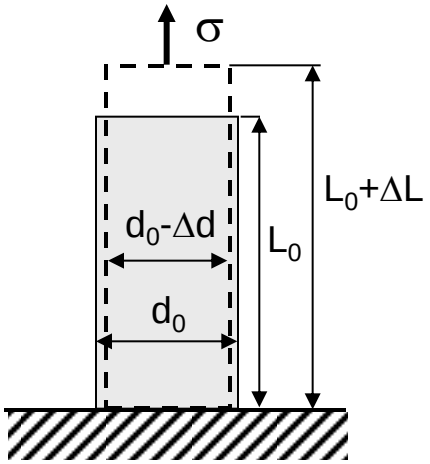

Tensile strain

Stress and Strain

Any force or load applied on the material will result in stress and strain in the material. Stress represents the intensity of the reaction force at any point in the body as imposed by service loads, assembly condition, fabrication, and thermal changes. Stress is measured as the force acting per unit area of a plane.

$$\sigma(stress) = \frac{Force}{Area}$$

The alternation in the shape or deformations of a body resulting from stress is called strain. Tensile strain is expressed as elongation per unit length

$$\varepsilon(strain) = \frac{L - L_0}{L_0}$$

where L and L_0 is length after and before deformation, respectively.

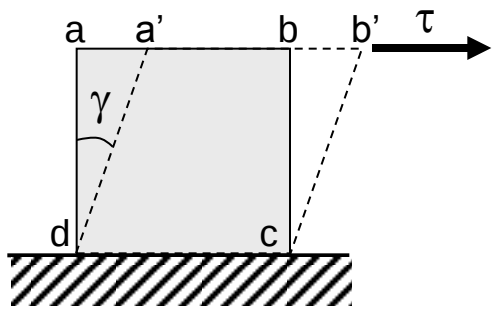

Shear strain, γ=aa'/ad

1.3.0 Introduction (4)

In structures, geometrical discontinuities, fillets and notches, and cracks in particular, give rise to a stress concentration, i.e. a local region where the stresses are higher than the nominal or average stress.

Stress concentration

At blunt notch (instead of a sharp cut), every discontinuities forms an interruption of **load flow lines**. (load low lines are imaginary lines indicating how one unit of load is transferred from one loading point to the other.) Local stress at a notch tip σ_l is higher than the nominal stress σ_{nom}. The ratio between local stress and nominal stress is called the theoretical stress concentration factor.

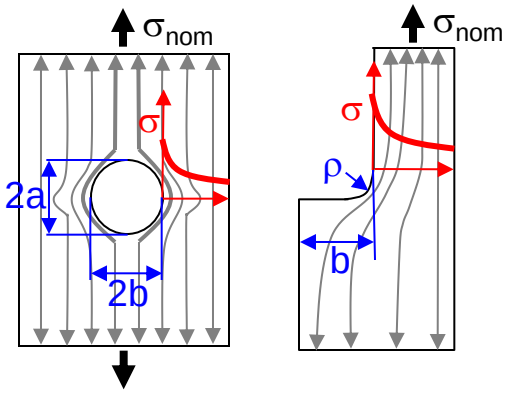

$$k = \frac{\sigma_l}{\sigma_{nom}} = 1 + 2\frac{b}{a} = 1 + 2\sqrt{\frac{b}{\rho}}$$

Stress intensity

The concept of stress concentration dose not provide a quantitative measure. Stress intensity factor, K, gives us the value of the stress intensity at tip of the crack, which remains constant for particular environmental conditions and geometry of a crack. The value of K is defined in general form as

$$K = C\sigma\sqrt{\pi a}$$

where C is shape factor which depends on the geometry and variety of conditions, a is the half-length of the crack.

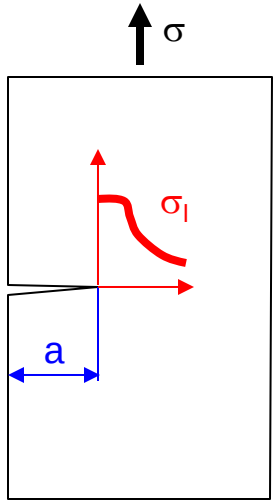

1.3.1 Failure Modes and Mechanisms

Metals can deform elastically and plastically.

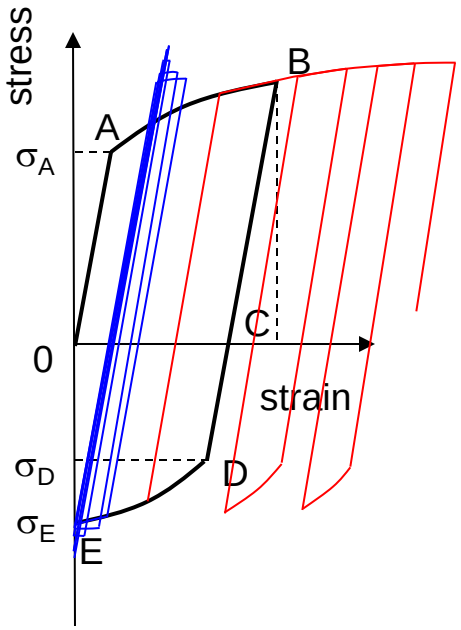

(1) Elastic deformation

Hook's Law: $\sigma=E\varepsilon$, E: young modulus

(2) Plastic deformation

Plastic deformation occurs either by slip or by twining. (mainly by slip)
Slip occurs due to formation and moving of dislocation.
(Dislocation is imperfect arrangement of atoms.)
The force required to move a dislocation are many times smaller than those required to exceed the elastic limit of a perfect crystal.
Nonrecoverable deformation occur after removal of the stress.
Bauschinger effect: $|\sigma_A|>|\sigma_D|$
Residual stress, σ_E, exists after deformation to zero strain.

(3) Creep deformation (flow)

The slow and progressive deformation of a material with time under a constant stress.
Creep occurs if the stress is smaller than the elastic limit. Metals usually exhibit creep at a temperature T>0.35 Tm (Tm is the melting point), where the moving of dislocation is thermally activated.

(4) Cyclic deformation

When alternating (cyclic) stress or strain are loaded, usually stress-strain behavior shows hysteresis loop (Shake down). However at some conditions, progressive distortion accumulates. (Rachet).

1.3.2 Short-Term Mechanical Properties (1)

(1) Tensile properties

The ability of a material to resist breaking under tensile stress is one of the most important and widely measured properties of materials used in structural applications.

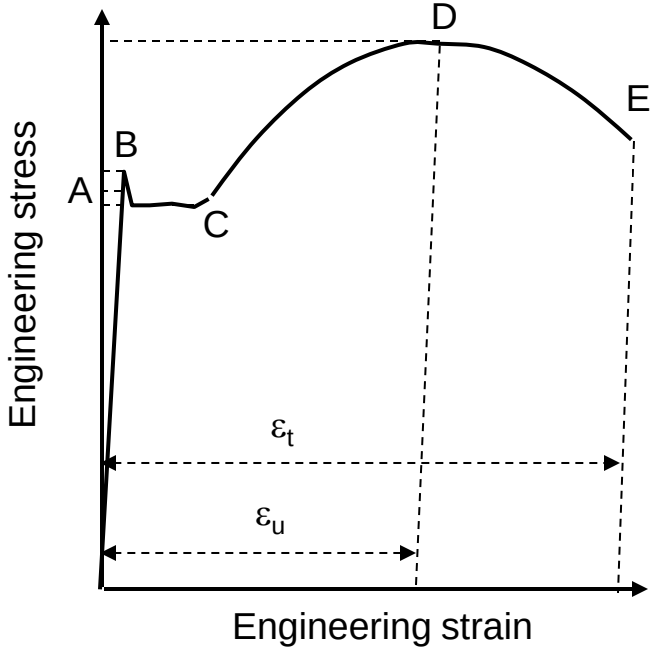

A: Elastic limit, B: Upper yield stress
C: Lower yield stress (σ_y), D: Ultimate tensile strength (UTS)
E: Fracture

Body-Centered Cubic (BCC) metal
(Low carbon steel, mild steel, low alloy steel, Martensitic steel)

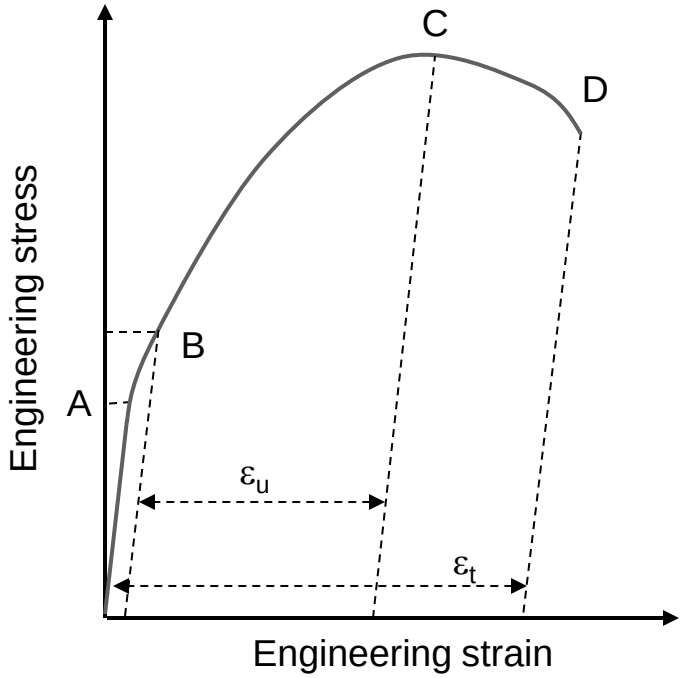

A: Elastic limit, B: 0.2% offset stress ($\sigma_{0.2}$)
C: Ultimate tensile strength (UTS), D: Fracture

Face-Centered Cubic (FCC) metal
(Austenitic steel, Ni-base alloy, Cu alloy)

1.3.2 Short-Term Mechanical Properties (2)

Ductile manner and brittle manner

- Brittle fracture
  - Low ductility or toughness
    little deformation, flat surface normal to stress
  - Irradiation embrittlement
    cleavage fracture, intergranular fracture

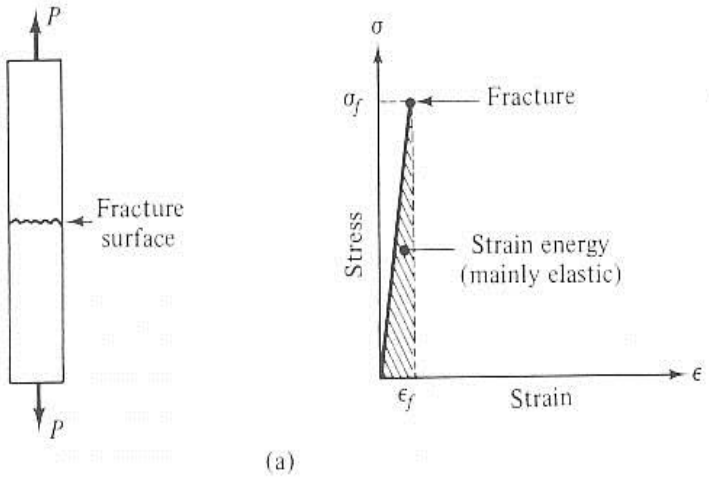

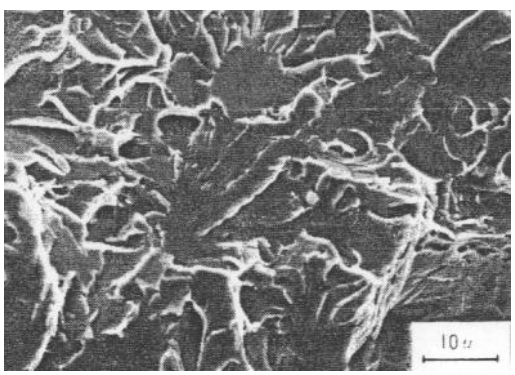

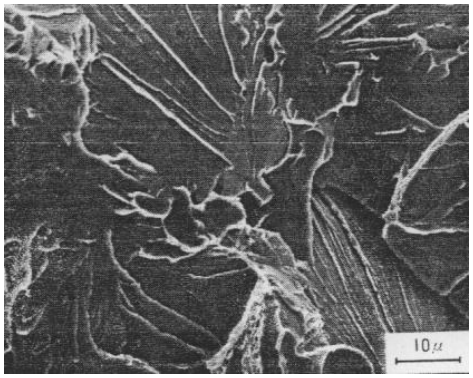

Fracture appearance of cleavage fractured specimen

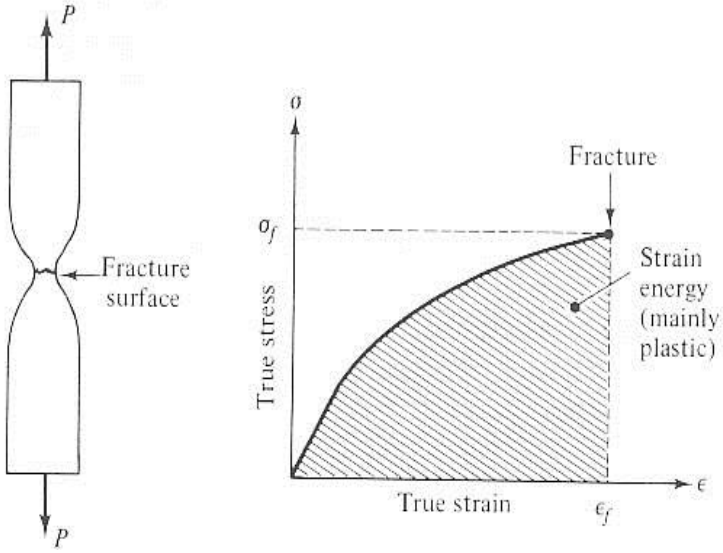

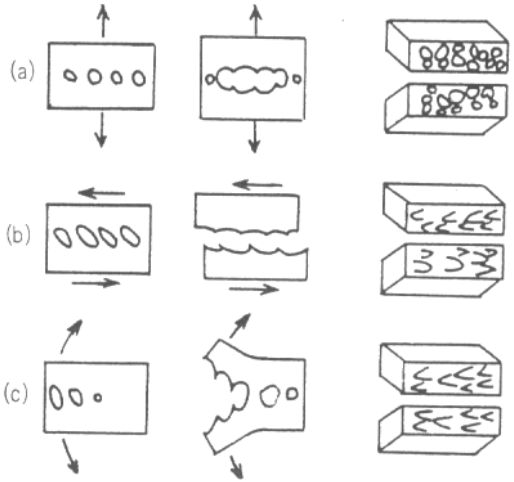

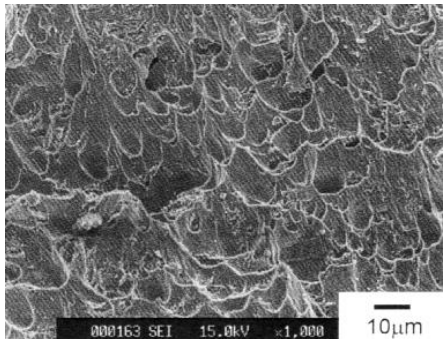

Ductile-fractured surface

Dimple creation in ductile fracture
(a) Equi-axial dimples
(b) Sheared dimples
(c) Tearing dimples

1.3.2 Short-Term Mechanical Properties (3)

(2) Impact property

Charpy impact test

- Impact loading by hammer to break specimen at a certain temperature
  - Charpy specimen of 10mm square with 2mm V-notch

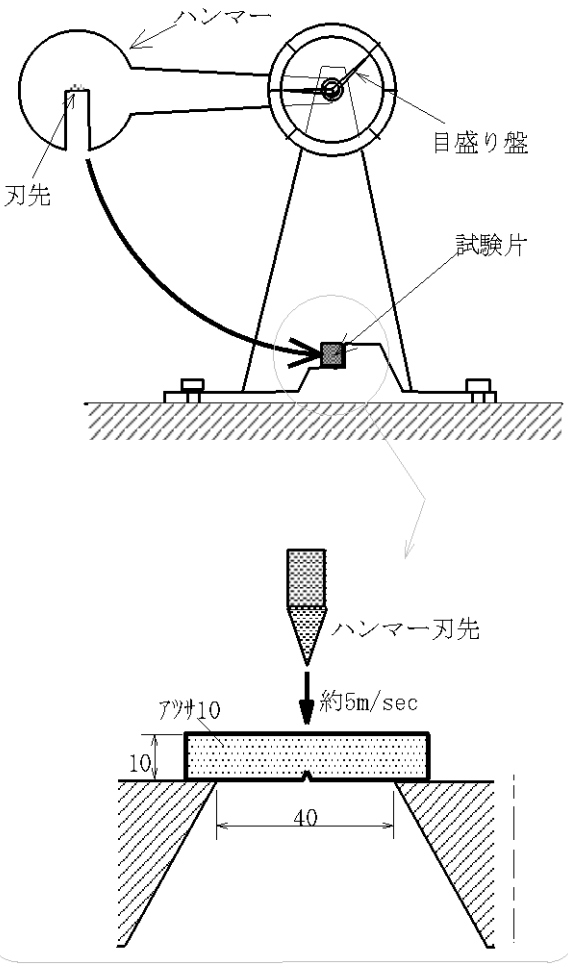

Charpy impact specimen
(JIS Z2202 No.4)

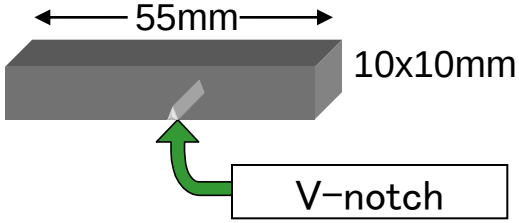

1.3.2 Short-Term Mechanical Properties (3) (cont.)

Charpy impact test

- Measurements of absorbed energy, lateral expansion and percent shear fracture
  - Calculate the absorbed energy from the angle of the hammer after specimen broken
  - Measure lateral expansion and shear area from the broken specimen

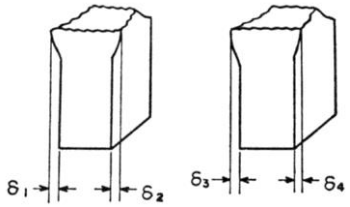

$$\delta = Max(\delta_1,\delta_4) + Max(\delta_2,\delta_3)$$

Measurement of LE

- The amount of plastic deformation
- Index of transition behavior

Example of Charpy impact test results

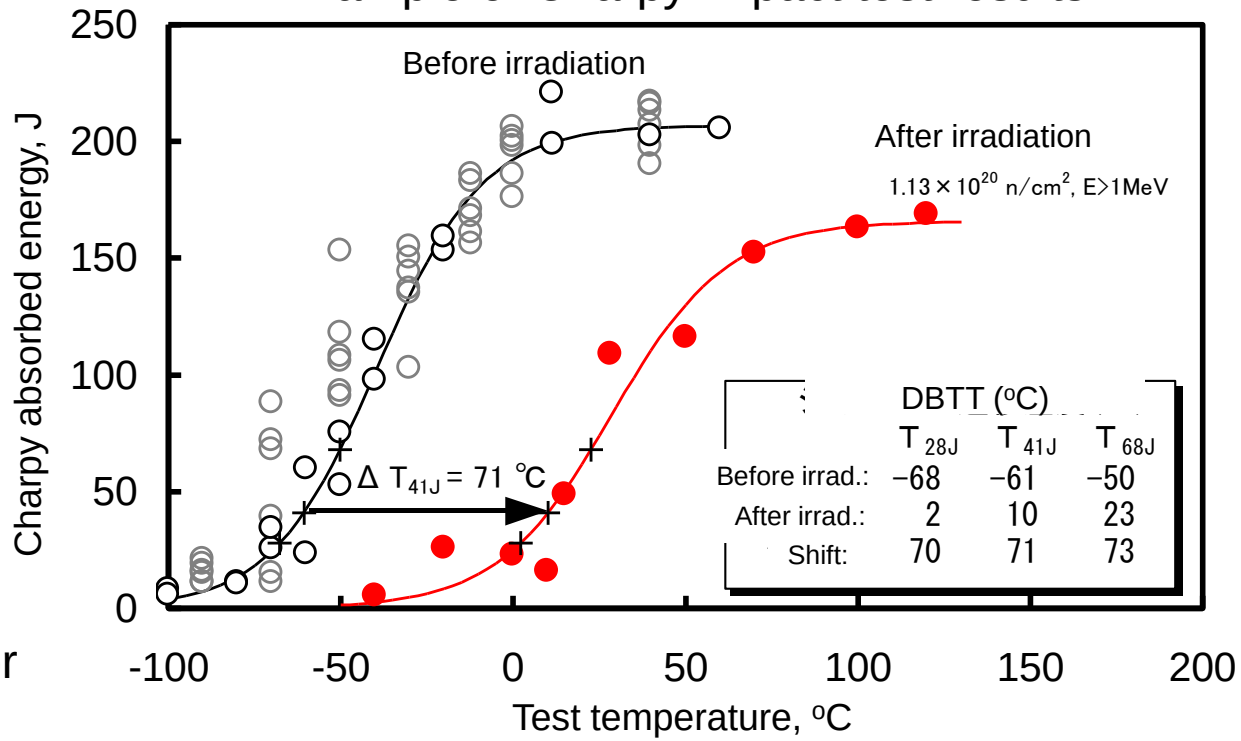

1.3.2 Short-Term Mechanical Properties (4)

Thermal embrittlement

Cast austenitic-ferritic (duplex) stainless steels with significant amount of delta ferrite will experience a reduction of toughness when aged at around 475ºC. DBTT increases, and both room-temperature and operating temperature toughness decrease. This temperature is well above the maximum temperature of BWR and PWR, nevertheless, a reduction of toughness dose take place at the BWR and PWR operating temperature but requires longer times.

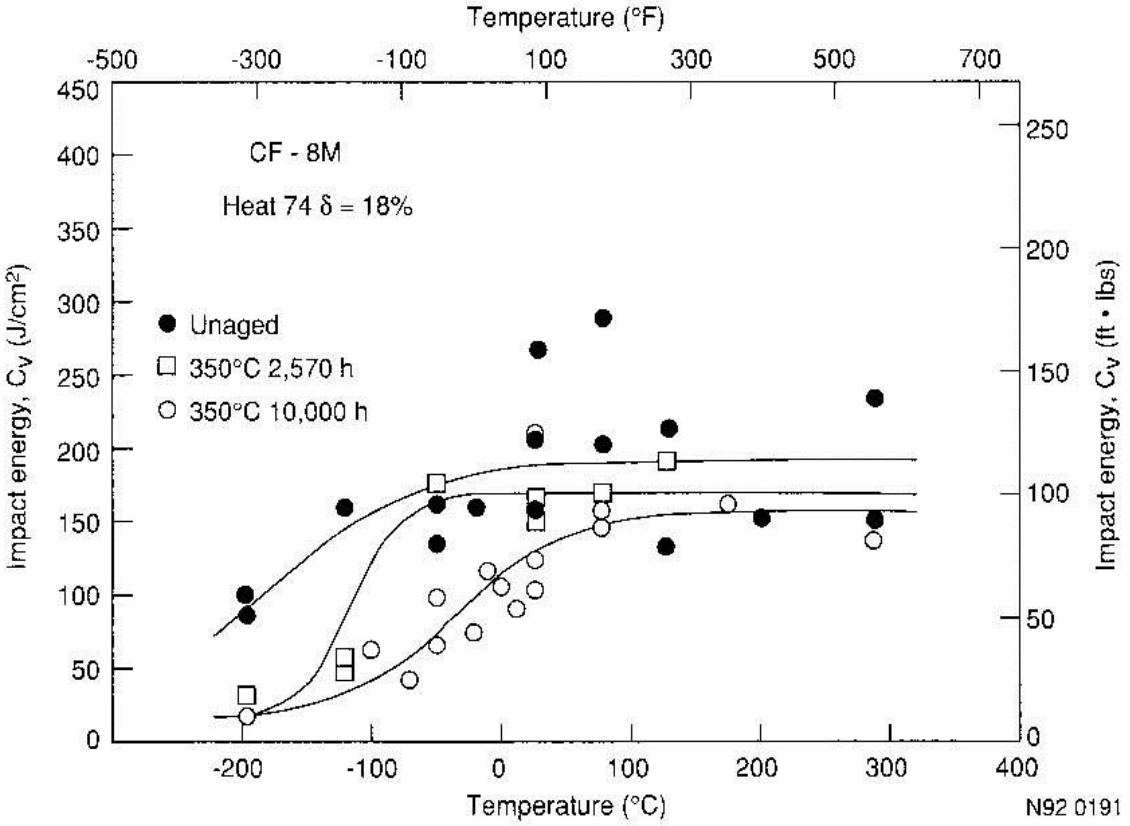

1.3.2 Short-Term Mechanical Properties (5)

(3) Fracture toughness

Fracture processes are enhances by the presence of cracks since they concentrate stress and strain at the crack tip. Fracture mechanics is concerned with a description of stress and strain distribution at crack tips and the mechanism of crack propagation. Thus, fracture mechanics provides a basis for predicting conditions that could lead to component failure and which should be avoided.

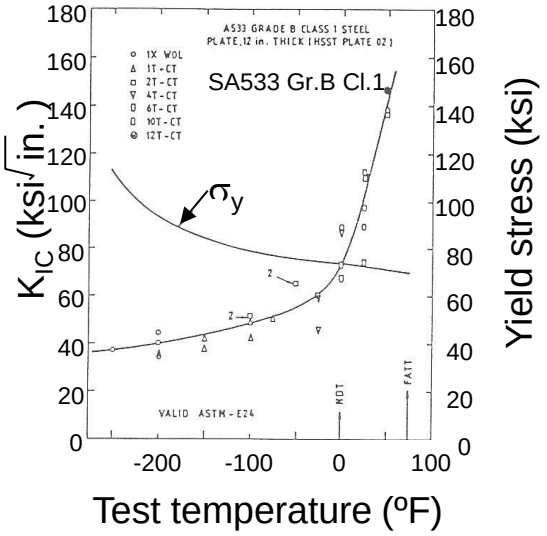

Linear elastic fracture mechanics: stress intensity factor K

When the stress intensity factor is larger than K_{IC} at crack tip, material fails in a brittle manner.

Elastic-plastic fracture mechanics: J-integral J

When the J-integral is larger than J_{IC} at crack tip, cracks propagate in a ductile manner.

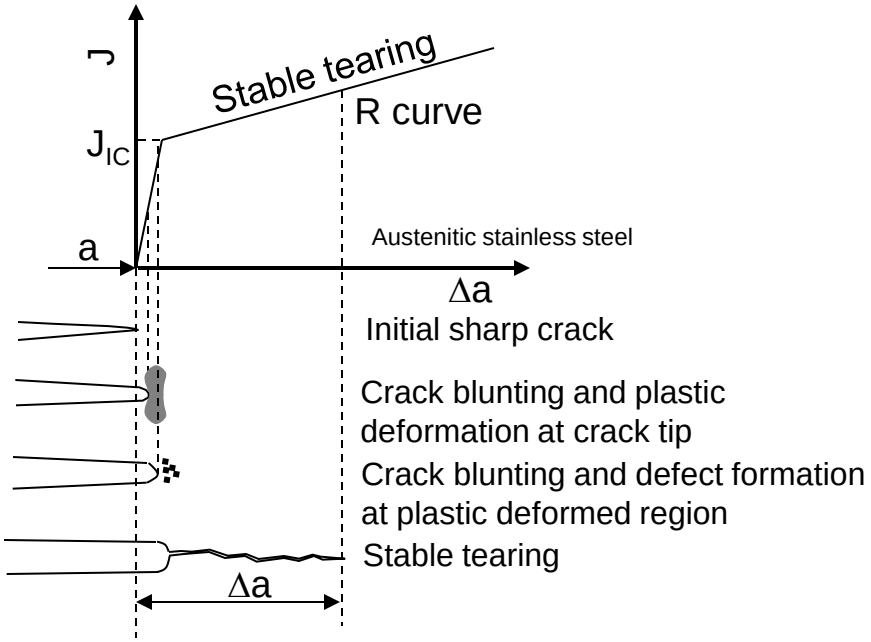

1.3.2 Short-Term Mechanical Properties (5) (cont.)

Fracture Toughness

Fracture toughness test specimens

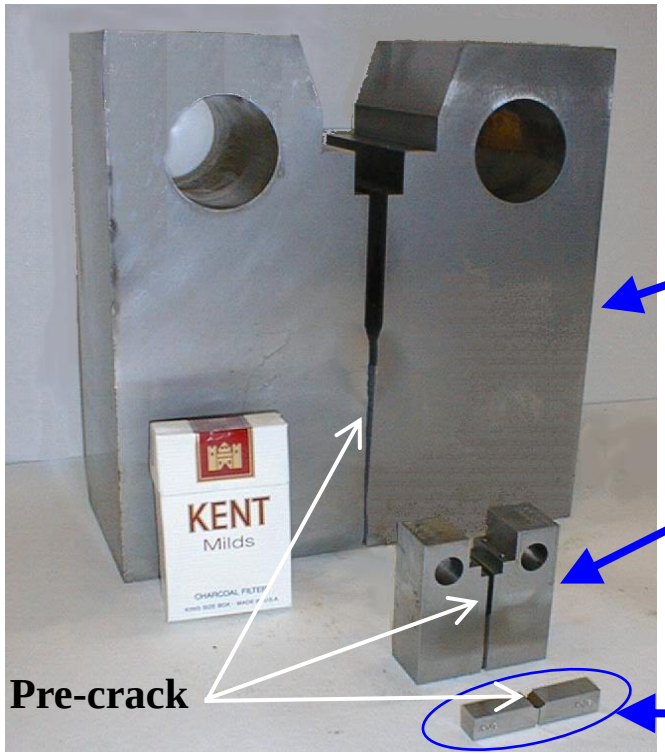

Large CT
(100mm thick)

Standard CT
(25mm thick)

Charpy size
(10mm thick)

Standardized specimen geometry

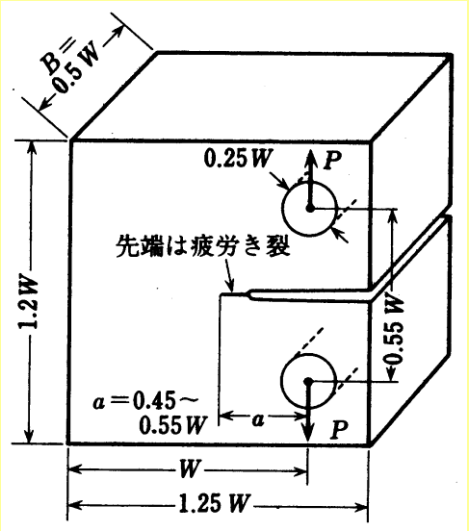

Compact tension specimen

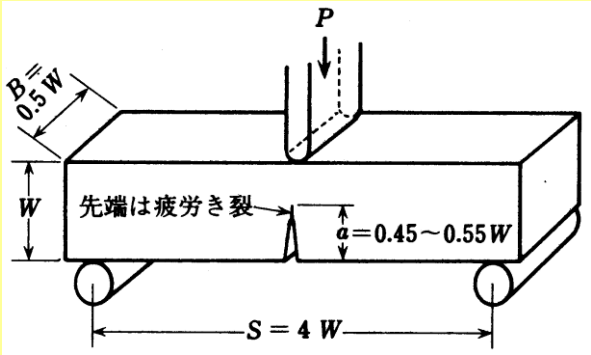

Three-point bend specimen

Plane strain fracture toughness (K_{Ic})

Fracture criterion:

$K_I \geqq K_{Ic}$

1.3.2 Short-Term Mechanical Properties (5) (cont.)

K_{IR} curve in ASME B&PV Code Sec. III

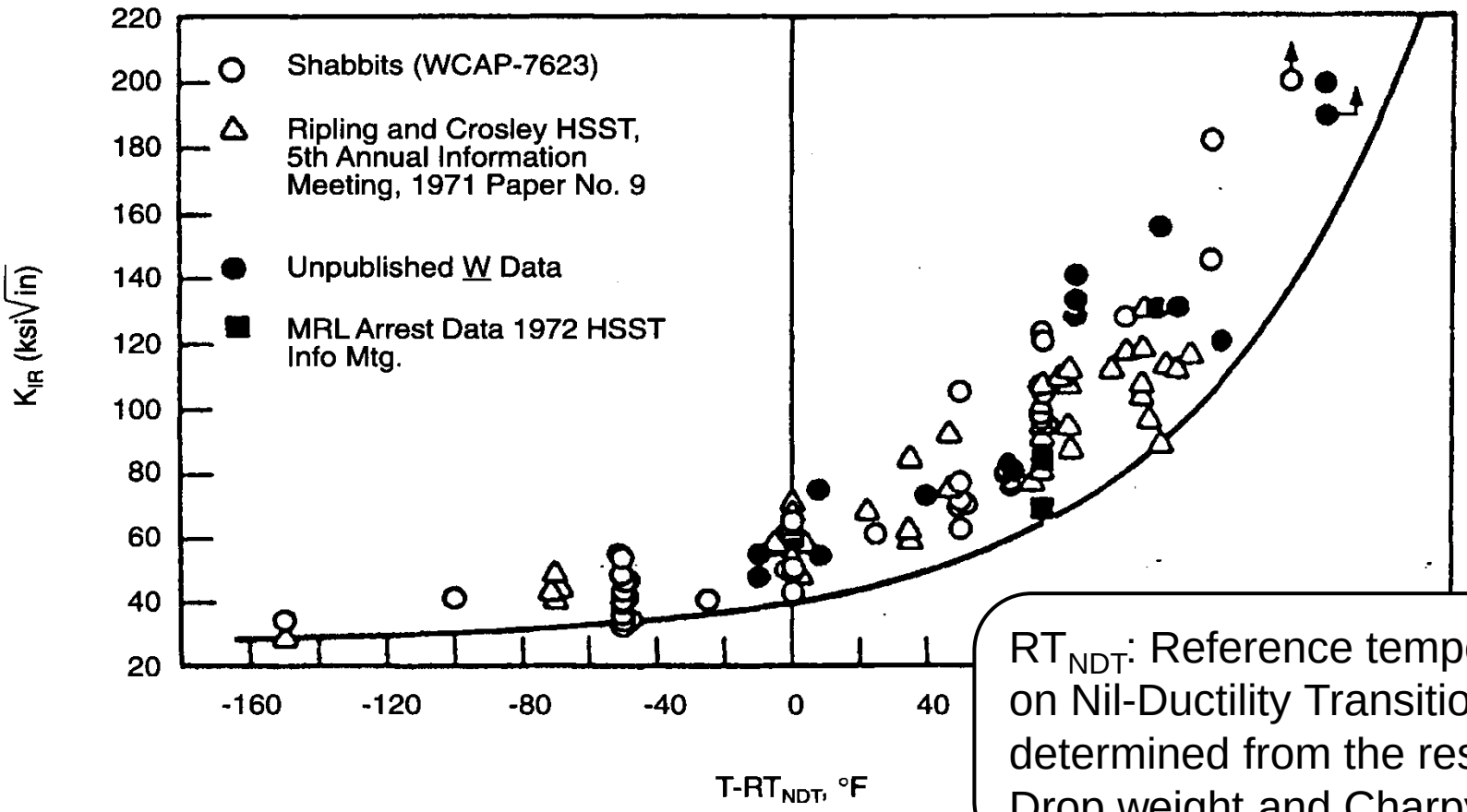

RT_{NDT}: Reference temperature on Nil-Ductility Transition determined from the results of Drop weight and Charpy tests

✓K_{IR} curve: Lower bound curve of all types of fracture toughness data (static K_{Ic}, dynamic K_{Id}, crack arrest K_{Ia})

→For Ferritic steels, fracture toughness can be bounded by this curve.

1.3.3 Fatigue Property (1)

(1) Fatigue life

At temperature range from RT to 350ºC, there is little difference on fatigue lives.

Langer equation

$$S_a = \frac{E}{4\sqrt{N_f}} \ln \frac{1}{1-RA} + B$$

Universal slopes equation

$$\frac{\Delta\varepsilon}{2} = \frac{\Delta\varepsilon_{elastic}}{2} + \frac{\Delta\varepsilon_{plastic}}{2} = 3.5\frac{\sigma_{UTS}}{E} N_f^{-0.12} + D^{0.6} N_f^{-0.6}$$

$$D = -\ln(1-RA)$$

RA : reduction of area

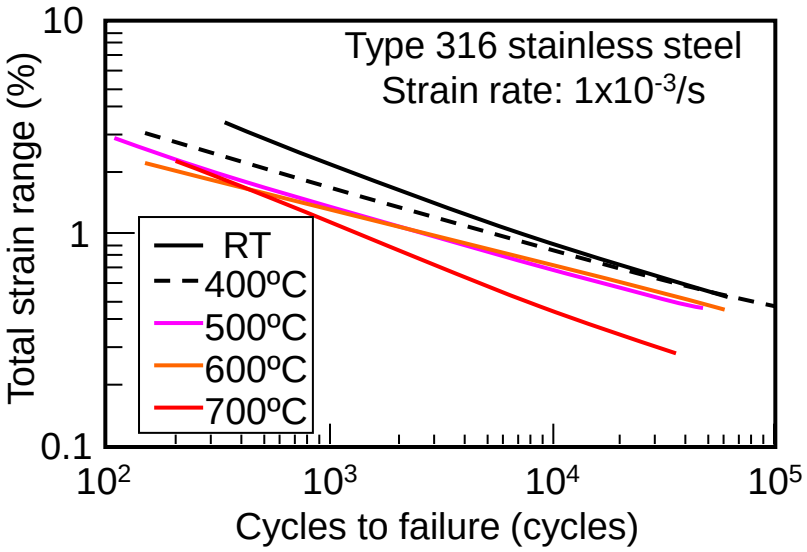

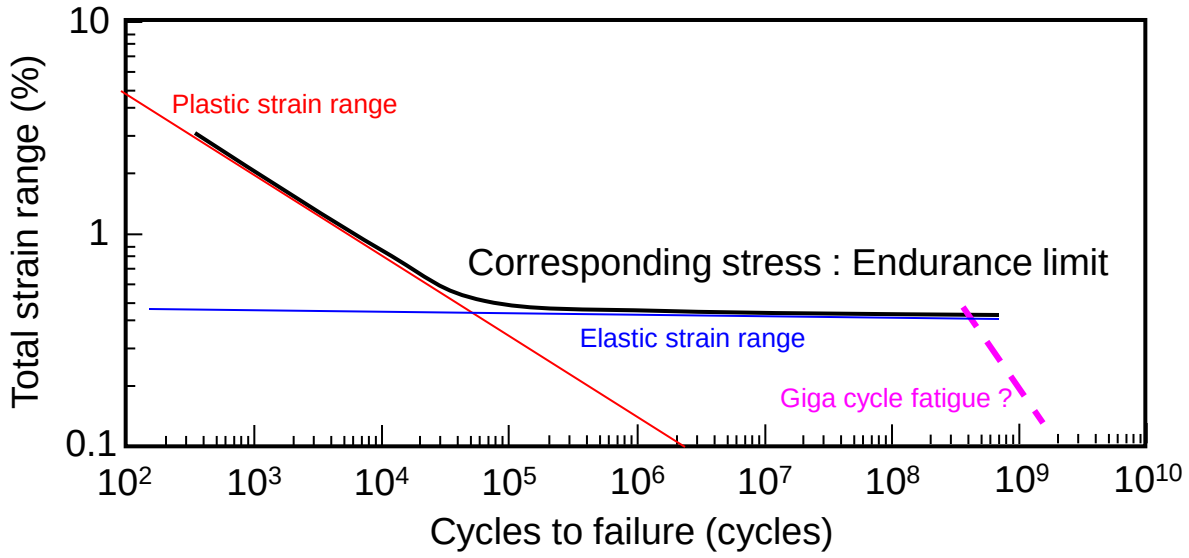

1.3.3 Fatigue Property (2)

Design for Fatigue

The class 1 plant design analyses have considered the well-defined thermal transients such as plant startup and shutdown. (low cycle fatigue)

The turbulence in the mixing layer at the interface between the hot and cold coolant layer introduces cyclic thermal stress at the inside surface of the pipe in the vicinity of the mixing layer. (high cycle fatigue)

Best-fit curve by Langer equation

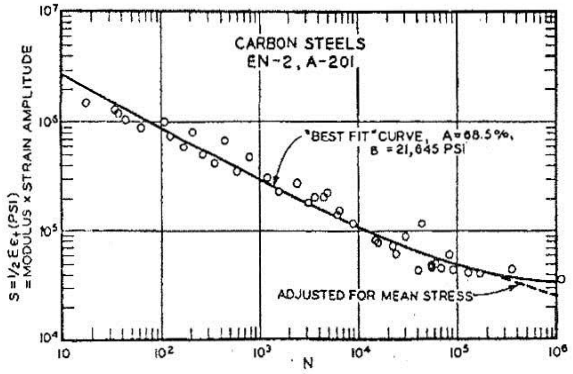

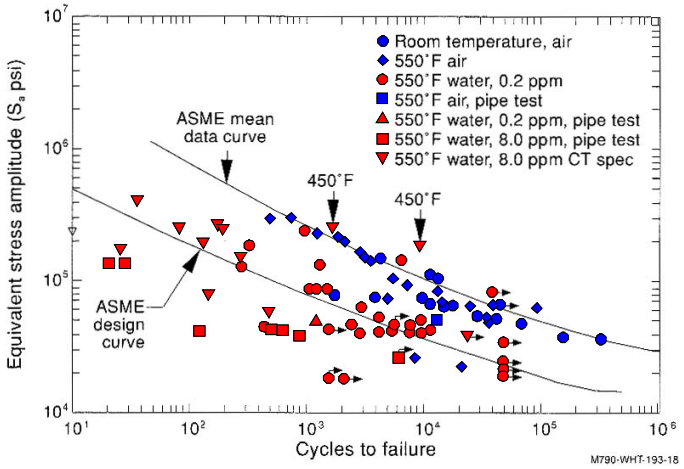

Environmental effects

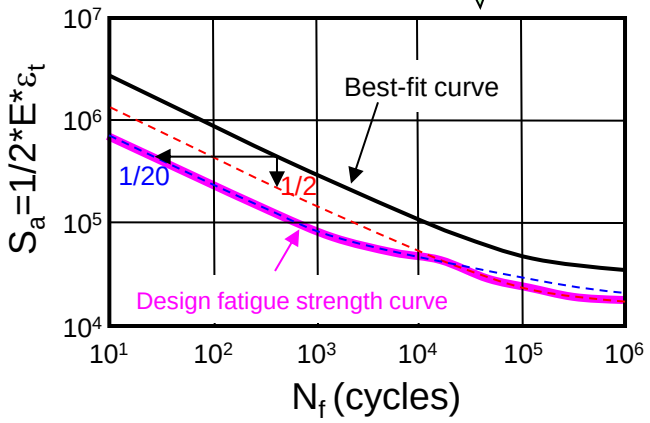

A least-squares curve was fitted through the data, and a factor of 2 on stress or 20 on cycles, whichever was more conservative for a given point, was used to establish the design curve.

A factor of 20 is divided to sub factors.

- deviation of fatigue lives : 2
- size effect : 2.5
- circumstantial effect, surface roughness : 4

Sa: pesudo-stress ampitude

1.3.3 Fatigue Property (3)

Fatigue damage evaluation

In Most real service application, the type of controlled stress fluctuations evident in laboratory experiments dose not exist. Instead a given stress level may prevail for a certain number of cycles, a different level for another number of cycles, and so forth.

Palmgren-Miner cumulative damage theory, or Miner's rule

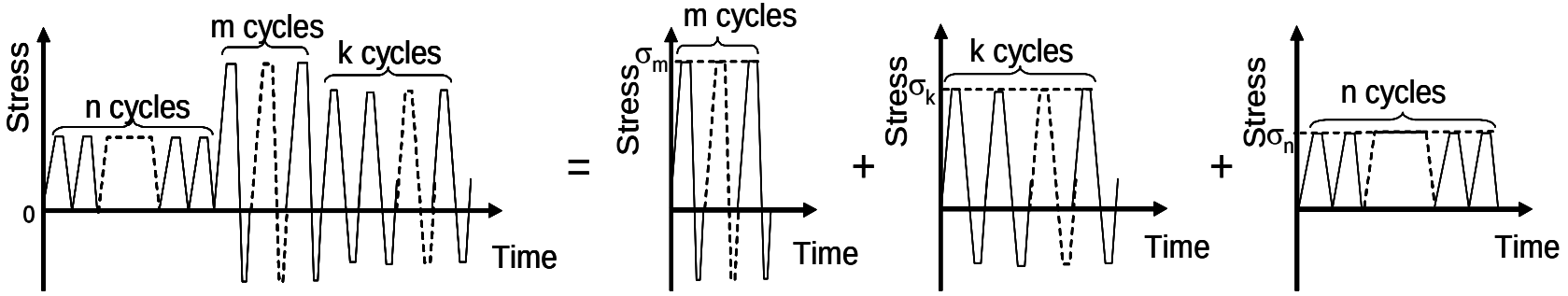

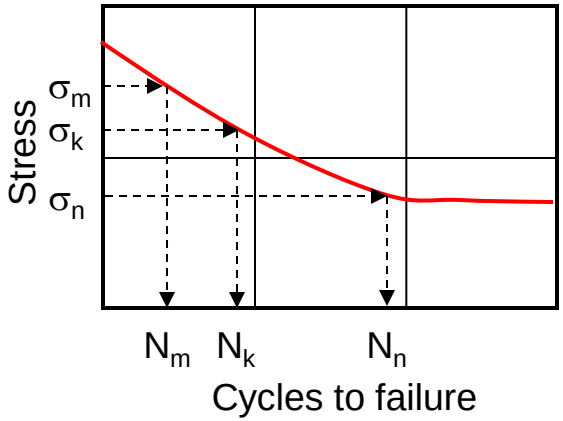

$$\phi_f = \frac{m}{N_m} + \frac{k}{N_k} + \frac{n}{N_n} = \sum_{i=k}^{n} \frac{n_i}{N_i}$$

When ϕ_f is equal to or larger than 1, fracture occurs.

1.3.3 Fatigue Property (4)

(3) Fatigue crack propagation

Under cyclic stresses the crack propagation can occur at a stress intensity factor K much lower than the fracture toughness factor K_I. As a consequence of accumulative damage strain, hardening occurs, causing the plastic zone around the crack to be much smaller than the initial plastic zone during the application of load.

$$\frac{da}{dN} = C(\Delta K)^n$$ 2a: crack length

Paris' law

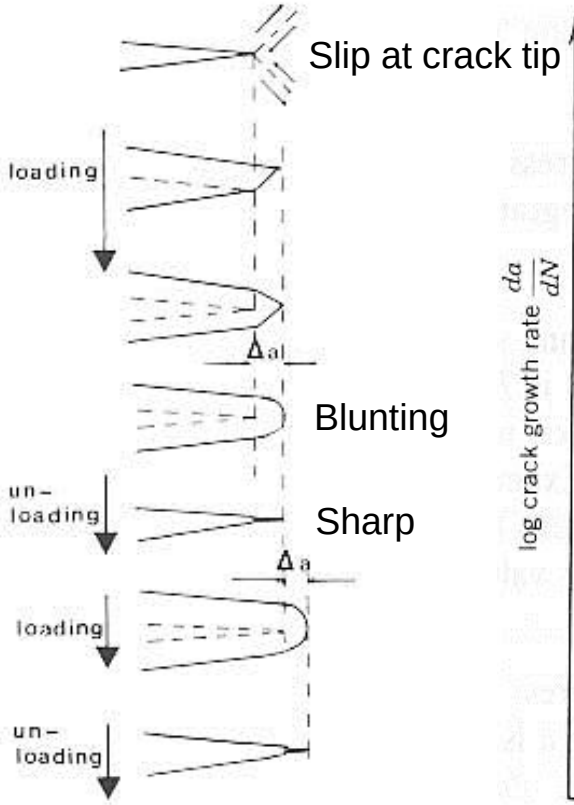

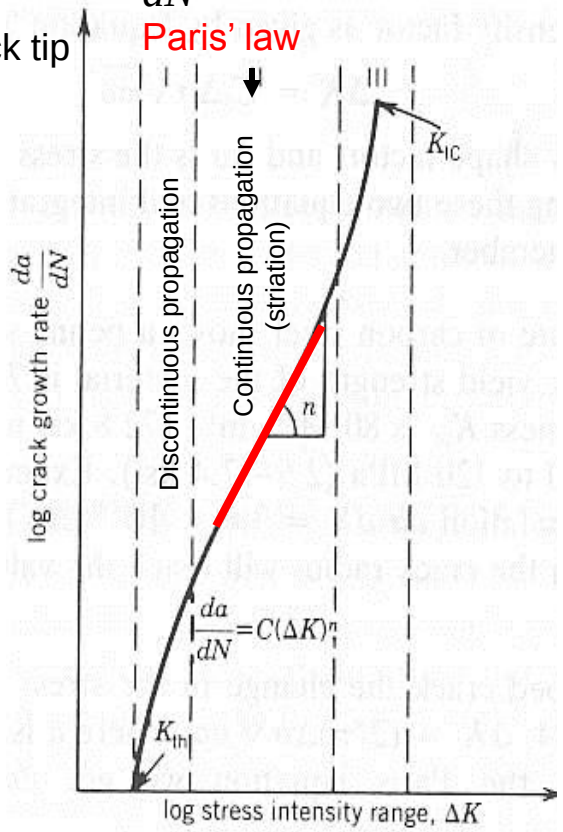

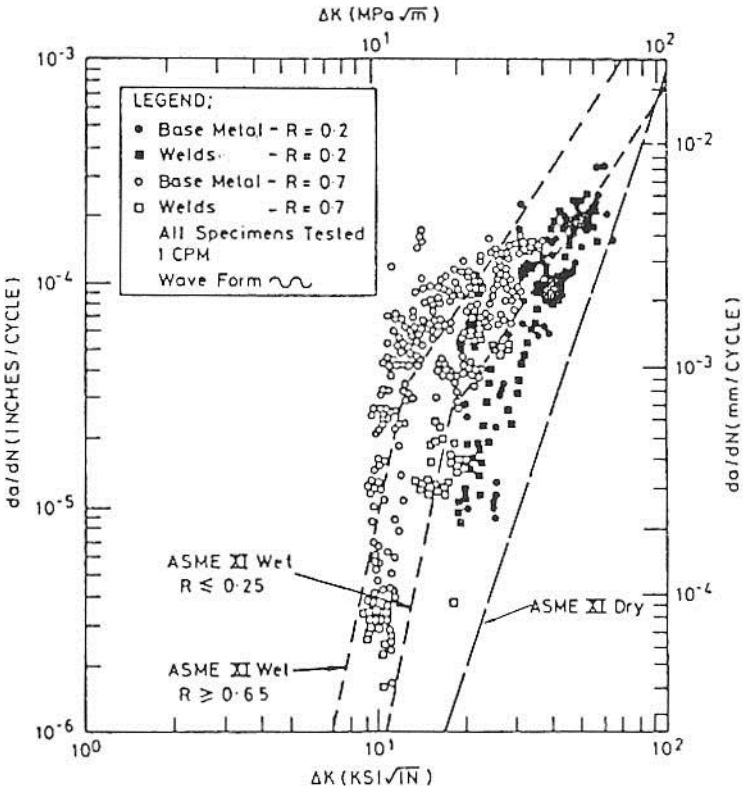

Environmental effects
(in high temperature water)

1.3.4 Creep Property

Usually creep is not considered in LWR conditions.

In ASME code section III, the use of ferritic steel and austenitic steel is restricted below 371 and 427 ºC, respectively, where the creep is ignored.

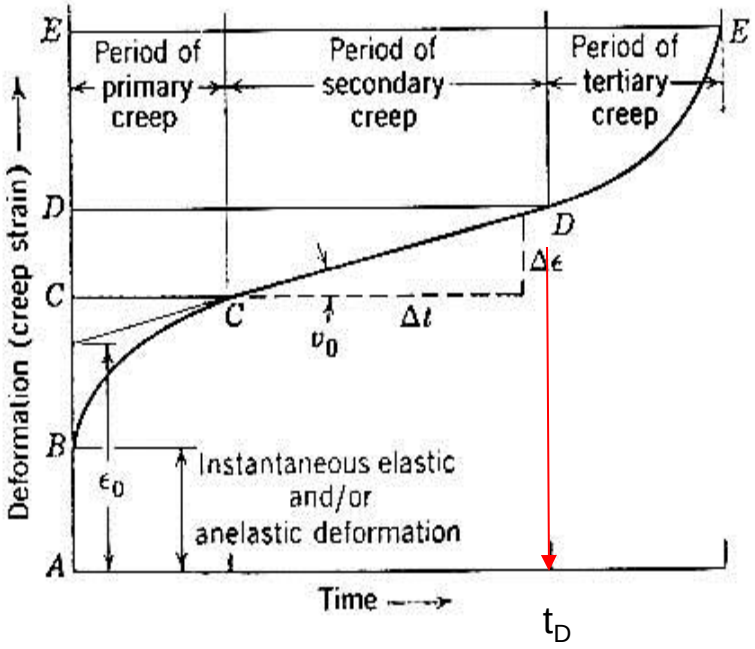

Minimum creep rate $\Delta\varepsilon/\Delta t$ and creep rupture time (t_D) is important.

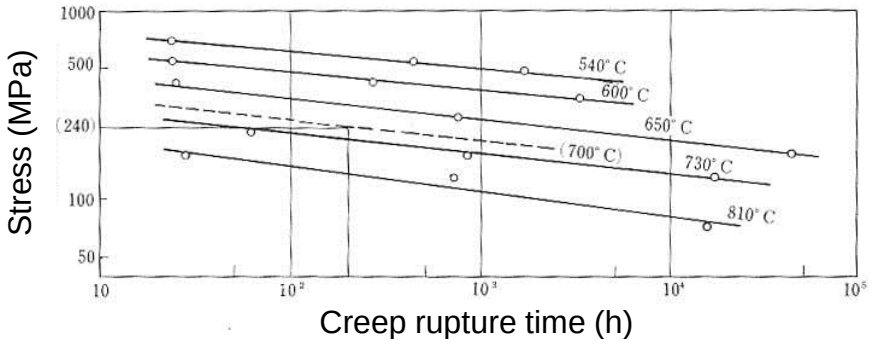

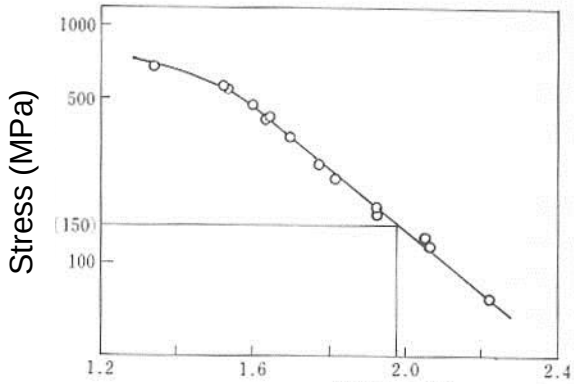

Larson-Miller parameter, 1.8T(ln t_r + C)

In some circumstances, creep can be advantageous in the relief of thermal stress resulting from temperature differences.

1.4 Welding

1.4.1 Welding Technique (1)

Welding is important not only for construction but also for maintenance (repair, replacement of component).

(1) Type of welding process

- Shielded metal arc welding, (SMAW)
- Submerged-arc welding, (SAW)
- Gas shielded are welding,
- Inert-gas arc welding: Tungsten-inert-gas (TIG), Metal-inert-gas (MIG)
- CO_2 arc welding,
- Laser beam welding

(2) Important parameter in welding process

- Groove shape: RPV, internals ⇨ Butt joint
- Heat input power:
- Minimum preheat and interpass temperature
- Post weld heat treatment

Table 8.4. Preheat, interpass and post-welding heat treatment temperatures for various steels

Steel type	Minimum preheat and interpass temperature (°C)	Postweld heat treatment temperature range (°C)
Carbon steel <19 mm	None	None
Carbon steel >19 mm	100	580–650
C½Mo	100	650–690
1Cr½Mo	150	650–700
2¼Cr1Mo	200	690–740
5Cr½Mo, 9Cr1Mo, 12CrMoV	200	700–760
3½Ni	None	580–620
9Ni	None	None
Austenitic Cr–Ni steel	None	Normally none (see text)

1.4.1 Welding Technique (2)

(3) Weld defects

● : often ▲ : occasionally

* Stress Relief

Material	Hot cracking	Cold cracking		Lamellar tear	SR cracking
		Delayed crack	Quenching crack		
Low carbon steel		▲		▲	
Low alloy steel		●			●
Cr-Mo steel		●			●
Martensitic stainless steel	▲	●	▲		
Austenitic stainless steel	●				▲
Ni-base alloy	●				
Cu alloy	●				▲

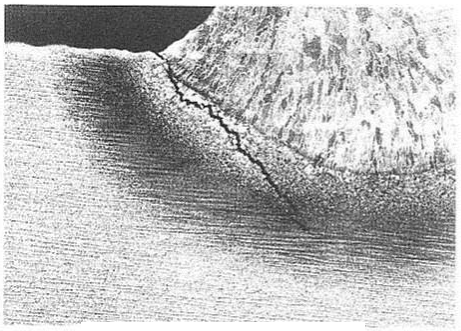

8.36 Cra ste a fillet weld in higher-tensil

Delay cracking

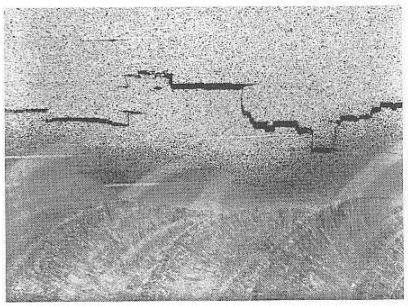

8.48 A lamelli morphol parallel t steel. Note the steplike dency to run in planes ph courtesy of TWI).

Lamellar tear

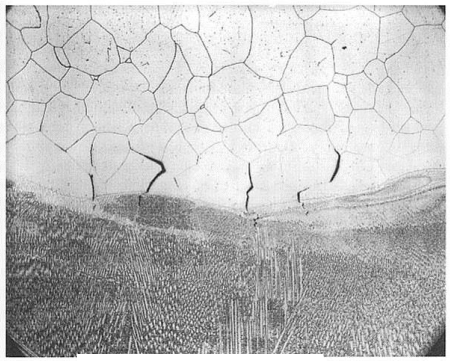

9.12 Hot c nicke (phot ustenitic chromium–ıring welding (×200)

Hot cracking

1.4.2 Material Issues Related to Welding (1)

Position of welding

– Reactor pressure vessel (RPV), Vessel support, ⇨Heavy steel
Reduce weld lines.

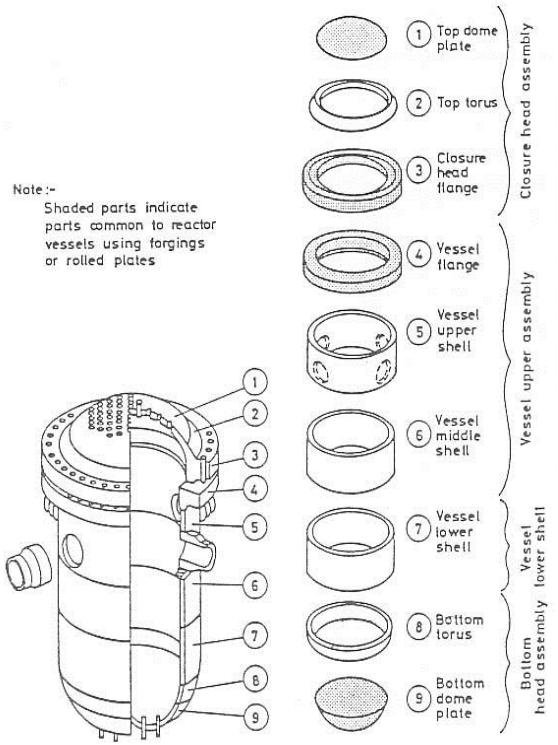

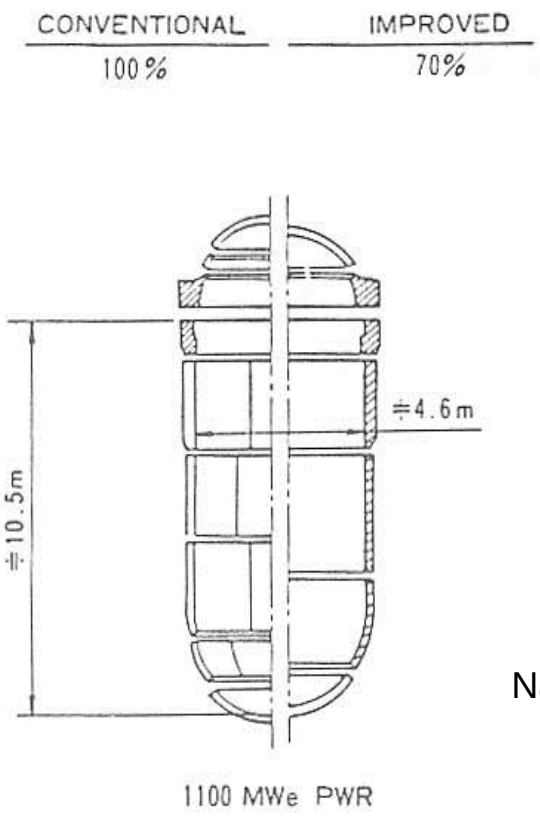

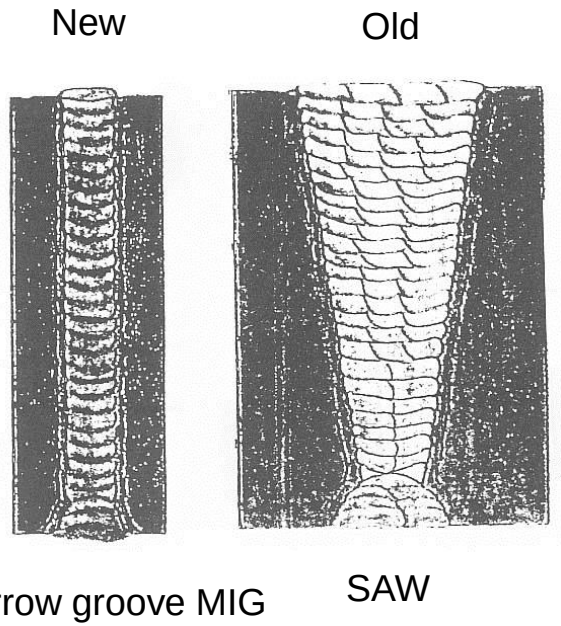

No longitudinal weld lines

1.4.2 Material Issues Related to Welding (2)

Inner surface of RPV; Overlay cladding

Under-clad cracking

Stainless steel
(308,309,309L)
Inconel
clad

RPV
SGPV

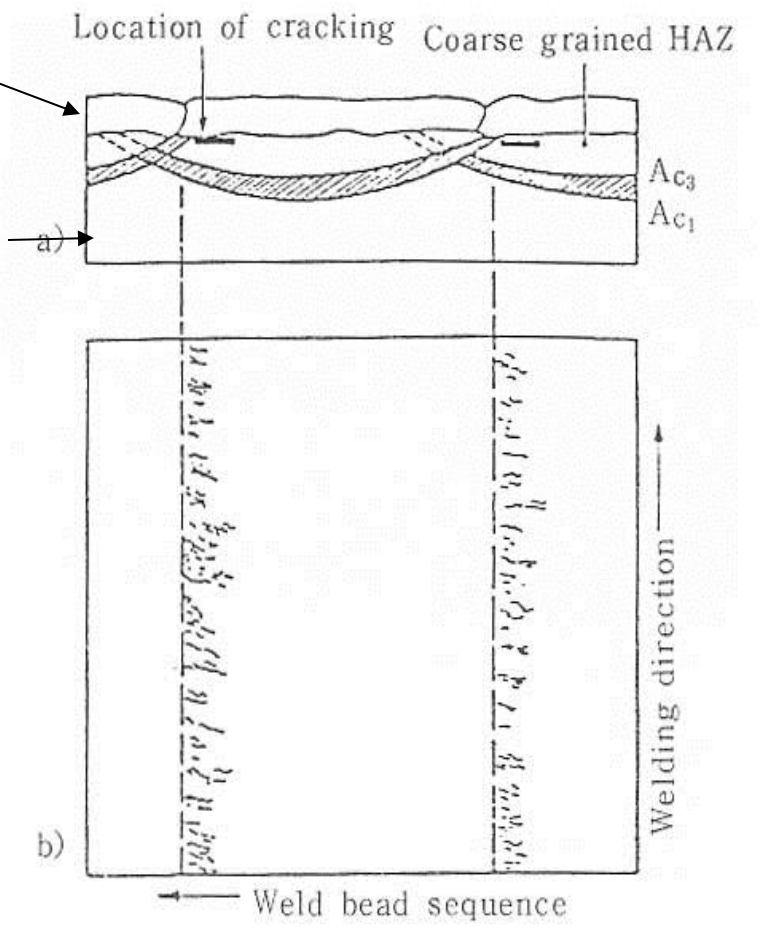

1.4.2 Material Issues Related to Welding (3)

- Nozzle to safe end (RPV, pressurizer)

  Dissimilar metal welding

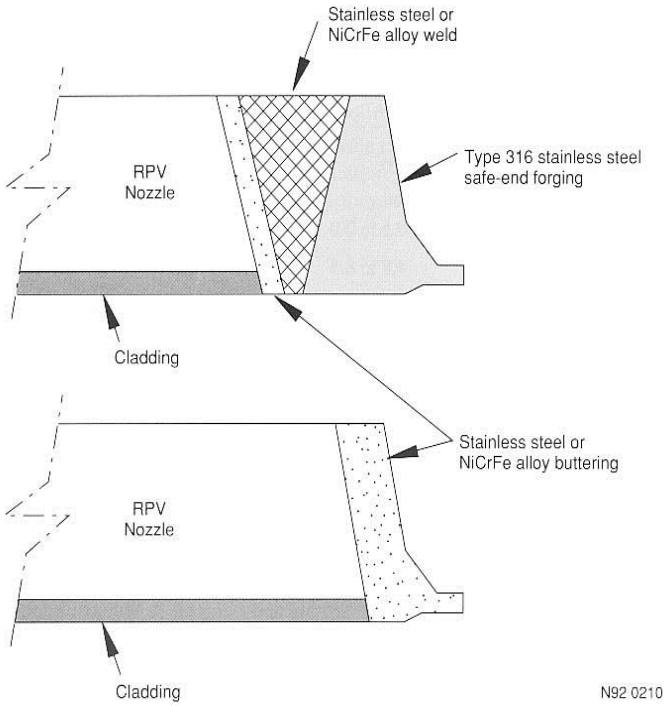

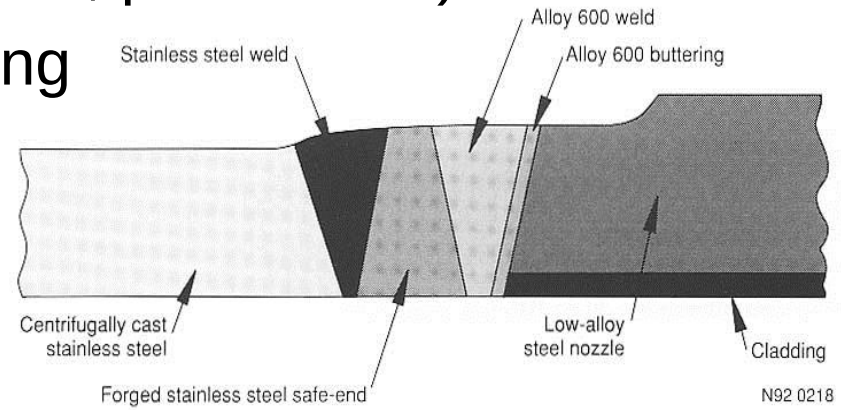

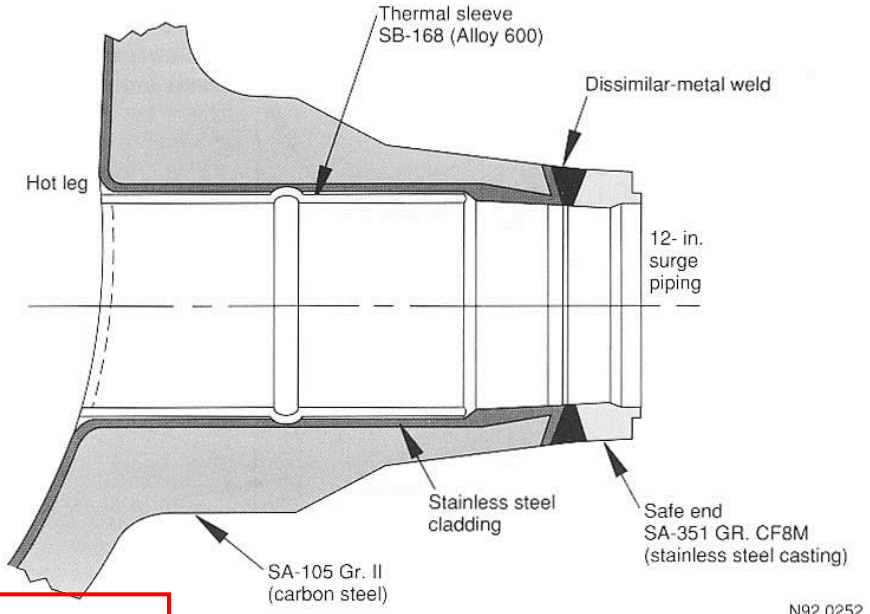

Buttering of Ni alloy on low alloy steel

1.4.2 Material Issues Related to Welding (4)

- RPV head, control rod drive nozzle

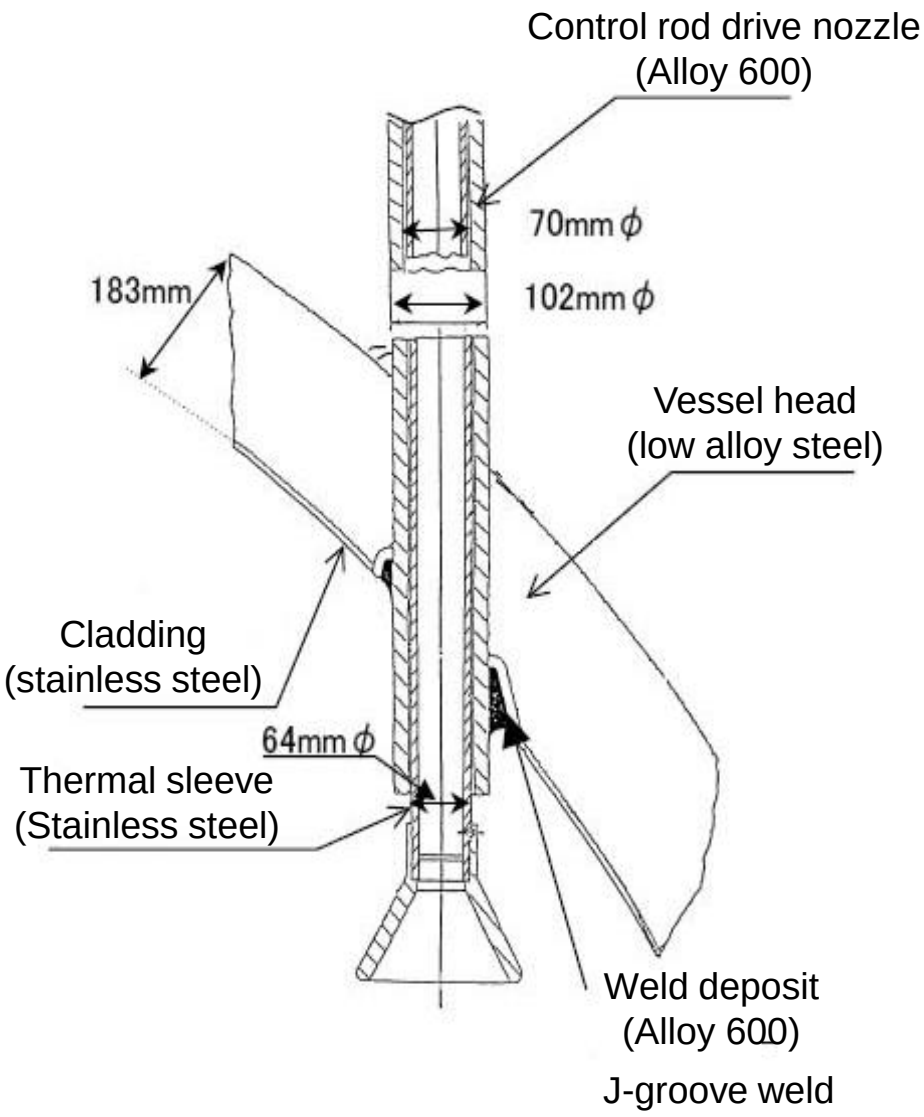

1.4.2 Material Issues Related to Welding (5)

The deposited weld metal contains a characteristic microstructure consisting of long columnar grains. These nucleate from favorably orientated grains in the heat affected zone and grow epitaxially from bead to bead in a multipass weld. In austenitic stainless steels, each grain contains a network of δ-ferrite and subgrain structure, dislocation network etc.

Moreover, welding affects not only on the as-welded deposit but also on the surrounding parent metals.

(1) Dissimilar metal welding

Dilution of alloying element, Post Welded Heat Treatment (PWHT)

⇨ Formation of new phase

Welding of safe end to nozzle, Buttering, cladding,

(2) Thermal cycles

There is an influence of localized reheating and chilling during the overlapping of successive weld metal. Regions adjacent to each new weld bead experience short-time, high-temperature, reheats. Then considerable variations in dislocation density also occur depending upon position in the welds, resulting in the heterogeneous hardness distribution. Shrinkage and thermal stresses experienced on welding cause significant deformation of inner weld bead compared to surface bead. These also affect on the surrounding parent metals.

1.4.2 Material Issues Related to Welding (6)

– Heat-affected zone (HAZ)

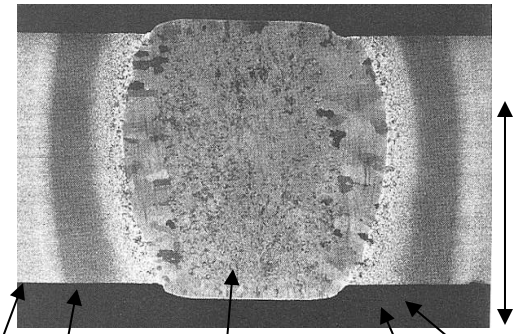

The heat-affected zone adjacent to weld fusion line has known to give lower toughness value than other regions, since the local temperature peak from the welding process rise above 1200ºC and the zone is cooled slowly.

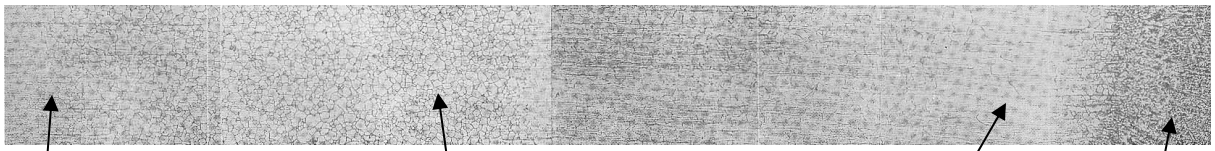

Austenitic stainless steel

Thermal sensitization :

1.4.2 Material Issues Related to Welding (7)

– Residual stress

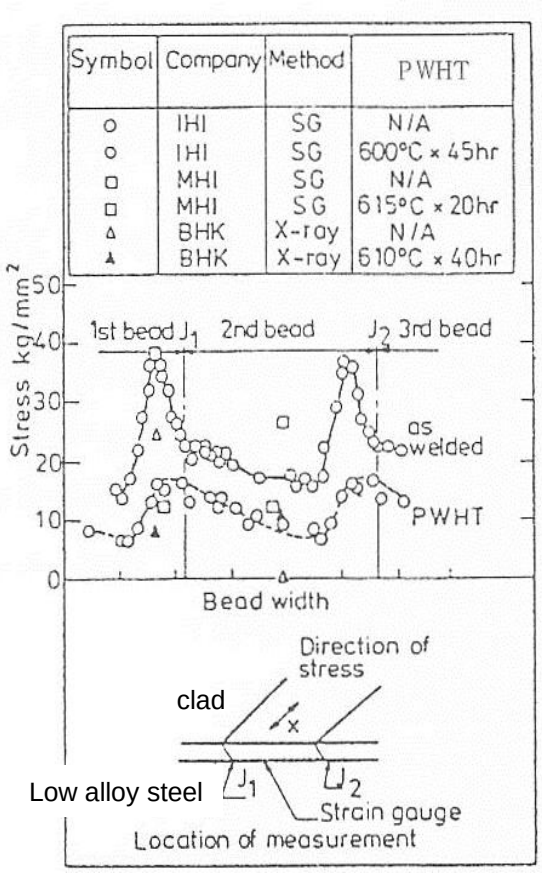

Residual stress by cladding has peak at position just below overlap of beads. The residual stress decreased after PWHT.

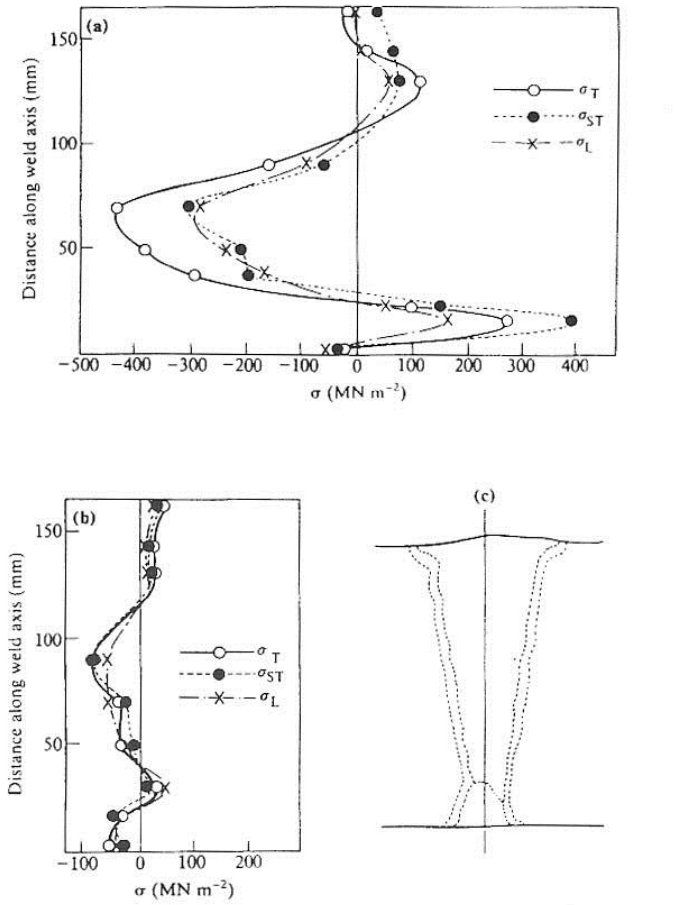

7.29 The distribution of residual stress along the centreline (c) of a submerged arc weld in 165 mm thick Mn–Mo steel: (a) postweld heat treatment 15 min at 600 °C; (b) postweld heat treatment 40 h at 600 °C. Curves are σ_T, stress transverse to weld; σ_{ST}, stress at right angles to plate surface; σ_L, longitudinal stress (from Suzuki *et al.*, 1978).

1.4.2 Material Issues Related to Welding (8)

- Remedy of residual stress for pipes

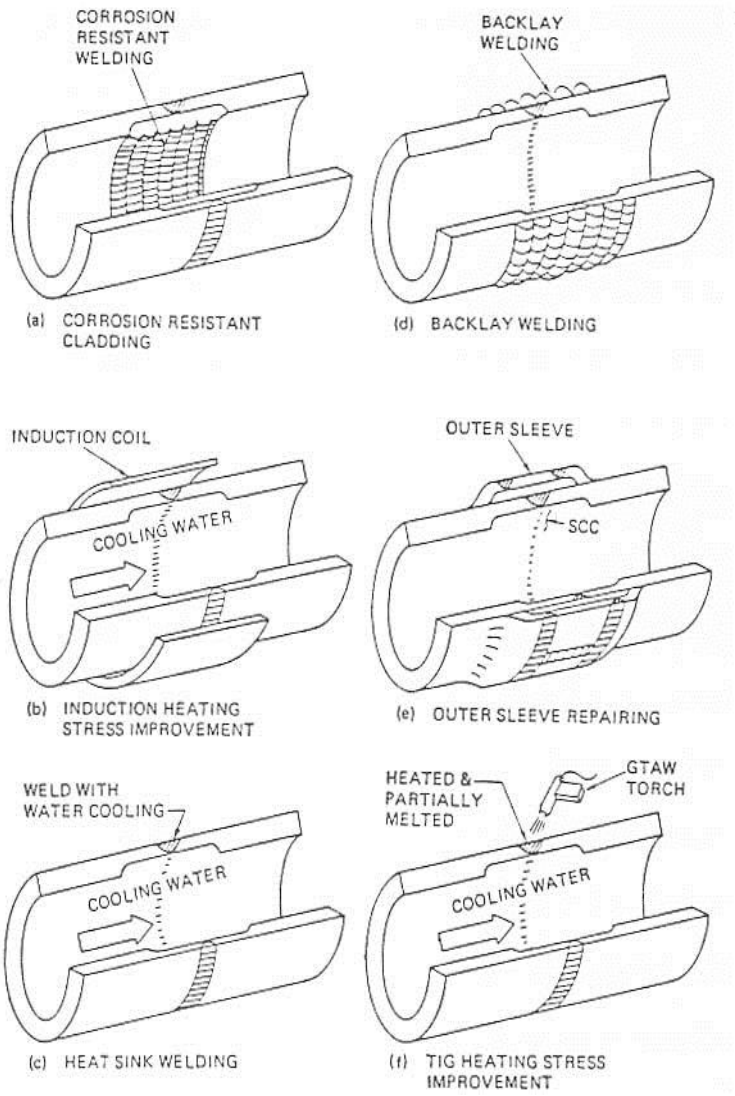

- For J-groove welding at penetration
  - ✓ Water jet peening
  - ✓ Laser peening

1.4.3 Repair by Welding

- Repair welding of pressure vessel nozzle
  - Thermal sensitizing of austenitic stainless steels such as clad during welding process and PWHT.
  - Residual stress.

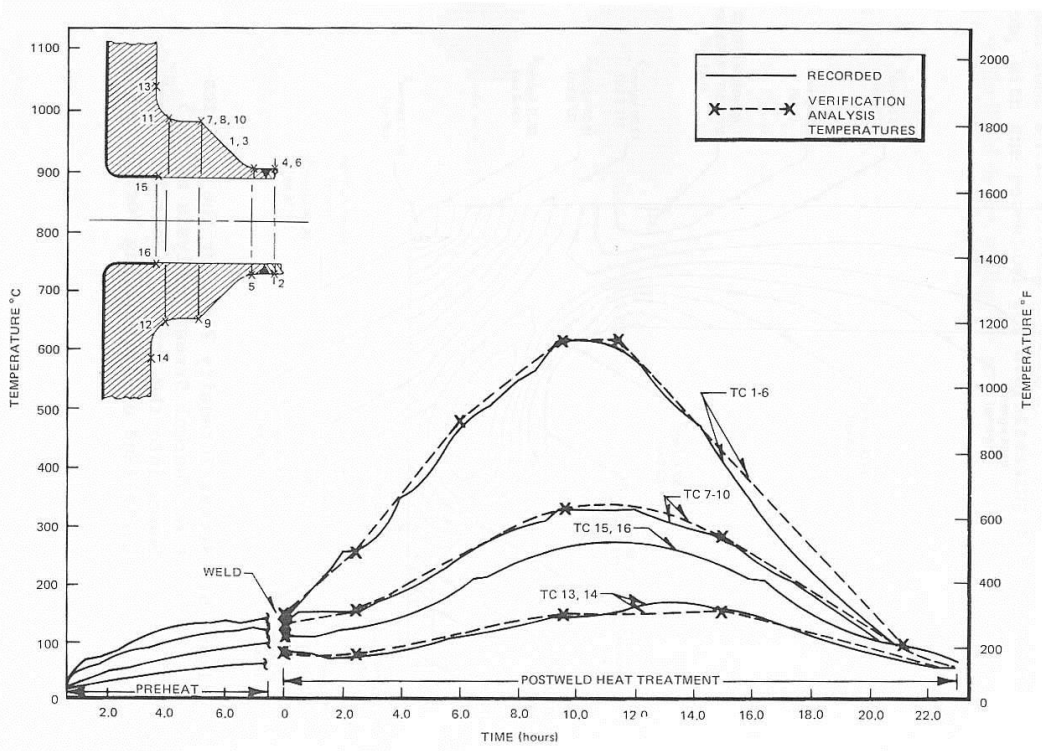

Recorded and Verification Analysis Temperature Versus Time for Nozzle N4B

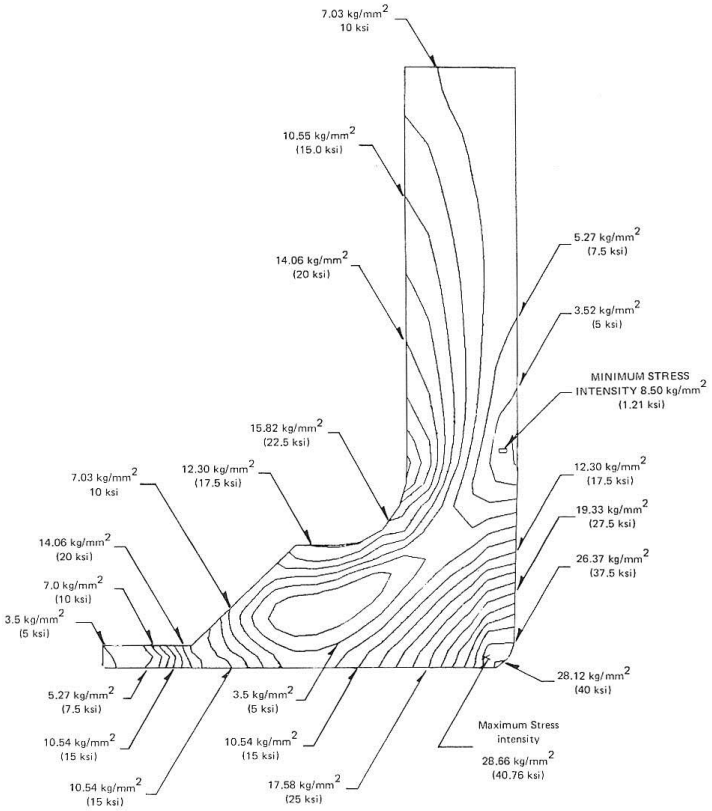

Figure 6. Stress Intensity Plot for the Verification Thermal Stress Analysis at 10.5 Hours into the Postweld Heat Treatment Cycle (End of the Holding Period)

1.5 Radiation Effects in Materials

1.5.1 General Principle (1)

Radiation damage

The radiation damage event is defined as the transfer of energy from an incident projectile to the solid and resulting distribution of target atoms after completion of event. This energy per atom is much larger than the usual chemical reaction energy.

1. The interaction of an energetic incident particle with a lattice atom
2. The transfer of kinetic energy to the lattice atom giving birth to primary knock-on atom (PKA)
3. PKA ionizes and displaces surrounding atoms from their lattice sites
4. The passage of the displaced atoms through the lattice and accompanying creation of additional knock-on atoms
5. The production of a displacement cascade
6. The termination of the PKA as an interstitial

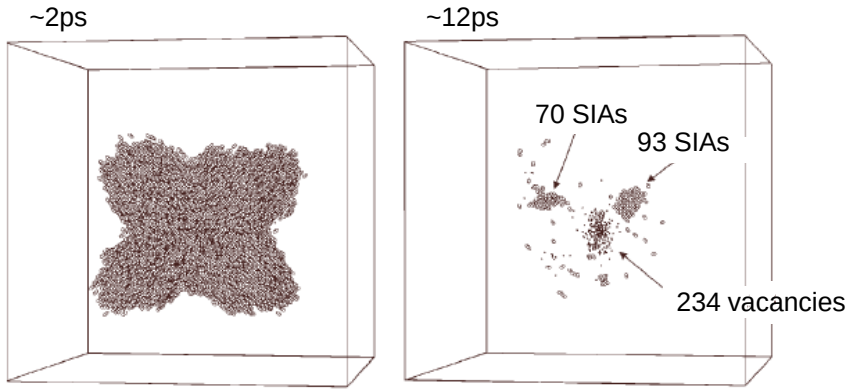

SIA : Self-interstitial atom

1.5.1 General Principle (2)

Displacement damage

2 step reactions
$^{58}Ni(n,\gamma)^{59}Ni(n,\alpha)^{56}Fe$
$^{58}Ni(n,\gamma)^{59}Ni(n,p)^{59}Co$

Fig. 7.5. Interactions of thermal and fast neutrons with a solid.

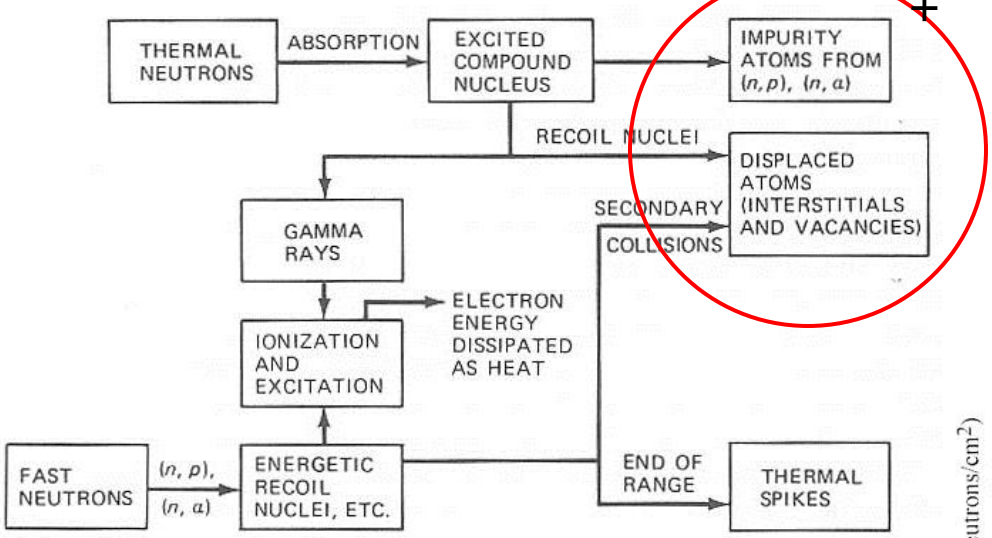

Parameters in radiation damage for metal

dpa (displacement per atom)
This is a measure of the amount of radiation damage in neutron-irradiated materials, for example, 10 dpa means each atom in the material has been displaced from its site within the structural lattice of the material an average of 10 times (due to interactions between the atoms and the energetic neutrons irradiating the material.

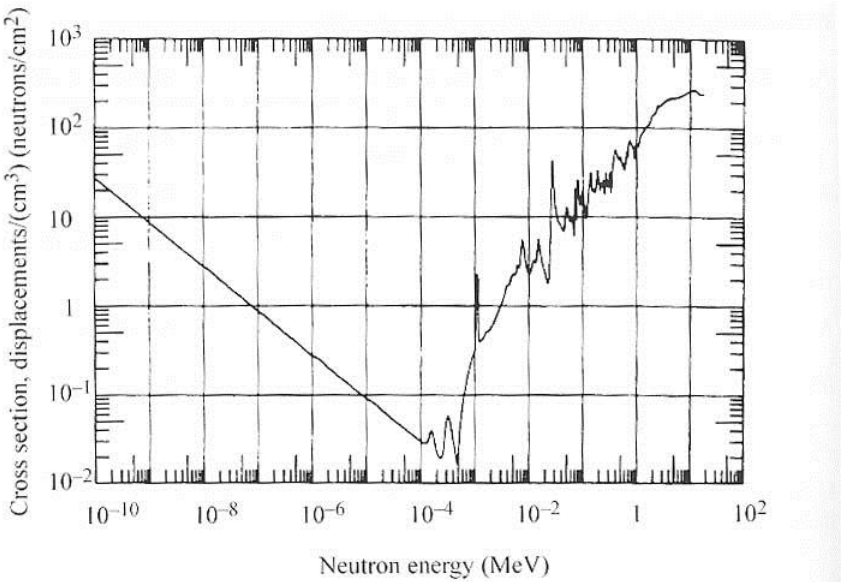

Fig. 2.18. The displacement cross section for stainless steel based on a Lindhard model and ENDF/B scattering cross sections (after [21])

1.5.1 General Principle (3)

Formation of radiation defects

- Interstitial cluster, dislocation loop
- Vacancy cluster, Stacking fault tetrahedron, Cavity (He bubble, void)
- Precipitates

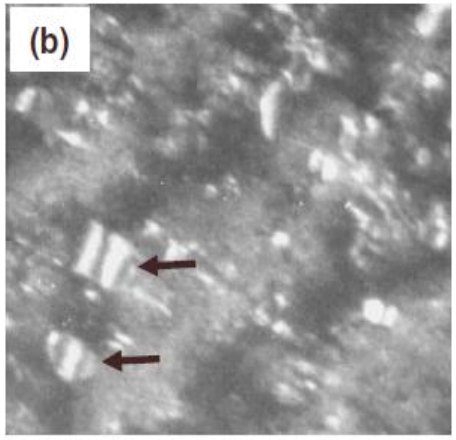

Dislocation loop

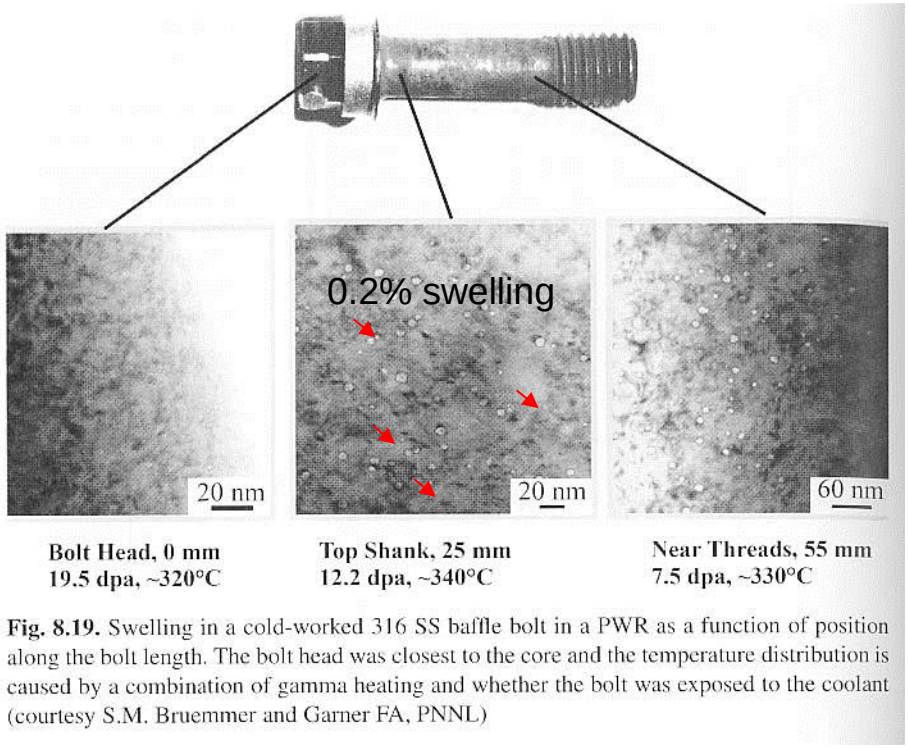

Fig. 8.19. Swelling in a cold-worked 316 SS baffle bolt in a PWR as a function of position along the bolt length. The bolt head was closest to the core and the temperature distribution is caused by a combination of gamma heating and whether the bolt was exposed to the coolant (courtesy S.M. Bruemmer and Garner FA, PNNL)

Cavity (He Bubble)

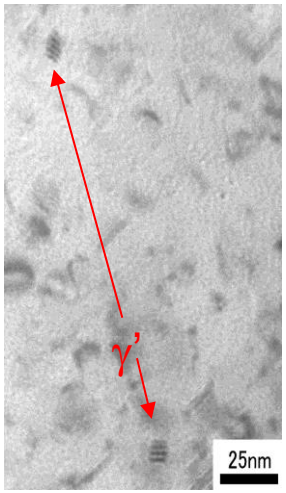

Precipitate

1.5.2 Irradiation Hardening (1)

- In austenitic stainless steels, 0.2% offset stress increases with increasing dose, dpa.

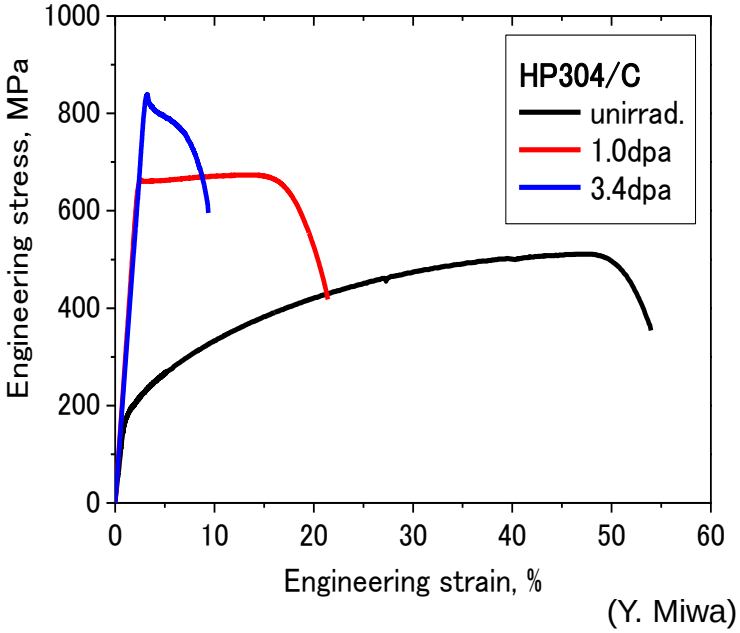

(Y. Miwa)

Plastic instability occurs just after yielding

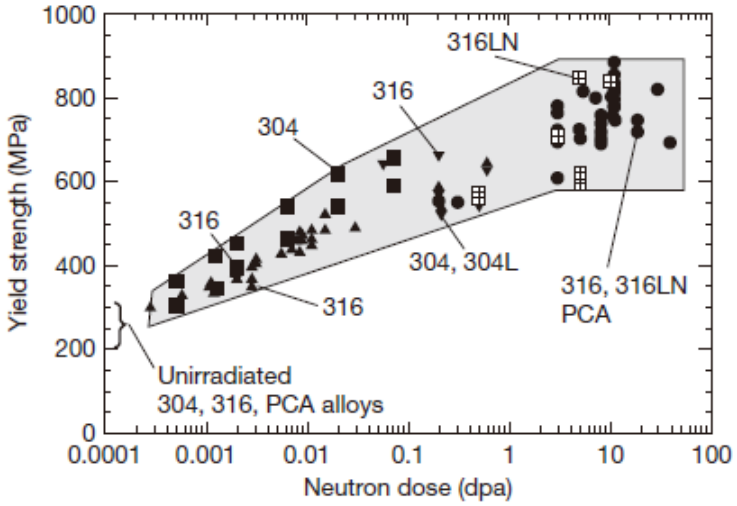

Figure 19 Strengthening of various annealed 300 series stainless steels versus dpa in various water-cooled reactors at relatively low temperatures (280–330 °C). Reproduced from Pawel, J. P.; Ioka, I.; Rowcliffe, A. F.; Grossbeck, M. L.; Jitsukawa, S. In *Effects of Radiation on Materials: 18th International Symposium*; ASTM STP 1325; 1999; pp 671–688. At these temperatures strengthening saturates at ~10 dpa.

The strength increase usually saturates at relatively low exposure levels (<10 dpa) as shown in Figure 19, reflecting a similar saturation of microstructural densities.

1.5.2 Irradiation Hardening (2)

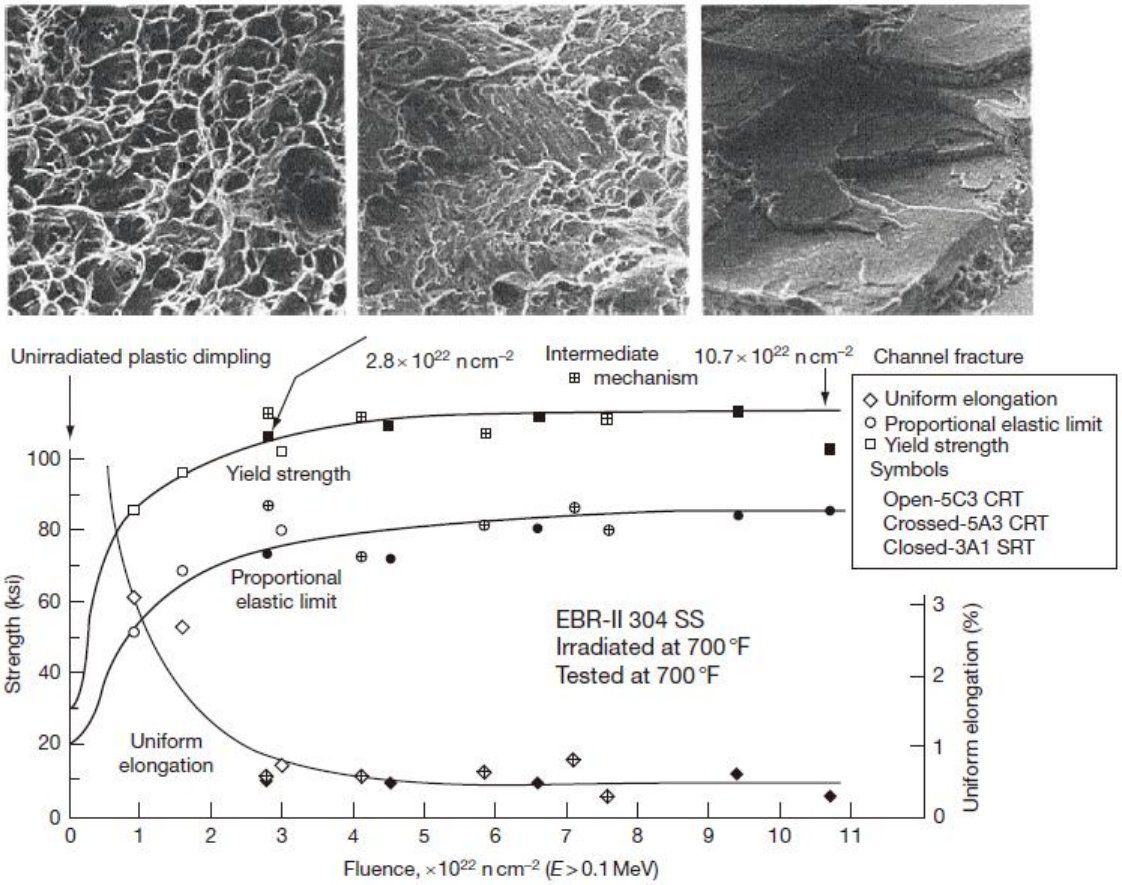

Figure 31 Increase in strength, loss of ductility, and change in failure mode observed during tensile testing in annealed 304 safety and control rod thimbles (SRT and CRT) after irradiation at ~370 °C in EBR-II. Reproduced from Fish, R. L.; Straalsund, J. L.; Hunter, C. W.; Holmes, J. J. In *Effects of Radiation on Substructure and Mechanical Properties of Metals and Alloys*; ASTM STP 529; 1973; pp 149–164.

- Concurrent with an increase in radiation-induced hardening is a loss of ductility.
- The flat faces observed at highest exposure are often referred to as ‘channel fracture’, but they are not cleavage faces. They are the result of intense flow localization, resulting from the first moving dislocations clearing a path of radiation produced obstacles, especially Frank loops, and thereby softening the alloy along that path.

1.5.2 Irradiation Hardening (3)

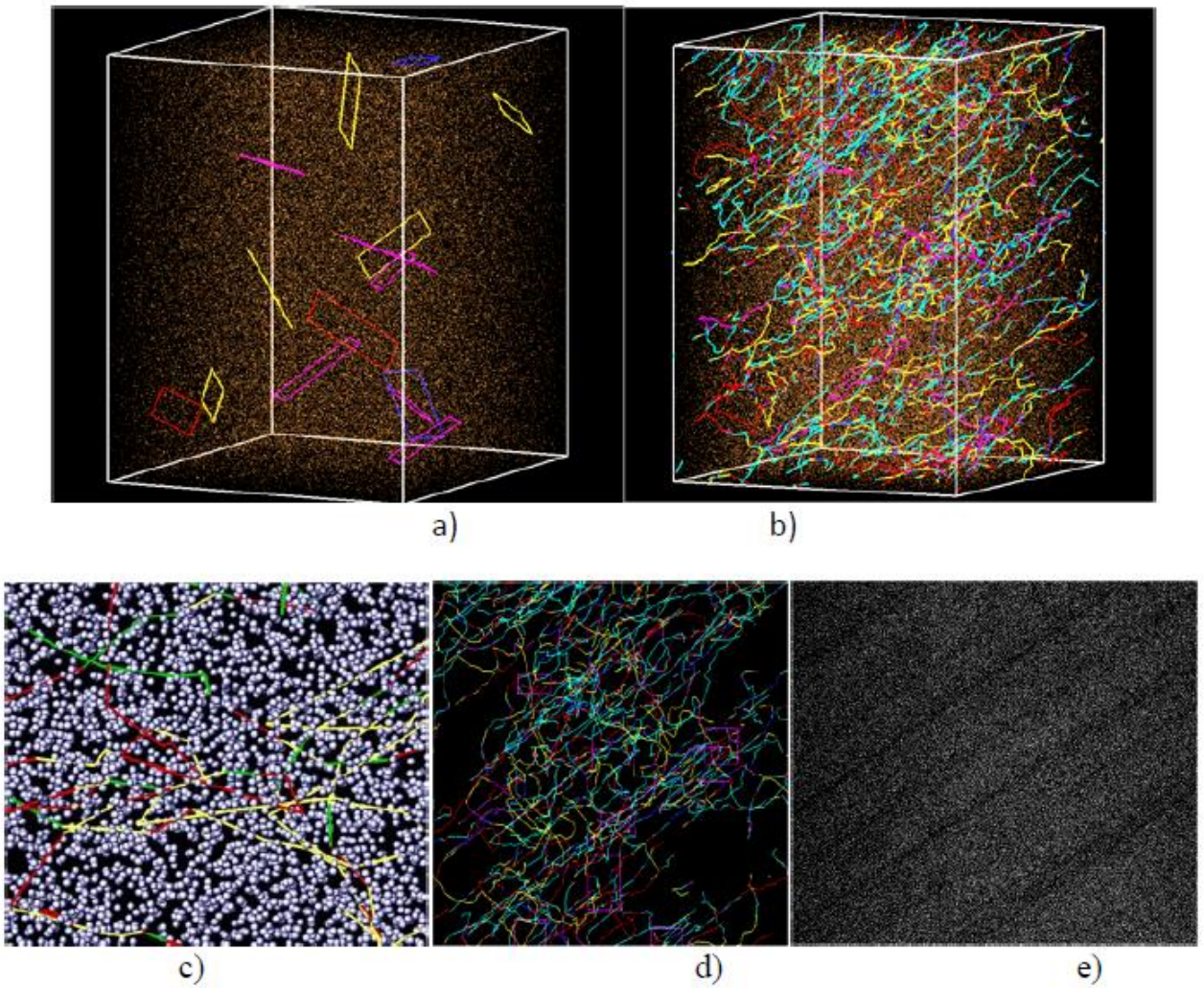

Fig. Typical dislocation dynamics simulation: a) Simulation cell with initial random distribution of Frank-Read dislocation sources and Frank-Sessile (FS) loops, b) dislocation-defect structure after plastic deformation, c) a close-up view showing the interaction between dislocations and FS loops, d) underlying dislocation structure resulting from cross-slip, e) FS loops structure showing the formation of defect-free channels.

1.5.3 Fatigue Property

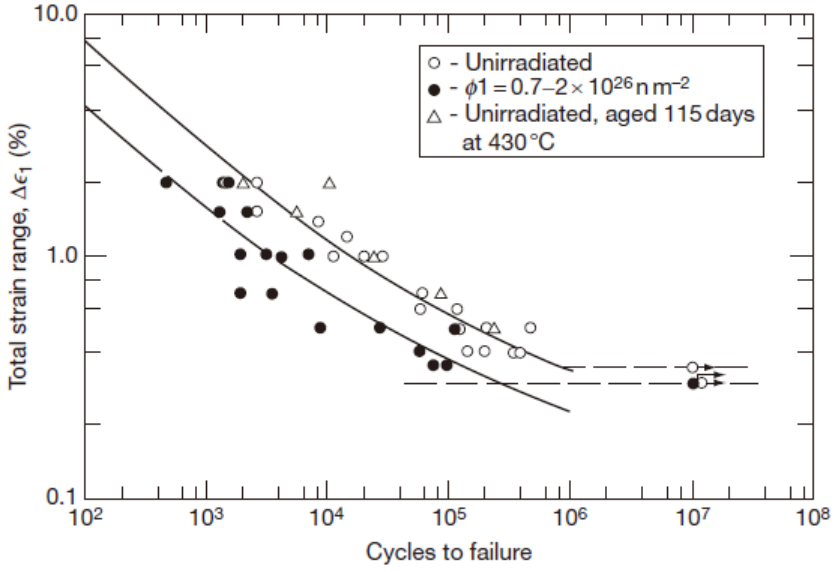

Fig. Fatigue life of 20% cold-worked AISI 316 stainless steel irradiated in HFIR to a maximum dose of 15 dpa and 900 appm He. Reproduced from Grossbeck, M. L.; Ehrlich, K.; Wassilew, C. *J. Nucl. Mater.* **1990**, 174, 264-281.

The lifetimes of irradiated and unirradiated materials are not really so dissimilar. The observed difference is the result of competing influences, degradation due to irradiation, and improvement due to hardening.

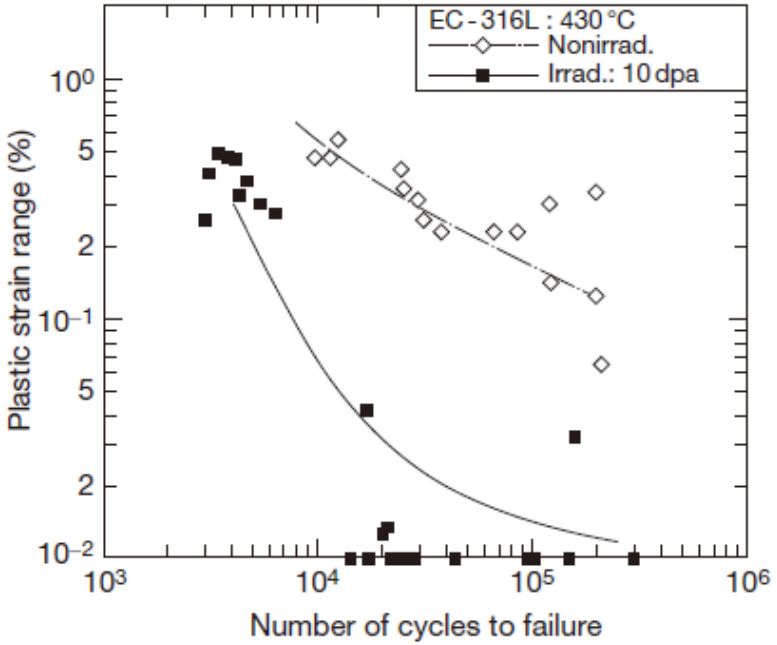

Fig. Plastic strain versus number of cycles to failure of annealed EC-316L irradiated to 10 dpa at ~430℃ in BR2. Reproduced from Grossbeck, M. L.; Ehrlich, K.; Wassilew, C. *J. Nucl. Mater.* **1990**, 174, 264-281; Vandermuelen, W.; Hendrix, W.; Massault, V.; Van de Velde, J. *J. Nucl. Mater.* **1988**, 155-157, 953-956. Using total strain rather than plastic strain, the reduction of life was only a factor of ~2, relatively independent of strain range.

There is a significant effect of radiation on the lifetime at a given plastic strain. The lower the plastic strain, the greater the decrease in lifetime. Under conditions where the crack initiation phase controls the lifetime of the unirradiated material, irradiation will result in much earlier crack formation and much earlier failure.

1.5.4 Irradiation Creep (1)

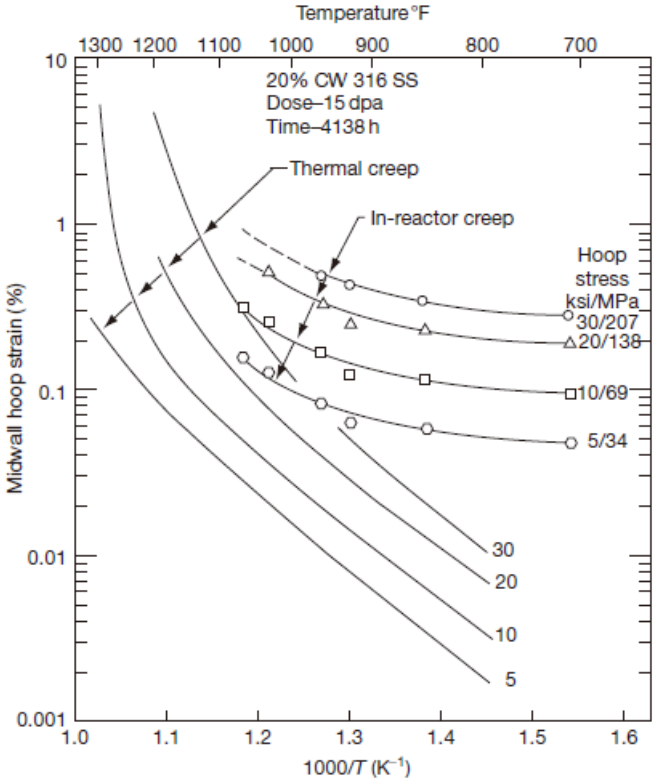

Figure 63 Early comparison of thermal creep and irradiation creep in EBR-II of 20% cold-worked 316 pressurized tubes at 15 dpa and various stress levels. Reproduced from Gilbert, E. R.; Straalsund, J. L.; Wire, G. L. *J. Nucl. Mater.* **1977**, *65*, 277–294.

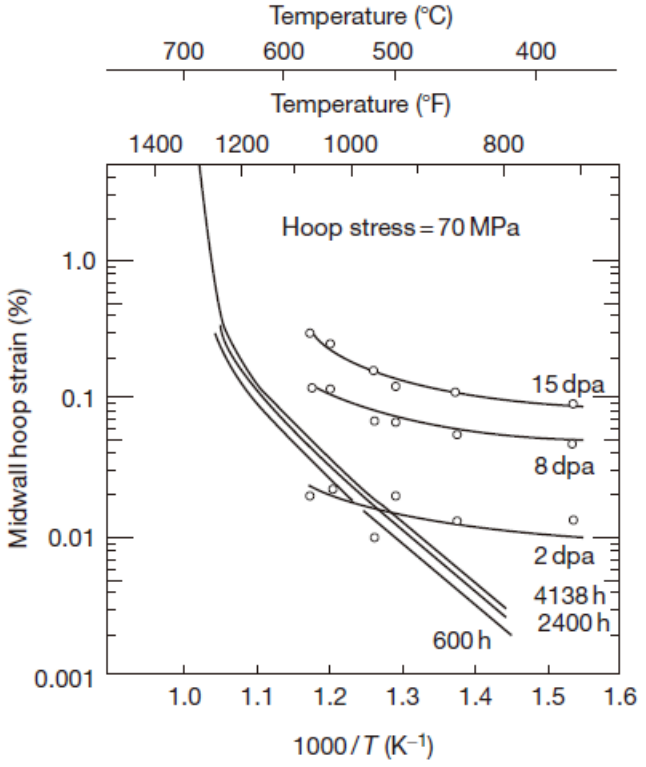

Figure 64 Another comparison of thermal creep and irradiation creep in EBR-II of 20% cold-worked 316 pressurized tubes at various dpa levels at 70 MPa hoop stress. Reproduced from Gilbert, E. R.; Bates, J. F. *J. Nucl. Mater.* **1977**, *65*, 204–209.

While the irradiation creep rate is much higher than that of thermal creep at relatively low temperatures, the difference decreases between the two as the temperature increases, as shown in Figures 63 and 64.

1.5.4 Irradiation Creep (2)

- Irradiation creep mechanism (Still unknown)

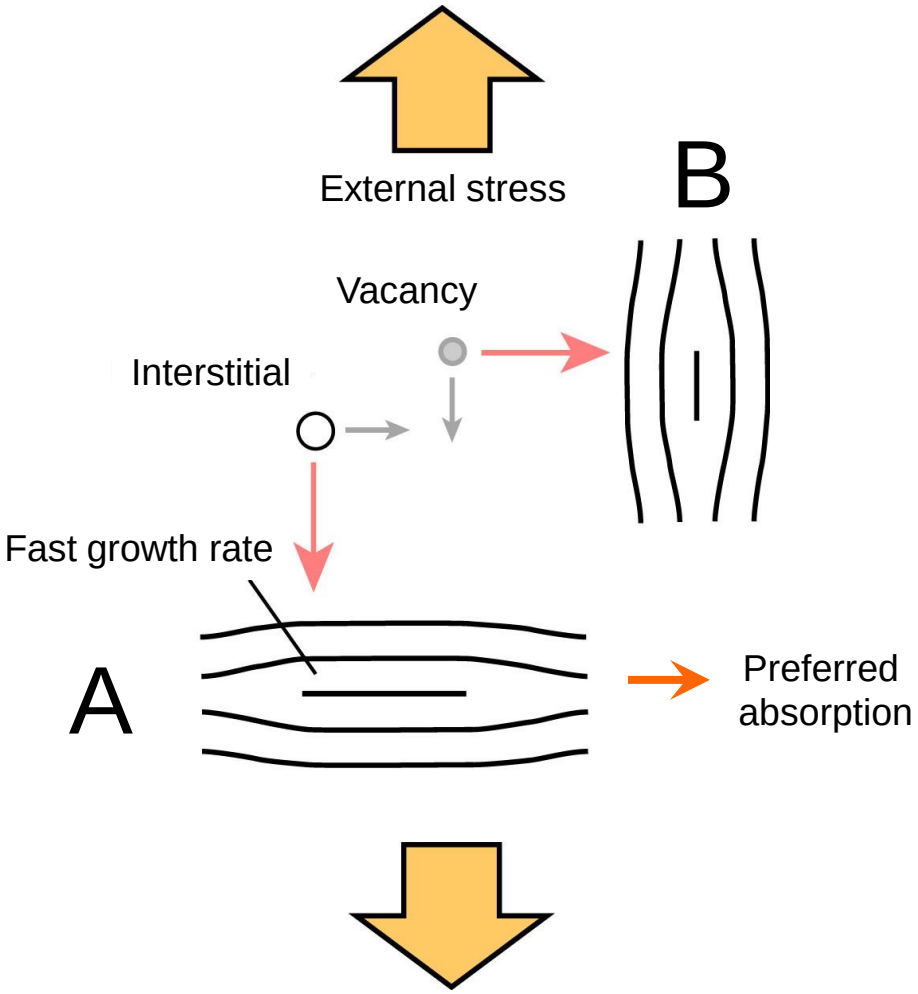

Irradiation increases the number of interstitials and vacancies in the solid, but the effect of this increase is not merely to accelerate thermal creep. In fact, irradiation does not accelerate diffusional creep rates.

Rather, irradiation creep needs to be understood in the context of enhanced defect production, the application of a stress and the developing irradiation microstructure. The formation and growth of loops and voids play important roles in the creep process.

The stress-induced nucleation of dislocation loops and the bowing of dislocation lines by stress-assisted preferential absorption of interstitials can account for the transient portion of the creep behavior, but climb and glide are required to explain steady state creep.

1.5.5 Radiation Induced Segregation (RIS) (1)

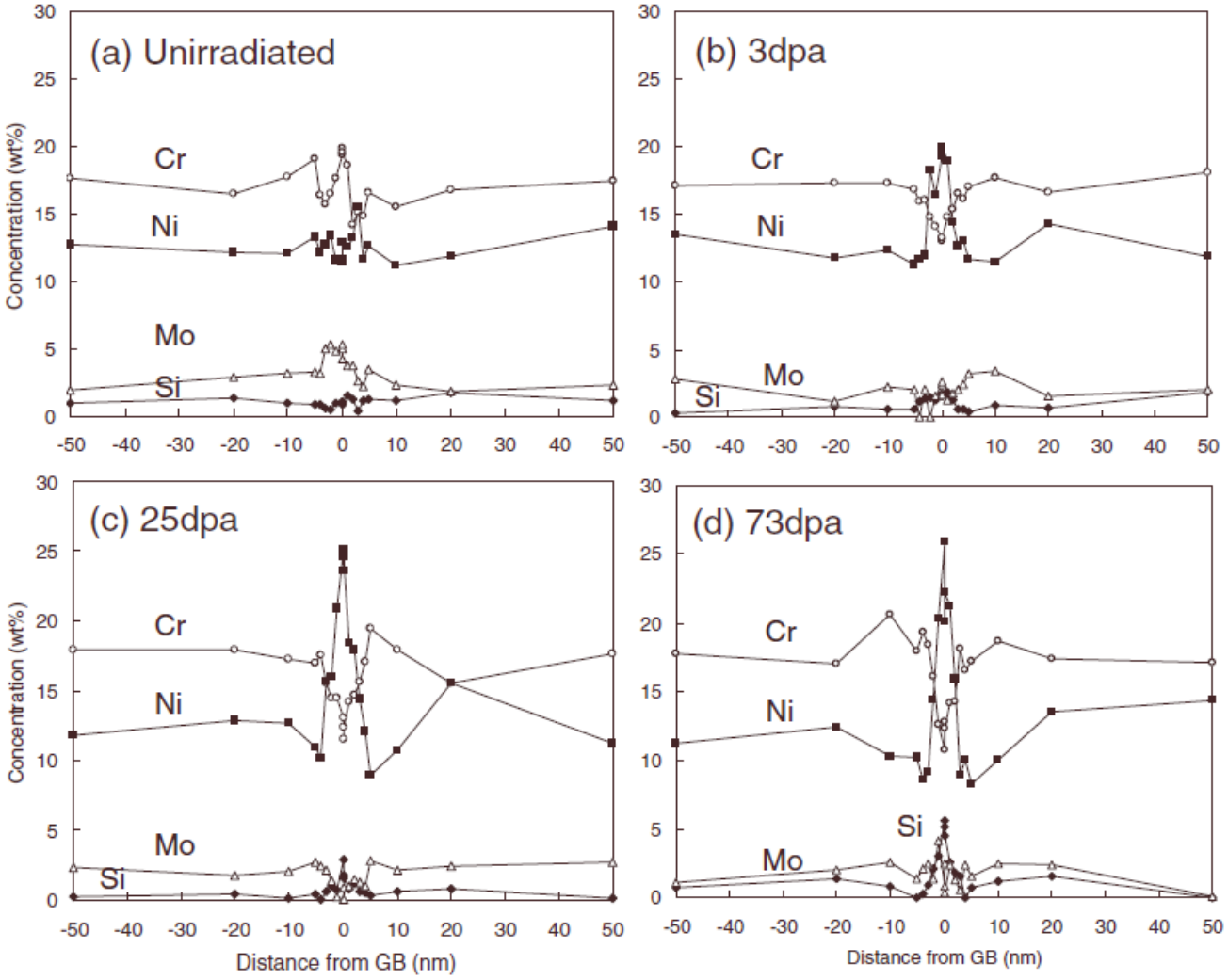

Fig. 7 Typical compositional profiles near grain boundary in PWR-irradiated CW316 stainless steels

1.5.5 Radiation Induced Segregation (RIS) (2)

Cr

Ni

Si

Mo

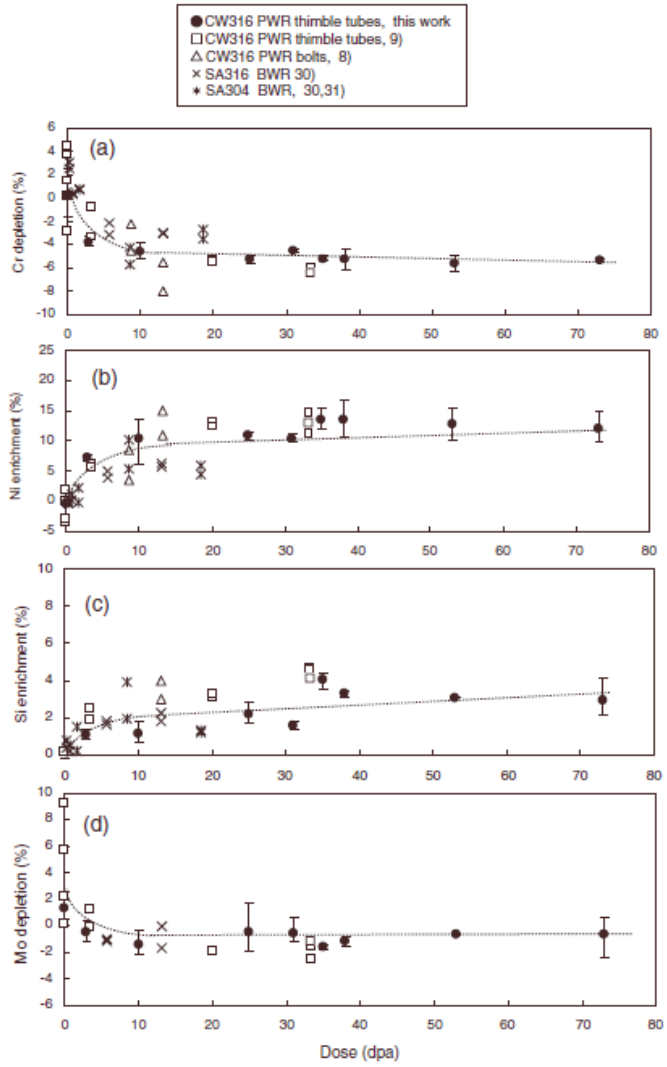

Fig. 13 Depletion of (a) Cr and (d) Mo and enrichment of (b) Ni and (c) Si against dose in LWR-irradiated stainless steels

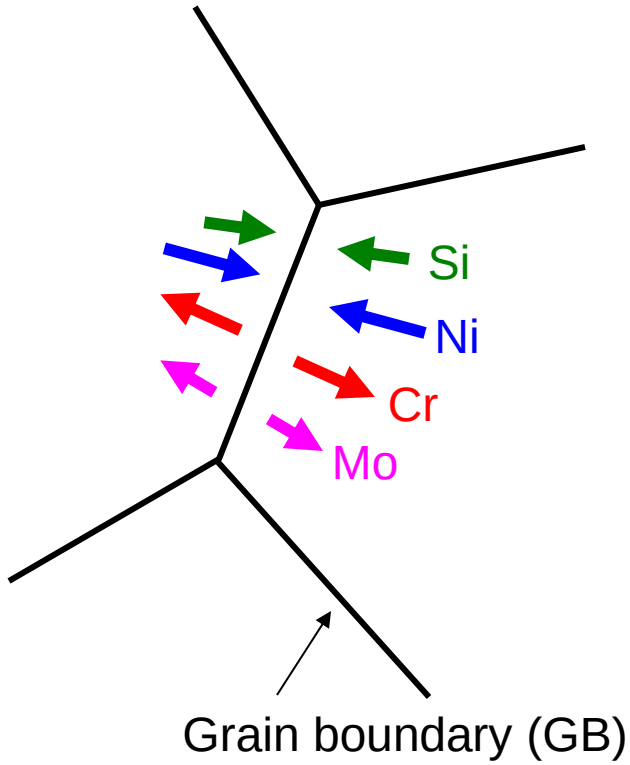

Enrich at GB : Ni, Si

Deplete at GB : Cr, Mo

1.5.6 High Temperature Embrittlement

- He embrittlement
  - He: formed by transmutation reaction
    insoluble to steels

After irradiation,

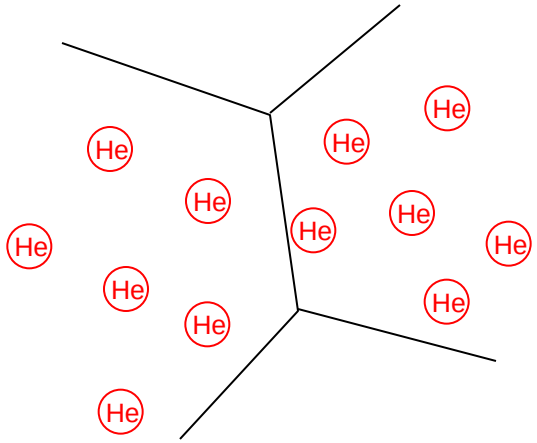

At high temperature such as weld repair,
He atoms aggregate and form bubble especially at GBs.

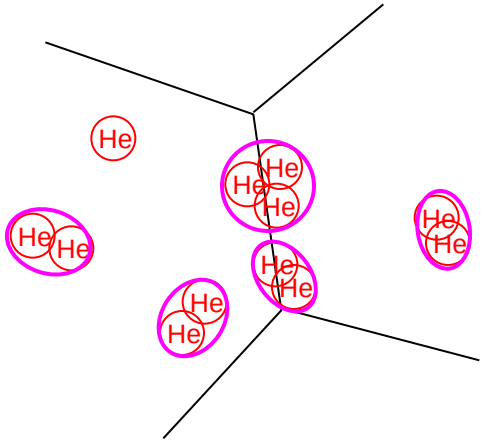

Cracking during welding
Intergranular fracture

Microscopically ductile,
but macroscopically brittle.

1.5.7 Irradiation Embrittlement

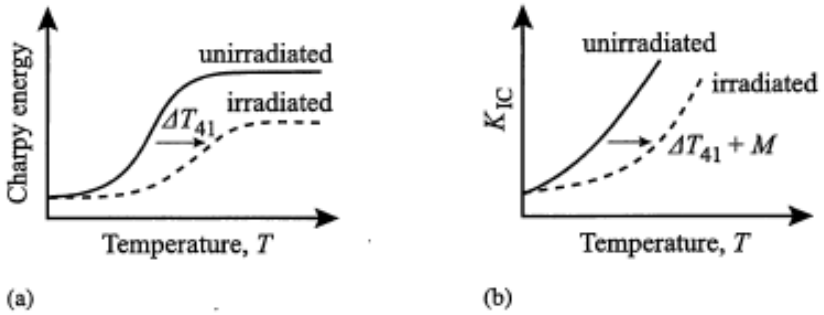

Fig. 13.19. Application of the transition temperature shift in a Charpy test to the fracture toughness test. (a) Charpy impact energy, and (b) fracture toughness (from [24])

Reactor surveillance programs:
Charpy test using V-notch specimens

The temperature shifts in impact energy due to irradiation are all that is available to determine the shift in fracture toughness due to irradiation.

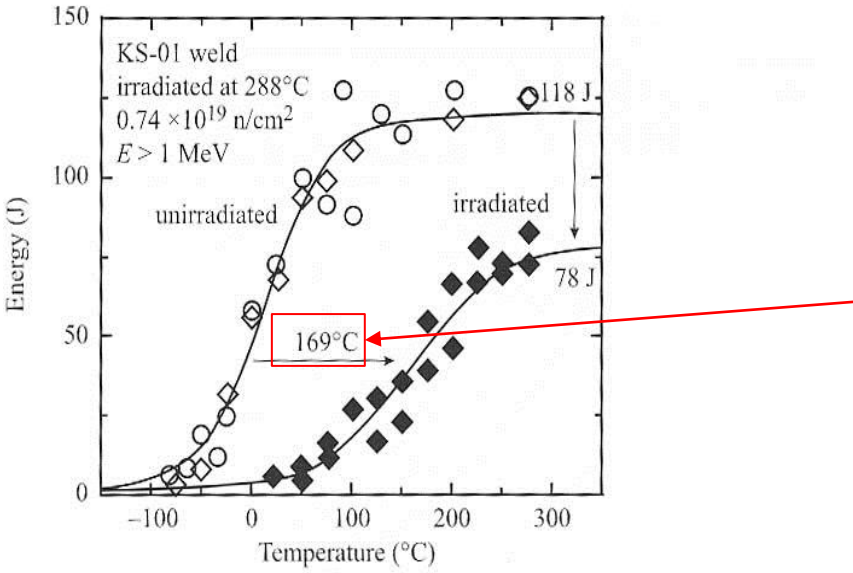

Fig. 13.20. Charpy impact energy vs. test temperature for weld metal in the unirradiated condition and following irradiation to 0.74×10^{19} n/cm^2 ($E > 1.0$ MeV) at 288 °C (from [25])

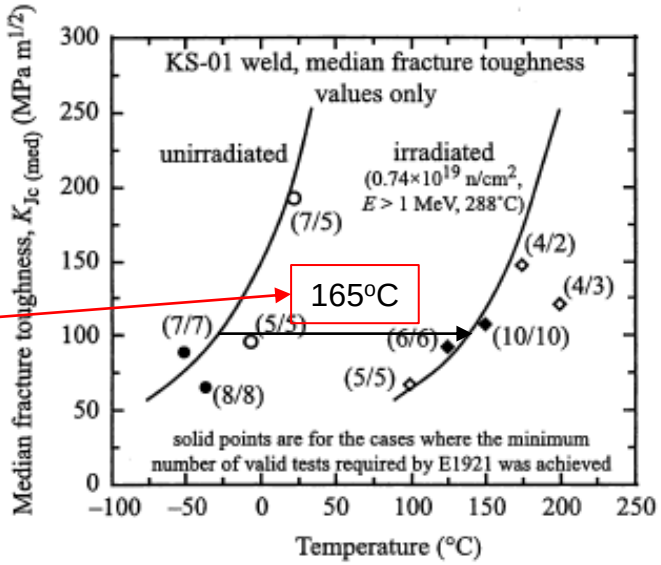

Fig. 13.21. Median fracture toughness of the same weld metal in the unirradiated condition and following irradiation under the same conditions as for the Charpy test in Fig. 13.20 (from [25])

1.5.7 Irradiation Embrittlement (cont.)

Pressurized Thermal Shock

- Injection of ECCS water into RPV during Accident

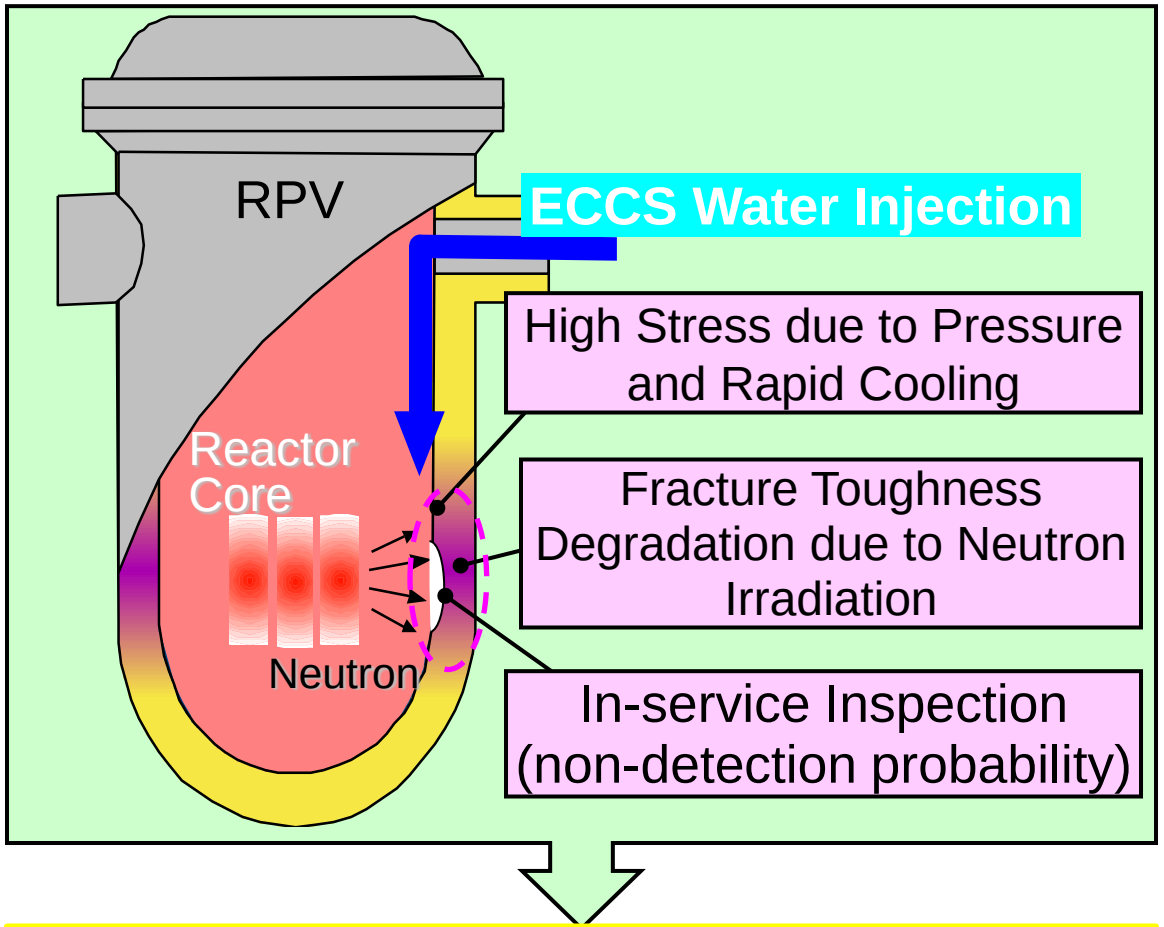

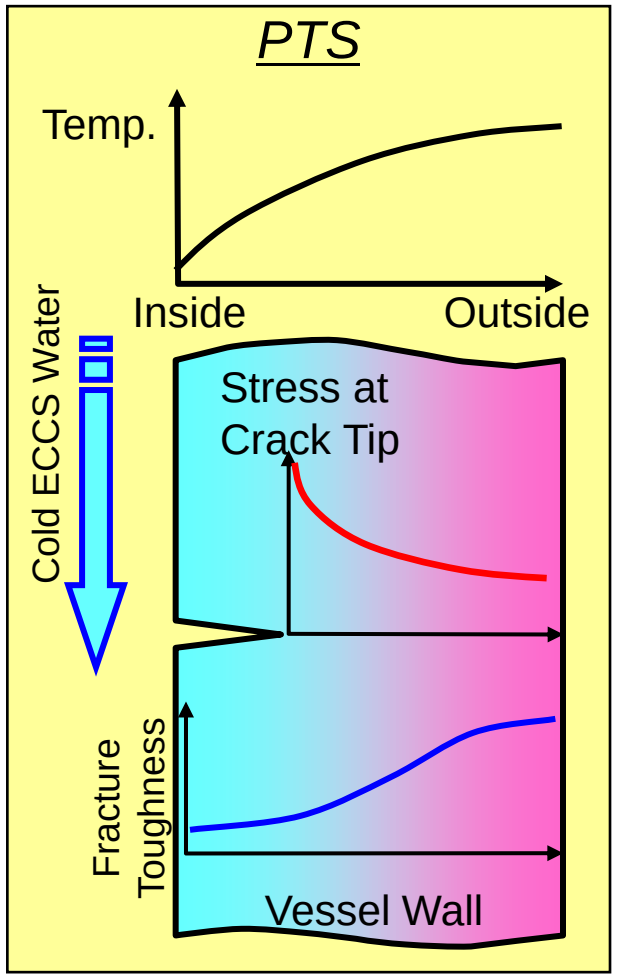

✓Non-ductile fracture must be avoided.

✓Deterministic analysis method is prescribed in Codes/Standards.

1.5.7 Irradiation Embrittlement (cont.)

Structural Integrity Assessment of RPV during PTS

Fracture Toughness (K_{Ic}) > Stress Intensity Factor (K_I)

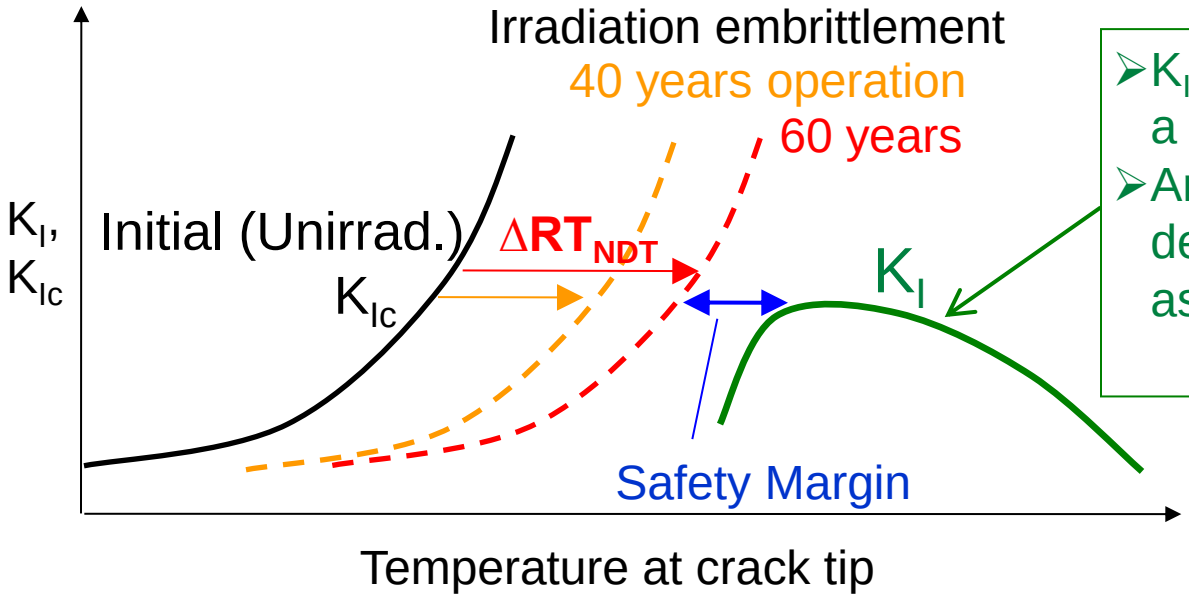

- K_I histories analyzed through a PTS transient
- An axial crack having 10mm depth and 60mm length is assumed in RPV wall. (Japanese procedure)

- Regulations require that the fracture toughness is maintained in an enough level throughout the plant operation.
- In addition to the prediction of fracture toughness decrease, ΔRT_{NDT} have to be monitored by the surveillance tests during plant operation.

2. Material-Related Issues in PWR and BWR

2.1 Introduction

Major Components and degradation mechanism

1. Reactor pressure vessel

   Radiation embrittlement, Primary water stress corrosion cracking (PWSCC), Boric acid corrosion

2. Reactor coolant piping and safe ends

   Low and high cycle thermal fatigue, Thermal embrittlement, High cycle mechanical fatigue

3. Steam generator

   PWSCC, Intergranular stress corrosion cracking (IGSCC), Intergranular attack, Pipe fretting, Denting, Corrosion fatigue, High cycle fatigue, Wastage

4. Reactor coolant pumps

   Thermal embrittlement, boric acid corrosion, high cycle mechanical and thermal fatigue

5. Pressurizer

   Low cycle thermal fatigue, PWSCC

6. Control rod drive mechanism

   Thermal embrittlement, PWSCC, wear, insulation breakdown

7. RPV internals

   Irradiation induced stress corrosion cracking (IASCC), High cycle mechanical fatigue, IGSCC, Stress relaxation, IG cracking

8. Feedwater piping and nozzles

   High and low cycle thermal fatigue, Flow accelerated corrosion (FAC), SCC

Advanced Pressurized Water Reactor (APWR)

- Larger reactor pressure vessel
  - Longer distance from core, reduction of neutron fluence at RPV (~1/3)
- Neutron reflector
  - Thick ring block structure : nuclear heating, high displacement damage

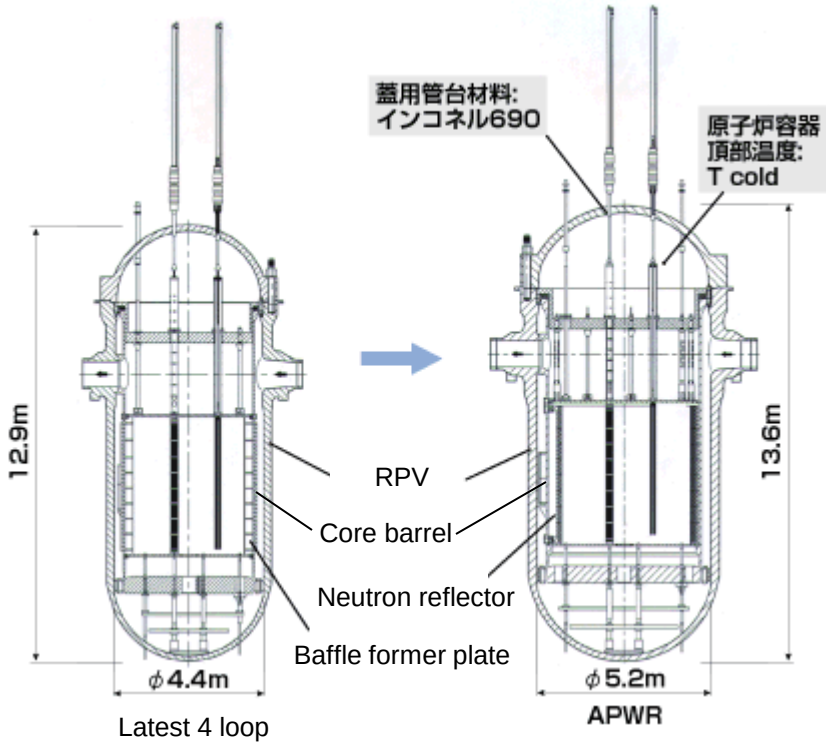

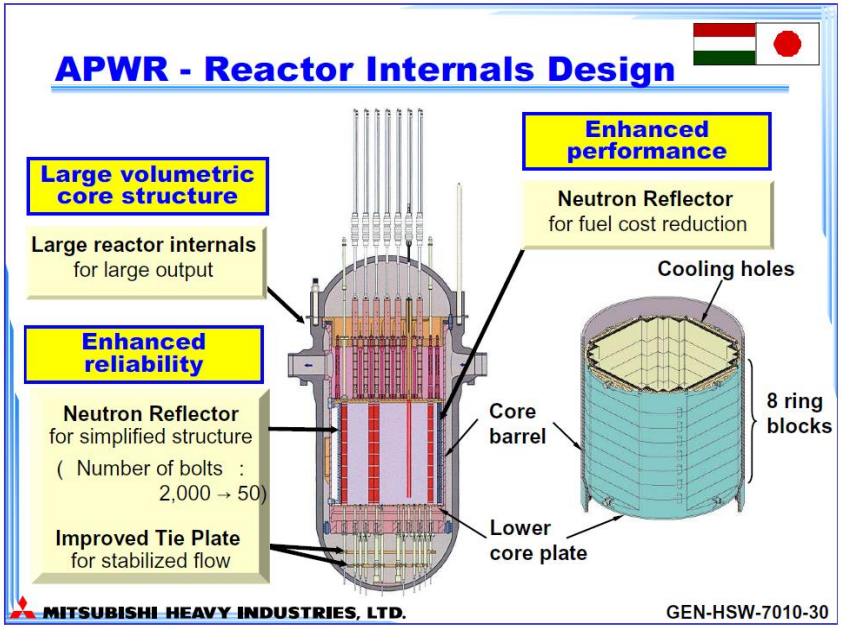

2.2 Design and Materials of PWR Components

2.2.1 Reactor Pressure Vessel

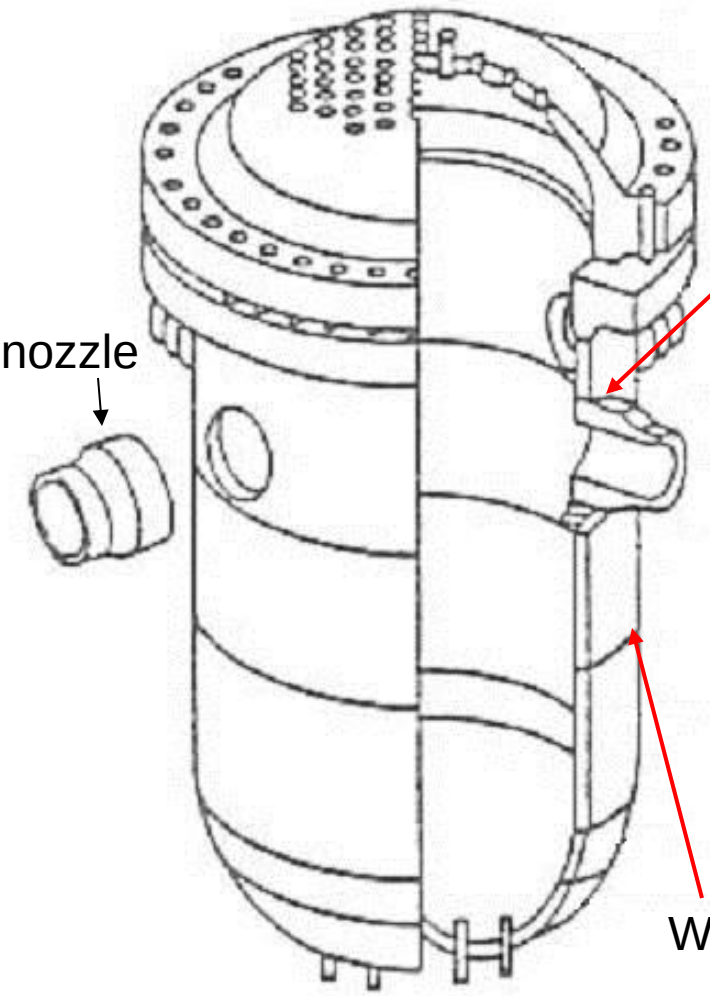

Material : SA508 Cl.2
Thickness : 200mm
Cladding : Type 308 or 309

Weld : SMAW

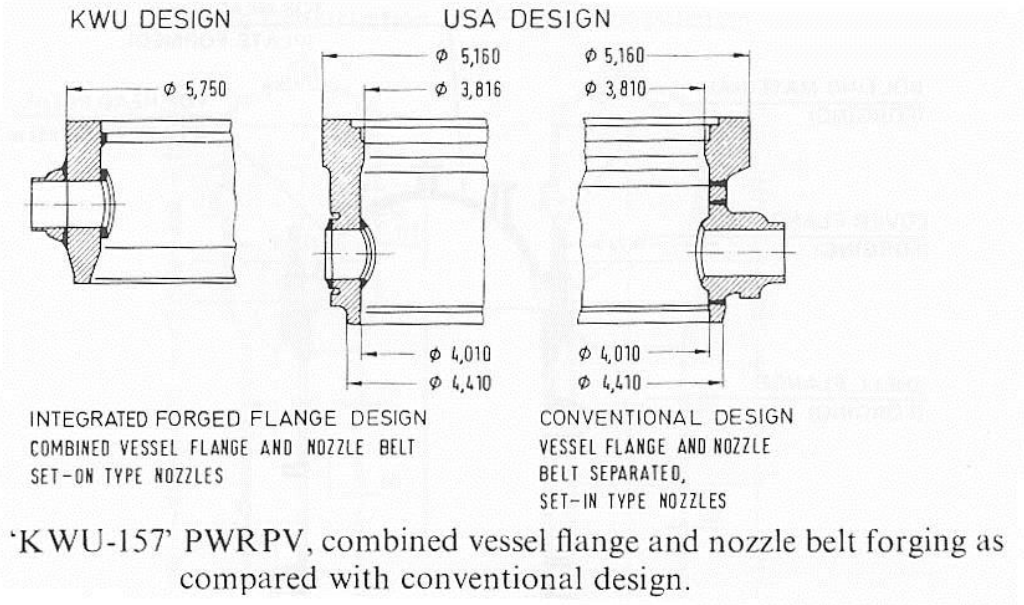

'KWU-157' PWRPV, combined vessel flange and nozzle belt forging as compared with conventional design.

Weld line: automatic SAW

PWHT: 610ºC for 20 h followed by a furnace cooling
to reduce residual stress and
to temper any martensite in the HAZ

2.2.2 Neutron Reflector

- Baffles

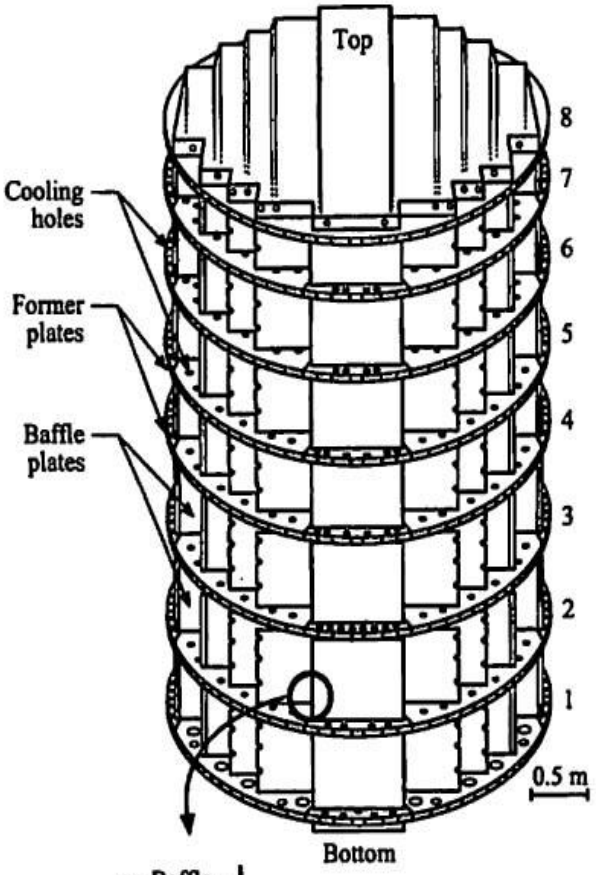

Baffle plates : Type 304 SS
Former plates : Type 304 SS

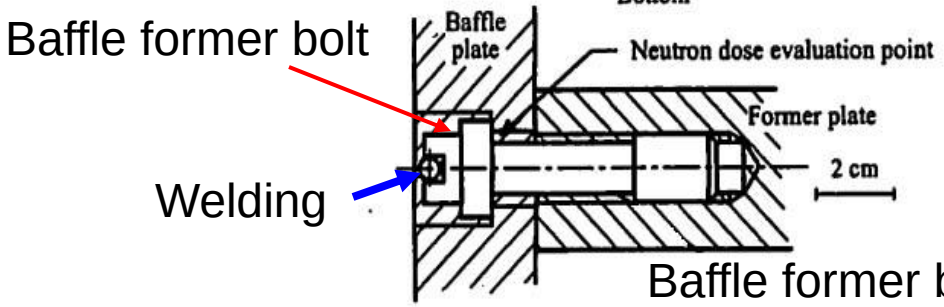

Baffle former bolts : 20% cold worked type 316 SS

2.2.3 Control Rod and Guide Tube Assemblies

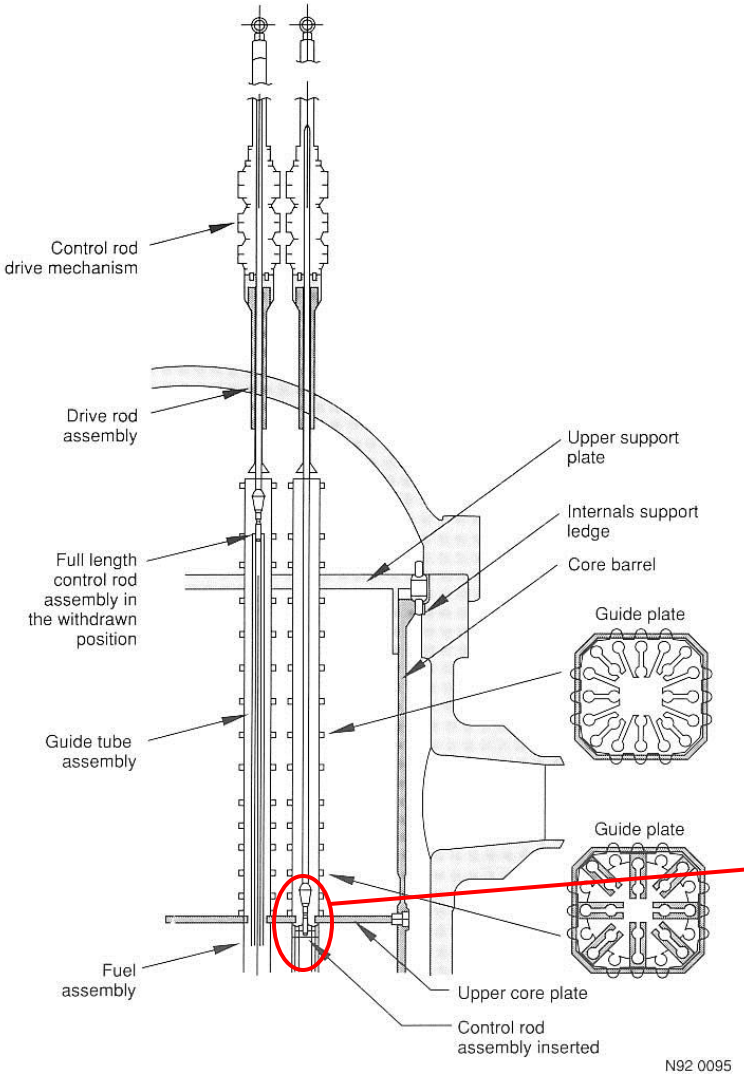

Figure 13-2. Elevation and plan cross-section views of two Westinghouse full-length control rod and guide tube assemblies, one fully withdrawn and one inserted.

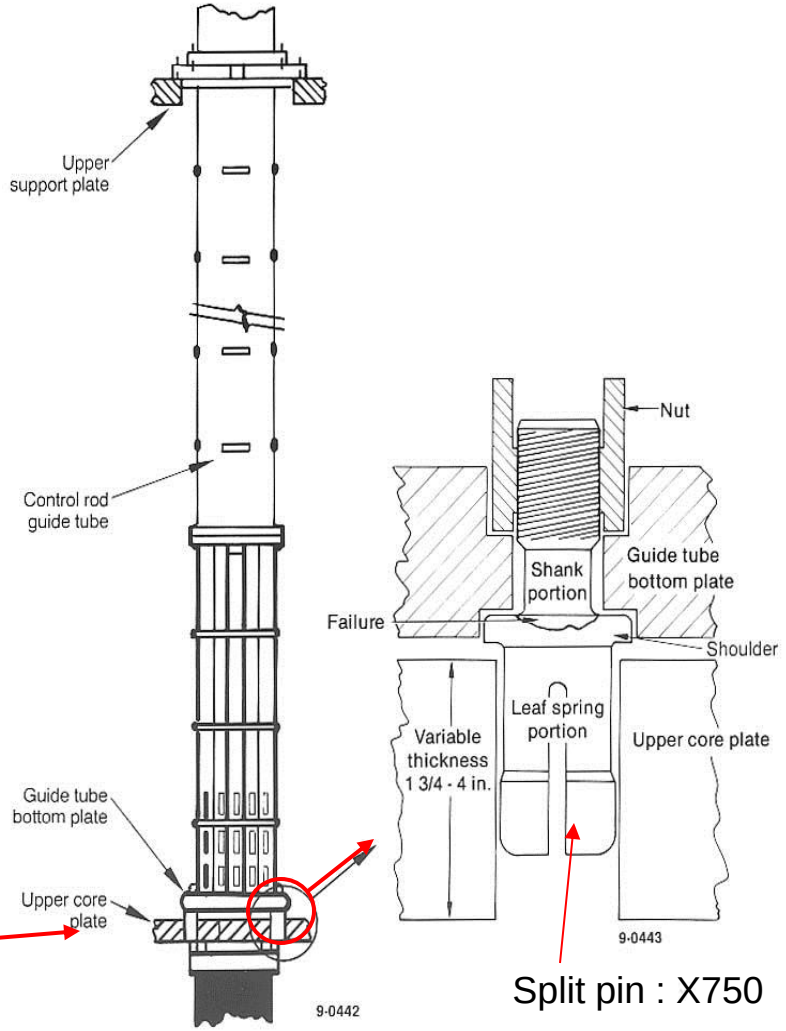

Figure 13-3. Westinghouse control rod guide tube assembly and split pin. A typical failure location in a split pin is also shown (Urquhart 1986, Mager 1983). Copyright American Nuclear Society; reprinted with permission.

2.2.4 Water Coolant Piping (1)

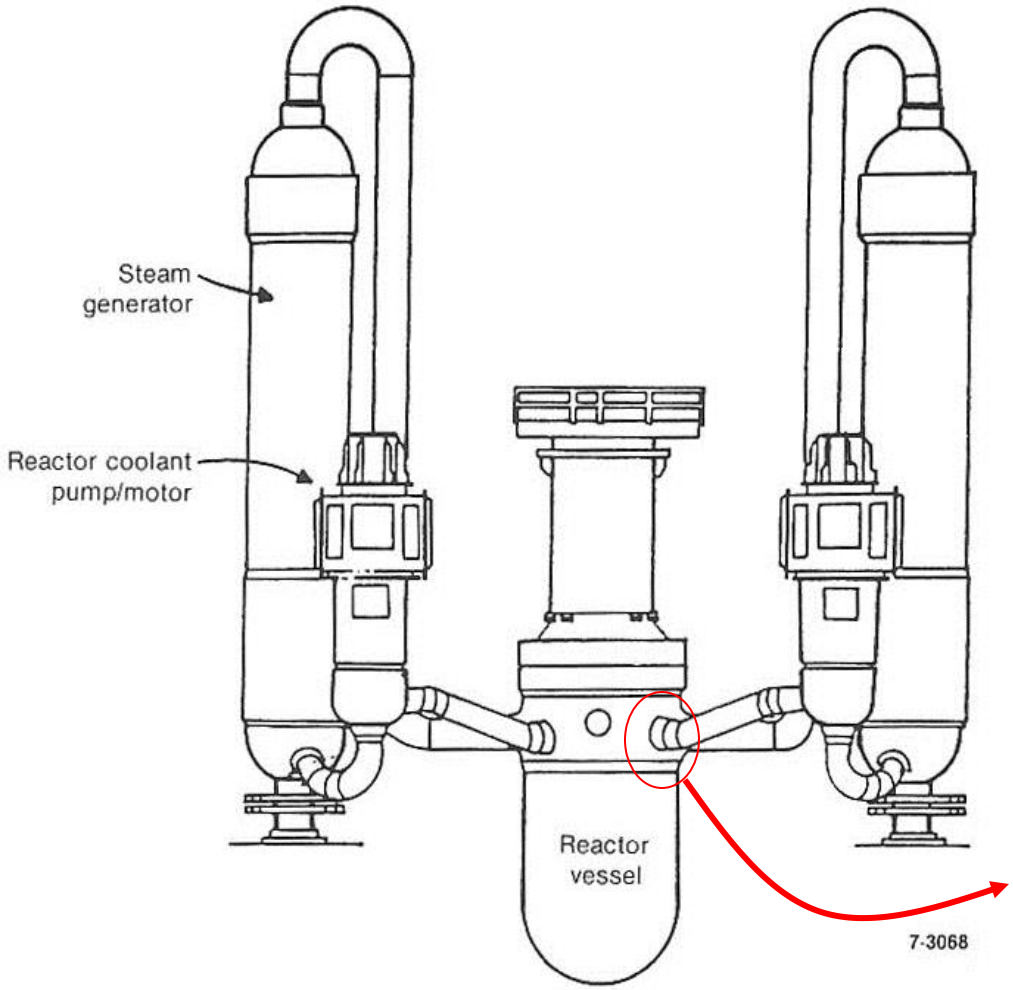

Primary

Piping : Type 316 SS, CF-8M, CF-8A
Fitting : Wrought and cast SS
(CF-8M, CF-8A)
Safe ends : Type 316 SS

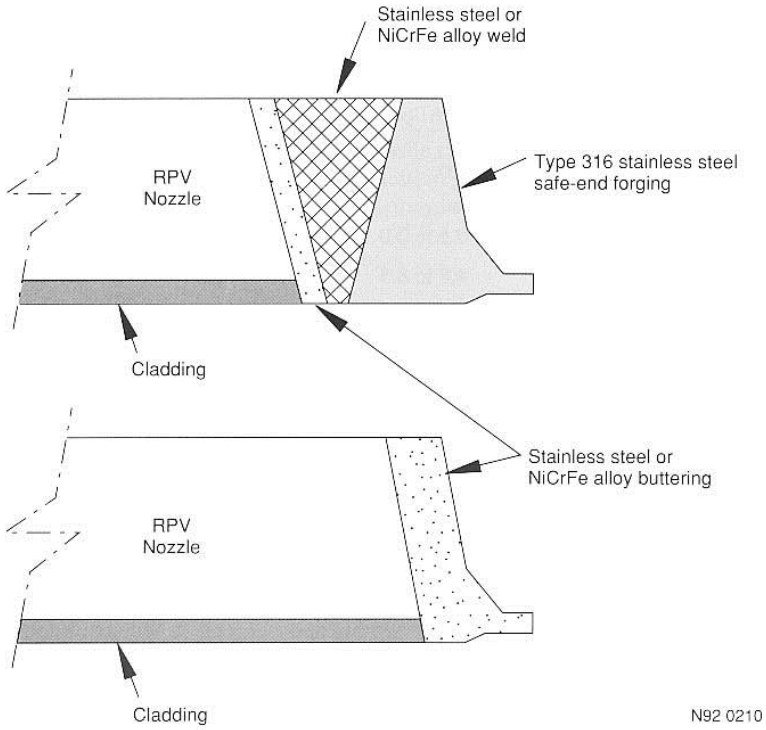

Figure 5-1. Schematic of a Babcock and Wilcox PWR reactor coolant system.

2.2.4 Water Coolant Piping (2)

- Secondary

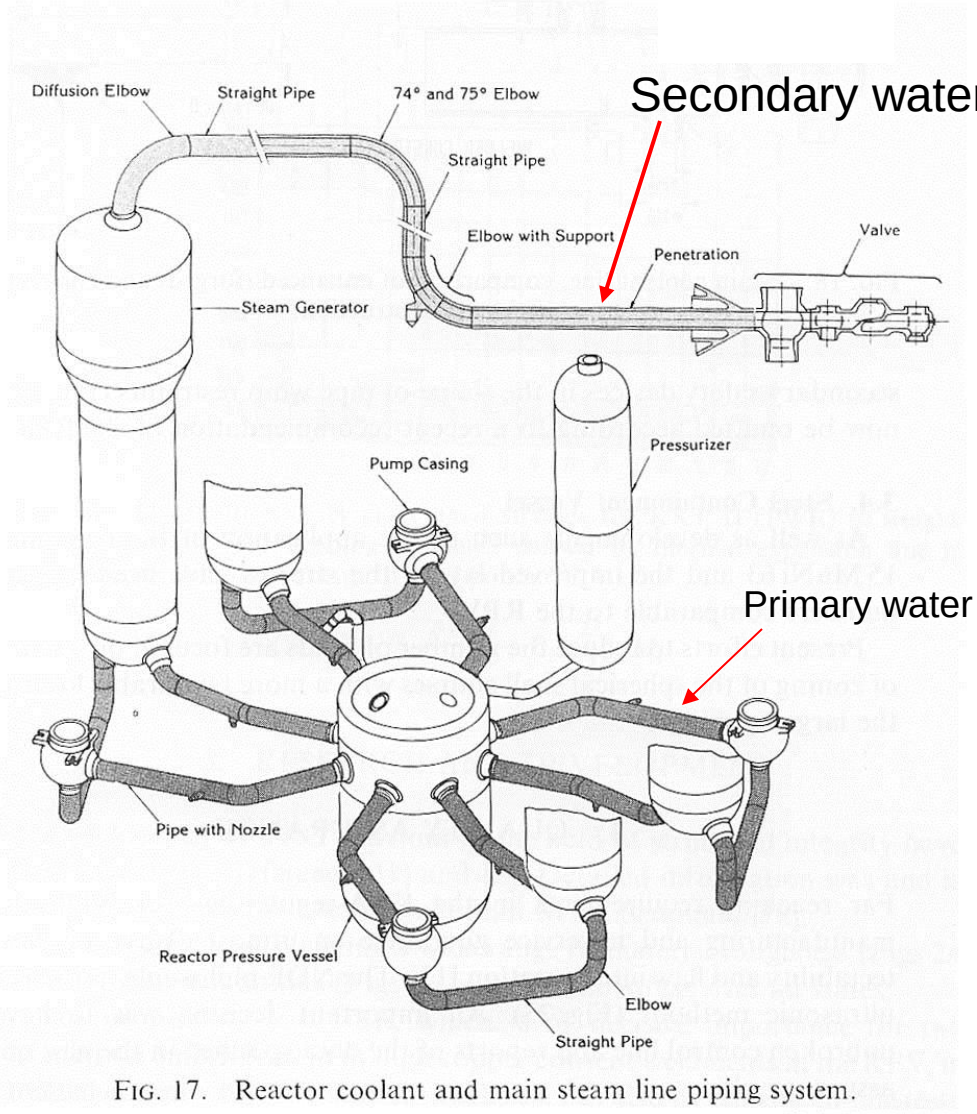

FIG. 17. Reactor coolant and main steam line piping system.

Secondary water coolant piping

Piping : SA106B
Elbow : A234WPB

Primary water coolant piping

2.2.5 Steam Generator

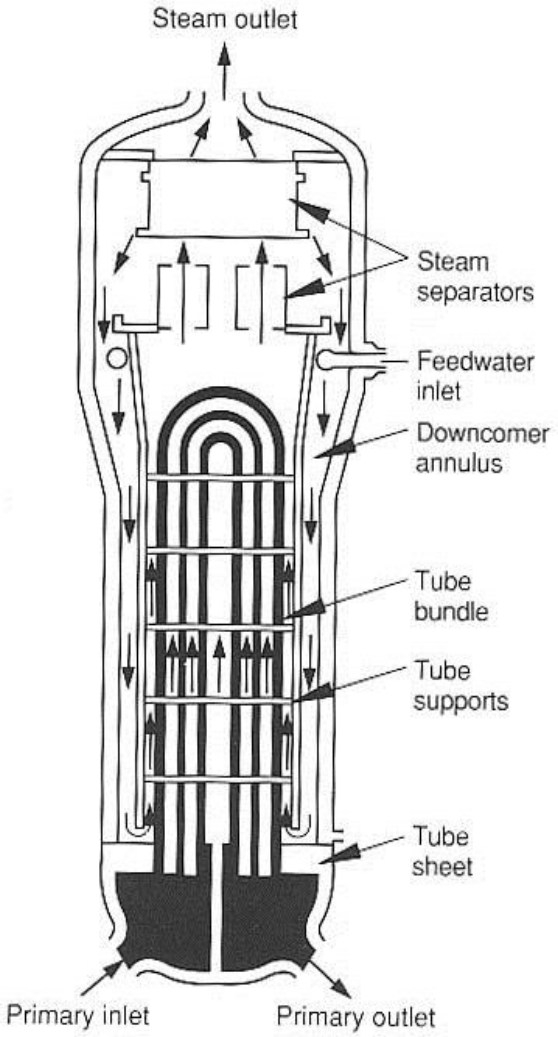

Recirculating steam generator N93 0022

Pressure vessel : SA533B Cl.2
Tube sheet : SA508 Cl.3
Clad : Type 308 or 309
Tube : Alloy 600 TT ➡ Alloy 690 TT

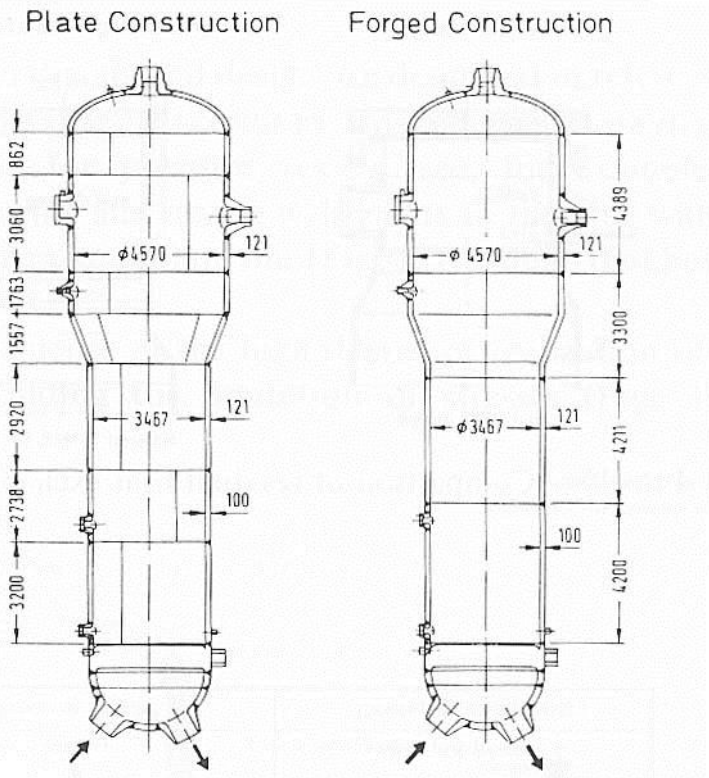

Number of Welds

Circumferential Welds	9	Circumferential Welds	7
Longitudinal Welds	10	Longitudinal Welds	-
Nozzle Welds	15	Nozzle Welds	14

Plate and forged design of a steam generator.

2.2.6 Pressurizer

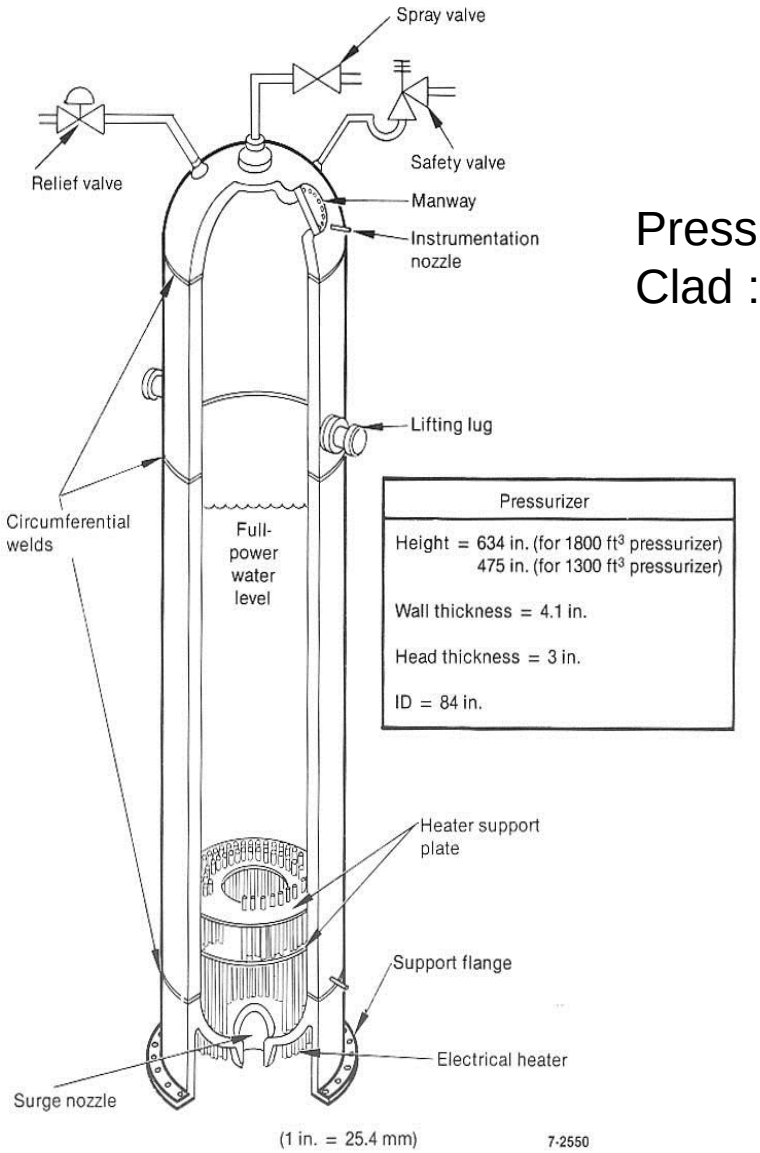

Figure 11-5. Westinghouse pressurizer (Diablo Canyon 1 and 2 FSARs).

Pressure vessel : Low alloy steel
Clad : Type 308, 309

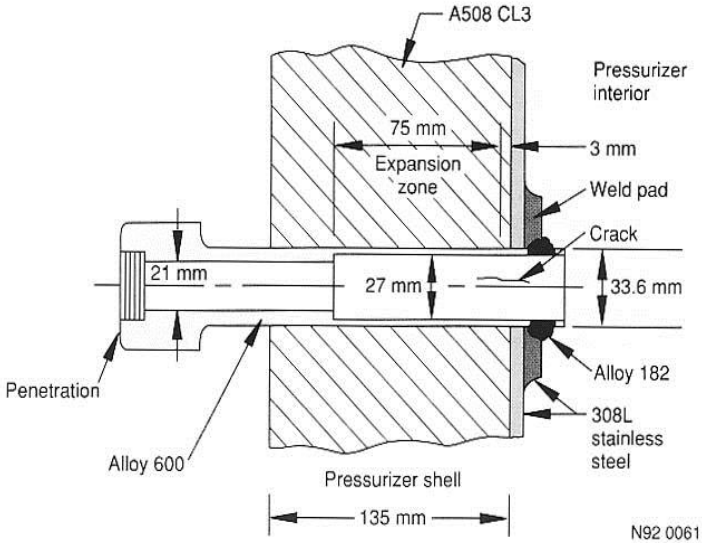

Figure 11-14. PWSCC in Électricité de France instrument penetrations (O'Neill and Hall 1990). Copyright Electric Power Research Institute; reprinted with permission (modified).

2.3 Corrosion-Related Issues in PWR

2.3.1 Introduction (1)

- Material degradation events

Sweden (PWR: 3 plants, BWR: 11 plants)

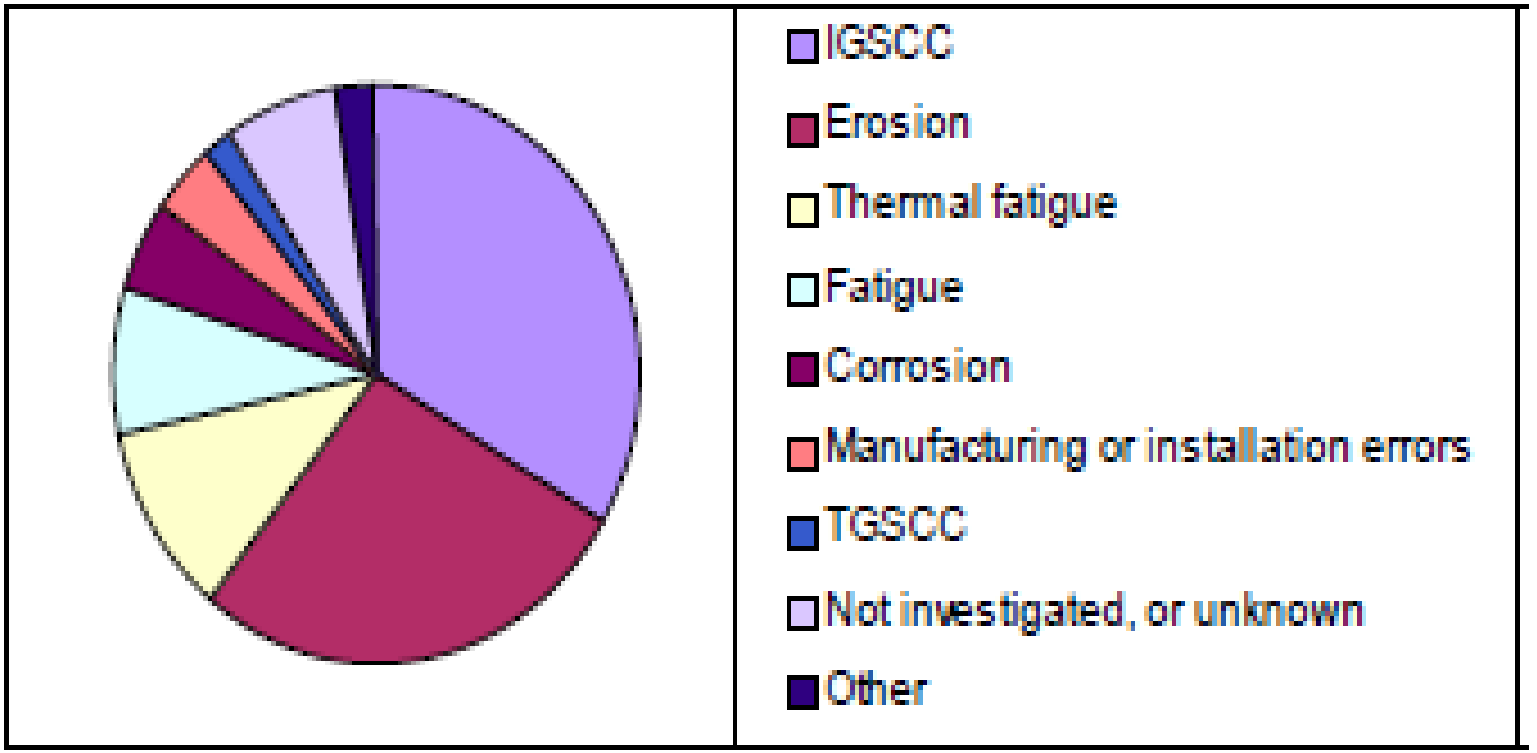

K. Gott, Proc. 10th Int. Conf. Environmental Degradation of Materials in Nuclear Power System –Water Reactors-, NACE, 2002.

2.3.1 Introduction (2)

Primary water stress corrosion cracking (PWSCC) events in U.S. PWRs during 1999 – 2005

Nozzles and pipes

Cracks in as-weld deposit

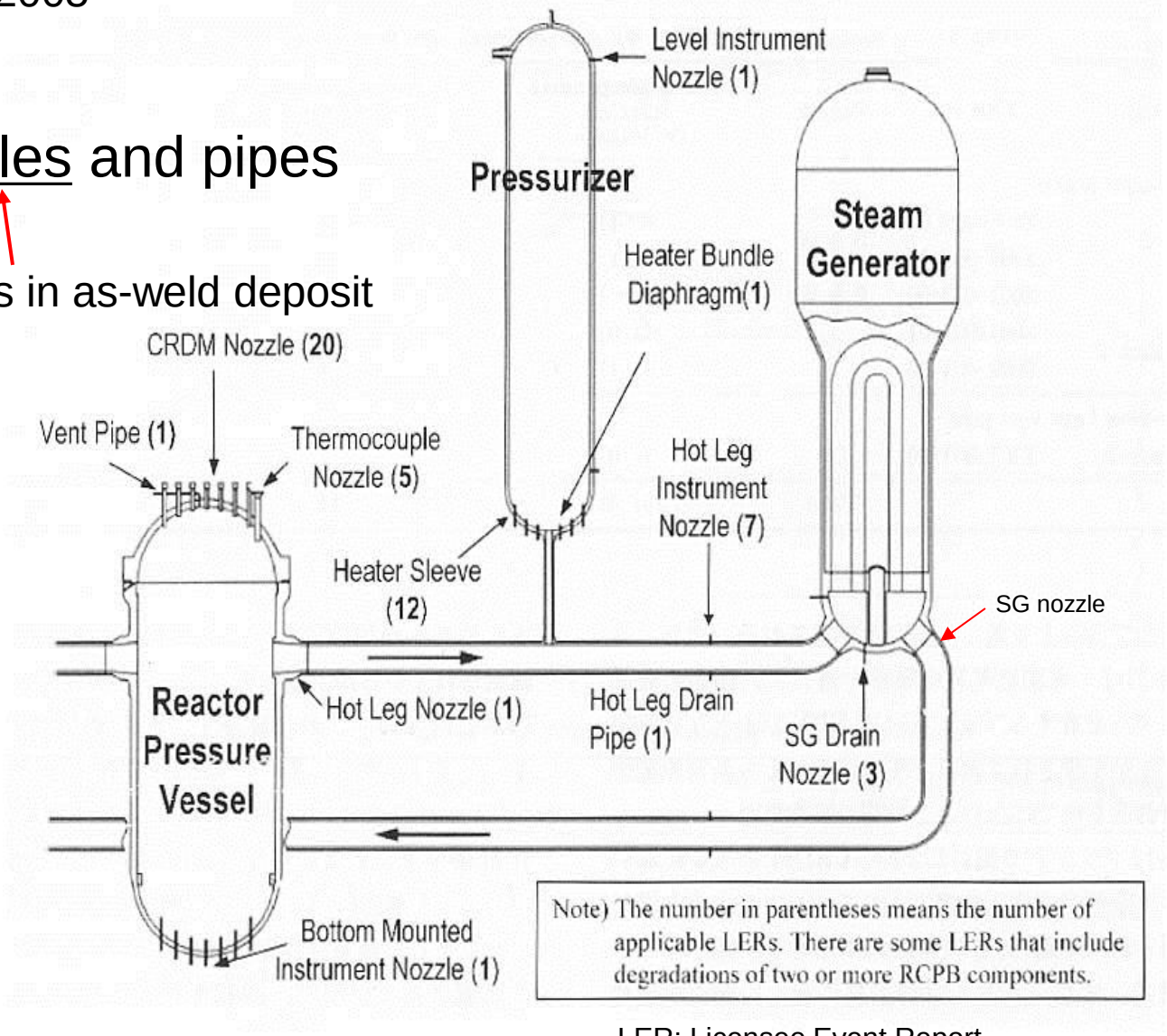

LER: Licensee Event Report

2.3.1 Introduction (3)

SG tubes

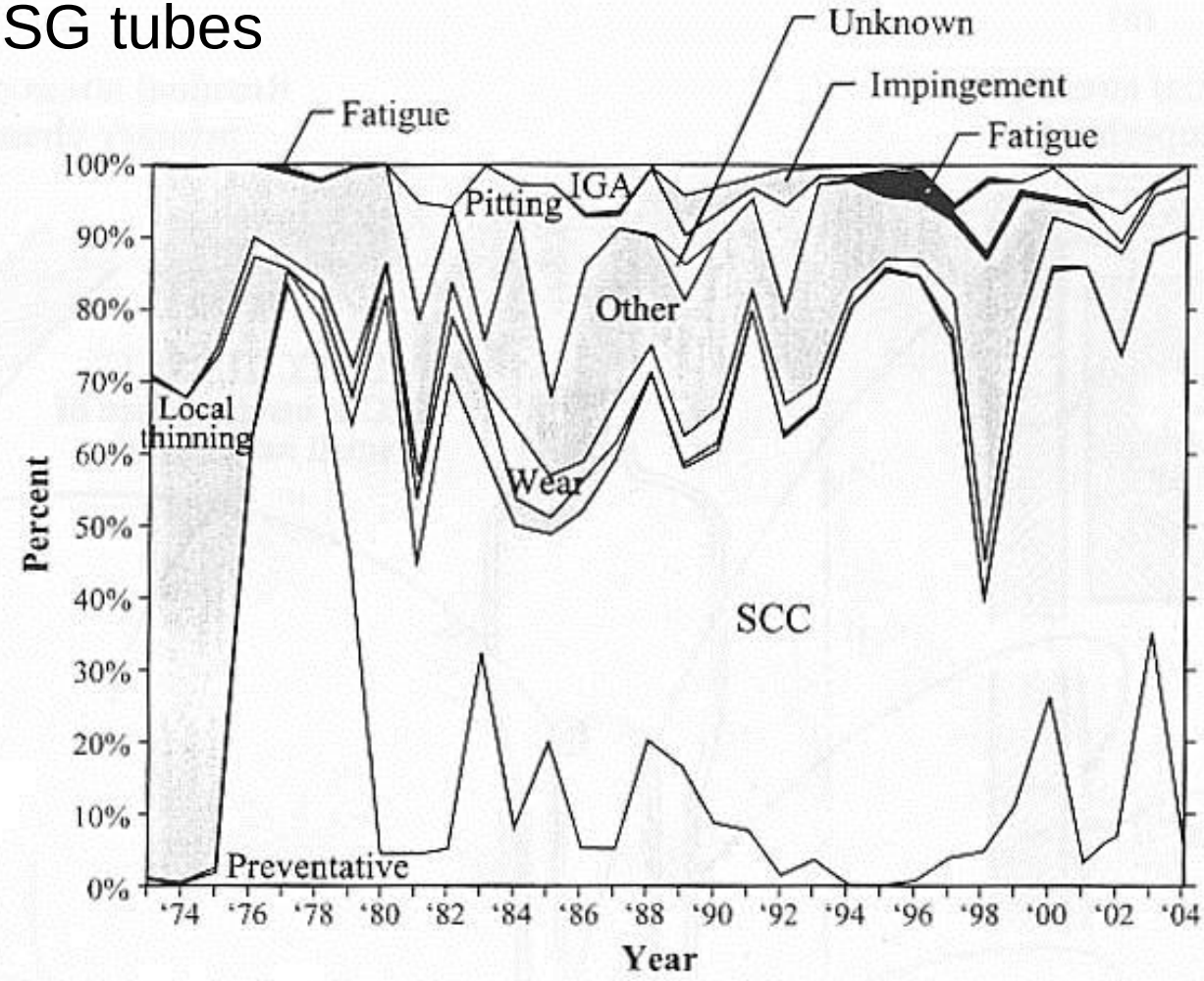

Evolution of modes of damage in PWR steam generator tubes with Alloy 600MA and drilled hole TSPs. Courtesy of EPRI

Primary water side
- PWSCC

Secondary water side
- Wastage
- Pitting
- IGSCC
- intergranular attack (IGA)

2.3.2 Water Chemistry

Structural materials of PWR/BWR are exposed to the high-temperature cooling water. In the corrosive environments, chemical interactions between the materials and water caused various kind of material degradation and consequent problems on the components. Therefore, a quality of cooling water or water chemistry is one of the most important issue for the operation of NPPs. In this section, an outlook of water chemistry mainly in PWR plant is given.

All viewgraphs are kindly provided by Dr. S. Uchida.

2.3.2 Water Chemistry

Major roles and adverse effects of cooling water

PWR primary cooling water

major roles: energy transporting medium
neutron moderating medium

adverse effects

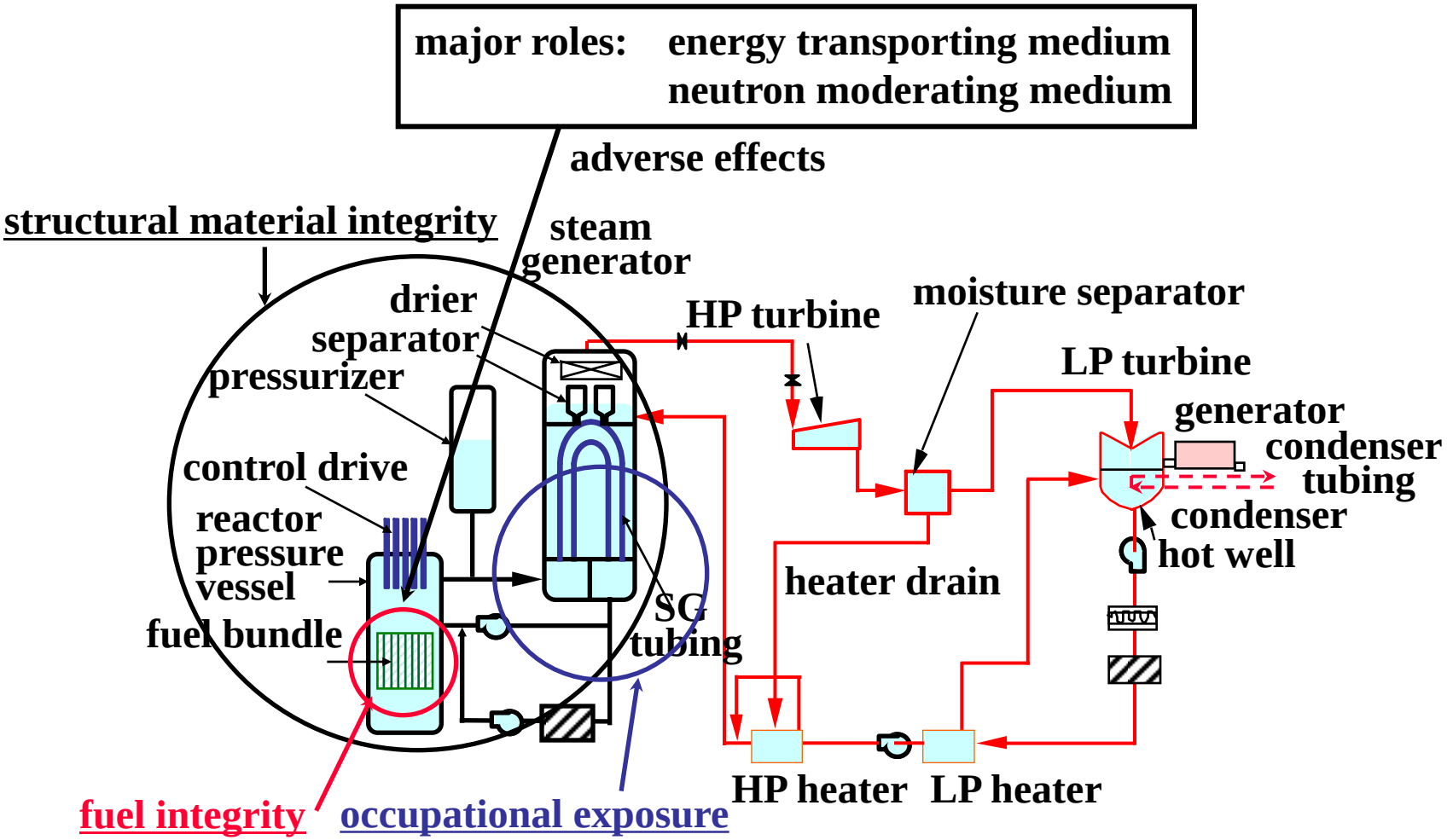

The under line shows items concerning adverse effects

2.3.2 Water Chemistry

Comparison of cooling system of BWRs and PWRs

item	BWR	PWR
reactivity control	control rod + void (core flow rate)	control rod + chemical shim (B)
corrosion control pH	neutral [pH_{RT}: 5.6-8.6]	alkaline [pH_{RT}>9]
corrosion control [O_2]	200 ppb [HWC : <10 ppb]	<1 ppb
corrosion control [H_2]	20 ppb [HWC : 50 ppb]	2 ppm
turbine dose rate	during operation ^{16}N during plant shutdown ^{60}Co,^{51}Cr	dose rate free

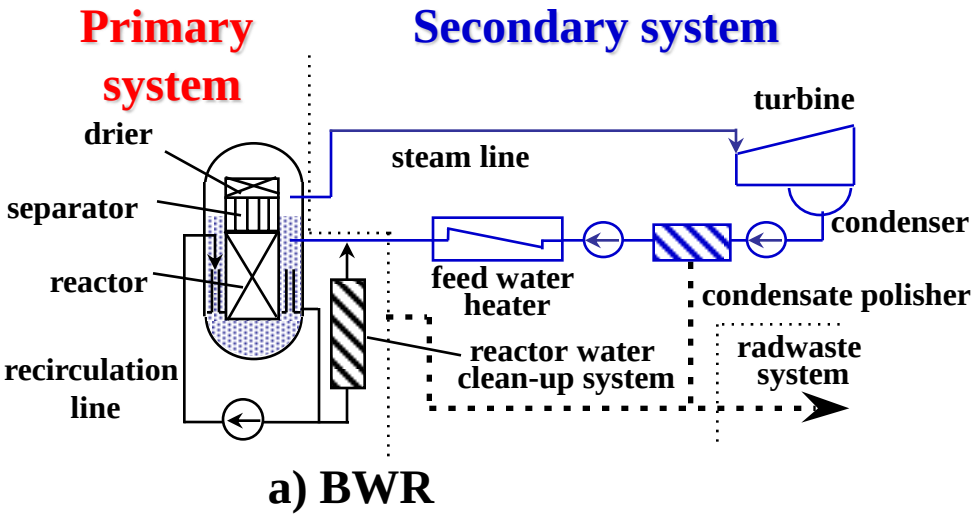

a) BWR

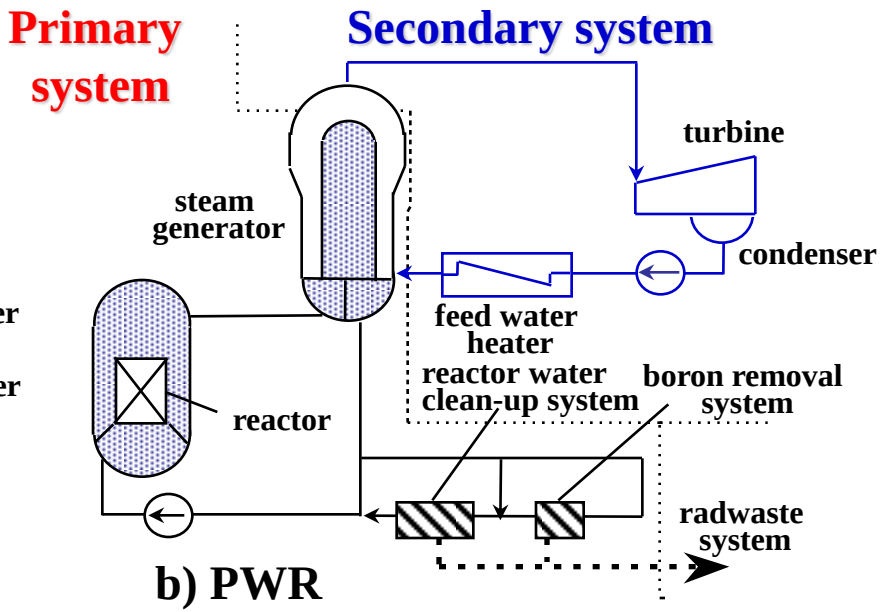

b) PWR

2.3.2 Water Chemistry

Material atlas of PWR primary and secondary cooling systems

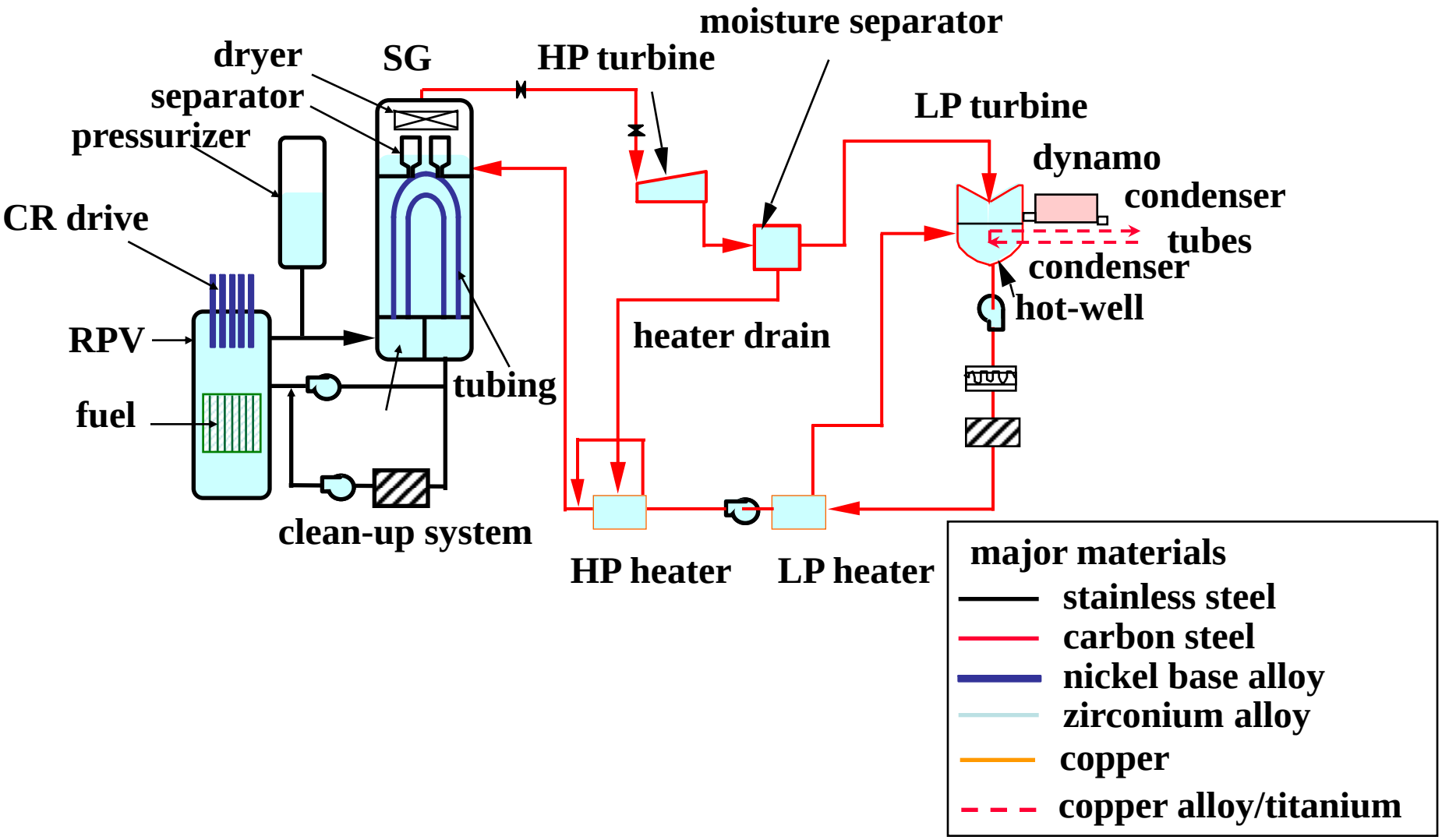

2.3.2 Water Chemistry

Material atlas of BWR primary cooling system

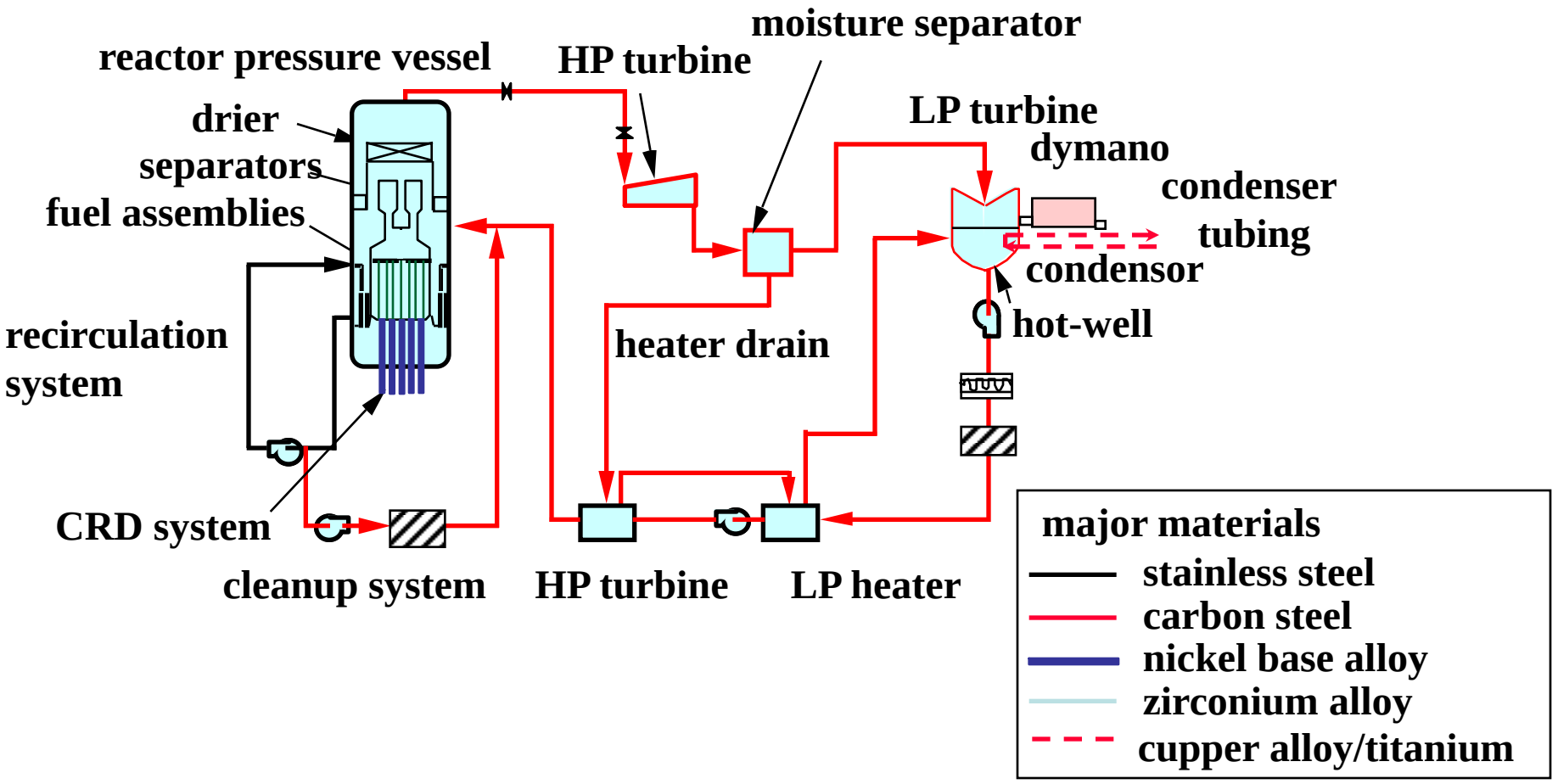

2.3.2 Water Chemistry

Major interactions between cooling water and structural materials

PWR (PWR primary)	PWR (secondary)	BWR
SCC of stainless steel	SCC of SG tubing	SCC
SCC of nickel alloy	wall thinning	erosion-corrosion
（PWSCC）	denting	
Radioactive corrosion	IGA	Radioactive corrosion
product accumulation	pitting	product accumulation
(dose rate buildup)	erosion-corrosion	(dose rate buildup)

2.3.2 Water Chemistry

Major achievements for water chemistry improvement

BWRs

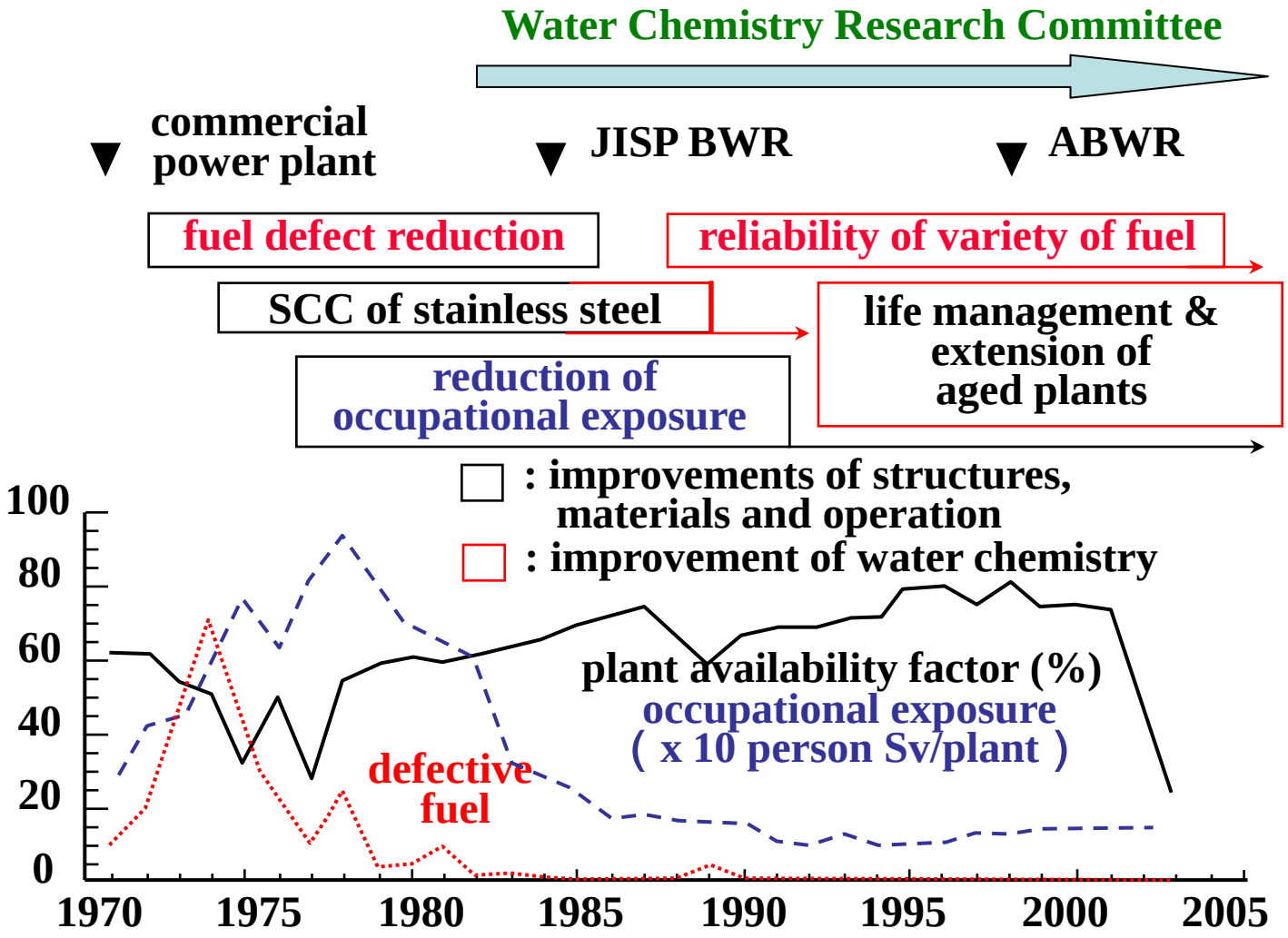

2.3.2 Water Chemistry

Major achievements for water chemistry improvement

PWRs

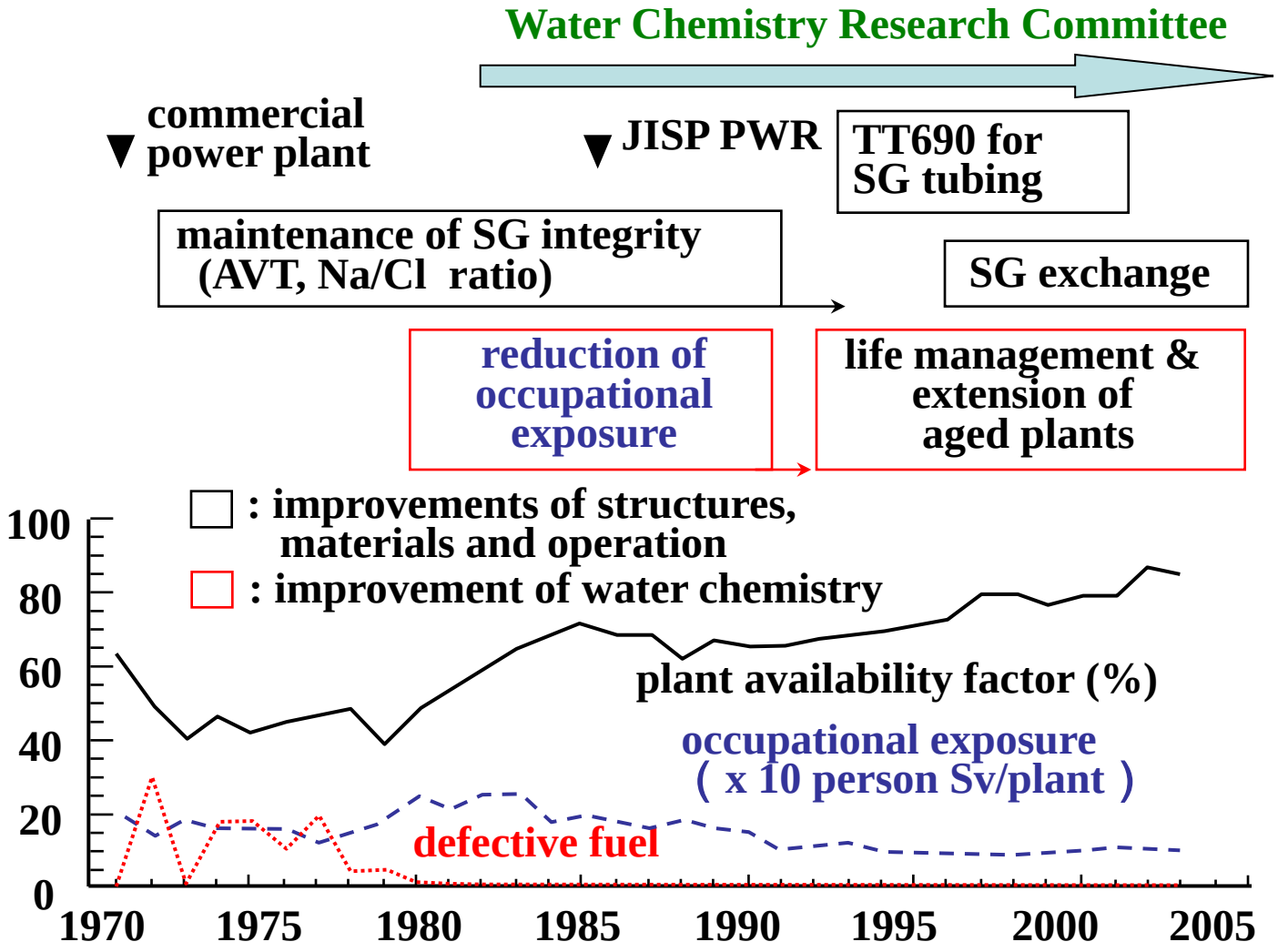

2.3.2 Water Chemistry

Locations for in-line monitoring and sampling in PWR

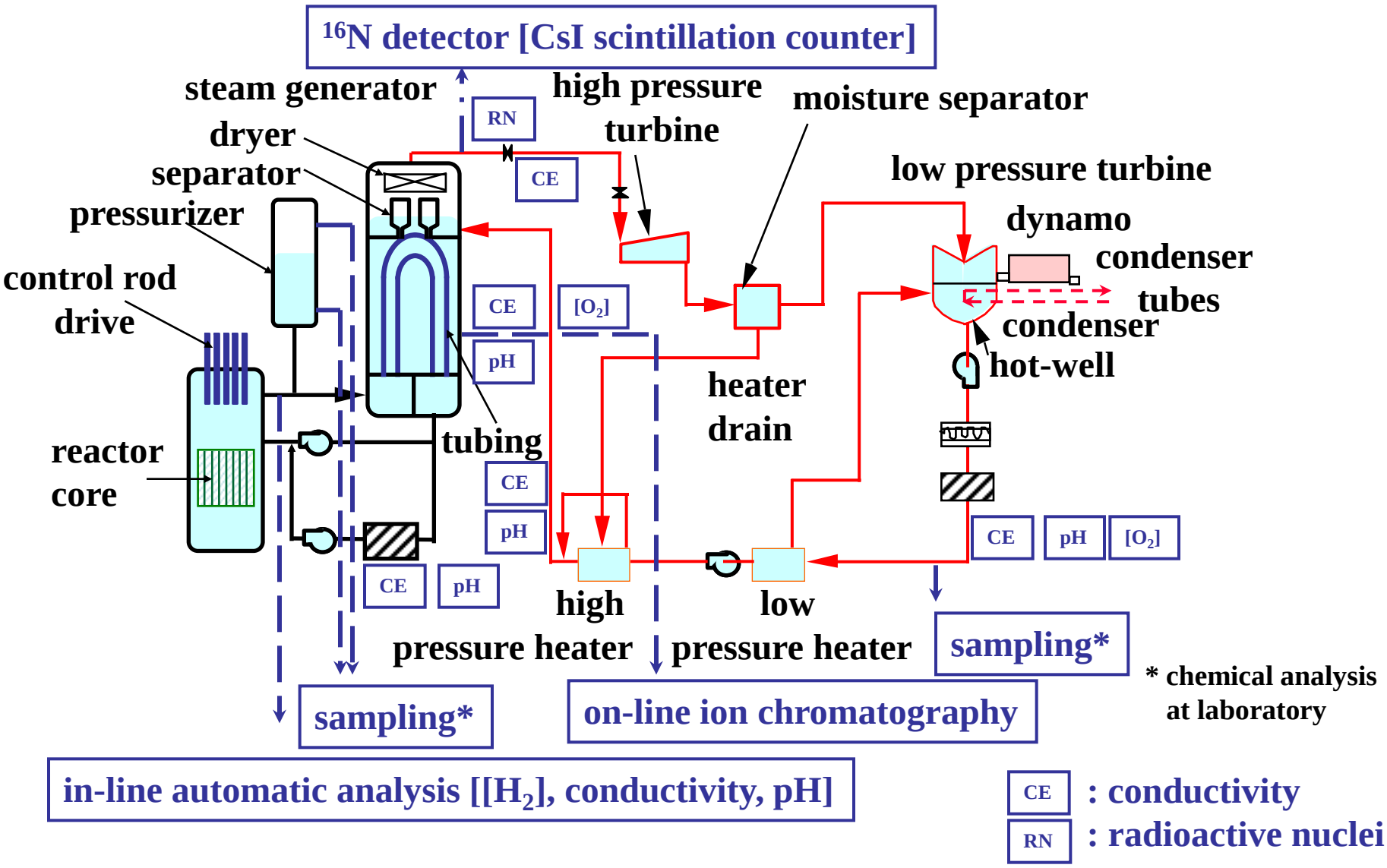

H. Takiguchi, H. Takamatsu, S. Uchida, K. Ishigure, M. Nakagami, M. Matsui, J. Nucl. Sci. Technol., 41, 214 (2004)

2.3.2 Water Chemistry

Optimal Water Chemistry Control

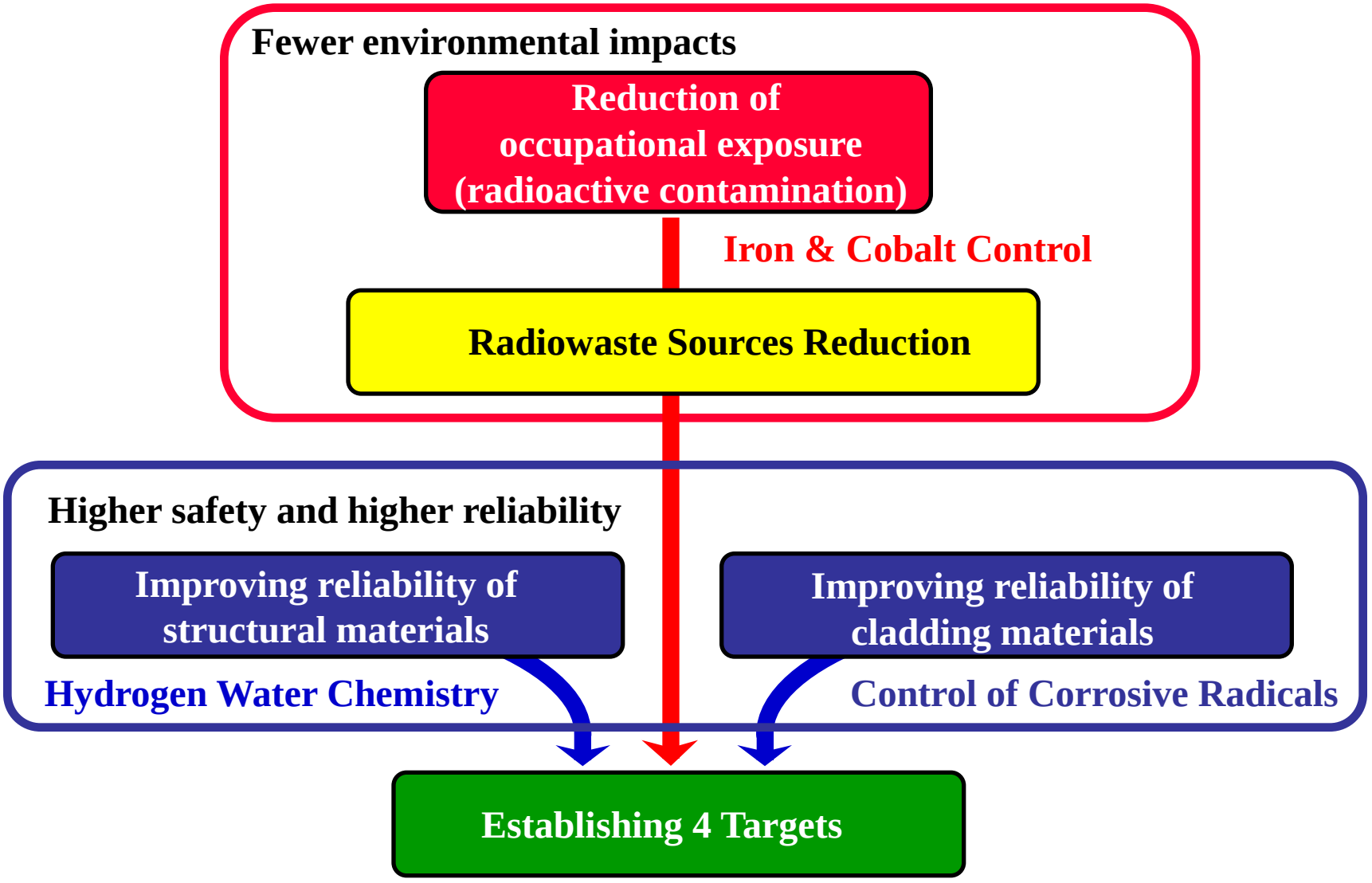

2.3.2 Water Chemistry

Water chemistry control targets

for PWR primary system

		Japan		EPRI	
Control item	**unit**	**target**	**standard**	**target**	**standard**
pH at 25°C	-	*1		*1	
conductivity	μS/cm	*1		*1	
boron	ppm	*2		*1	
Cl^- ion	ppm	<0.05	<0.15	<0.05	<0.15
$[O_2]$	ppm	<0.005	<0.1	<0.05	<0.1
$[H_2]$	cc-STP/kg-H_2O	25-35	15-50	25-50	>15
[Li]	ppm	0.2-2.2		zone control	
muddily	ppm	<1		<0.05	
$[SO_4^{2-}]$	ppm			<0.05	
[Si]	ppm-SiO_2	<0.5			

*1: combination of [Li] and [B] for optimal pH

*2: determined by reactor reactivity

2.3.2 Water Chemistry

Latest problems related to water chemistry

- **Latest experiences with problems related to water chemistry are as follows.**

1) Increasing occupational exposure

Challenge to more dose reduction by water chemistry improvement

2) Stress corrosion cracking of BWR core shrouds

Mitigation of corrosive conditions by water chemistry control

3) Flow accelerated corrosion of PWR feed water piping

Water chemistry improvement applying experience with BWR and fossil plants

2.3.3 Primary Water Stress Corrosion Cracking (PWSCC) (1)

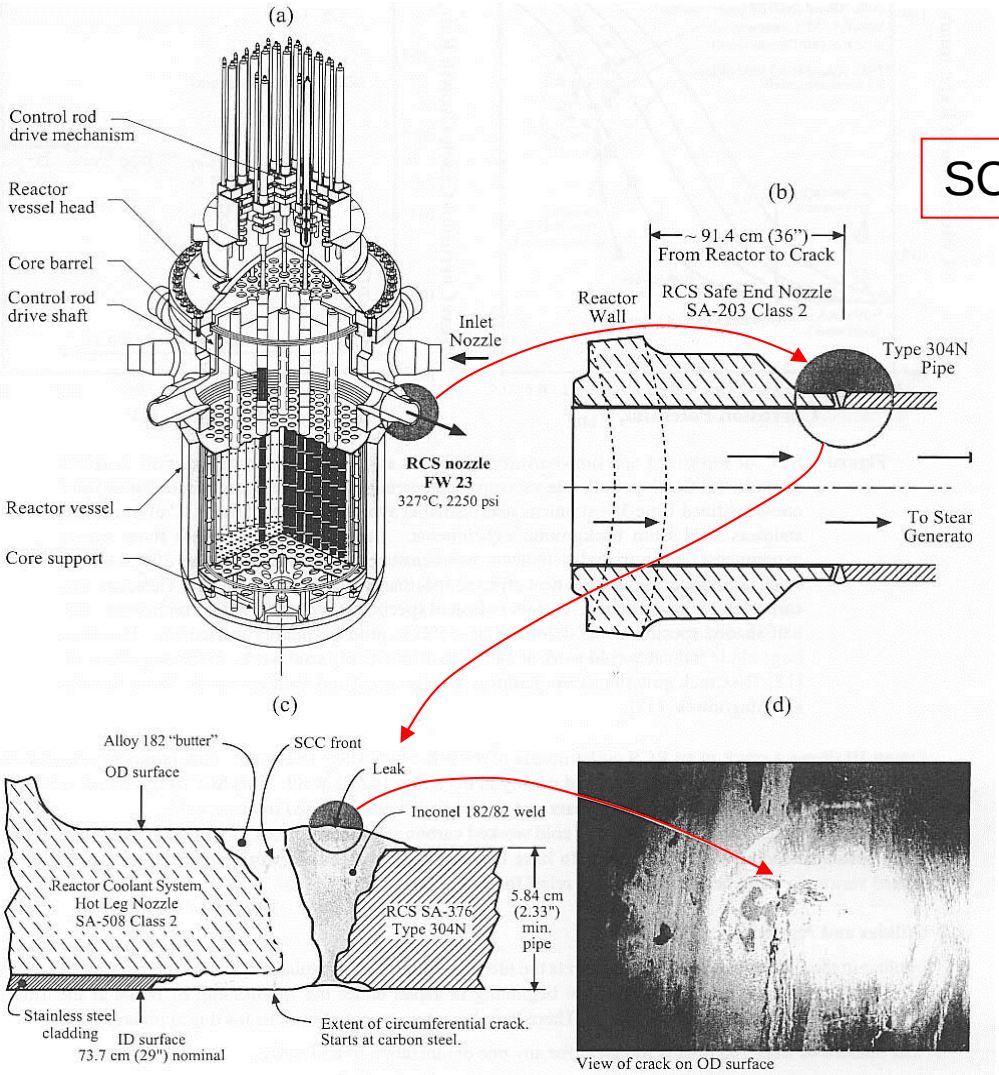

Figure 10 LPSCC of weld in primary piping of PWR outlet nozzle. (a) Schematic overview of reactor pressure vessel showing location of an outlet nozzle. (b) Cross section of nozzle, weld, and pipe. (c) Enlarged schematic cross section. (d) OD surface showing location of leak. From EPRI.

SCC occurred in Alloy 182/82 weld.

2.3.3 Primary Water Stress Corrosion Cracking (PWSCC) (2)

- Steam Generator at Tsuruga Unit 2 (1)

SG primary water inlet nozzle

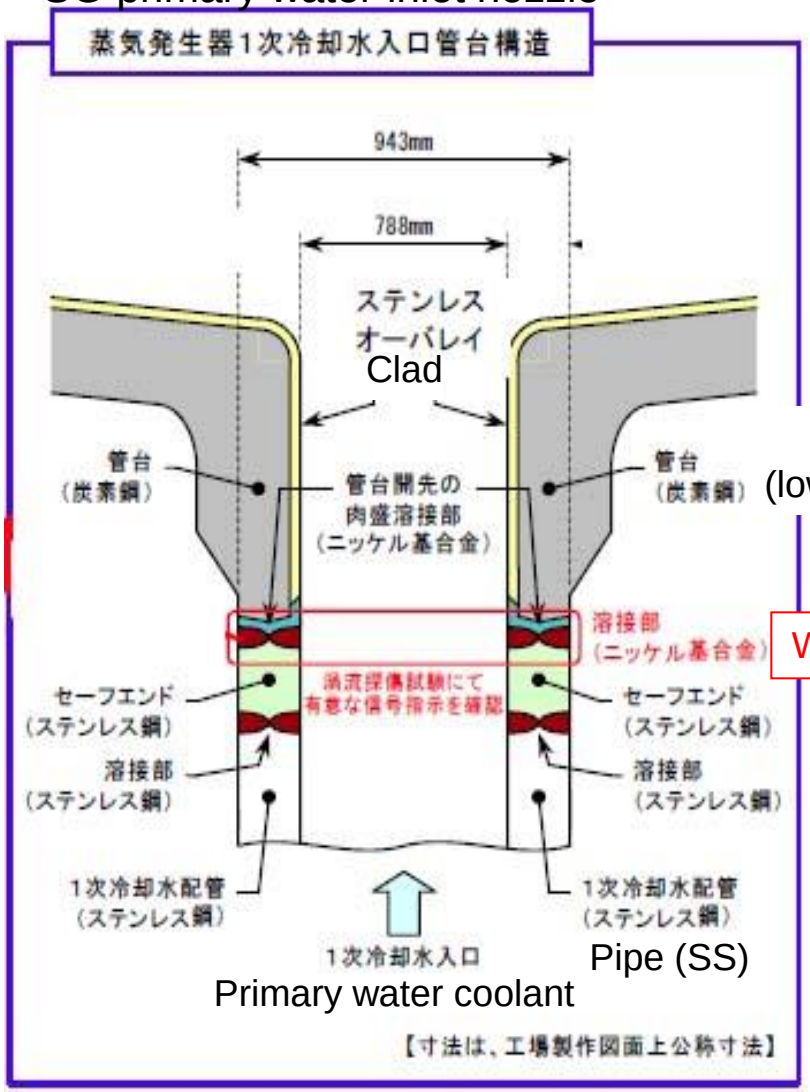

Nozzle
(low alloy steel)

Weld

Safe end

Weld (SS)

Pipe (SS)

Primary water coolant

PWSCC occurred in
Alloy 182/82 weld.

2.3.3 Primary Water Stress Corrosion Cracking (PWSCC) (3)

- SG at Tsuruga Unit 2 (2)

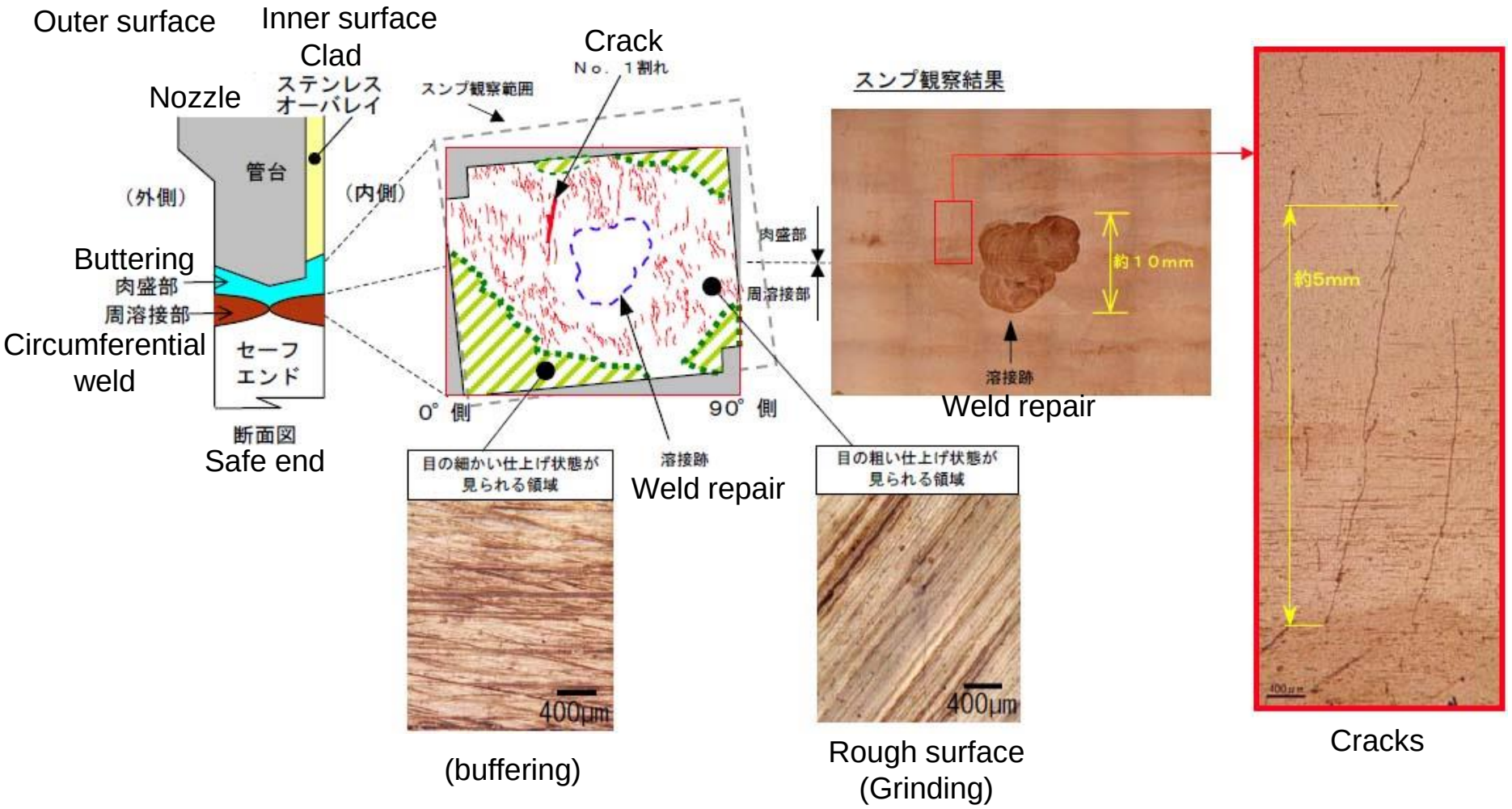

2.3.4 Corrosion of RPV (1)

- Boric acid corrosion

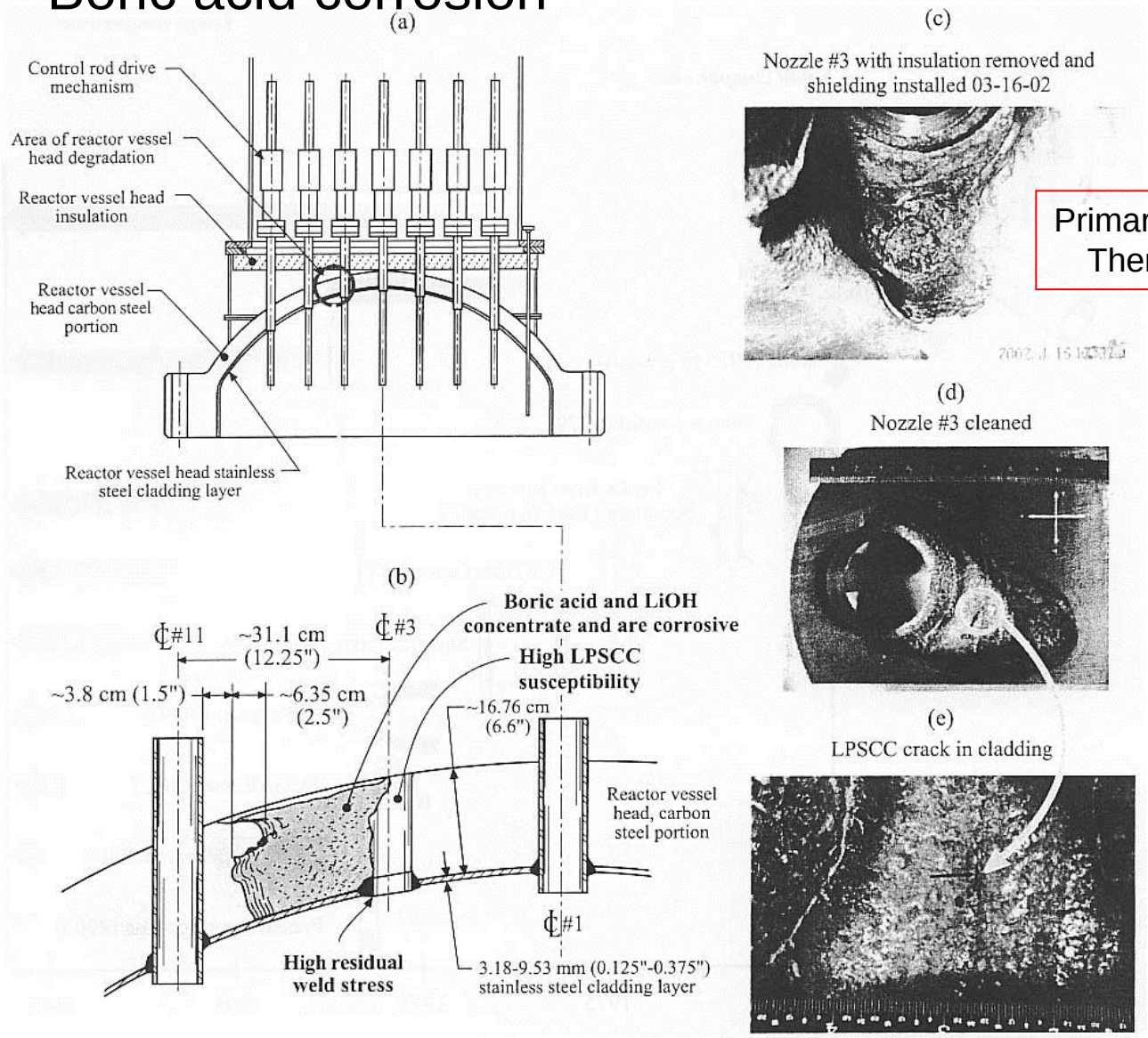

Figure 58 (a) View of pressure vessel head. (b) Cross section of pressure vessel head with location of corrosion. (c), (d), (e) view of corroded cavity with small crack in cladding in (e).

Primary water leaks after PWSCC.
Then the water corrodes RPV.

2.3.5 IASCC of Baffle Former Bolts (1)

- IASCC (Irradiation Assisted Stress Corrosion Cracking)
  - Baffle former bolt

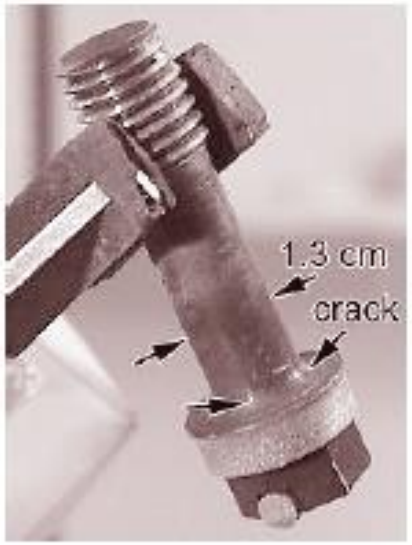

E. P. Simonnen et al., "Response of PWR Baffle-Former Bolt loading to Swelling, Irradiation Creep and Bolt Replacement as using Finite Element Modeling", Proc. Int. Conf. Environmental Degradation of Materials in Nuclear Power System –Water Reactors-, TMS, 2005, p.449.

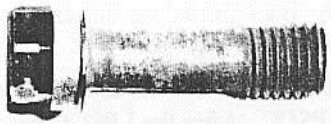

Baffle former bolt

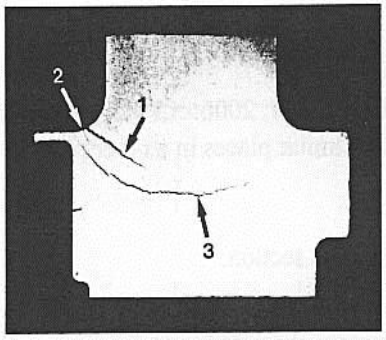

Cross section of SCC

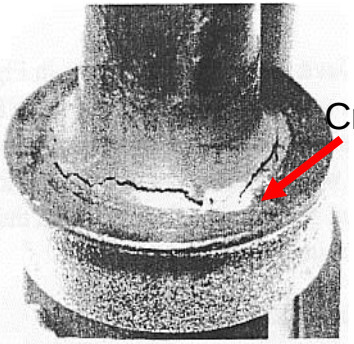

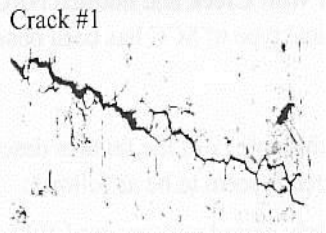

Optical micrograph of crack #1

2.3.5 IASCC of Baffle Former Bolts (2)

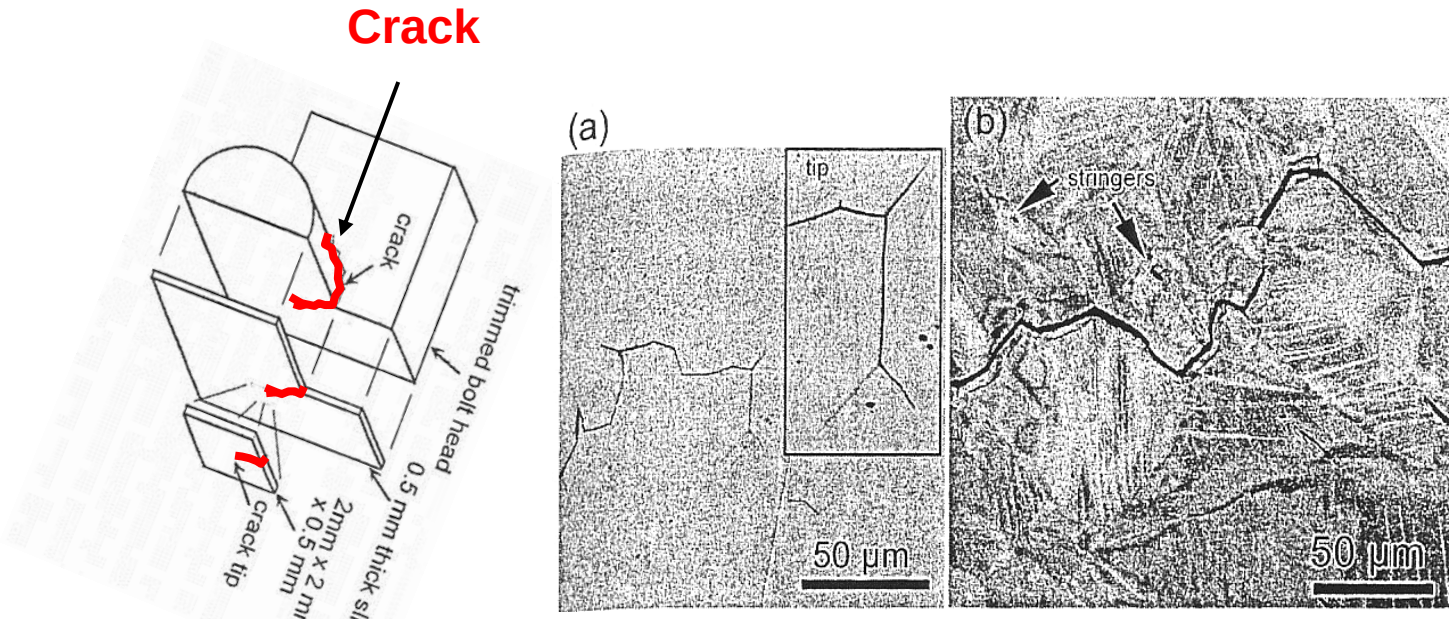

L.E. Thomas et al., Proc. Fontevraud 5, (2002) p.117

Cracks are discontinuous.

2.3.6 Corrosion Issues in Steam Generator

Many kinds of SCC mechanisms on SG tube

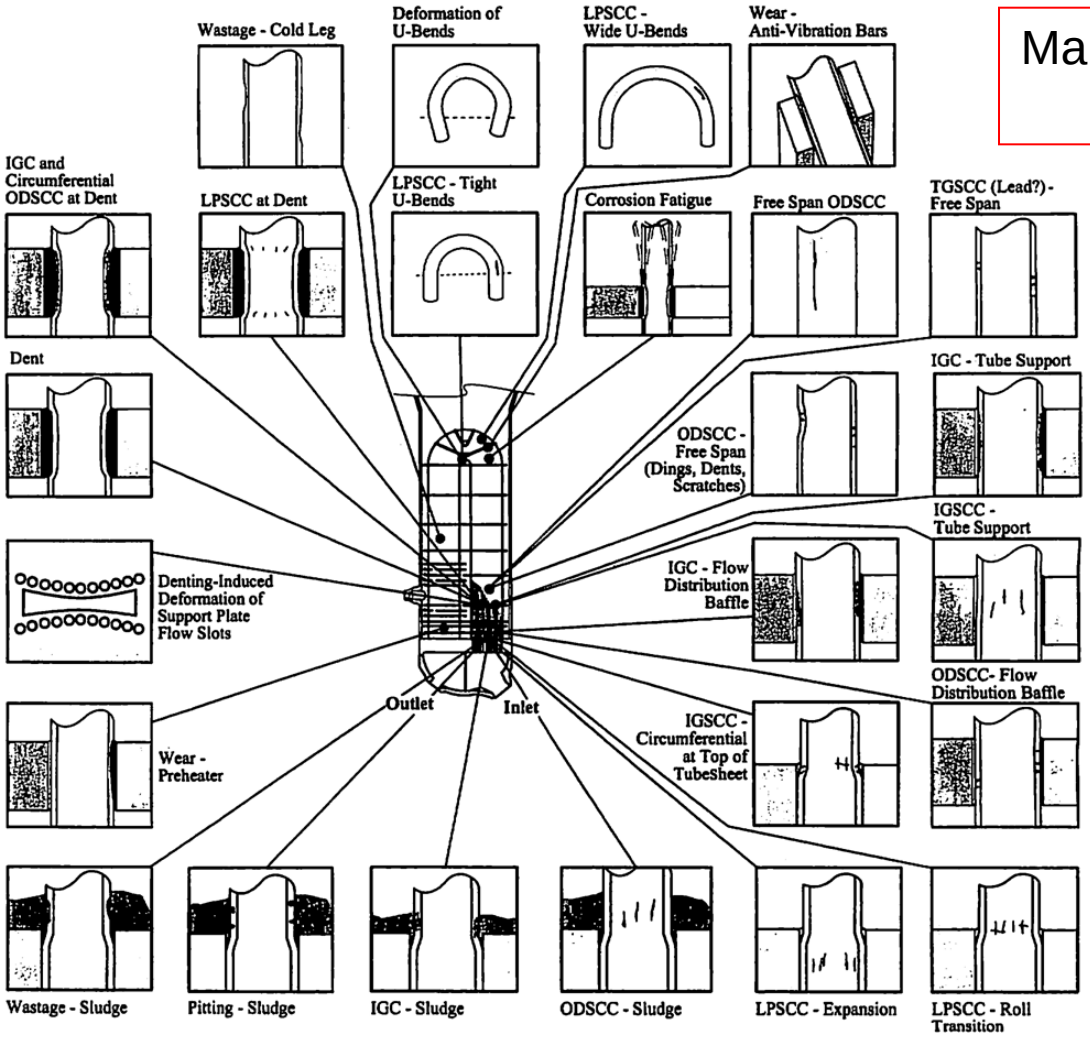

Figure 2 Array of modes of failures at various locations (mode-location cases) that have occurred in recirculating steam generators having Alloy 600MA tubes and drilled hole tube supports.

2.3.7 Flow Accelerated Corrosion (FAC)

Flow assisted (accelerated) corrosion (FAC) is one the most common problems in nuclear and fossil power plants.

Large scale rupture of the Surry-2, feed water piping which thinned locally due to FAC was experienced in 1986. Last summer, one of the feed water piping in Mihama-3 Nuclear Power Plant ruptured suddenly caused by FAC.

The mitigation of FAC to prevent such tragic accident is one of important subjects for corrosion engineers in nuclear power plants.

In this section, we discuss about the FAC issue based on the experience of accident at Mihama-3 NPP. In order to prevent such accident, the mechanistic viewpoint is effective and essential.

Viewgraphs are kindly provided by Drs. S. Uchida and T. Satho.

2.3.7 Flow Accelerated Corrosion (FAC)

Large scale piping rupture accident at Mihama-3 NPP

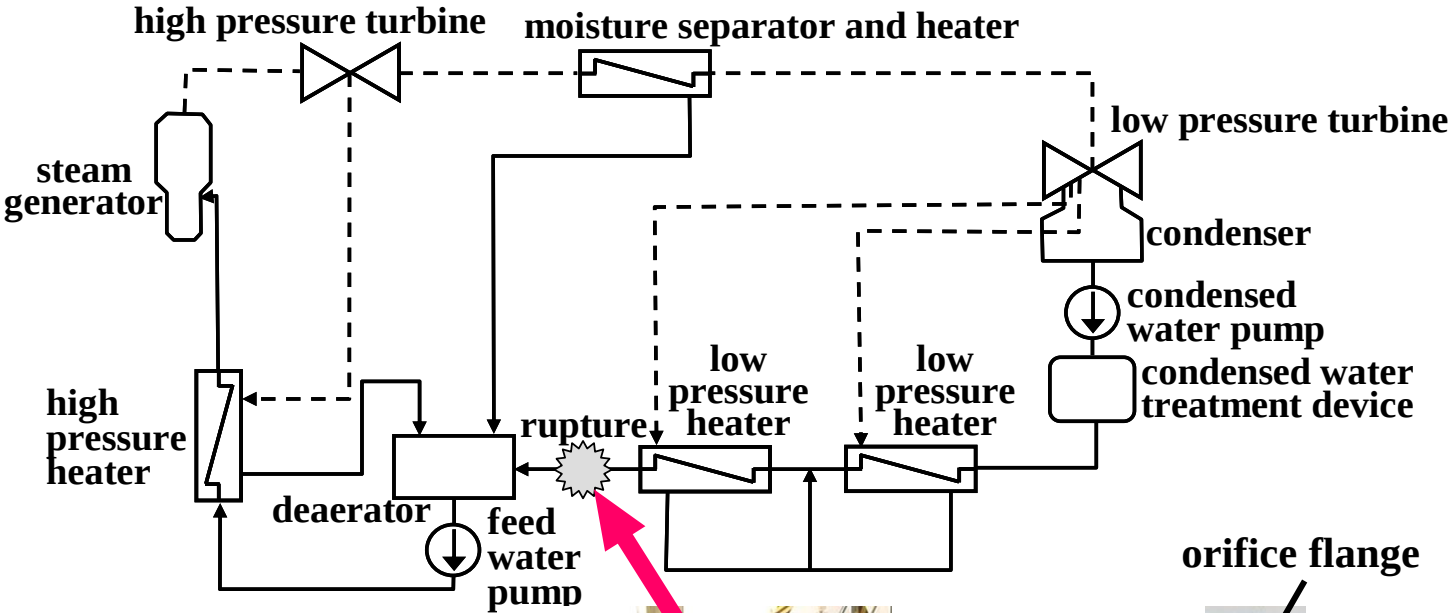

Parameter	
Operating time	185,700 h
Outer diameter	560 mm
Initial thickness	10 mm
Pressure	0.93 MPa
Temperature	142 °C
Flow velocity	2.2 m/s
pH	8.6 - 9.3
DO*	< 5 ppb

*DO: dissolved oxygen

2.3.7 Flow Accelerated Corrosion (FAC)

Materials and Water Chemistry at Mihama-3 NPP

Table 1 Chemical composition of material (%) (Mihama Unit 3)

	C	Si	Mn	P	S	Cr	Cu
Piping	0.16	0.24	0.67	0.009	0.011	0.01	0.01
Elbow	0.14	0.23	0.74	0.016	0.007	0.03	0.03

Table 2 Parameters in the rupture point (Mihama Unit 3)

	Parameter	
Piping	Material	JIS G3103 SB42
	Operating time	185,700 h
	Outer diameter	560 mm
	Initial thickness	10 mm
Flow condition	Mass flow rate	1,700 t/h
	Pressure	0.93 MPa
	Temperature	142 ºC
	Flow velocity	2.2 m/s
Water chemistry	pH	8.6 - 9.3
	DO*	< 5 ppb

*DO: dissolved oxygen

2.3.7 Flow Accelerated Corrosion (FAC)

A photo of ruptured piping of Mihama-3

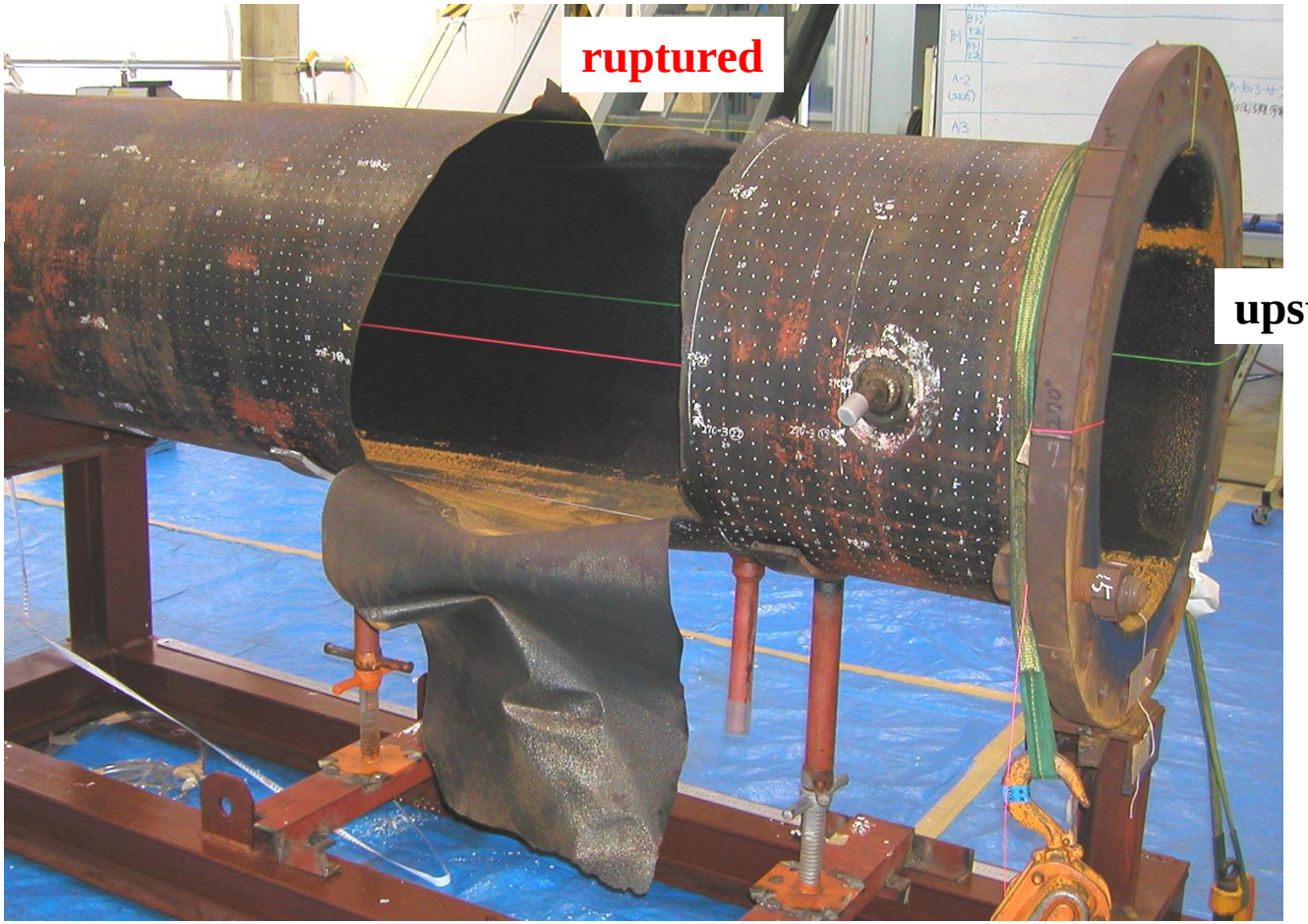

2.3.7 Flow Accelerated Corrosion (FAC)

Microscope image of rupture pares

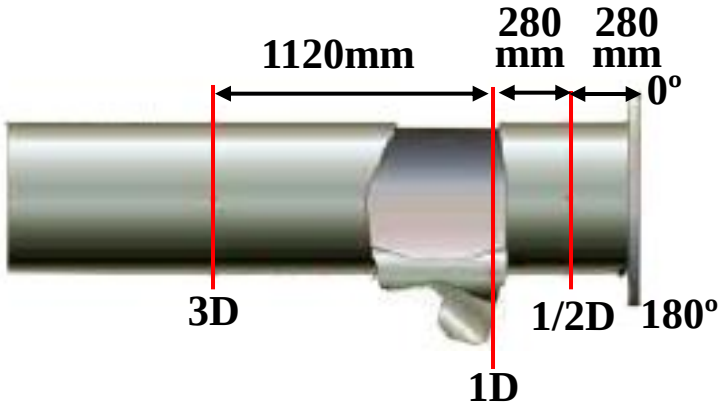

”scallop” surface
→ Single phase FAC

	3D	1D	1/2D
0º			
90º			
180º			
270º			

2.3.7 Flow Accelerated Corrosion (FAC)

Distribution of wall thickness

Azimuthal distribution

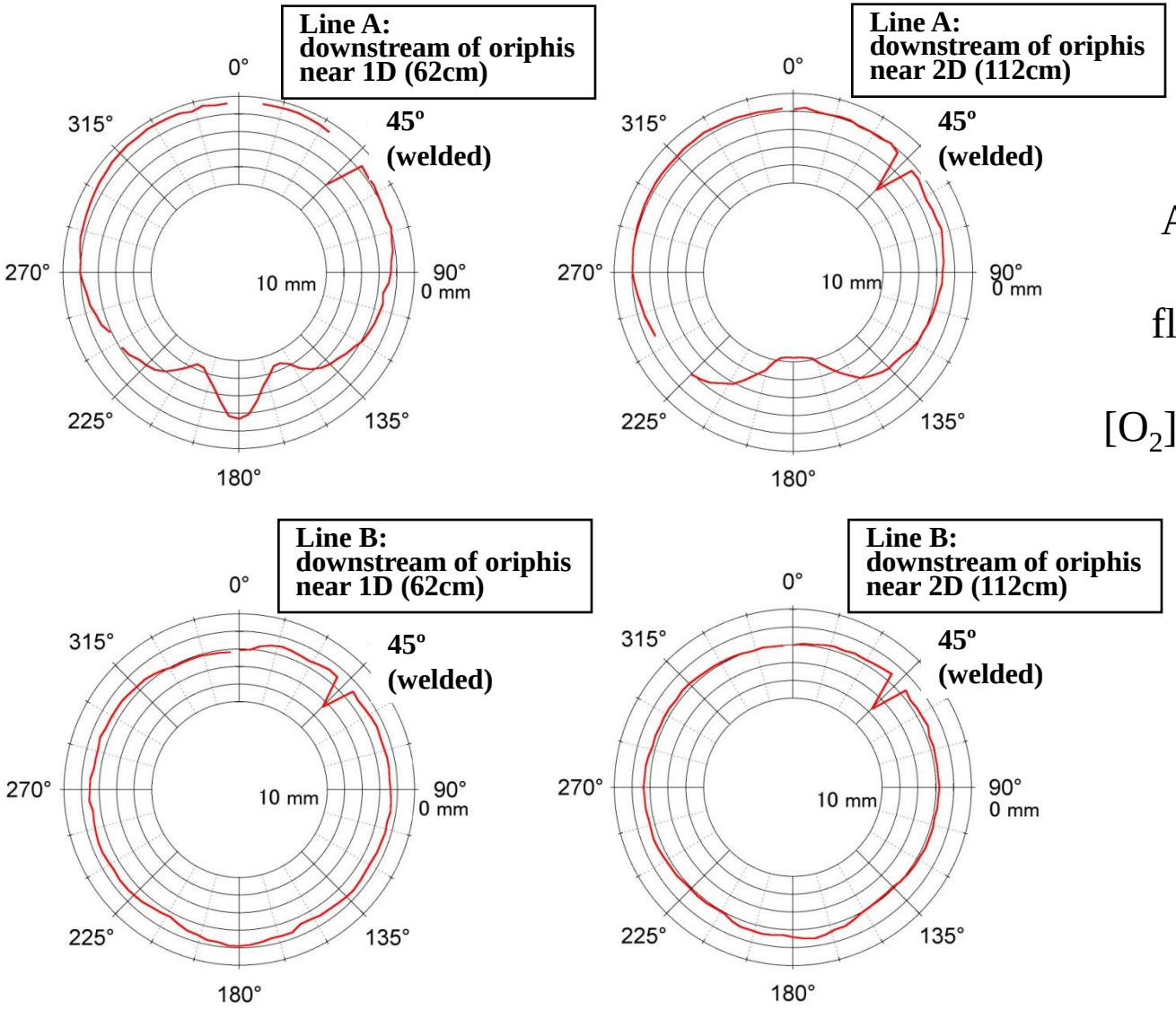

Azimuthal distributions
caused by either of
flow velocity distribution
or
$[O_2]$ distribution due to mixing

2.3.7 Flow Accelerated Corrosion (FAC)

Mechanism of FAC

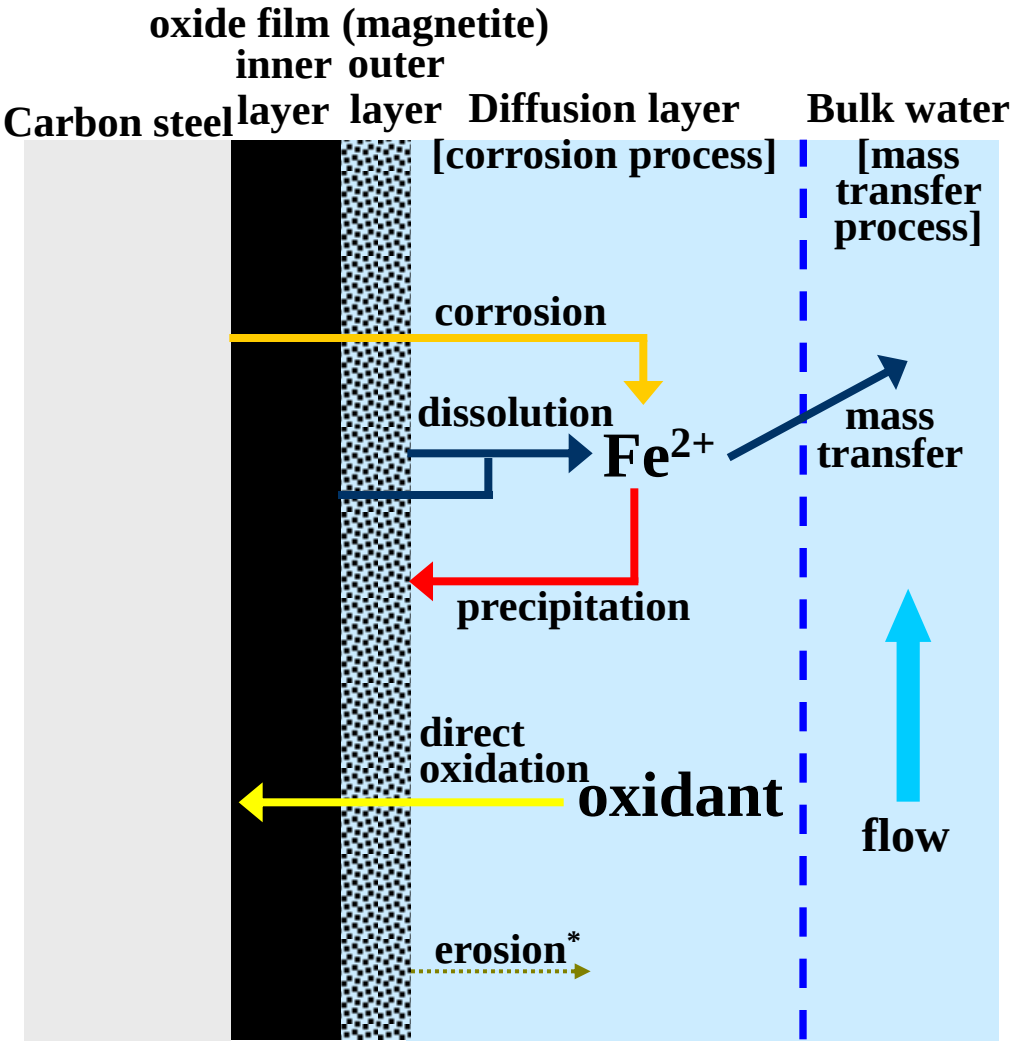

FAC mechanism: Two processes

1: corrosion process
[production of soluble Fe^{2+} and their accumulation at the oxide-water interface]

2: mass transfer process
[flowing water removes the soluble ferrous ions by a convective mass transfer mechanism]

In order to determine a process on FAC experimentally, the other process should be simplified.

[* Erosion may be occurred by share stress, however it can be neglected in FAC process.]

2.3.7 Flow Accelerated Corrosion (FAC)

Dependency of FAC on flow velocity and temperature

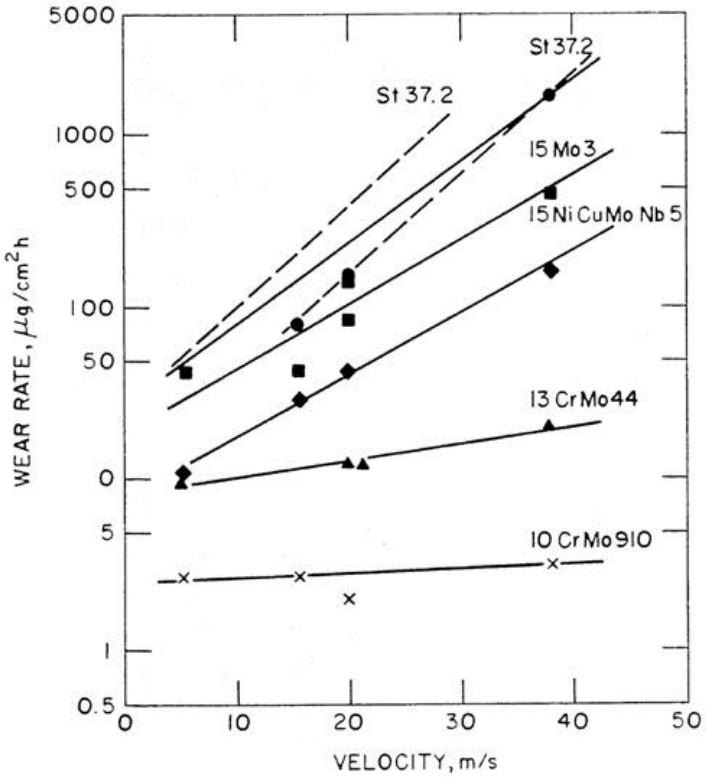

Figure 1 Dependency of FAC on flow velocity (pH=7.0, T=180°C, DO<5ppb)

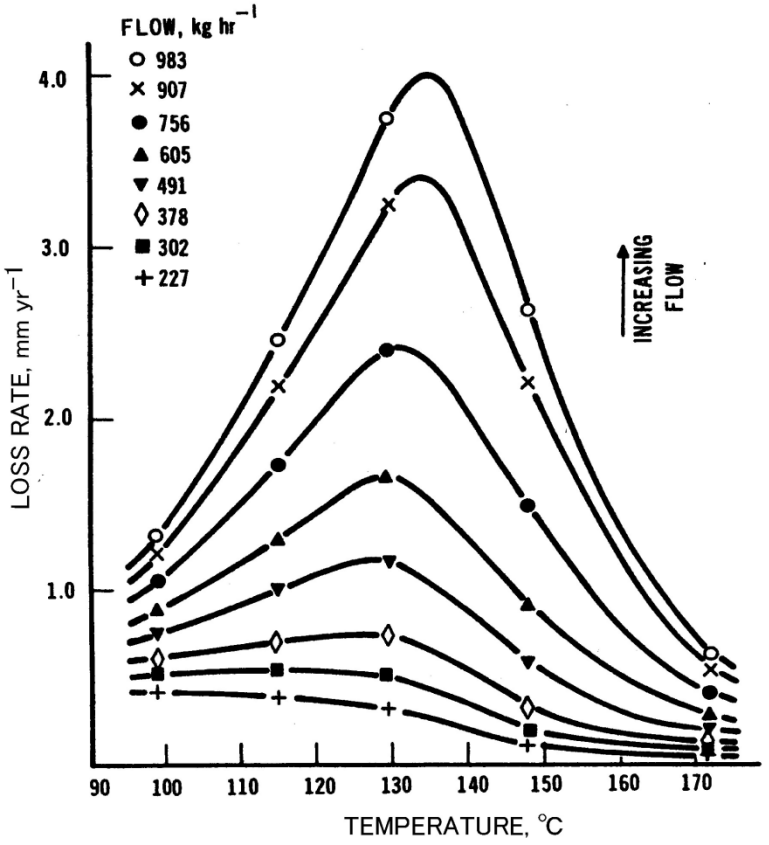

Figure 2 The dependency of FAC rate on temperature (pH=9.5)

2.3.7 Flow Accelerated Corrosion (FAC)

Effects of pH and [O_2] on corrosion of carbon steel

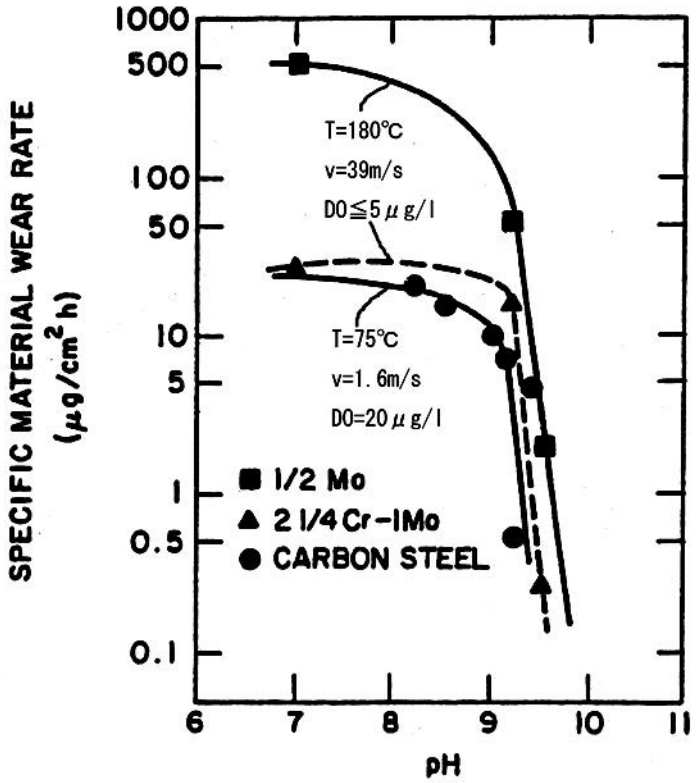

Figure 3 The dependency of FAC rate on cold pH

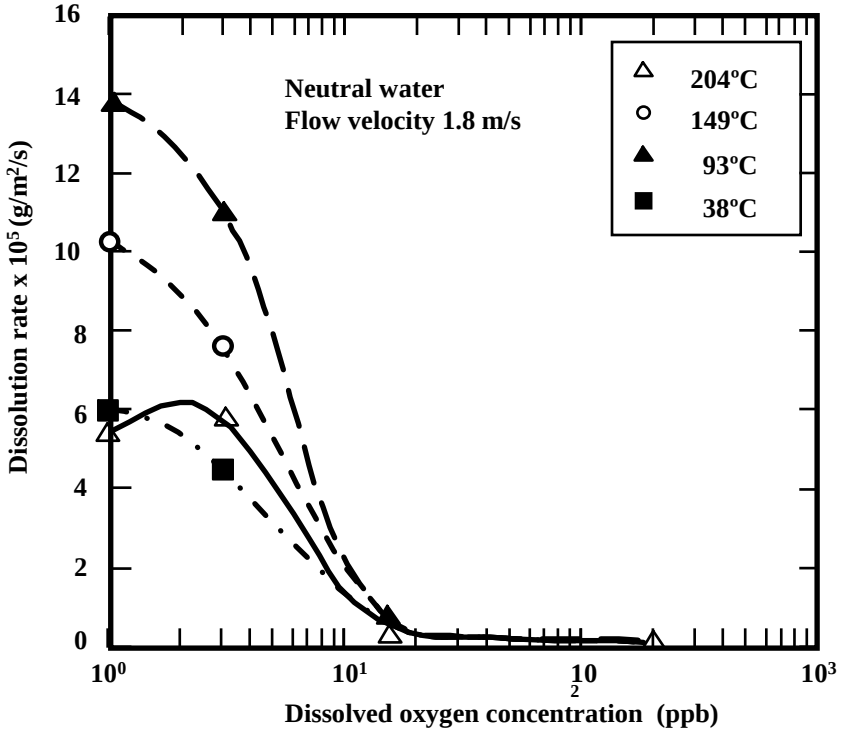

Figure 4 The relationship between DO and dissolution rate of iron in pure water

2.3.7 Flow Accelerated Corrosion (FAC)

Effects of chromium contents on corrosion rate

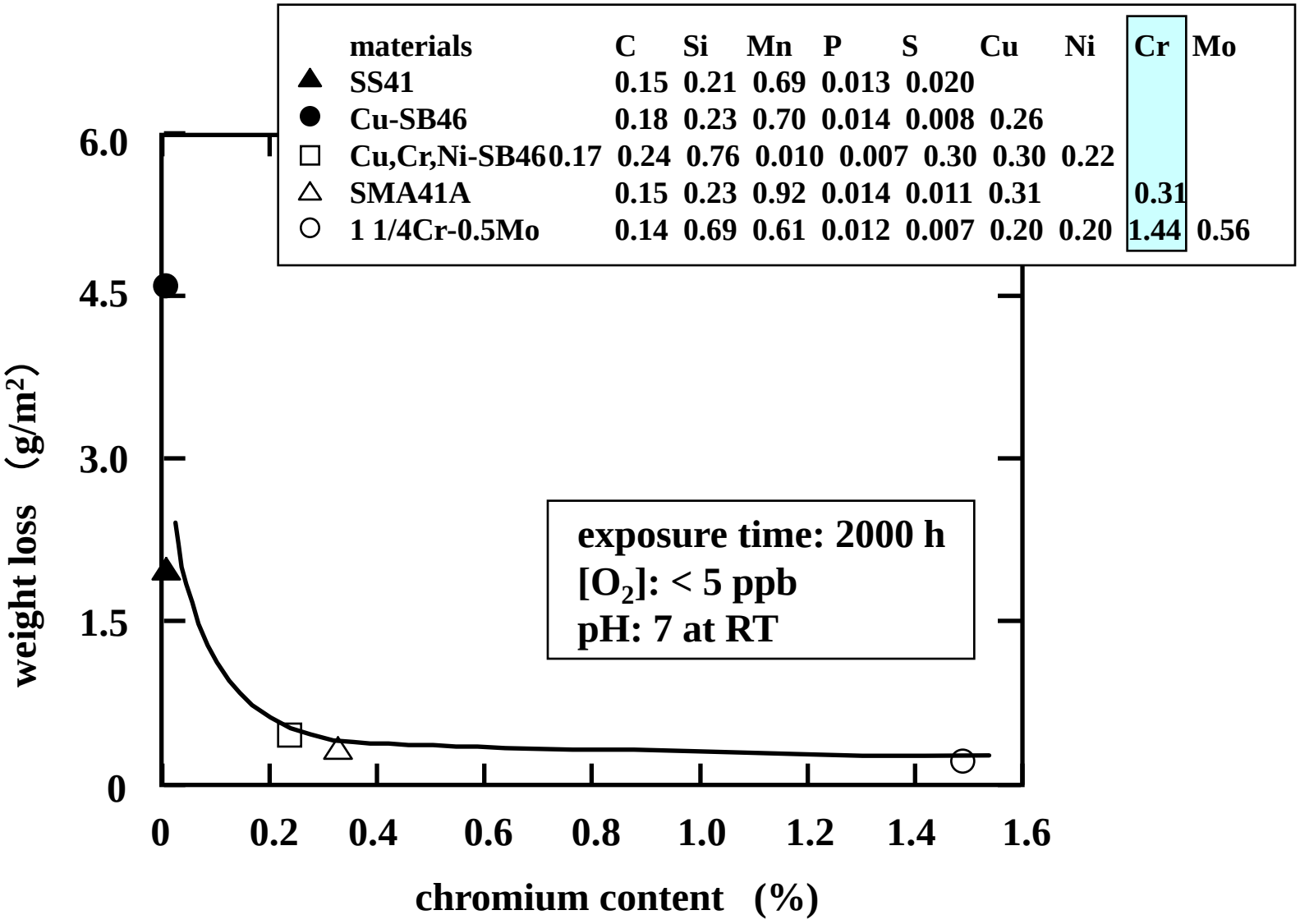

2.3.7 Flow Accelerated Corrosion (FAC)

Summary of effects of each parameter on FAC

Parameter	Effect on FAC
Flow velocity	proportion to flow velocity
Chromium content	mitigated with more than 0.5 % chromium content
Temperature	maximum at 130 - 150 ºC
Dissolved Oxygen	mitigated in more than about 20 ppb
pH	mitigated in more than about 9.2
Ferrous ion concentration	proportion to (C_{sat}-C)
	here, C_{sat}; saturation concentration, C; ferrous ion concentration
Electero-chmical potential (ECP)	mitigated at more than -500mV-SHE in alkali water (pH9.0)

2.3.8 IGSCC

- Intergranular Stress Corrosion Cracking (IGSCC)
  - Non-sensitized, but hardened materials
    - X-750 alloy
    - Alloy A-286

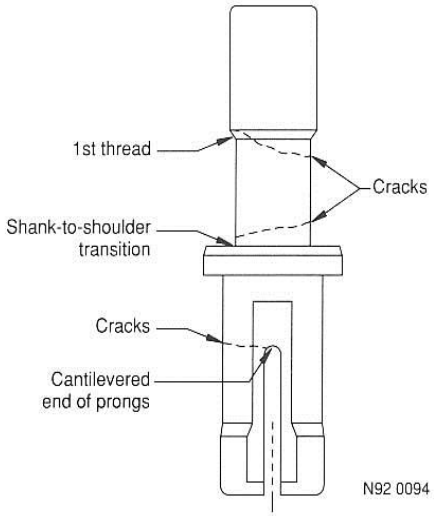

Figure 13-15. Locations of split-pin cracking in Framatome PWRs (Benhamon and Poitrenaud 1989). Copyright Electric Power Research Institute; reprinted with permission.

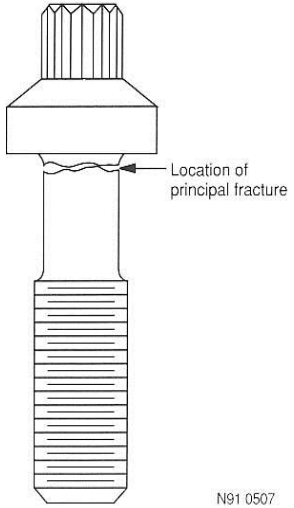

Figure 13-16. A Babcock & Wilcox bolt with the location of the principal fracture shown (Moore 1983).

2.4 Design and Materials of BWR Components

2.4.1 Reactor Pressure Vessel (1)

Material : SA533B Grade B
Cladding : Type 308 or 309

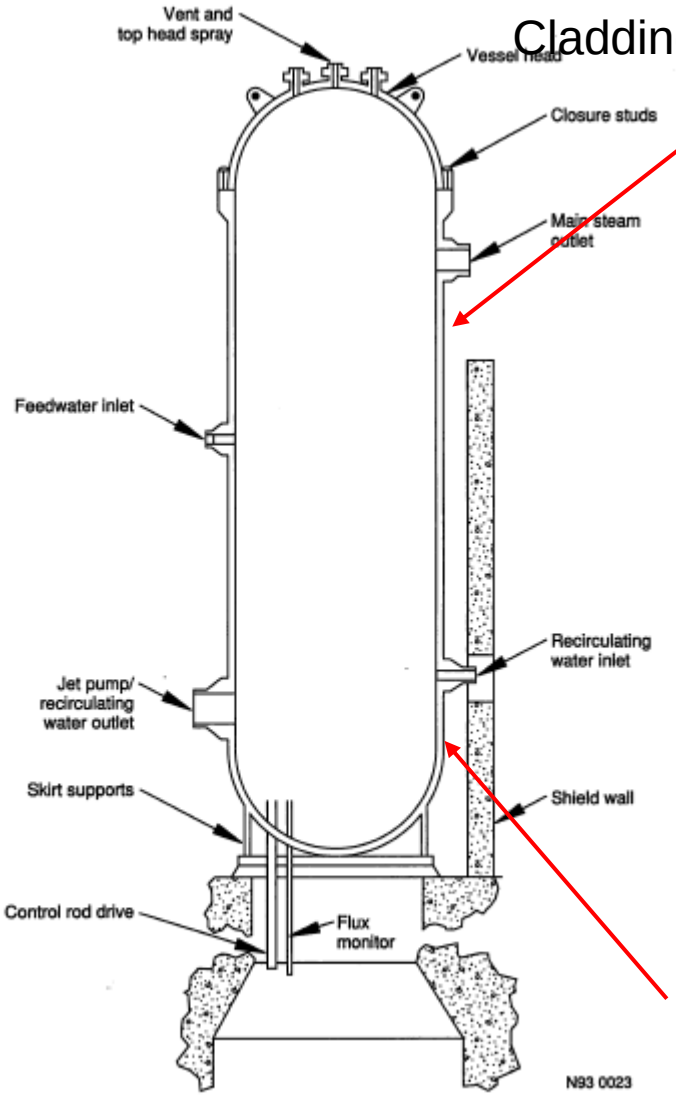

Figure 18-1. Typical BWR pressure vessel.

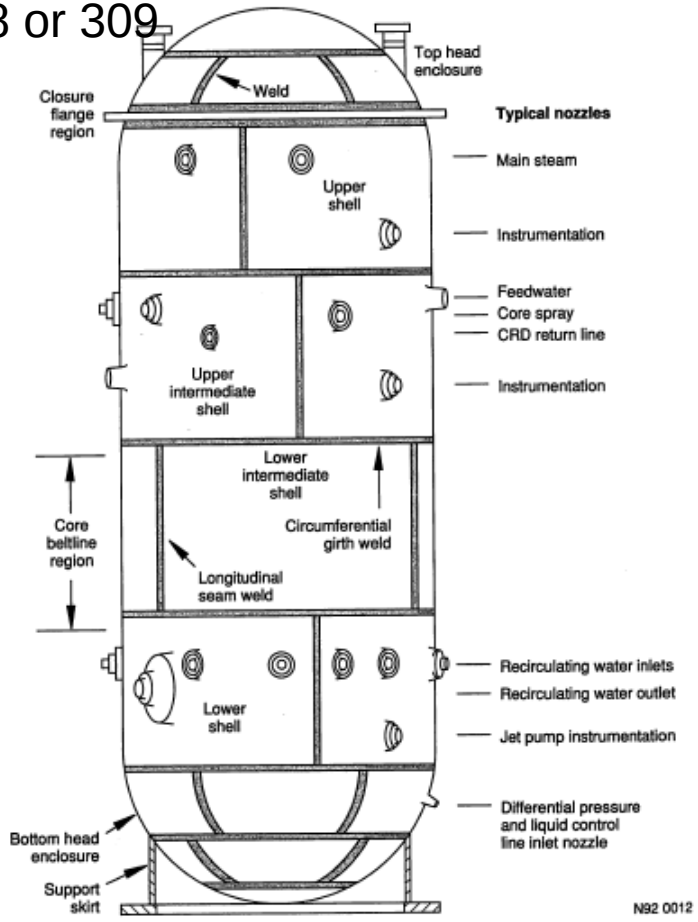

Figure 18-2. BWR pressure vessel showing vessel plates, seam welds, and nozzles.

PWHT: 610ºC for 1 h per inch thickness, followed by a furnace cooling

to reduce residual stress and

to temper any martensite in the HAZ

2.4.1 Reactor Pressure Vessel (2)

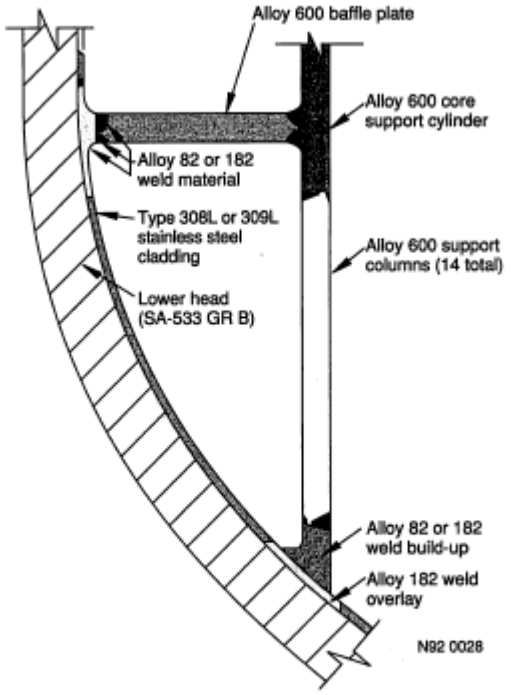

Figure 18-3. Sketch of a Chicago Bridge and Iron vessel shroud support structure attachment configuration.

Either Alloy 82 or Alloy 182 weld materials were used.

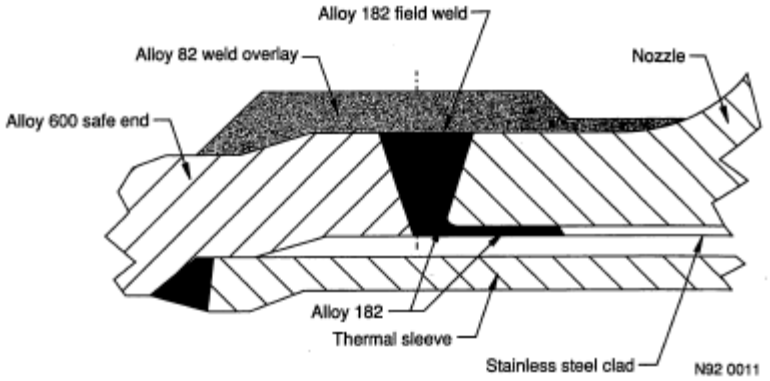

Figure 18-11. Nozzle-to-safe end weld overlay (Smith et al. 1990). Copyright Elsevier Science Publishers; reprinted with permission.

Temporary repair by weld overlay using corrosion resistant Alloy 82 material.

2.4.2 Reactor Internals

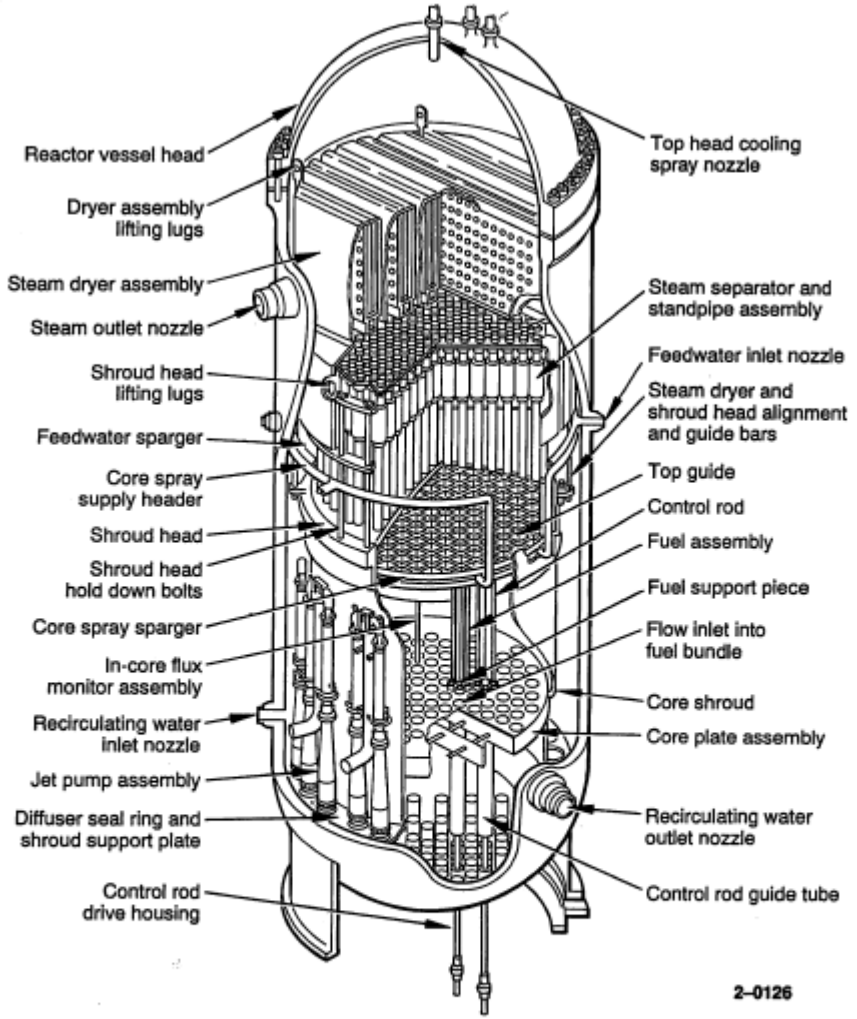

Figure 21-1. Arrangement of CRDM and reactor internals used in BWR/3 and BWR/4 designs (Herrera and Stancavage 1988). Copyright American Nuclear Society; reprinted with permission.

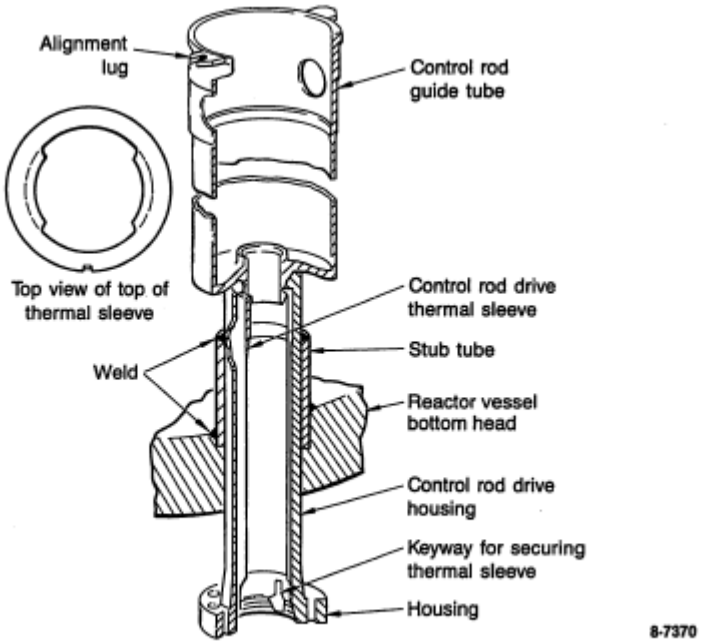

Figure 21-2. Arrangement of CRDM housing (USNRC Reactor Training Center).

In BWRs, the control rod drive mechanisms (CRDMs) are mounted at the bottom of the pressure vessels where they position the neutron absorbing control rod assemblies (CRAs) within the reactor core to provide reactivity control during startup and shutdown of the reactor, flux shaping at power, and emergency shutdown (scram).

2.4.2 Reactor Internals

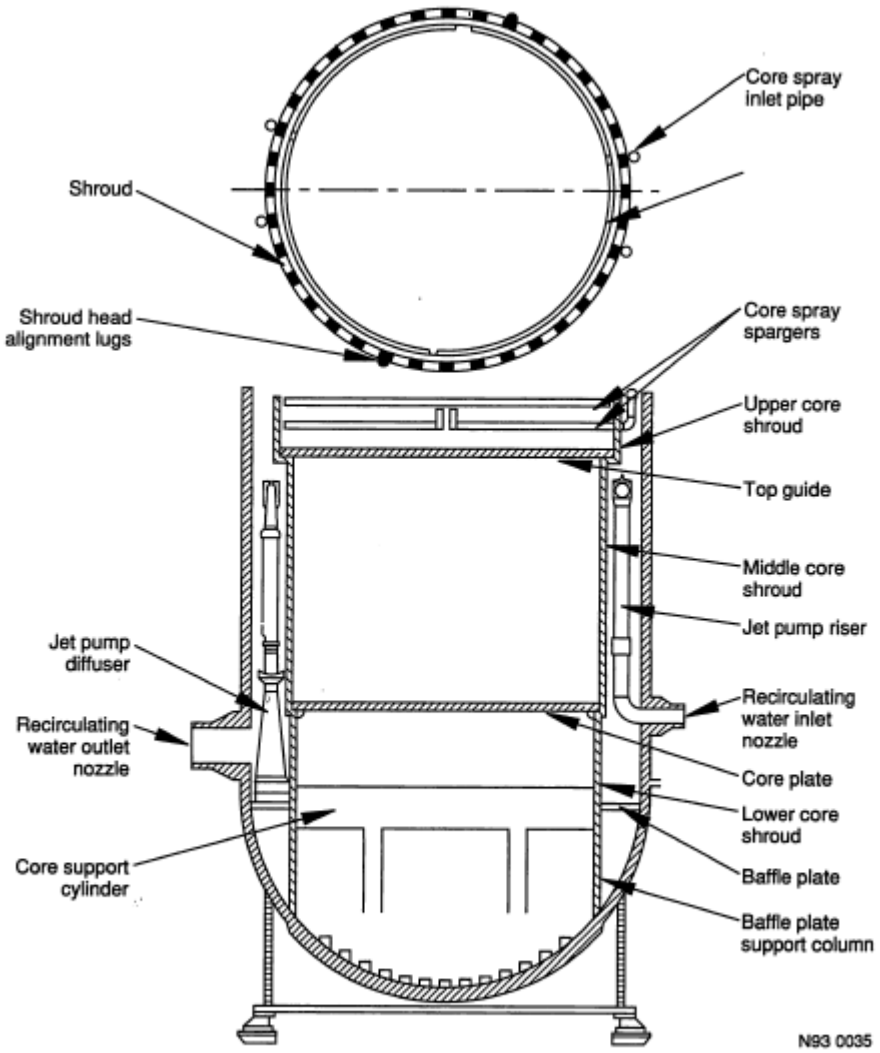

Figure 22-2. Arrangement of core shroud, core spray spargers, baffle plate, and jet pumps (USNRC Reactor Training Center).

The core shroud is a 51 mm thick cylindrical stainless steel assembly that provides vertical and lateral support for the core plate, top guide, and shroud head.

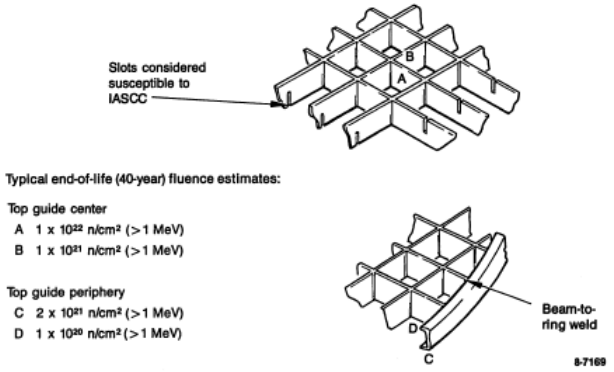

Figure 22-6. Top guide structure (Gerber et al. 1986). Copyright Electric Power Research Institute; reprinted with permission.

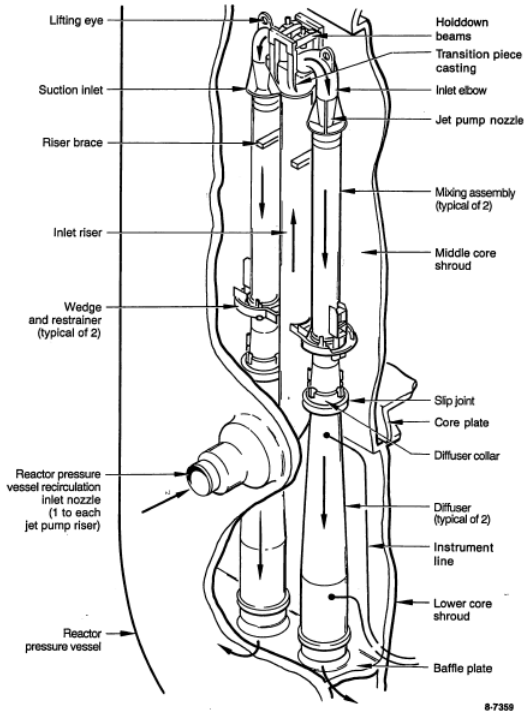

Figure 22-5. Jet pump assembly (USNRC Reactor Training Center).

The jet pump is primarily composed of forged Type 304 SS.

2.4.3 Recirculation Piping

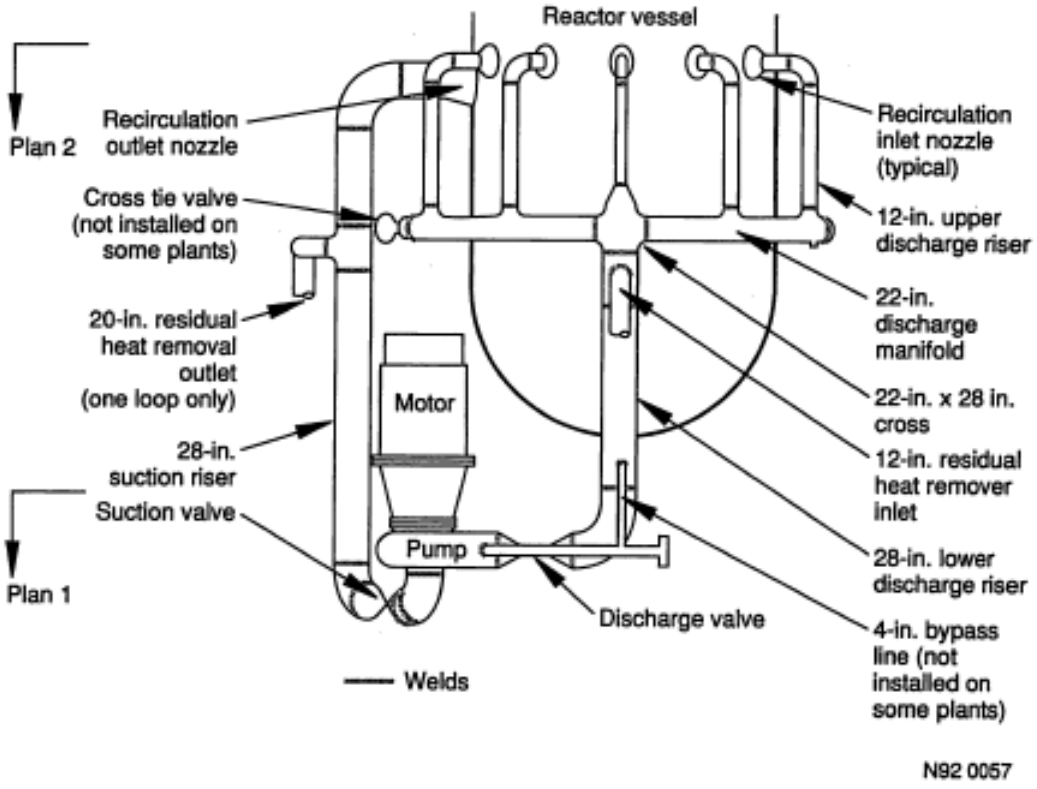

Figure 19-1. Loop B of a typical BWR-4 recirculation piping system, with the weld locations indicated by screened lines (Lo et al. 1989). (See Figure 19-2 for plan views.)

The stainless steel recirculation piping systems are connected to the low-alloy steel pressure vessels through vessel nozzles and transition pieces of pipe called safe end.

2.5 Corrosion-Related Issues in BWR

2.5.1 SCC in Piping

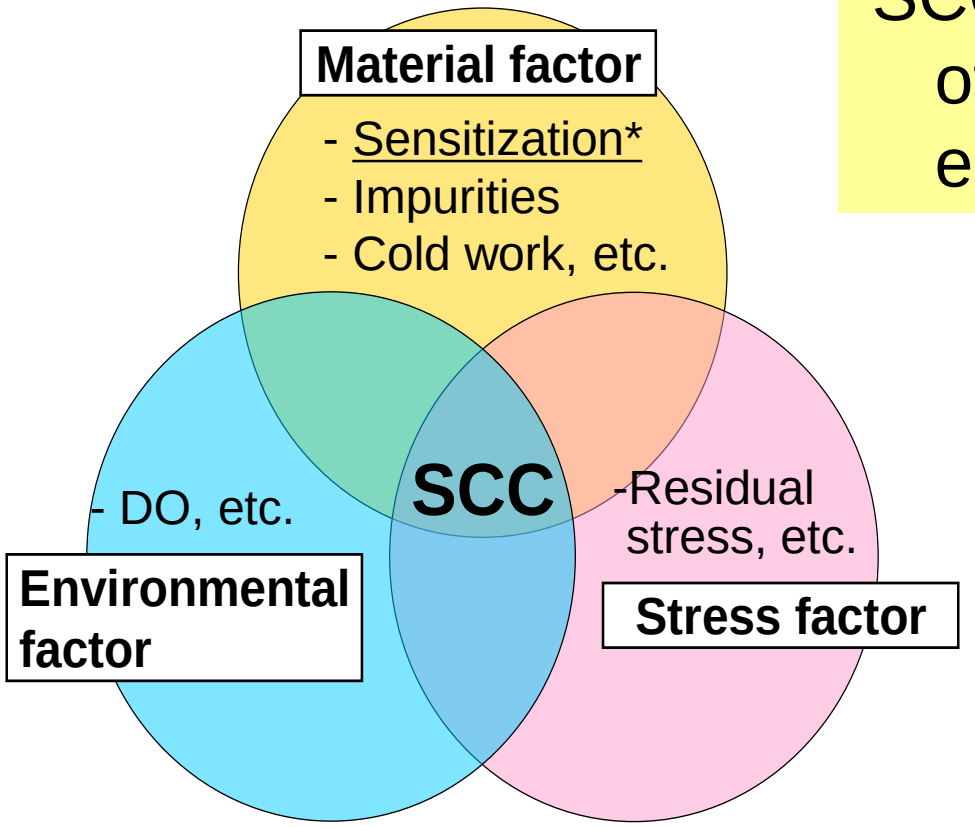

Fig. Factors governing SCC

SCC is a synergistic effect of material, stress and environmental factors.

The remedy for SCC is to remove any of the factors.

Sensitization*: Condition of alloy that becomes sensitized to SCC due to **thermal effect or irradiation effect**.

2.5.1 SCC in Piping

- Thermal sensitization due to $Cr_{23}C_6$ precipitate at grain boundary -

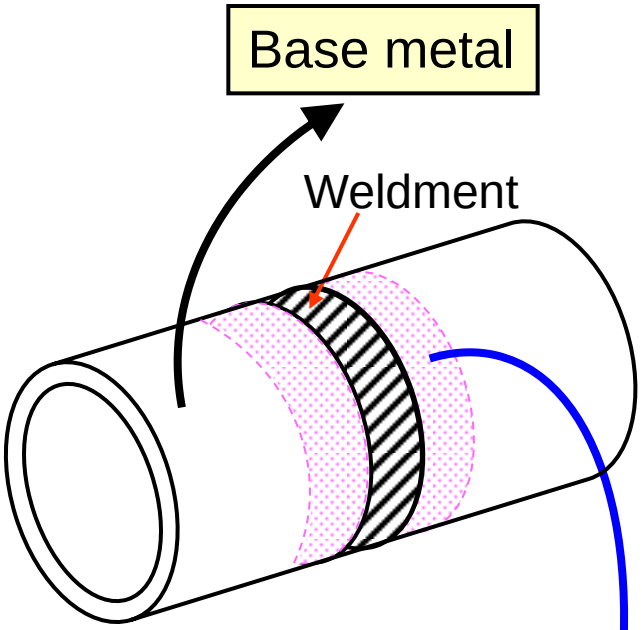

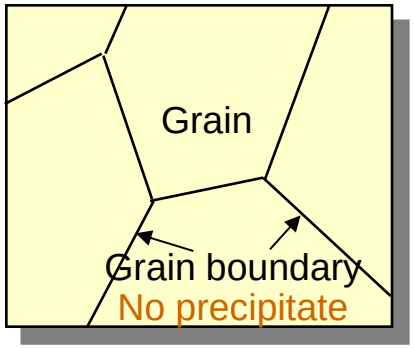

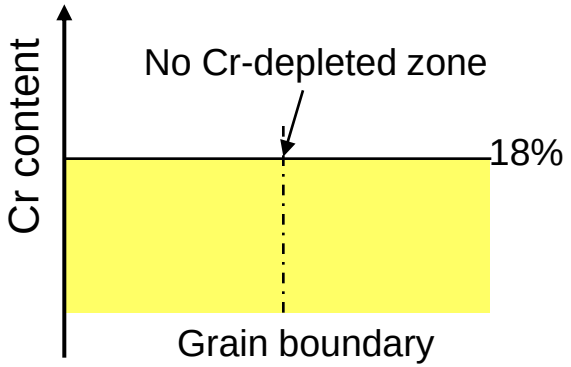

Corrosion resistance → Cr-rich passive film

Thermal sensitization

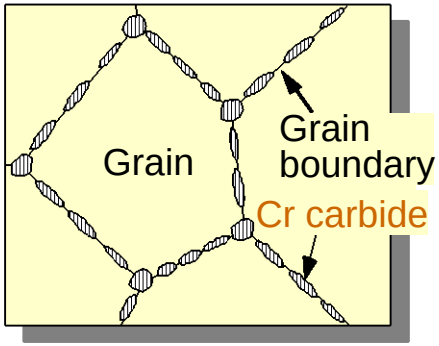

Heated at 500-800°C

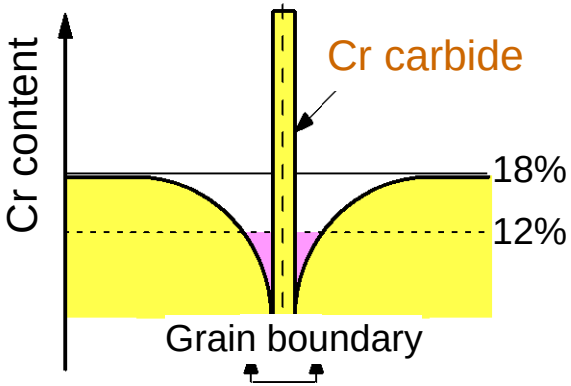

Formation of Cr-depleted zone

Initiation of IGSCC ← Lack of Cr at GB

2.5.1 SCC in Piping

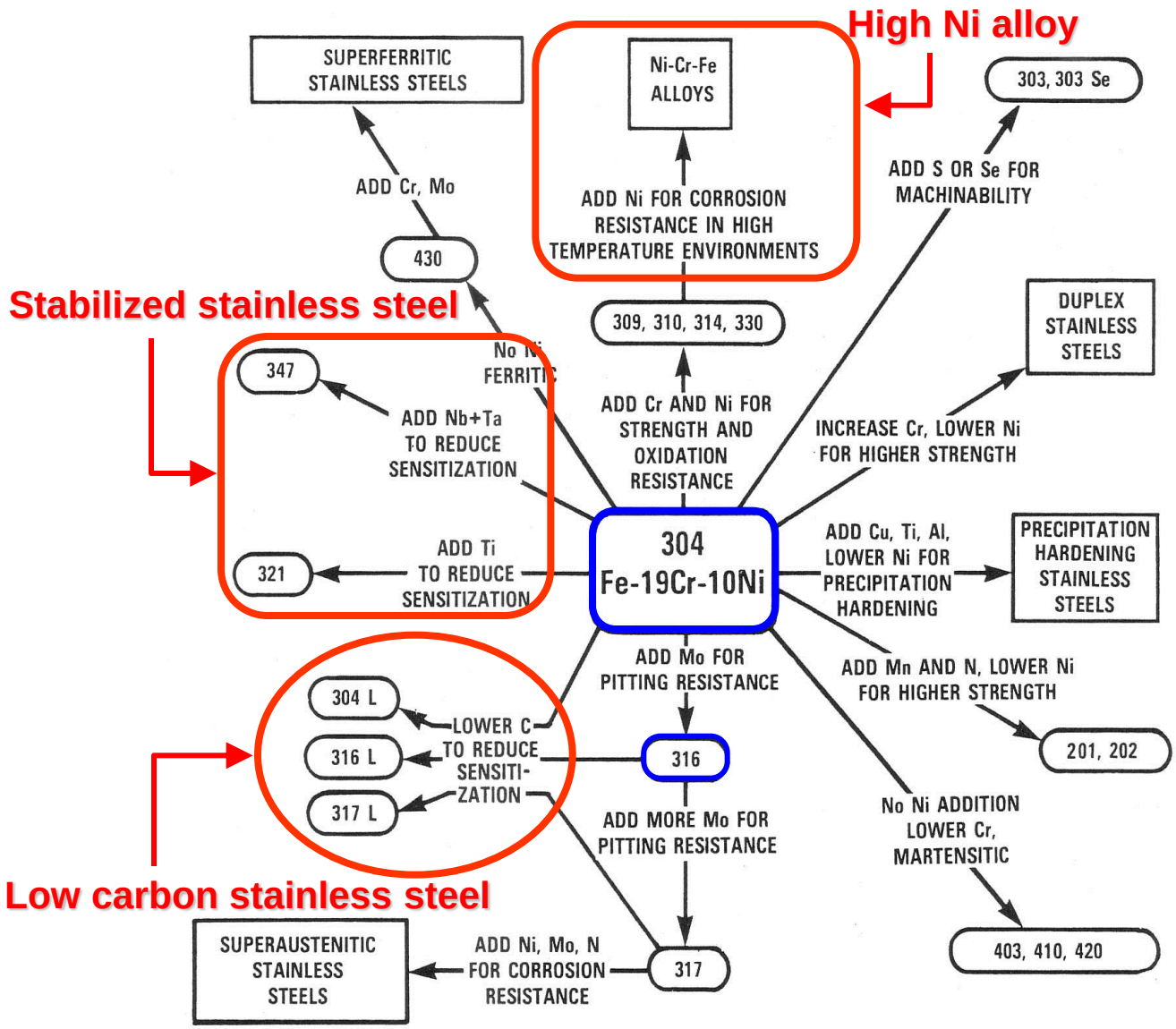

Figure 2.1 Compositional and property linkages in the stainless steel family of alloys.

SCC "resistant" alloys

??

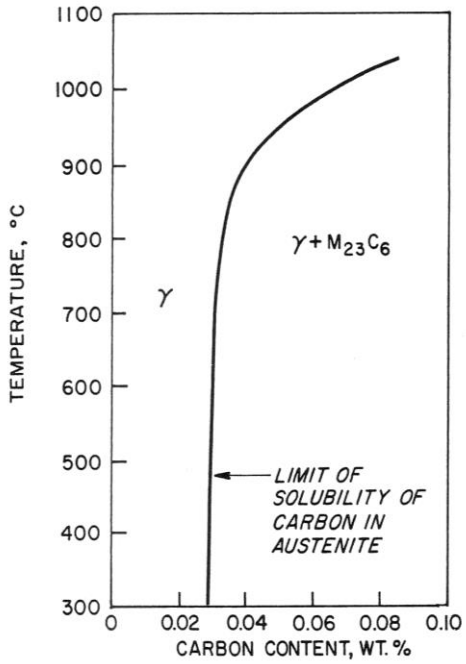

Fig. Carbon in 18Cr-8Ni-Fe alloy

Ref: J. Sedriks,
"*Corrosion of Stainless Steels*"

2.5.1 SCC in Piping

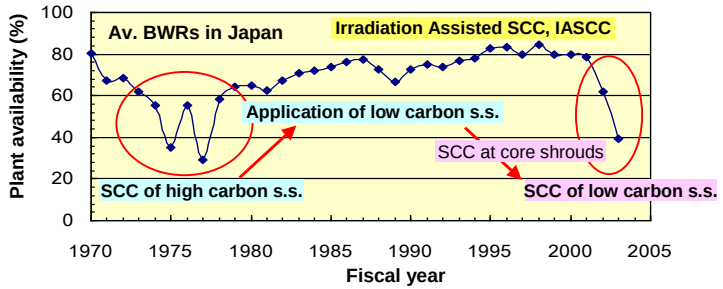

Updated

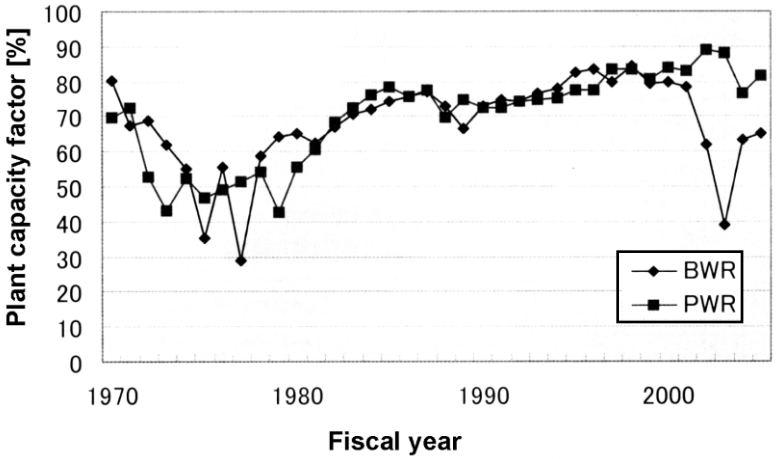

Fig. The history of LWR plant utilization rate in Japan.
T. Isogai; Maintenology, Vol. 6, No. 2, (2007) pp.23-28

Capacity Factor Losses Due to Corrosion-Related Damage in BWRs

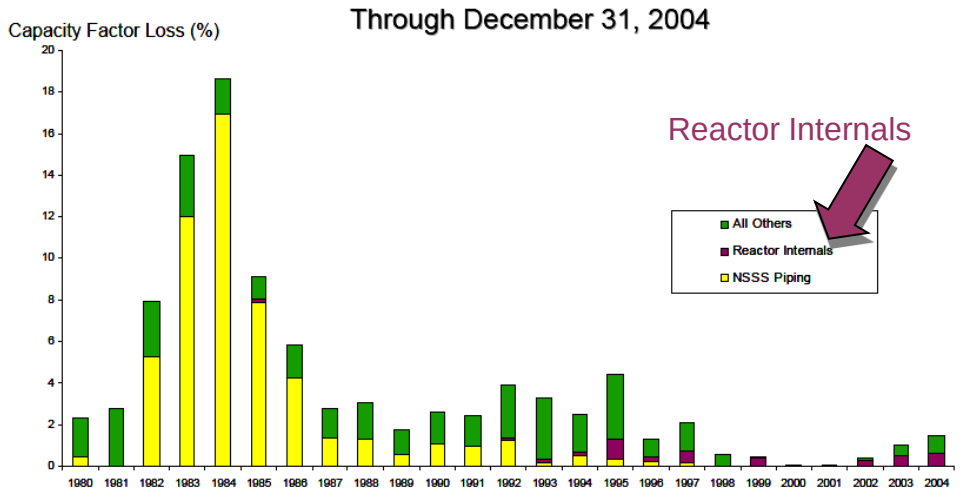

From: "EPRI's R&D Programs on Materials Degradation in LWR's" by Robin Jones, RIC 2006, Session Th5BC, Materials Degradation, March 9, 2006 (http://www.nrc.gov/public-involve/conference-symposia/ric/past/2006/)

Operational history of NPPs clearly shows the influence of material degradation due to various type of corrosion and SCC phenomena.

2.5.1 SCC in Piping

Type F316 SS(Forged material)
(0.016%C,16.7%Cr,12.7%Ni,2.6%Mo)
Operation condition:
・Temp.: about 275ºC , ・Pressure: about 70 kg/cm^2
・DO content: about 150 ppb, ・Conductivity: about 0.08 μS/cm

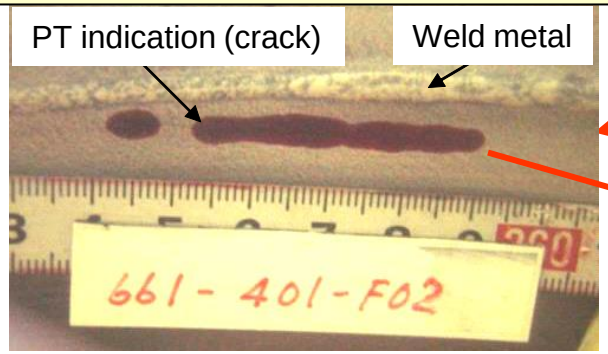

Indication image in Penetration Test (PT)

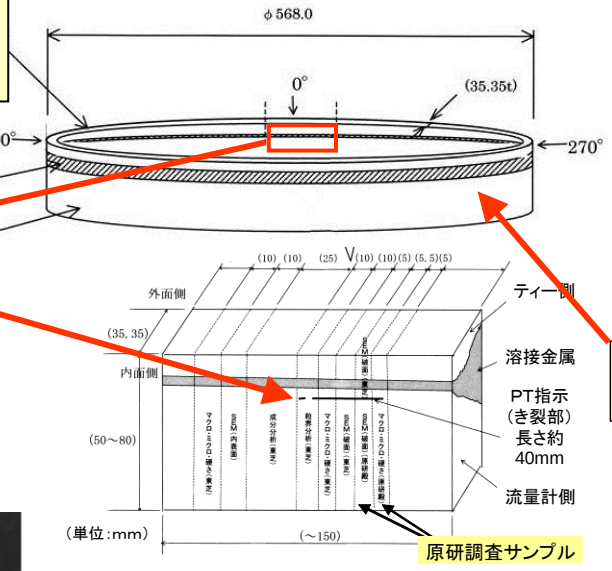

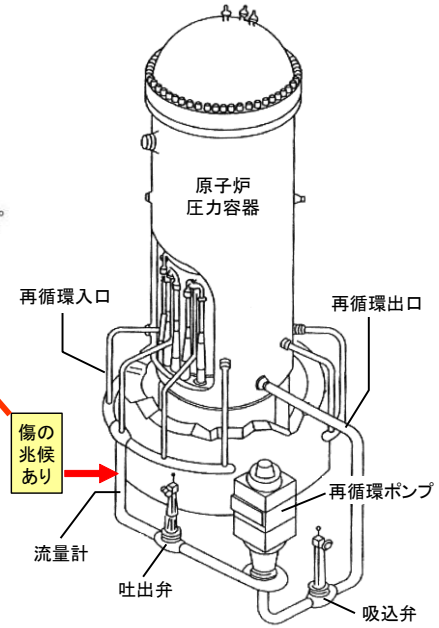

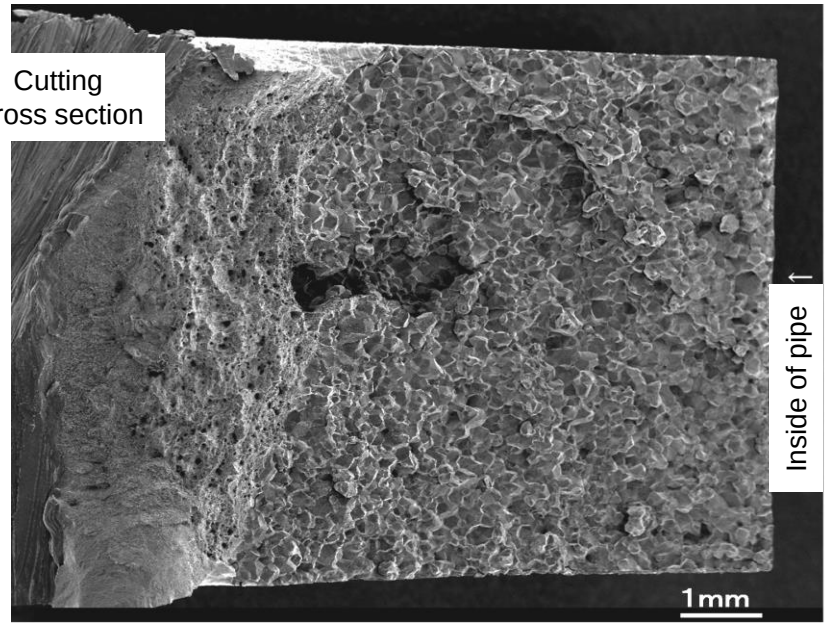

SEM observation of fracture surface
(Intergranular cracking on almost whole surface)

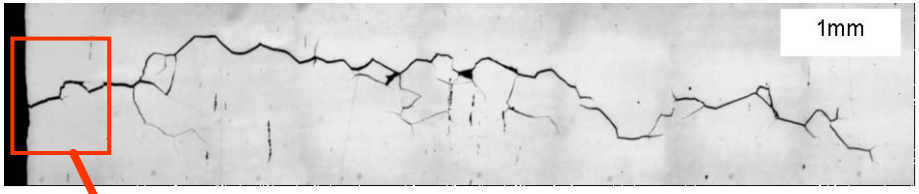

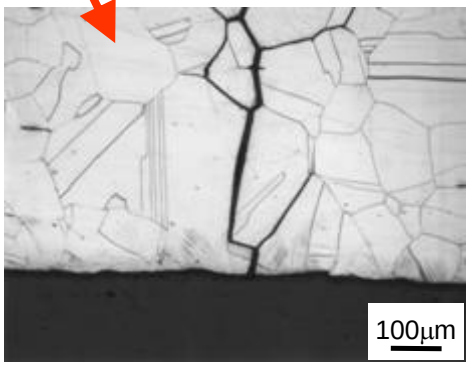

Hardened microstructure near surface
(Slip lines)

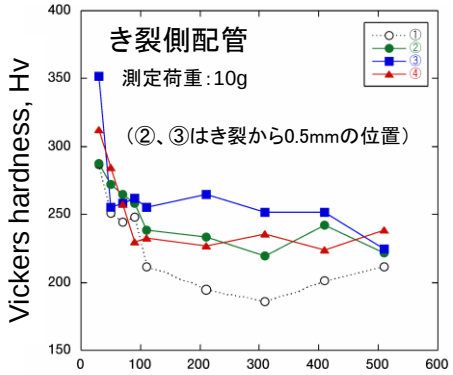

Distance from surface, μm

(JAERI-Tech2004－003)

2.5.2 SCC in Core Shroud

BWR: Boiling Water Reactor

Core shroud

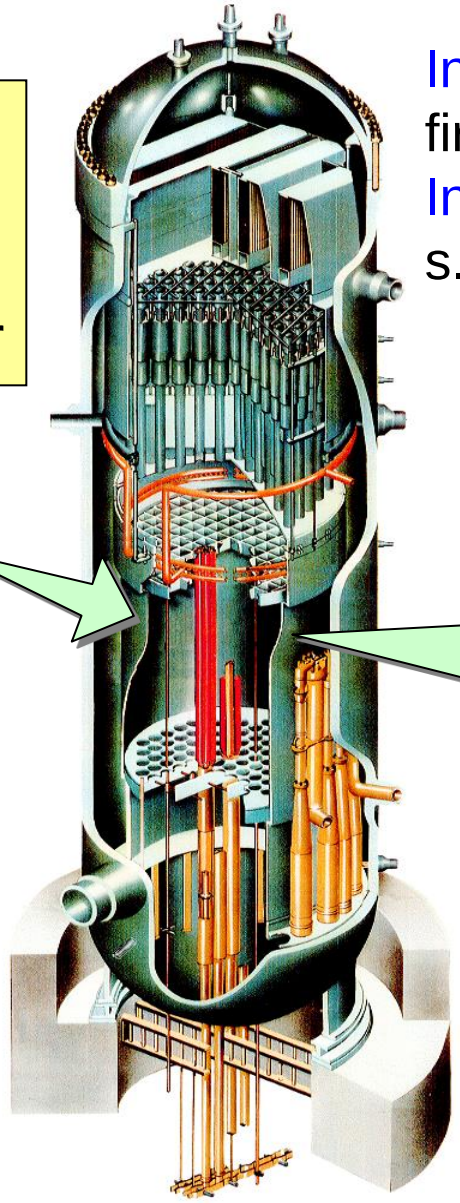

In 1990, cracking of core shroud was reported first at the Swiss NPP, and in 1994, in Japan. In 2001, cracking of a shroud made from 316L s.s. was reported from Fukushima NPP (2F3).

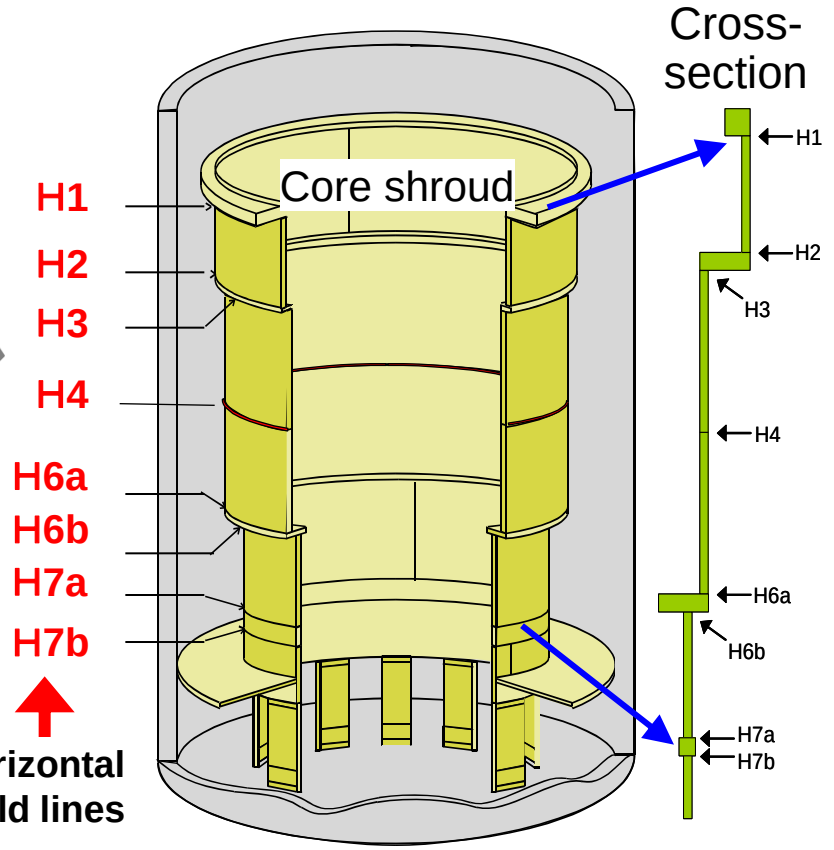

2.5.2 SCC in Core Shroud

SUS 316L
1.3X10^{22} n/m^2 (E>1MeV)

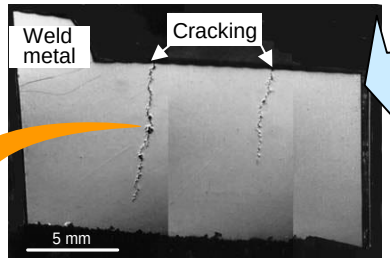

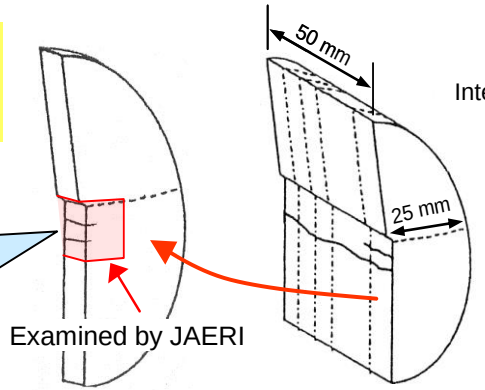

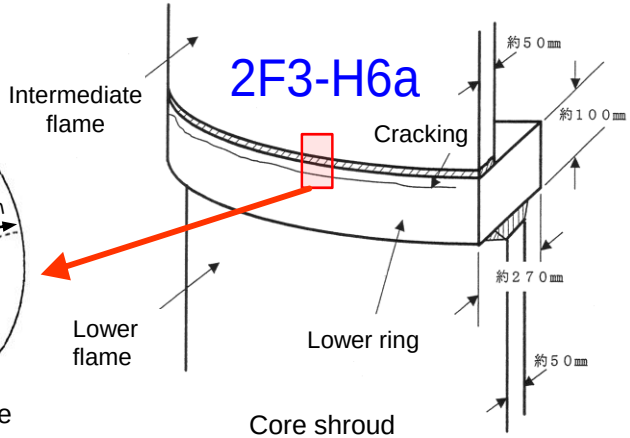

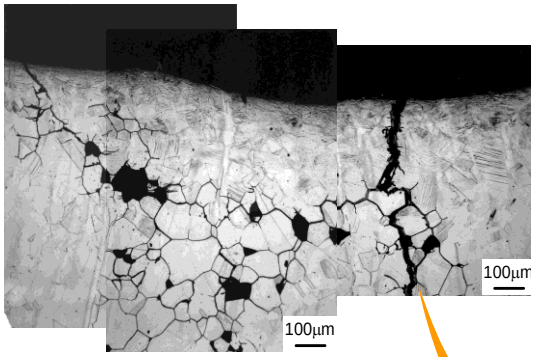

Cracking near outer surface

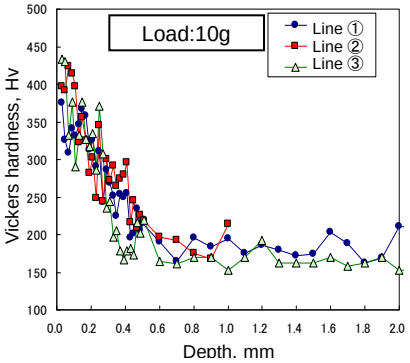

Hardness profile near surface

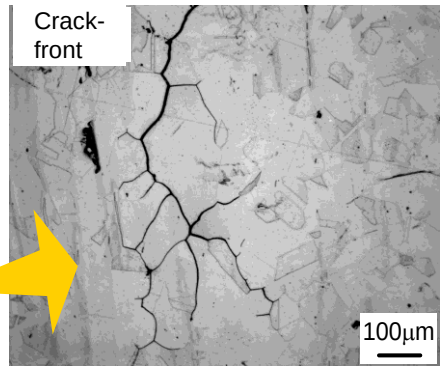

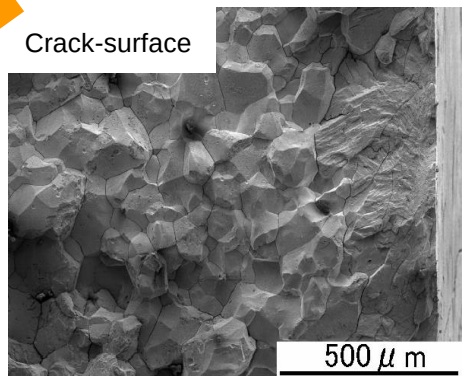

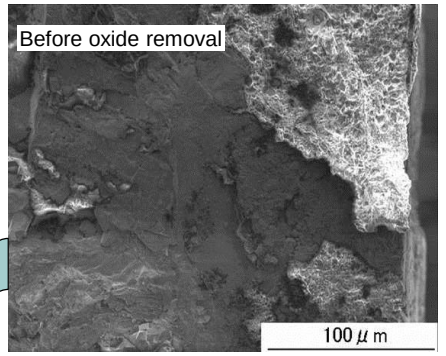

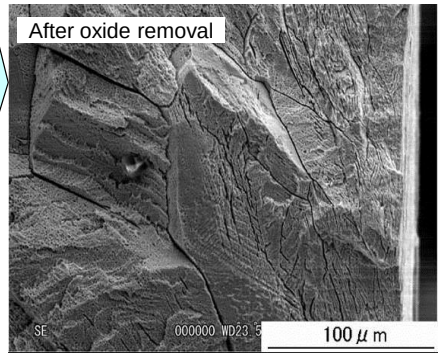

Cracking near outer surface

Ref.: JAERI-Tech 2004-044 (2004)

2.5.2 SCC in Core Shroud

Evaluation of SCC growth
- Rules on Fitness-for-Service for Nuclear Power Plants (JSME) -

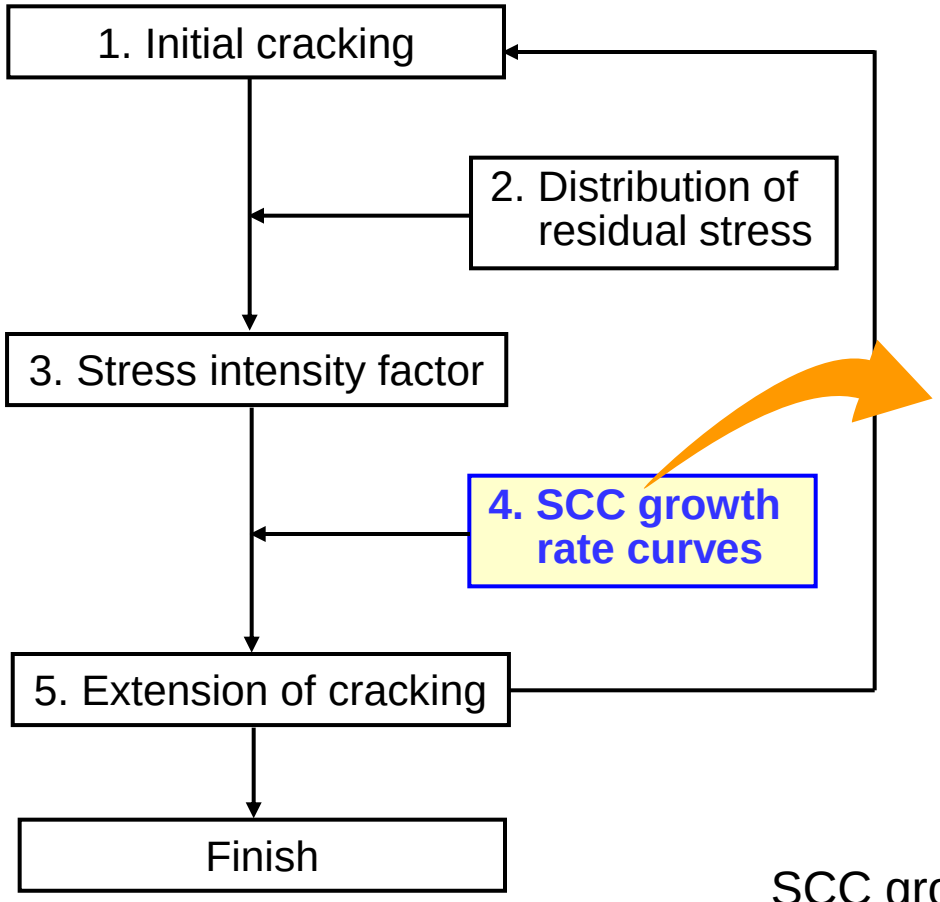

Flow of evaluation of SCC growth

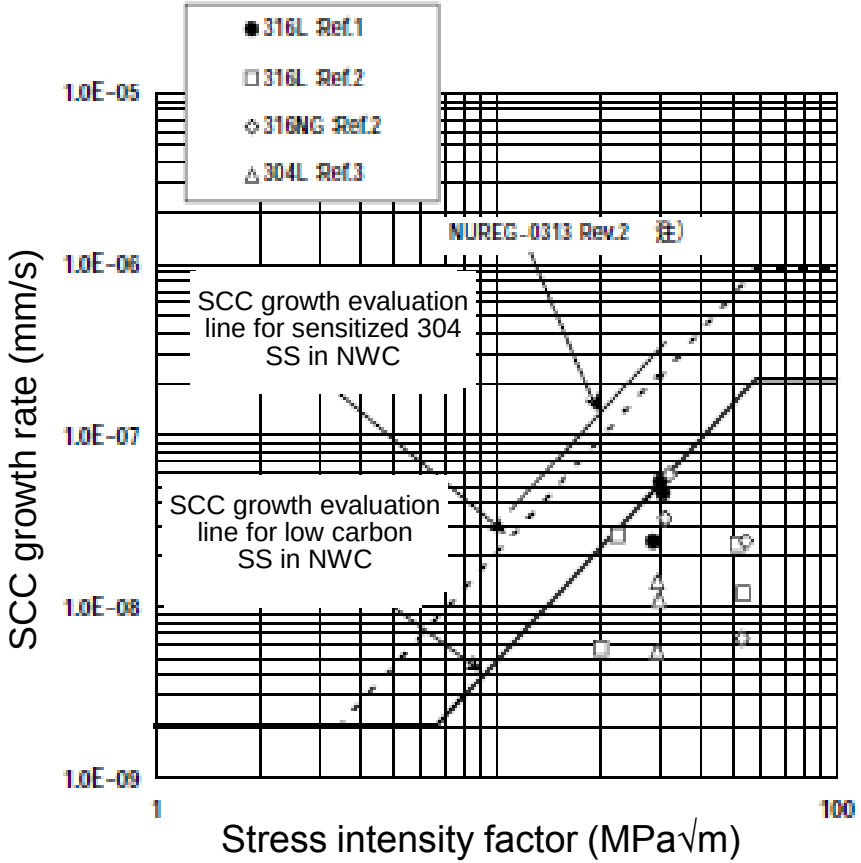

SCC growth rate vs. Stress intensity factor curves

Ref.: Nuclear and Industrial Safety Agency, Report on structural integrity evaluation for core shroud and PLR piping, Oct. 22, 2004.

2.5.3 SCC Mechanism of Low Carbon SSs

J. Kuniya: 3rd E.D.M. (1988) p.383

Influence of hydrogen on CBB tests of cold-worked non-sensitized Type 304 SS

(＊CBB: Creviced Bent Beam)

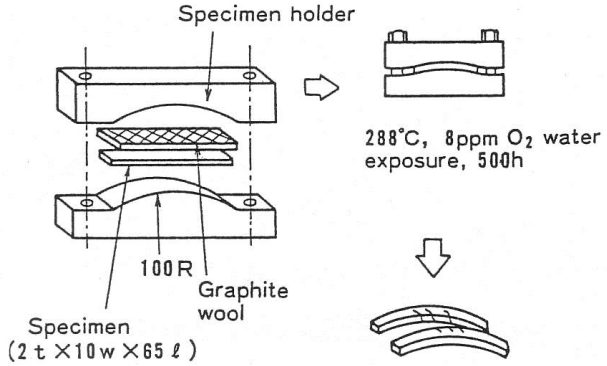

Figure 1 Crevice bent beam (CBB) test method

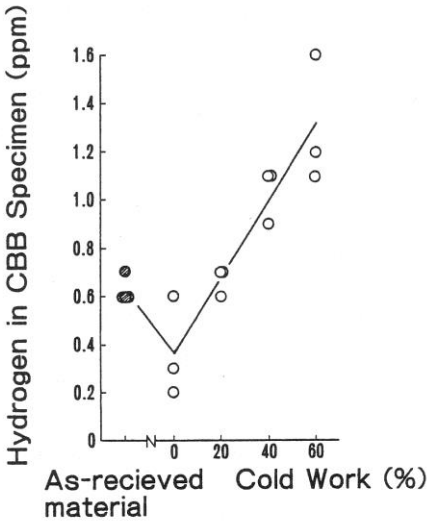

Figure 4 Hydrogen in CBB specimens analyzed just after testing as a function of the degree of cold work

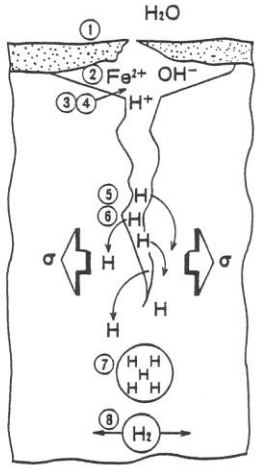

① rupture of film
② formation of crevice
③ consumption of oxygen

$O + 2H_2O + 4e \rightarrow 4OH^-$

④ pH drop

$Fe \rightarrow Fe^{2+} + 2e^-$

$Fe^{2+} + H_2O \rightarrow FeOH + H^+$

⑤ cathodic reaction
⑥ diffusion of H into metal
⑦ trapping of H
⑧ crack initiation

Figure 13 Schematic modeling for SCC in cold worked, annealed Type 304SS in 288°C water containing 8 ppm dissolved oxygen

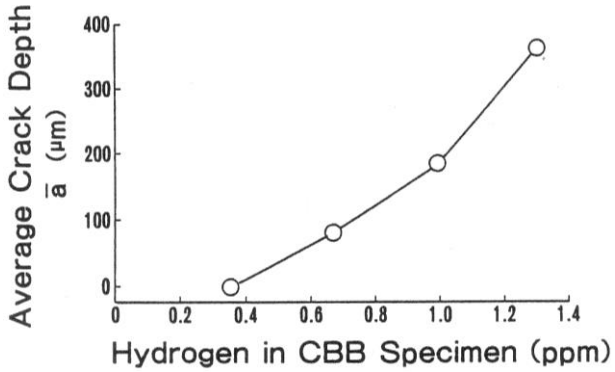

Figure 5 Correlation of average crack depth, ā, and hydrogen in CBB specimens

SCC of non-sensitized Type 304 SS was also initiated in CBB tests. Relationship between SCC and hydrogen contents was investigated.

2.5.3 SCC Mechanism of Low Carbon SSs

A. Sudo: 6th E.D.M. (1993) p.251

It was confirmed that IGSCC was observed in crack growth test of Type 316L SS under high conductivity conditions.

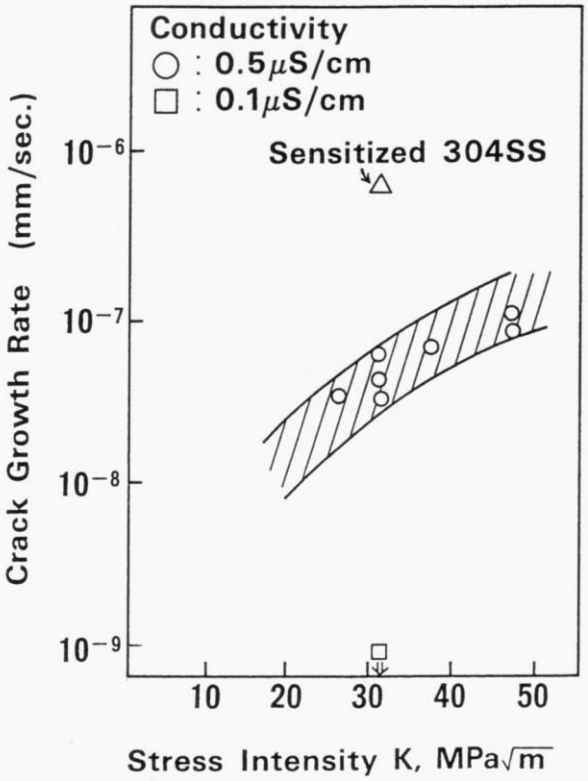

Figure 3- SCC growth rate of Type 316L stainless steel as a function of stress intensity factor, K in 288℃ water containing 0.2 ppm O_2 and conductivity of 0.5 and 0.1 uS/cm.

Relationship between stress intensity factor K and crack growth rate

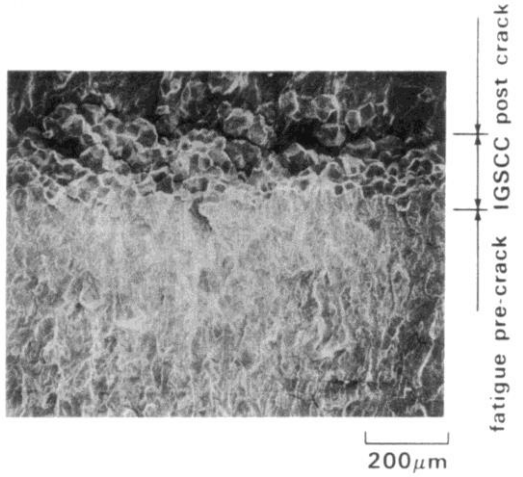

Figure 4- Fracture surface morphology of environmental cracking of Type 316L after SCC growth test at K=37 Mpa/m in 288 ℃ water containing 0.2 ppm O_2 and conductivity of 0.5 uS/cm.

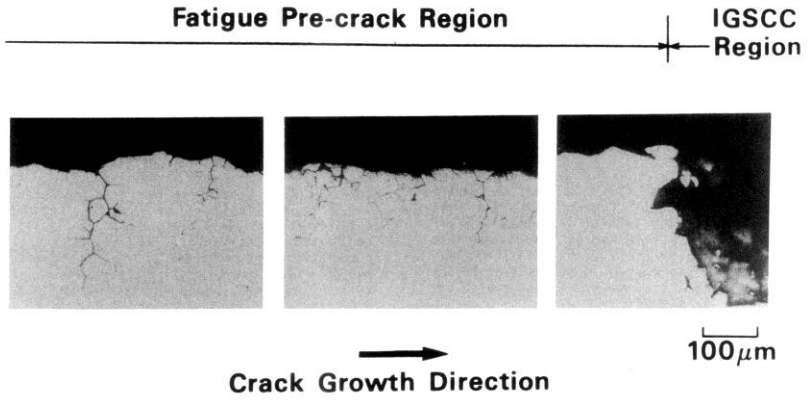

Figure 6- Longitudinal section of crack growth specimen of Type 316L after SCC growth test at K=37 MPa/m in 288℃ water containing 0.2 ppm O_2 and conductivity of 0.5 uS/cm.

2.5.3 SCC Mechanism of Low Carbon SSs

A. Jenssen: 7th E.D.M. (1995) p.553

It was confirmed that SCC growth rate highly increased with increase of cold work in Type 316NG SS.

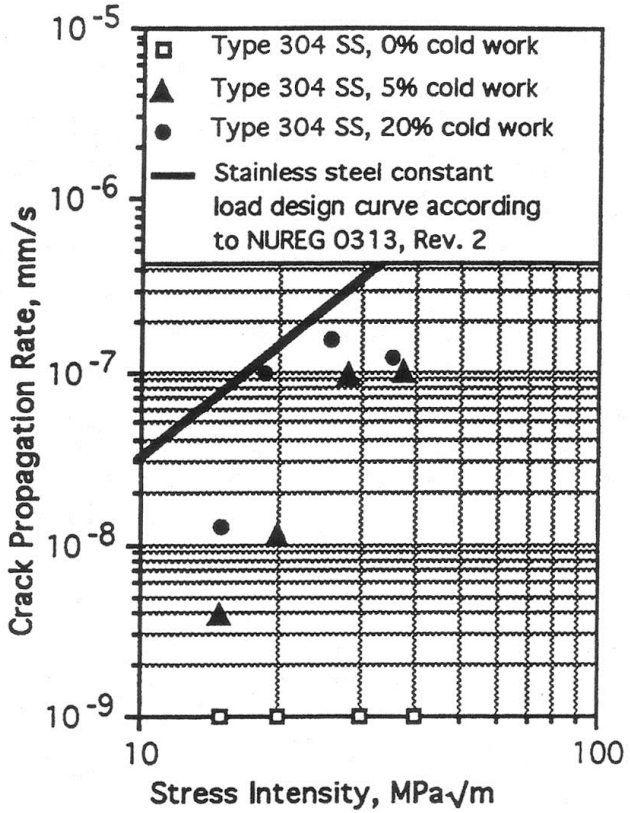

Figure 7. Crack propagation Rates for Cold Worked Type 304 SS

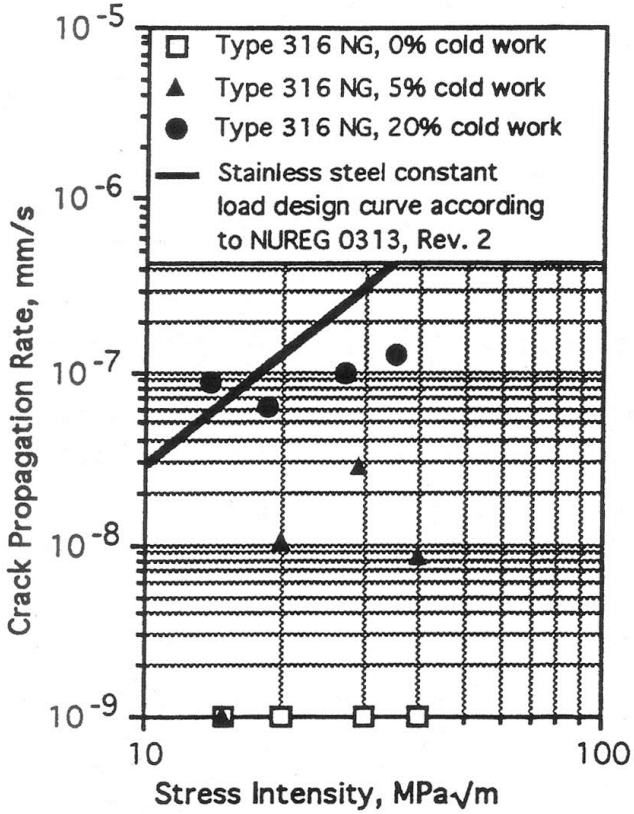

Figure 8. Crack propagation Rates for Cold Worked Type 316 NG Stainless Steel

K dependence on SCC growth rate is small in low carbon SS by cold work.

2.5.3 SCC Mechanism of Low Carbon SSs

M. Tsubota: 7th E.D.M. (1995) p.519

Relationship between cold work and SCC initiation was investigated in CBB test of Type 316L/304 SSs. (＊CBB: Creviced Bent Beam)

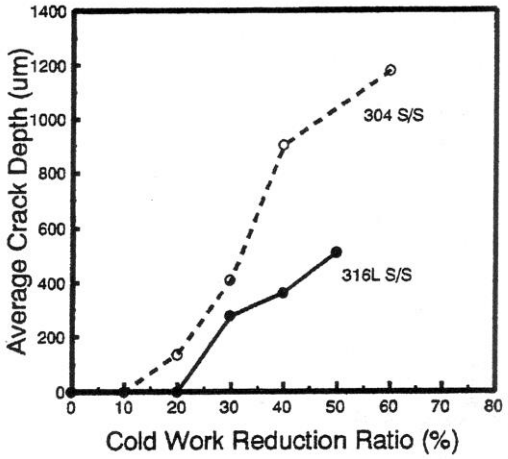

Fig. 2 CBB test results in 288°C high temperature water for cold rolled 304 S/S and 316L S/S.

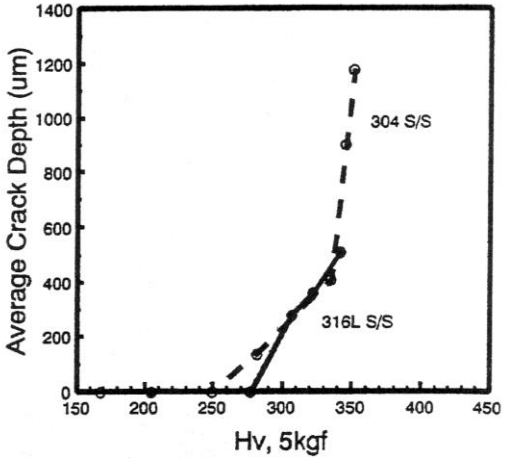

Fig. 3 Average crack depth measured in CBB specimens versus Vickers hardness.

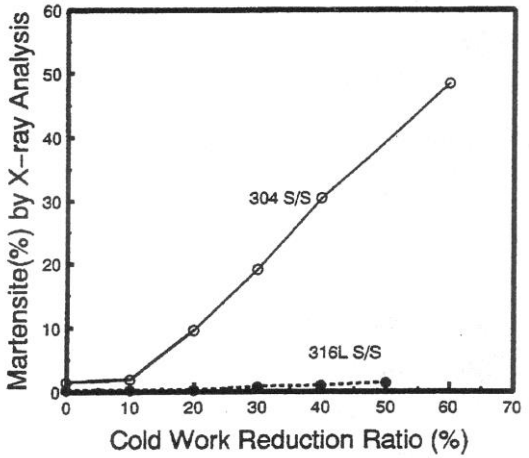

Fig. 4 Quantity of martensite estimated by X-ray Analysis for cold rolled 304 and 316LS/S.

TGSCC was initiated and susceptibility increased with increase of cold work reduction ratio.

Critical hardness in TGSCC initiation is Hv=300 in Type 316L SS and Hv=270 in Type 304 SS.

Martensite is not a control factor of TGSCC by cold work.

Cold work reduction ratio correlate with TGSCC initiation susceptibility in CBB test under high dissolved oxygen (DO) condition of Type 316L SS.

2.5.3 SCC Mechanism of Low Carbon SSs

Nishimoto, et al.: Proc. of the 52nd Japan Conference on Materials and Environments (2005) p.185

Influence of cold work on grain boundary sliding behavior was investigated in Type 316LN SS.

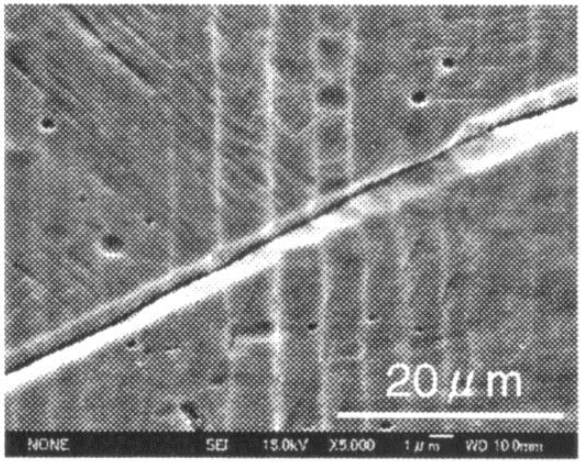

Fig.3 Surface appearance of tensile tested specimen.

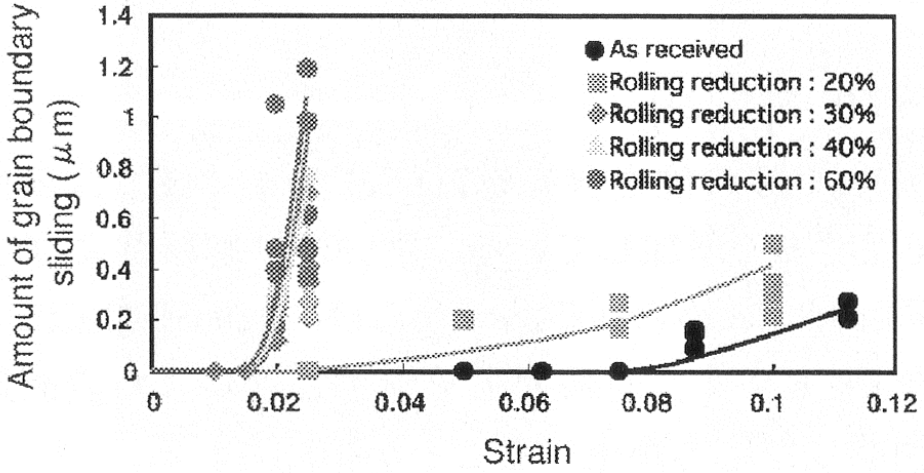

Fig.4 Relationship between strain and amount of grain boundary sliding.

It was found that grain boundary sliding was initiated in stress of above 500 MPa in constant strain rate test (strain rate=1.25X10^{-4}/s).

In cold work material, grain boundary sliding was initiated in lower strain condition and increase of amount of grain boundary sliding is remarkable compared in as received material.

It is considered that grain boundary energy increase with increase of amount of grain boundary sliding and encourage grain boundary corrosion.

2.5.3 SCC Mechanism of Low Carbon SSs

Y. Kaji, et al.: Japan Institute of Metal 2006 Autumn Meeting

Plastic strain distribution was investigated near crack tip of CT specimen of Type 316L SS by EBSD method.

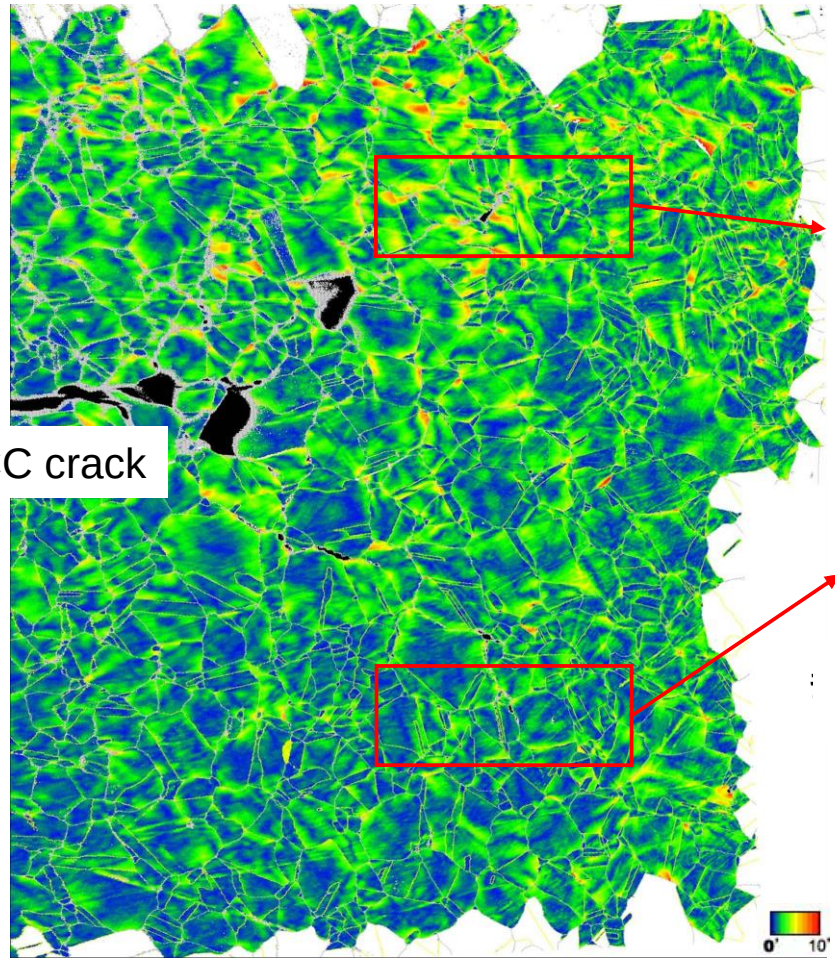

Misorientation distribution near crack tip

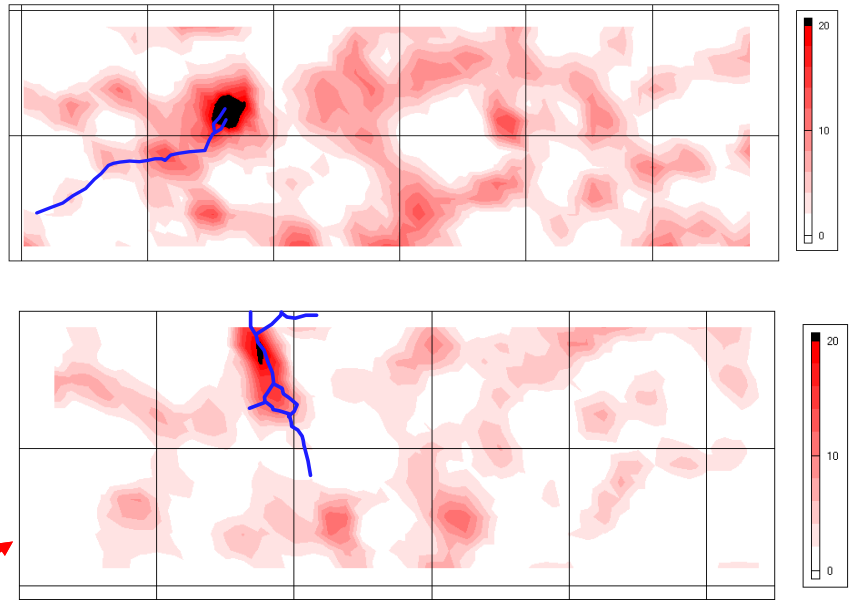

Plastic strain distribution near crack tip
(1 grid=200μm square)

- About 10-20% plastic strain generated at crack tip, and steep strain gradient was found within 1 or 2 grains.

2.5.3 SCC Mechanism of Low Carbon SSs

- Analysis of Grain Boundary Character near SCC -

Grain boundary character is known to influence crack growth path and segregation of chemical elements at grain boundary (GB). Relationship between cracked and the other grain boundaries was investigated by scanning electron microscope with Electron Back-Scattering Diffraction pattern (EBSD). Crystal orientation was measured in step interval and classified for misorientation degree into four categories which were small angle（Σ1）, twin（Σ3）, CSL（Σ5～Σ27）and the other GBs.

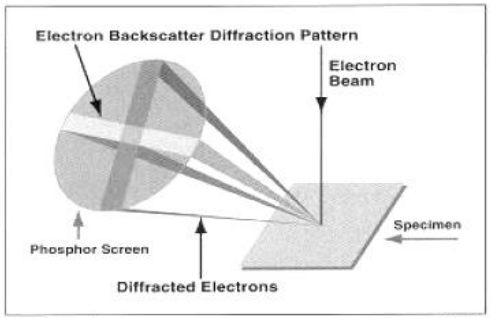

(a) EBSP(Electron Backscatter diffraction Pattern)装置の概念図

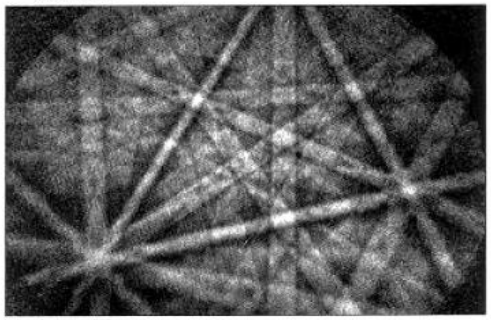

(b) カメラに写る菊地線の例
この白黒の線の角度関係を計算し結晶方位を求める。

Schematic drawing of EBSD and diffraction pattern

- Orientation map around crack

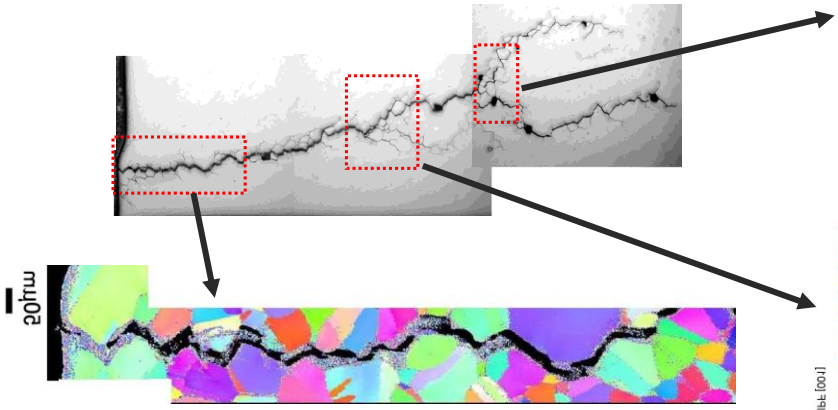

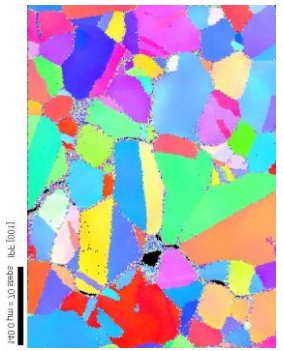

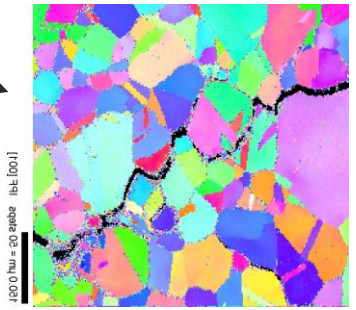

Main cracks extended with many secondary cracks.
Branched and discontinuous cracks were observed.

Y. Miwa, et al.: Proc. of the 52nd Japan Conference on Materials and Environments (2005)

2.5.3 SCC Mechanism of Low Carbon SSs

Local corrosion resistance on the hardened layer which had been carried out surface machining was investigated by atomic force microscope (AFM) after electro-chemical corrosion testing.

Y. Nemoto, et al.: Proc. of the 52nd Japan Conference on Materials and Environments (2005) p.197

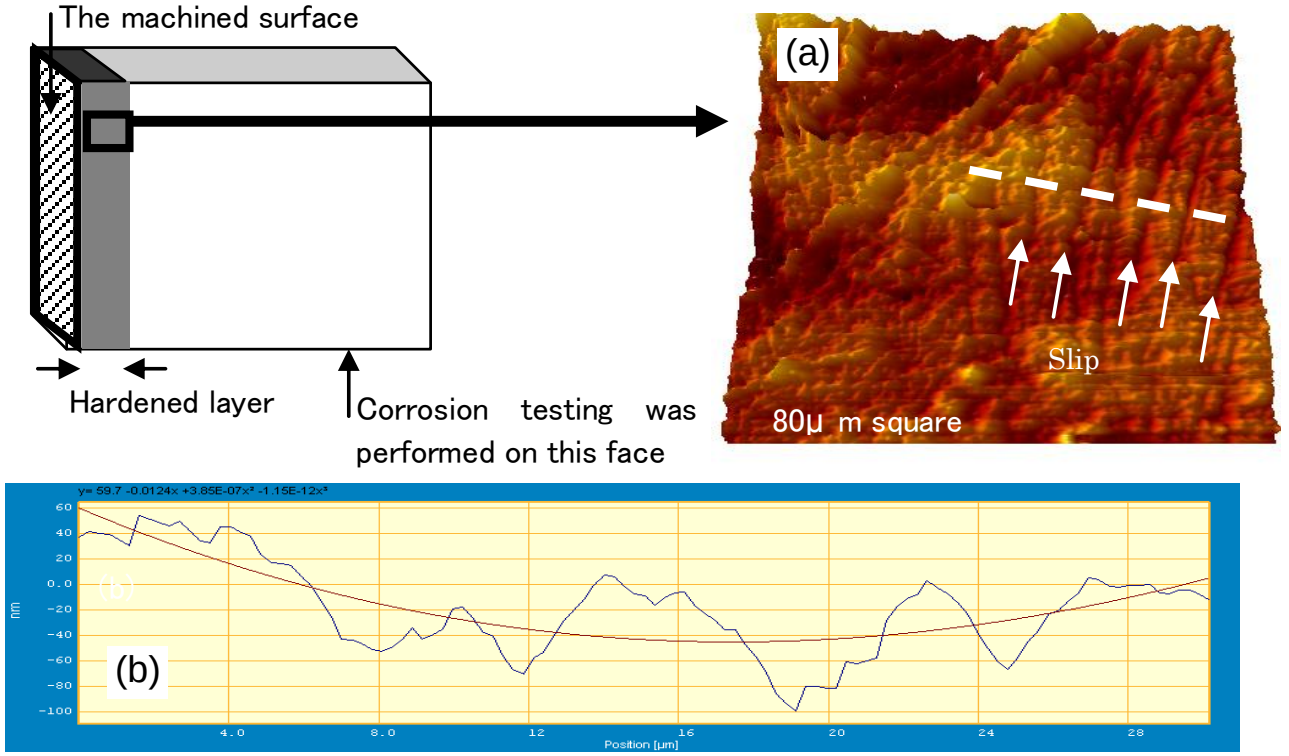

Fig.3 (a) Results of AFM observation after electro-chemical corrosion testing on the SUS316L specimen which had been carried out surface machining.
(b) The height distribution along the line drawn in the Fig.3(a).

From results of AFM observation, preferred corrosion was observed in hardened layer, especially slip line portion.

2.5.3 SCC Mechanism of Low Carbon SSs

AFM observation was performed near SCC cracks of core shroud material after electro-chemical corrosion test.

Y. Nemoto, et al.: Proc. of the 52nd Japan Conference on Materials and Environments (2005) p.197

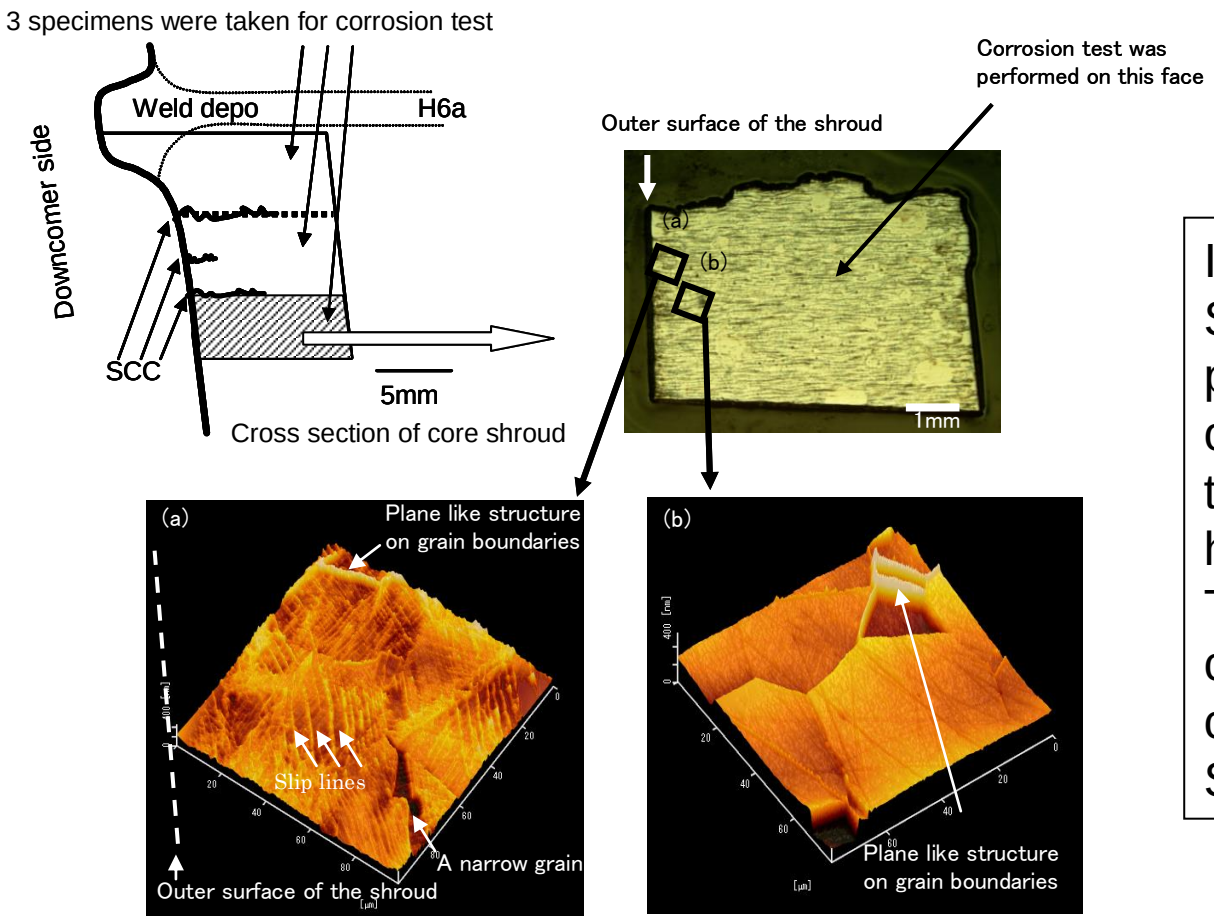

In low carbon Type 316L SS used in core shroud, preferred corrosion was observed in grain rather than grain boundary in hardened layer.
This phenomenon is considered to be one of cause of transgranular SCC initiation.

Fig.4 AFM topography observed after corrosion test on the cross sectional area of the shroud specimen. (a) Hardened layer near the surface. (b) Matrix layer.

2.5.3 SCC Mechanism of Low Carbon SSs

F. Ueno, et al.: Proc. of the 52nd Japan Conference on Materials and Environments (2005) p.193

Microscopic magnetic structure of surface hardened layer was measured by magnetic force microscope (MFM) and investigated relationship between SCC initiation and martensite phase.

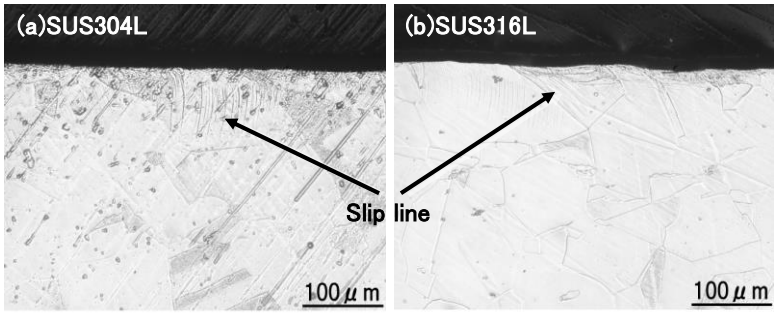

Fig.2 Microscopic images of surface hardened layers

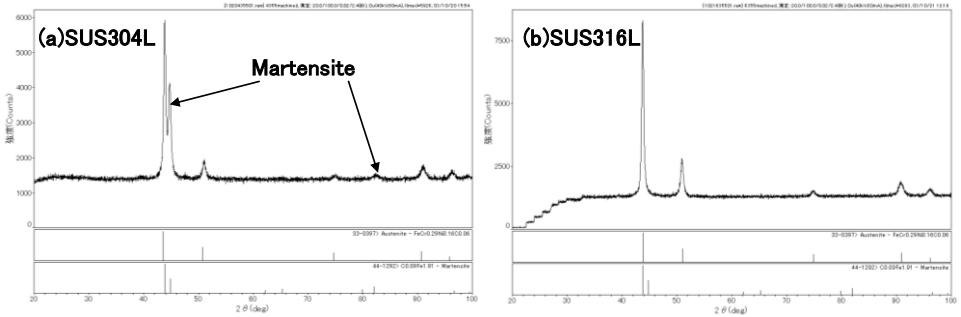

Fig.4 X-ray Diffraction patterns of surface hardened layers of stainless steels

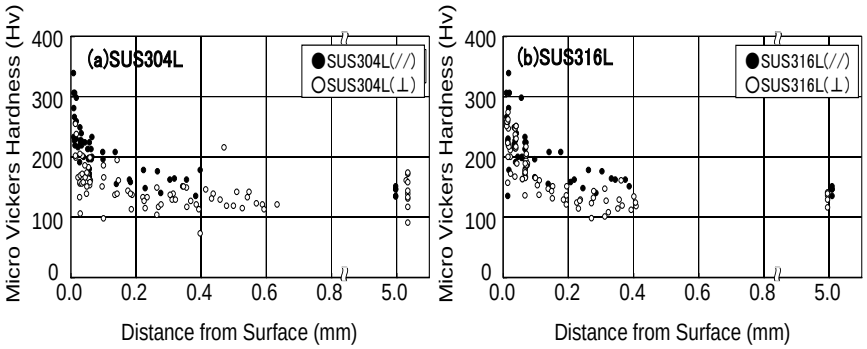

Fig.3 Hardness profiles of surface hardened layers of stainless steels

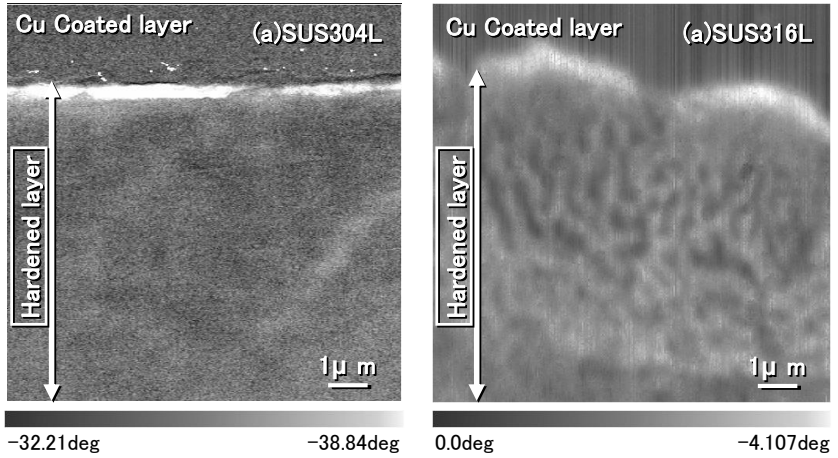

Fig.5 MFM images of cross-sections of surface hardened layers

It was considered that no or very small (nm order) martensite phase (α' phase) was observed in surface hardened layer of Type 316L SS. Magnetic phase in surface layer is not only martensite phase but also self-magnetization by large residual strain and plastic deformation.

2.5.3 SCC Mechanism of Low Carbon SSs

Y. Miwa,et al.: Proc. of the 52nd Japan Conference on Materials and Environments (2005) p.189
K. Kondo, et al.: Japan Institute of Metal 2005 Autumn Meeting

In order to investigate local chemical composition of core shroud material in high spatial resolution, 3-dimensional atom probe (3DAP) observation was performed in grain and grain boundary.

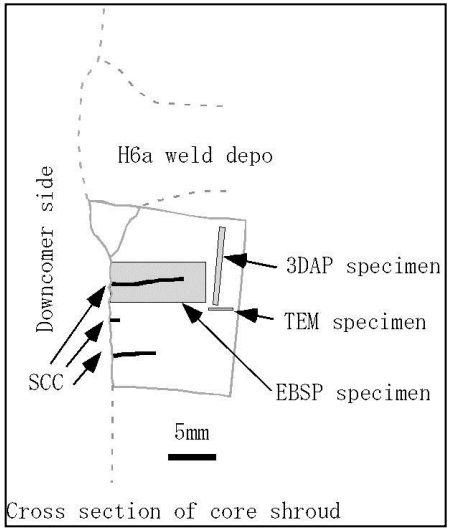

Fig.1 boat sample

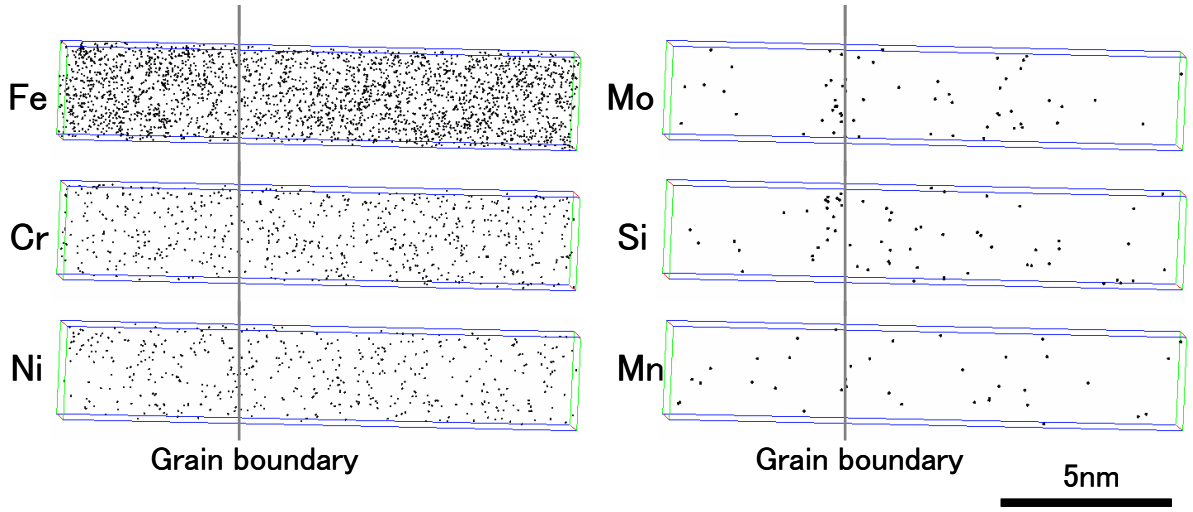

Fig.4 Atom maps at grain boundary on shroud sample

From 3DAP results in region of about 8×9×100nm including grain boundary, enrichment of Ni, Si and Mo was observed in 2nm width at grain boundary and no Cr depletion was observed. Amount of segregation in Si and Mo is larger than that of FE-TEM analysis and average amount of Si in 2nm region is about 8 at% (about 2 at% in EDX analysis) and about 10 at% (about 4 at% in EDX analysis) in Mo.

2.5.3 SCC Mechanism of Low Carbon SSs

3-Dimensional Atom Probe（3DAP）:

In 1988, by applying a position sensitive detector to a time-of-flight atom probe, Cerezo, Godfrey and Smith at the University of Oxford succeeded in determining both the mass to charge ratio (m/n) and the position of ions at the same time. It is possible to draw two dimensional element mapping with a subnanometer spatial resolution. Reconstruction of a series of two dimensional element mapping with a graphics workstation make it possible to draw a three dimensional element mapping in a 3D volume of a few nanometer region.

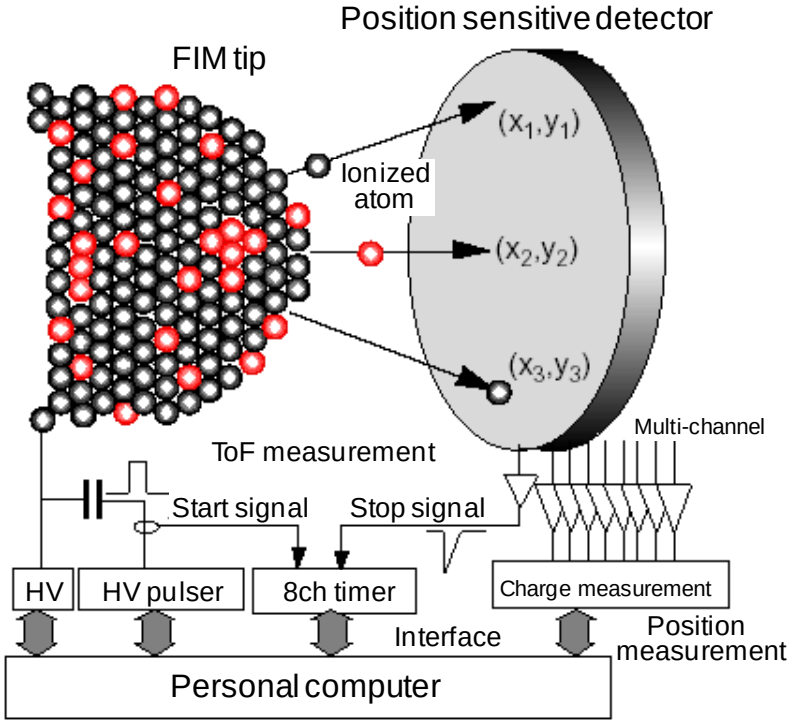

Reference：http://www.nims.go.jp/apfim/tutorial_j.html

A photograph of the three-dimensional atom probe

2.5.3 SCC Mechanism of Low Carbon SSs

Needle like sample and analysis region for 3DAP observation

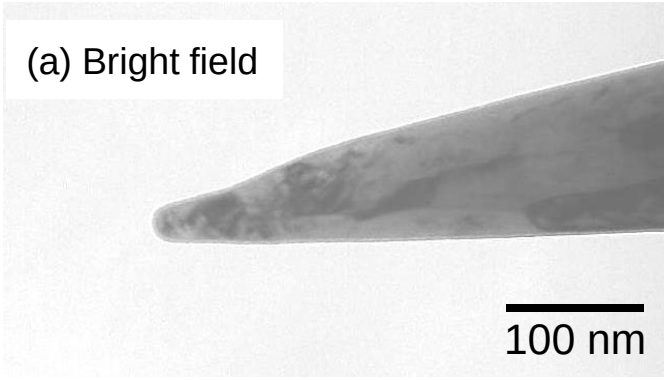

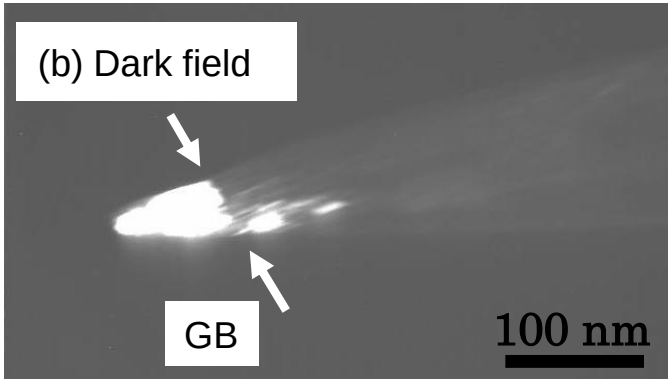

TEM observation

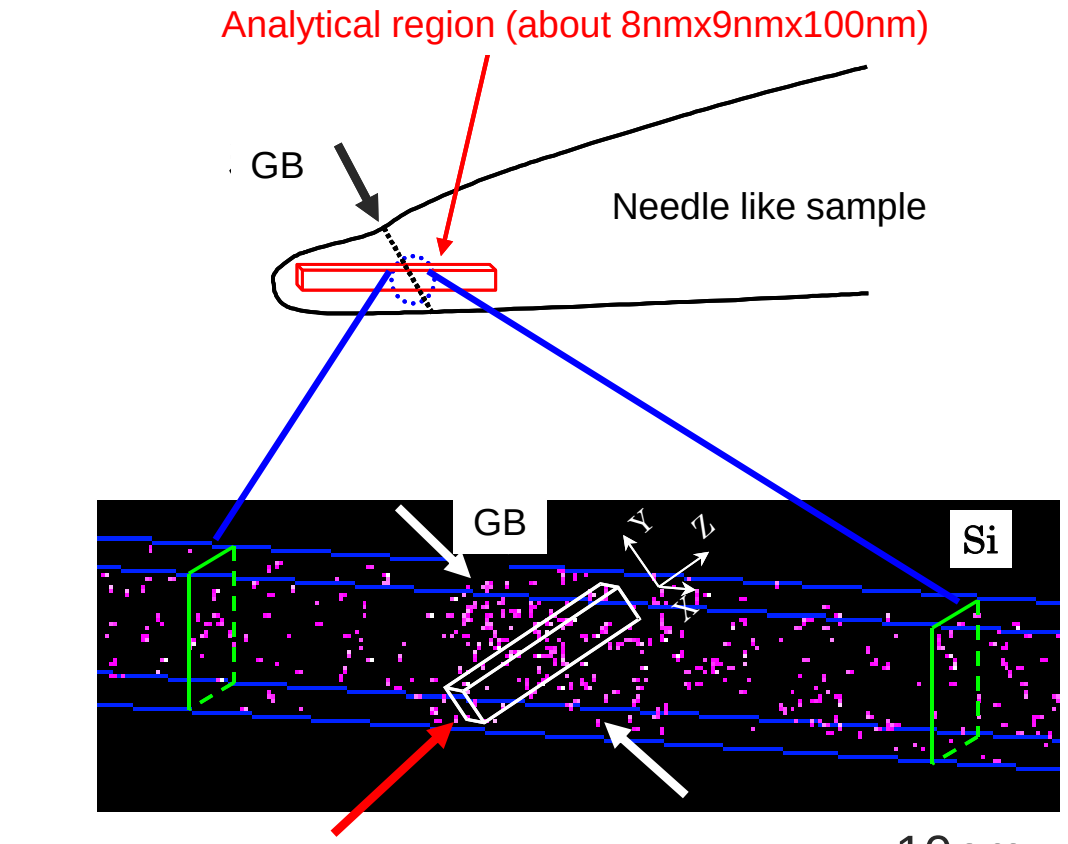

Sampling of analytical region perpendicular to GB

Data area shown in next slide

2.5.3 SCC Mechanism of Low Carbon SSs

Evaluation of solute elements distribution at grain boundary

1.4 nm × 3.5 nm × 19 nm

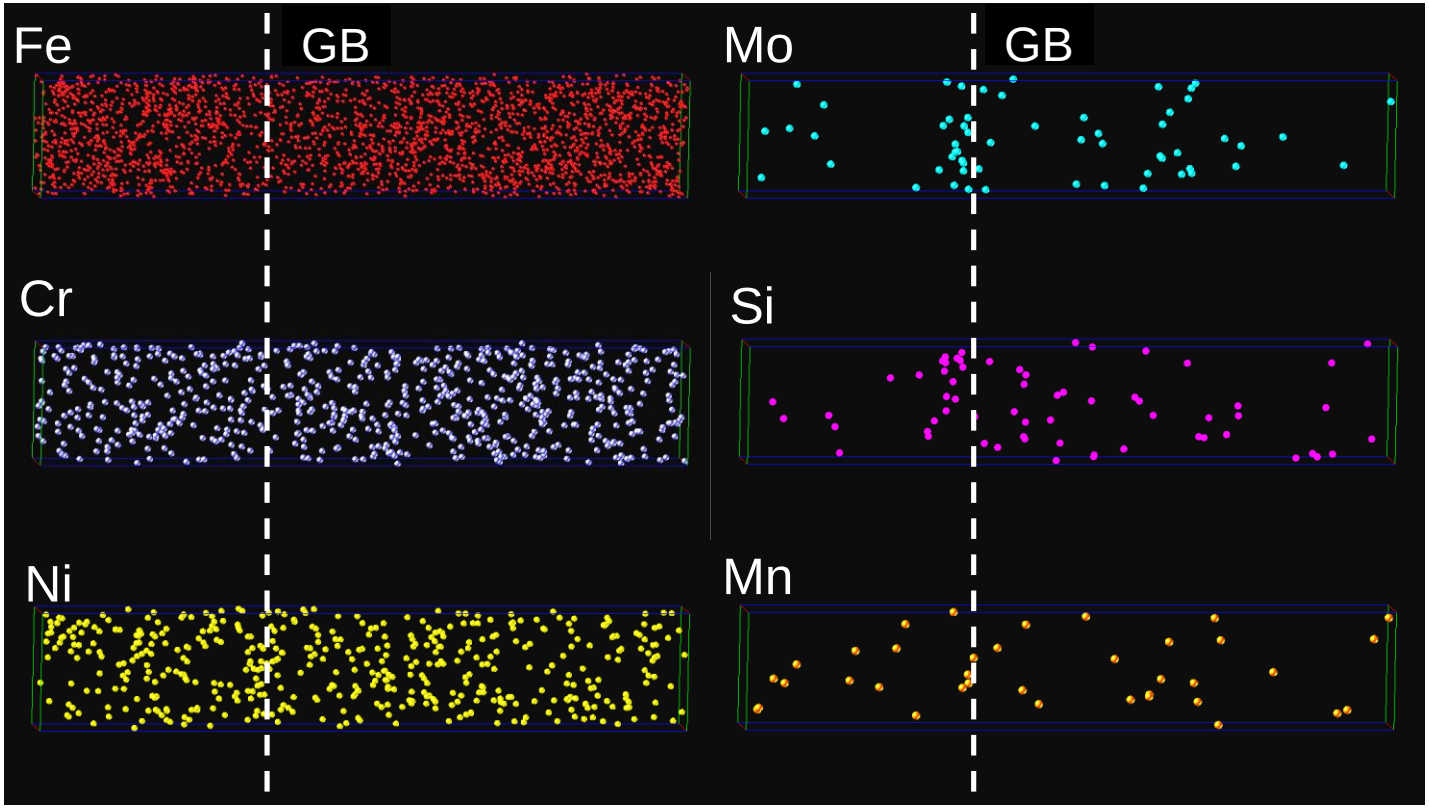

Solute segregation was segregated in about 2nm near grain boundary.

Dilution: Fe Enrichment: Ni, Mo, Si Uniform distribution: Cr, Mn

3DAP analysis results of solute elements distribution near grain boundary of core shroud (Type 316L SS)

Y. Miwa, et al.: Proc. of the 52nd Japan Conference on Materials and Environments (2005)

2.5.4 IASCC of In-Core Materials

Fluence dependence of SCC phenomena

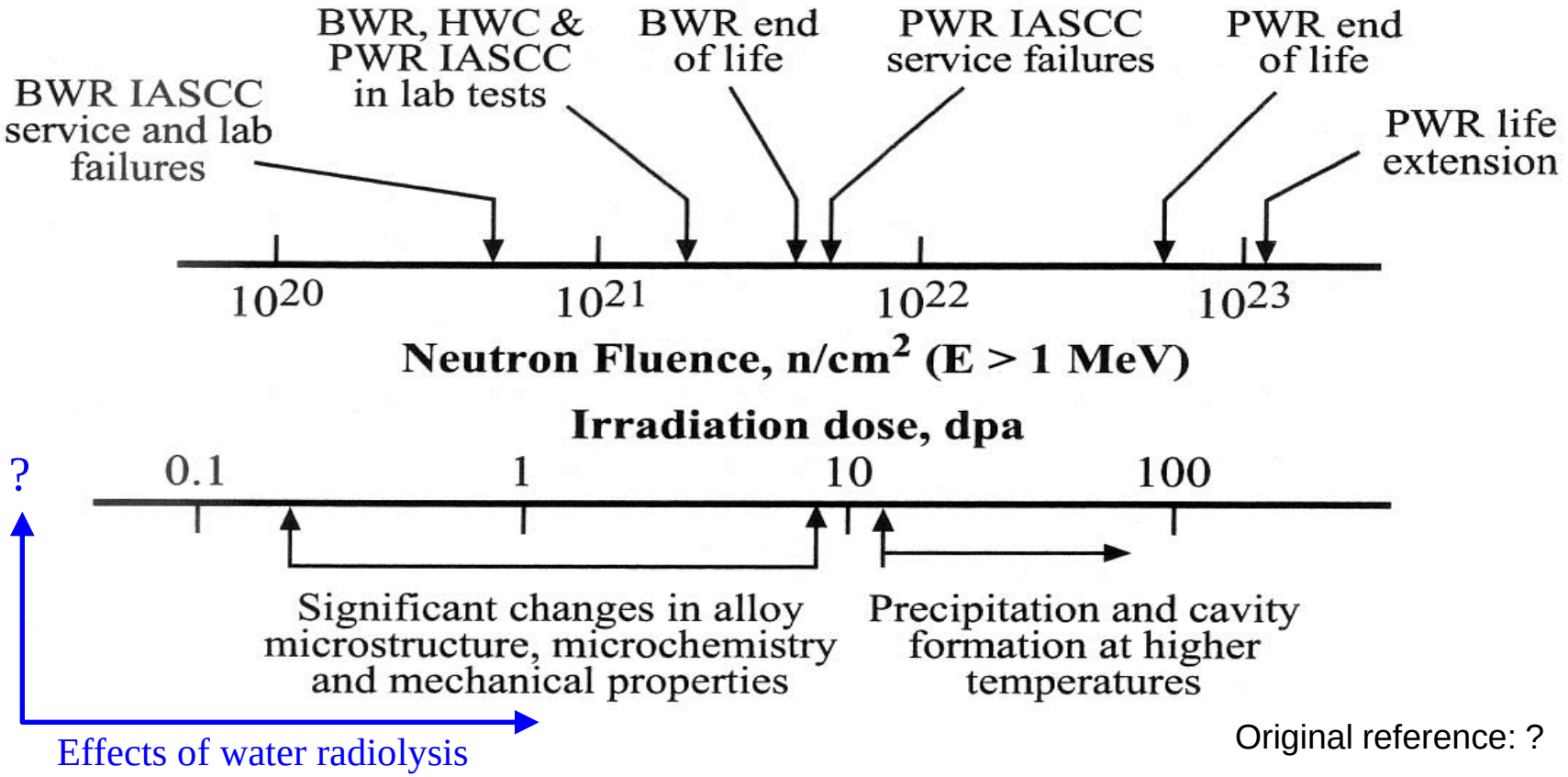

Original reference: ?

For BWR, IGSCC and IASCC must be understood from a viewpoint of continuous effect of neutron/gamma radiation on the material and also on the environment.

IASCC: Irradiation Assisted Stress Corrosion Cracking

2.5.4 IASCC of In-Core Materials

IASCC susceptible parts in BWR

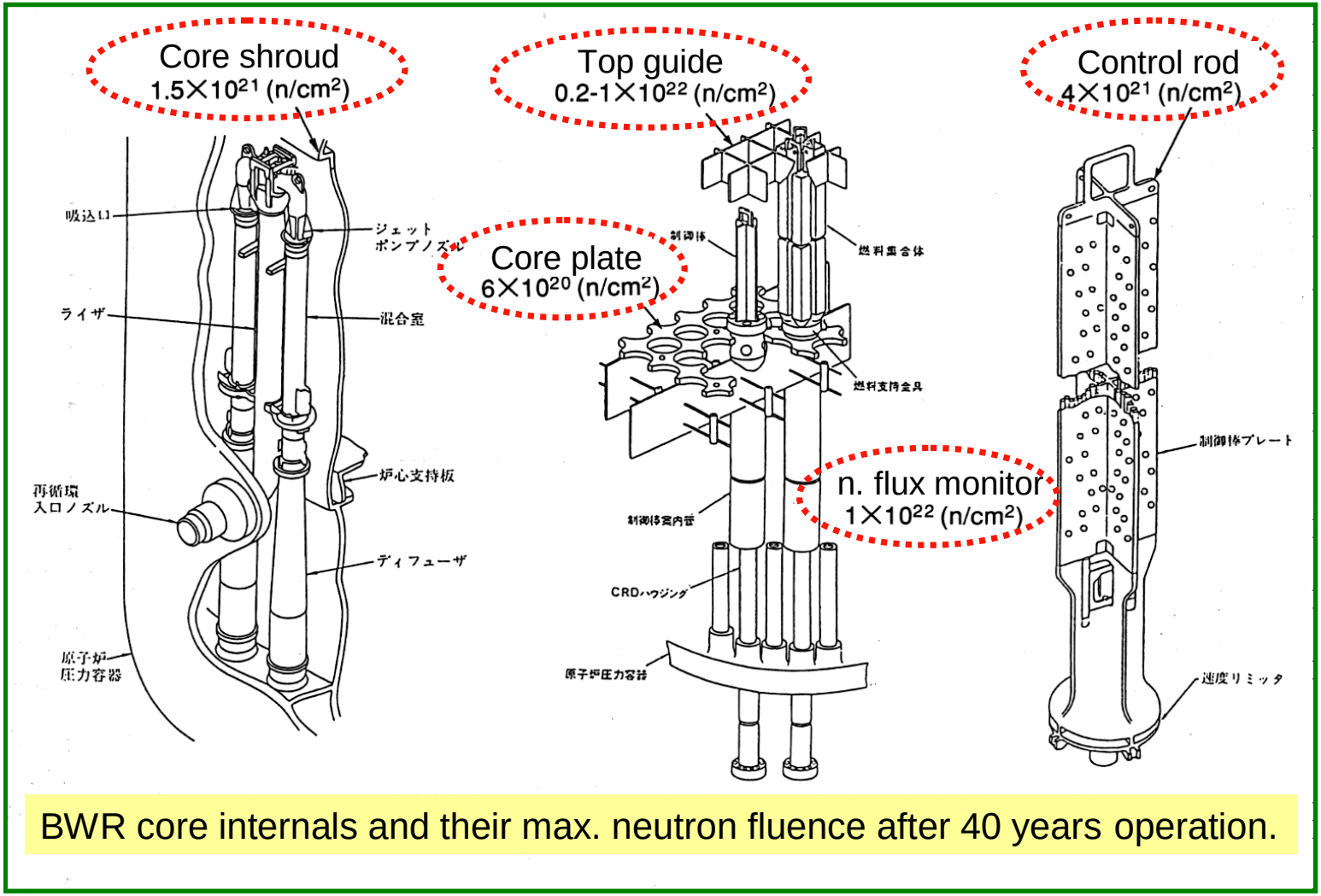

BWR core internals and their max. neutron fluence after 40 years operation.

Various components will be susceptible to IASCC from a viewpoint of the “threshold” fluence, but even below the fluence SCC were observed in BWR.

2.5.4 IASCC of In-Core Materials

IASCC of CR sheath material in BWR inspected in 2006

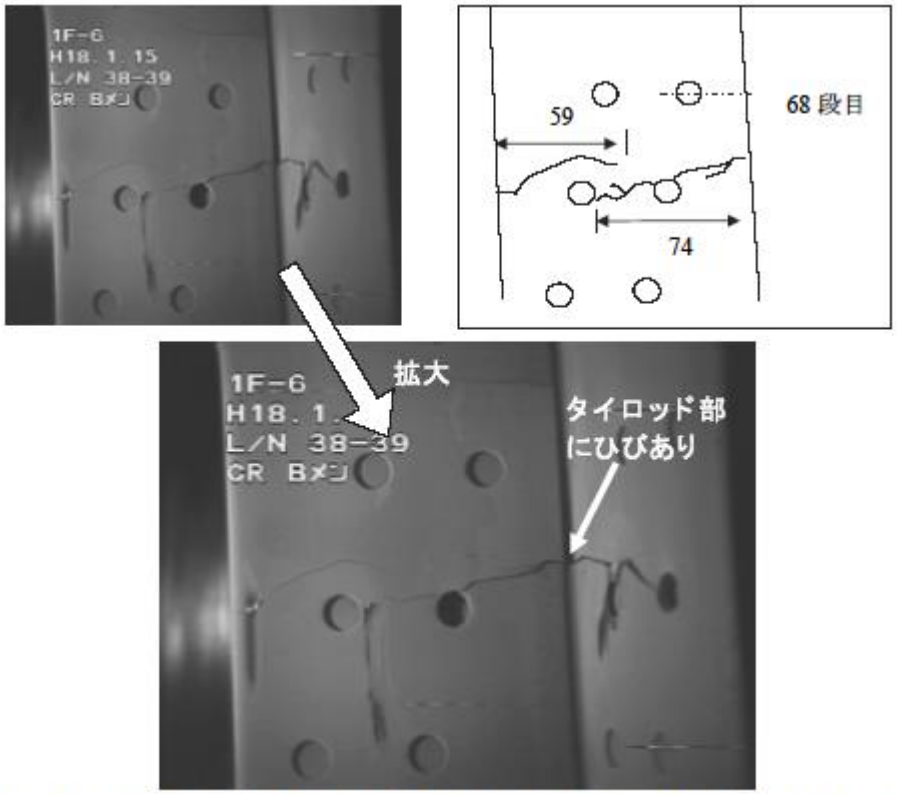

福島第一原子力発電所6号機の例 （制御棒シリアルナンバー99－022：装荷位置38－39）
部位：制御棒下側から68段目の冷却孔付近（シース下端から3443mm上）

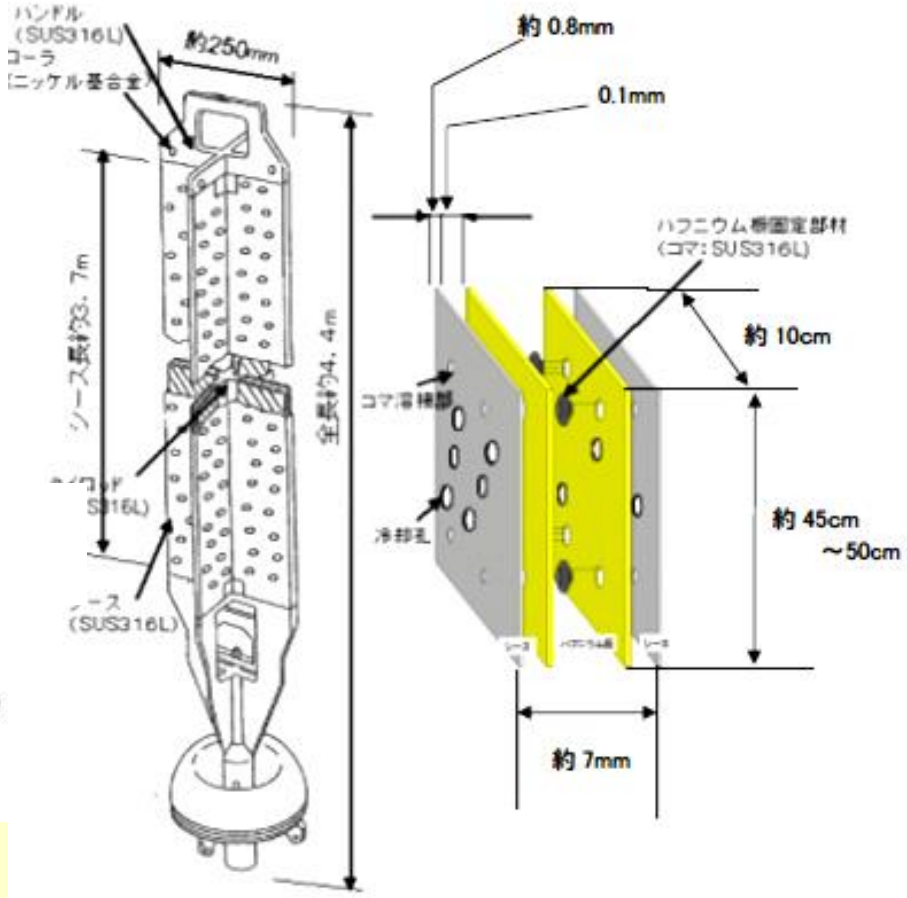

Sheath material: SUS316L

Fluence of failed part: $> 4.4X10^{21}$ n/cm^2

http://www.meti.go.jp/press/20060531005/houkokusho%20kouhyou-set.pdf

2.5.4 IASCC of In-Core Materials

Post Irradiation Examination (PIE) Facility for IASCC Research Activities

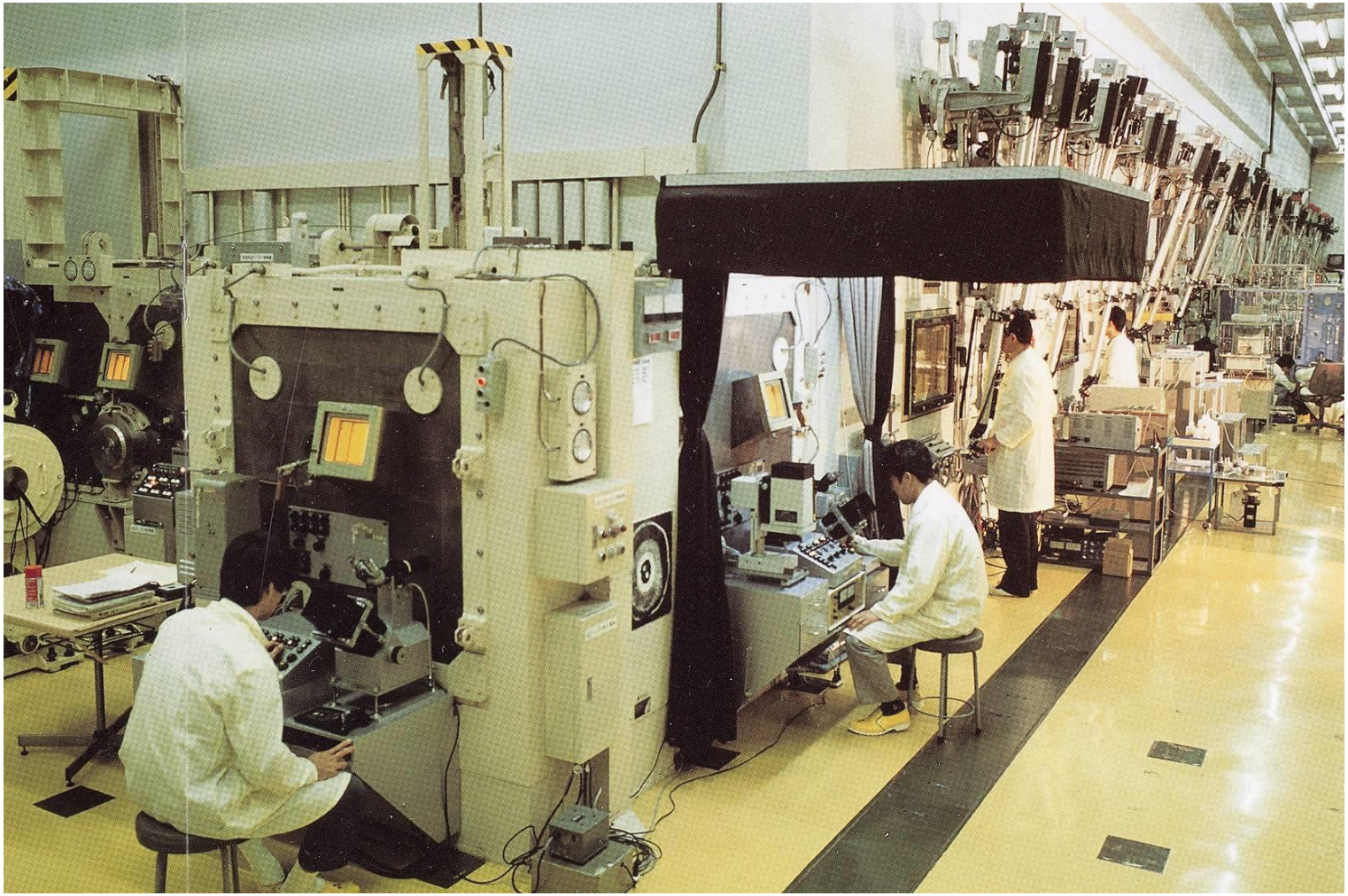

Hot Laboratory in Oarai Research Center of JAEA

2.5.4 IASCC of In-Core Materials

PIE Test Apparatus for IASCC Research

Test Apparatus for SCC Growth Test of Irradiated Materials

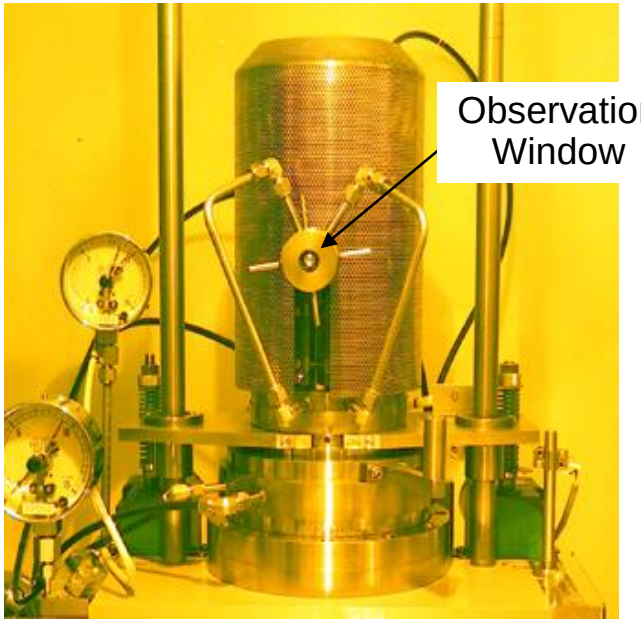

Test apparatus with two autoclave for crack growth tests and high temperature circulation pump (1000l/h) was installed inside hot cell of JMTR hot laboratory in Oarai Research Center.

Test Apparatus for SCC Initiation Test of Irradiated Materials

Test apparatus with four autoclave for uniaxial constant load (UCL) and slow strain rate testing (SSRT) tests was installed inside hot cell of WASTEF facility in Tokai Research Center.

2.5.4 IASCC of In-Core Materials

Slow Strain Rate Testing (SSRT) in High Temperature Water

Tensile test method at very slow strain rate compared with general tensile test to initiate forcibly SCC. SCC susceptibility is evaluated by ratio of SCC in fracture surface.

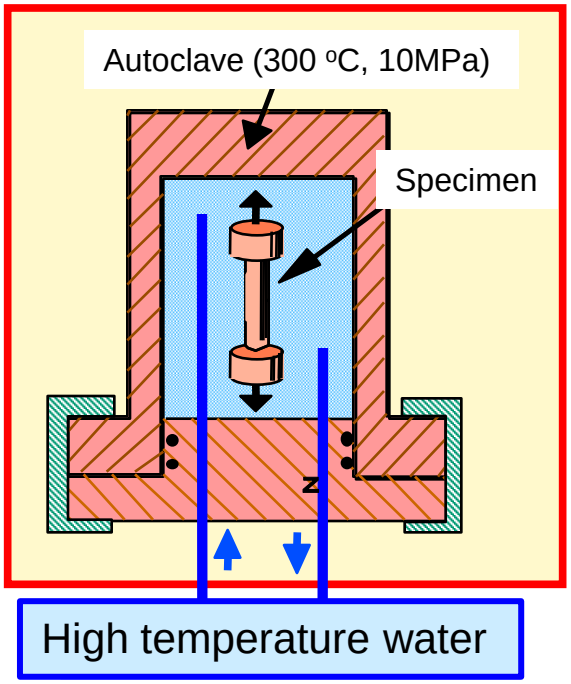

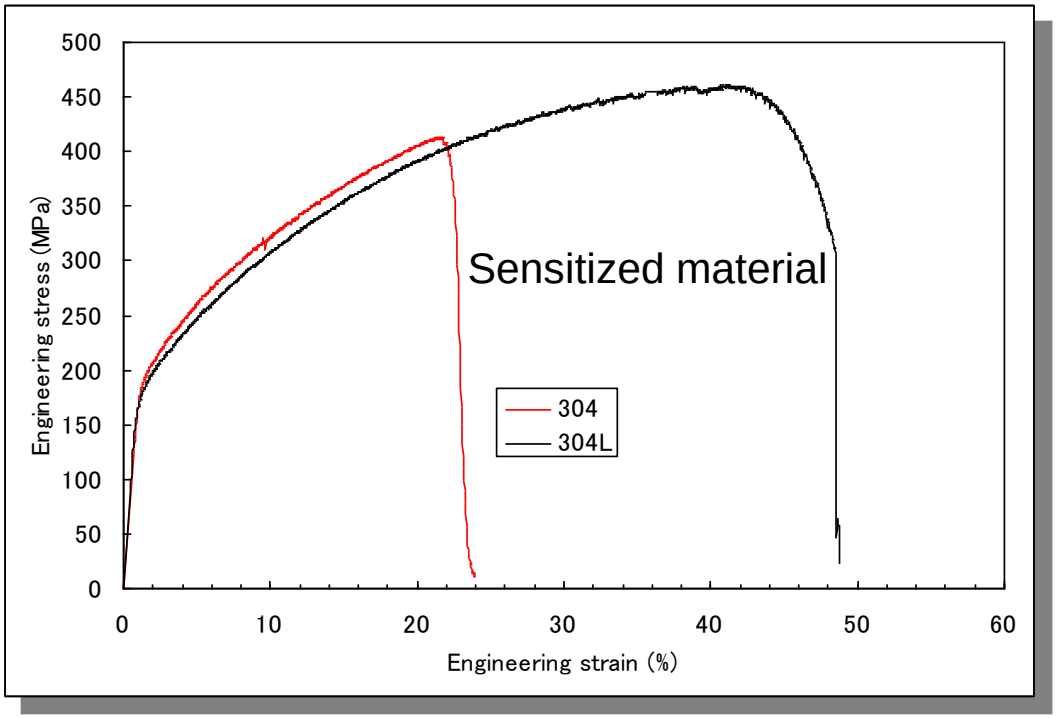

In high temperature water at 288℃
Dissolved oxygen (DO)content: 8 ppm
Strain rate: 2×10^{-7} s^{-1} (Tensile rate: about 0.4mm/day)
Fracture time: about two week or one month

2.5.4 IASCC of In-Core Materials

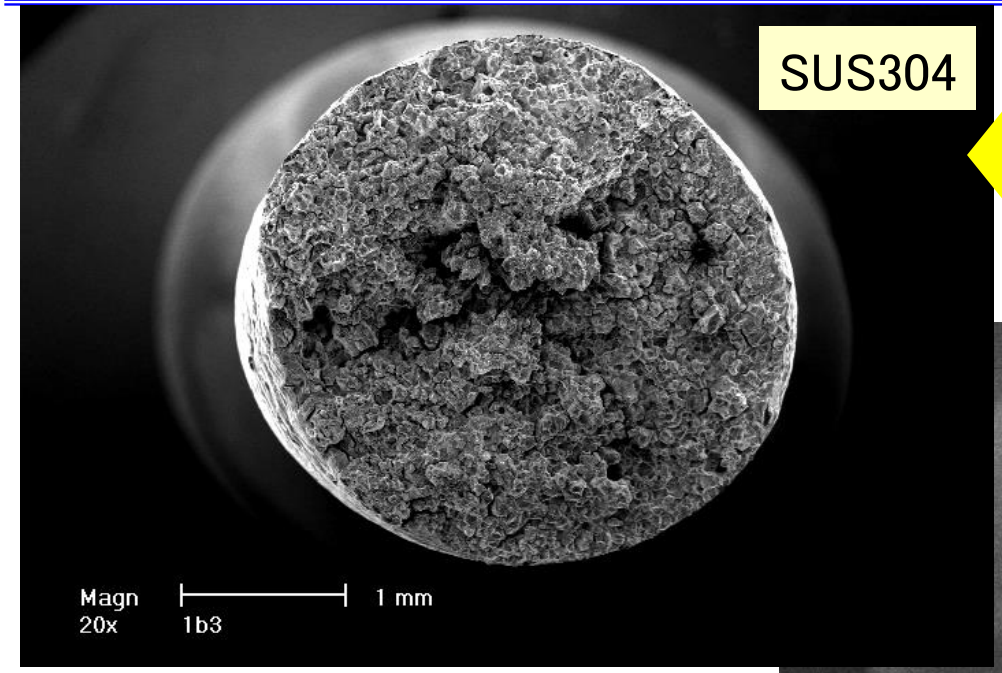

Intergranular SCC was observed on whole fracture surface. No reduction of area was almost observed.
(%IGSCC=100%)

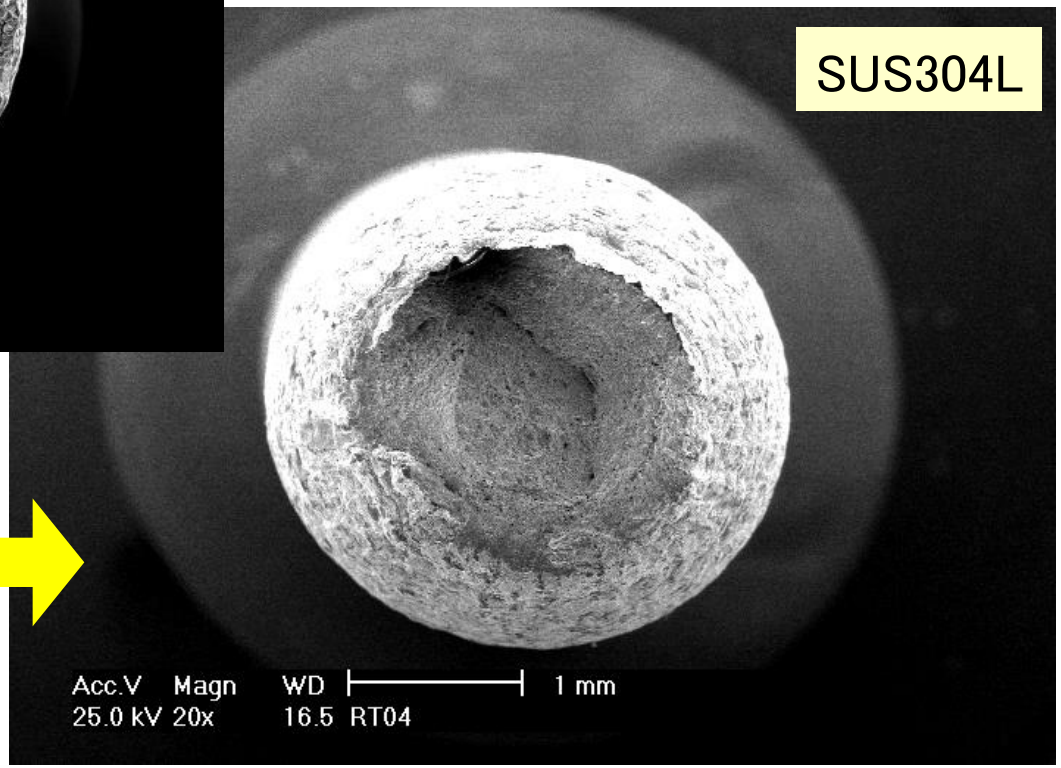

No SCC was observed. Reduction of area is large and ductile fracture was observed.
(%IGSCC=0%)

(Miwa, 2001)

Fracture Surface Observation in SSRT

(Unirradiated material)

2.5.4 IASCC of In-Core Materials

Important Knowledge derived by PIE

Neutron Fluence Dependence

B-IASCC: IASCC under BWR environmental condition
P-IASCC: IASCC under PWR environmental condition

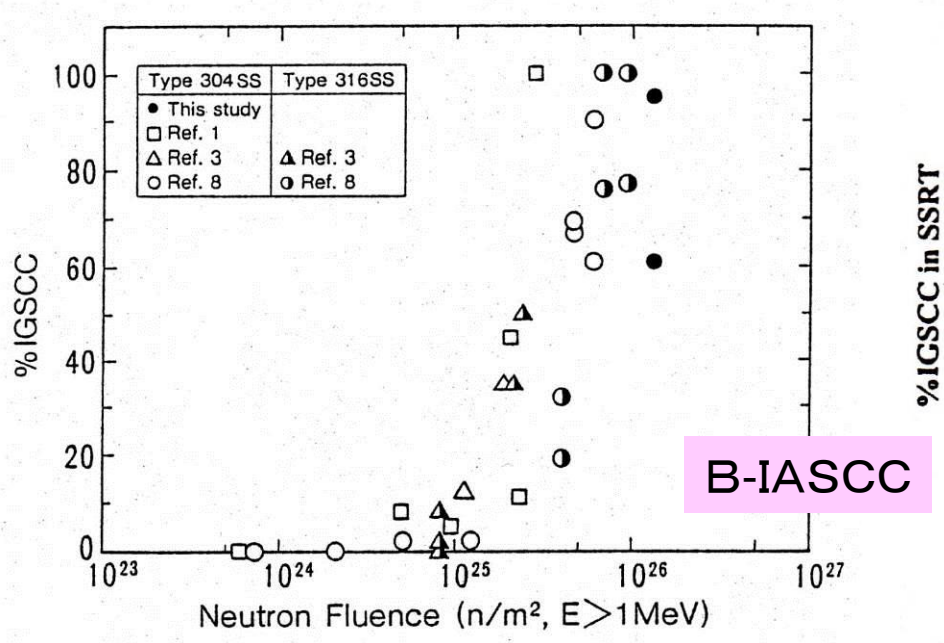

(Kodama, 1993)

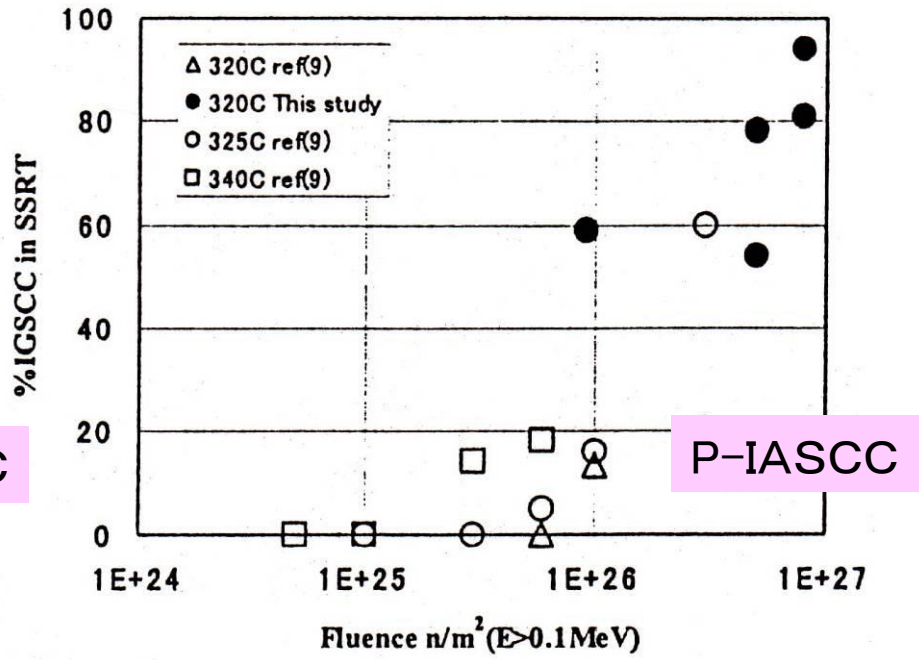

(Fukuya, 2001)

✓These figures show the existence of so-called “threshold” fluence of IASCC from SSRT results.

✓ Threshold fluence under PWR environment is larger than that under BWR environment.

2.5.4 IASCC of In-Core Materials

Common feature between B-IASCC injected H_2 and P-IASCC

SSRT: 288°C

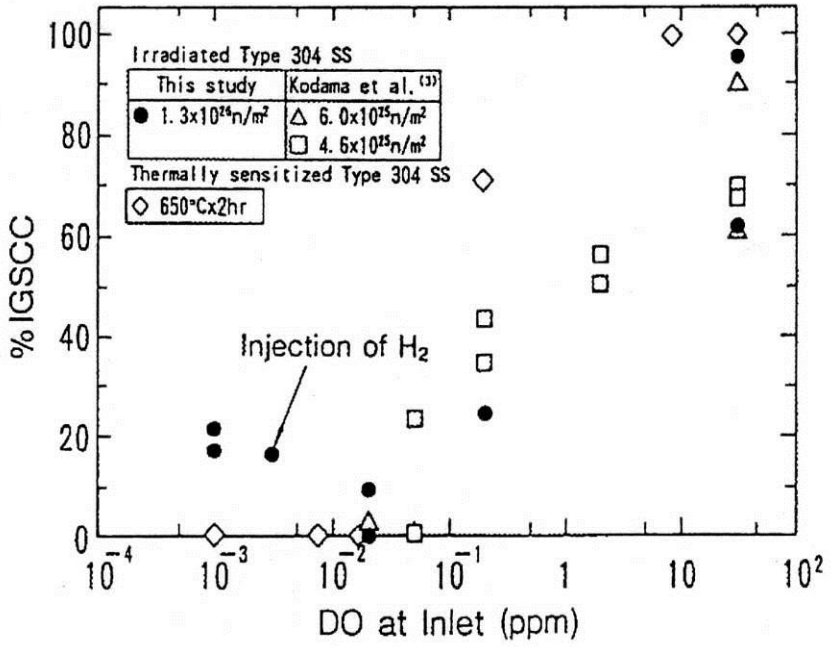

(Kodama, 1995)

SSRT: 320°C

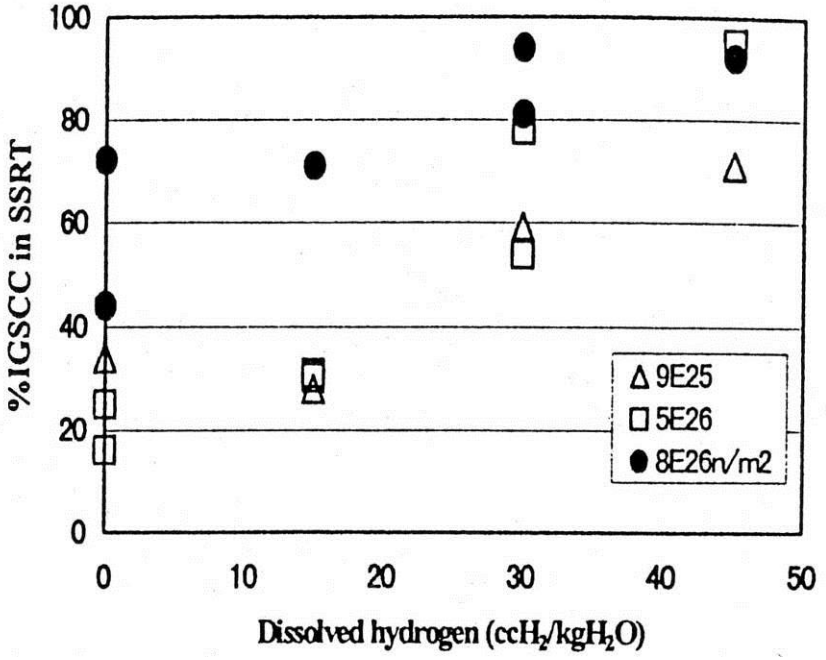

(Fukuya, 2001)

Influence of H_2 addition on B-IASCC P-IASCC vs. Dissolved Hydrogen (DH)

- Relation between hydrogen content in high temperature water and IASCC behavior
- Similarity between both IASCC morphology under hydrogen addition condition

2.5.4 IASCC of In-Core Materials

Relationship between IASCC susceptibility and water chemistry and fluence

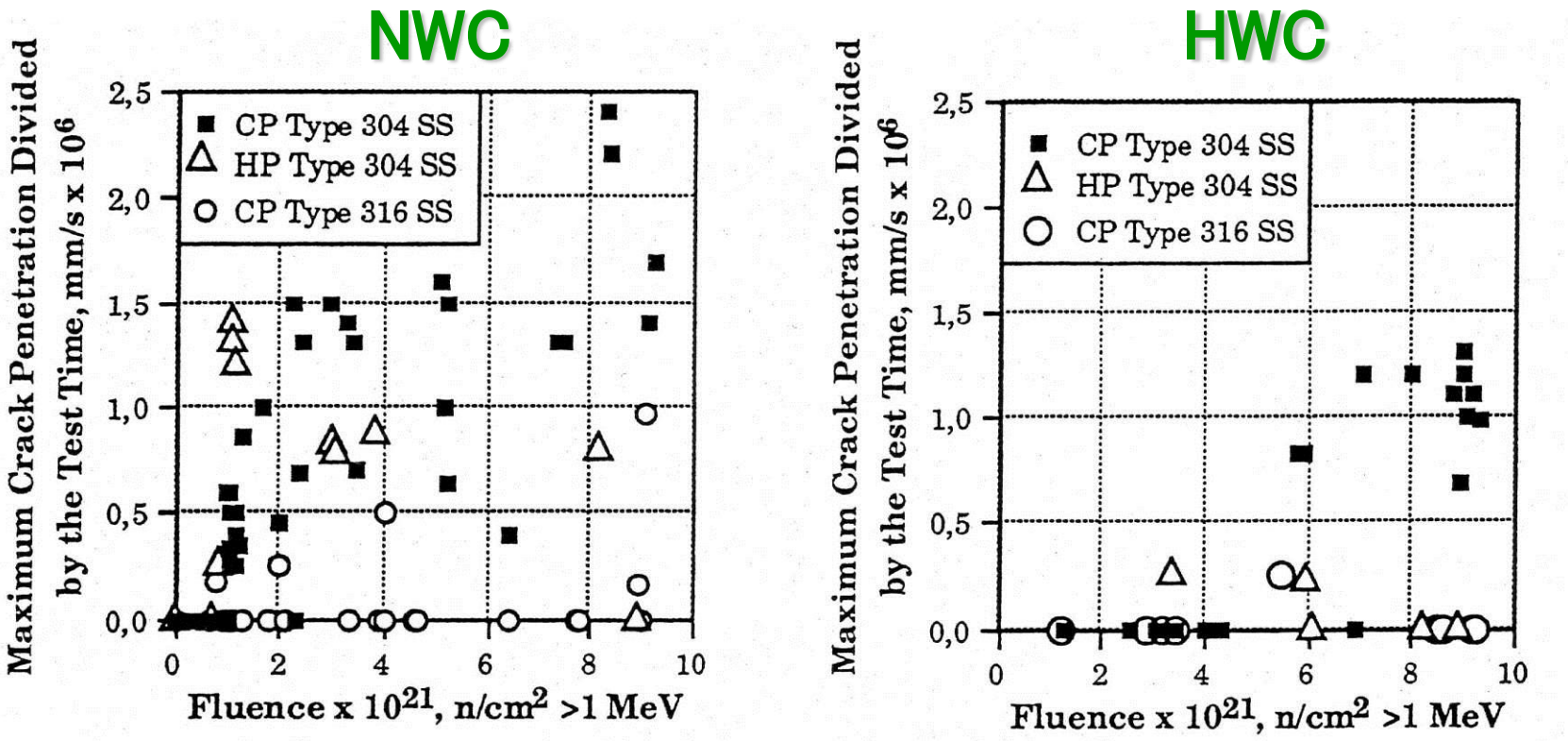

(Jenssen, 1996)

B-IASCC under NWC (left) and HWC (right) conditions

（NWC: Normal Water Chemistry, HWC：Hydrogen Water Chemistry）

- In high fluence regions, IASCC is uncontrollable by hydrogen injection.
- Different mechanism with dissolution of Cr depletion layer ?

2.5.4 IASCC of In-Core Materials

Summary of influence of environment and fluence on IASCC

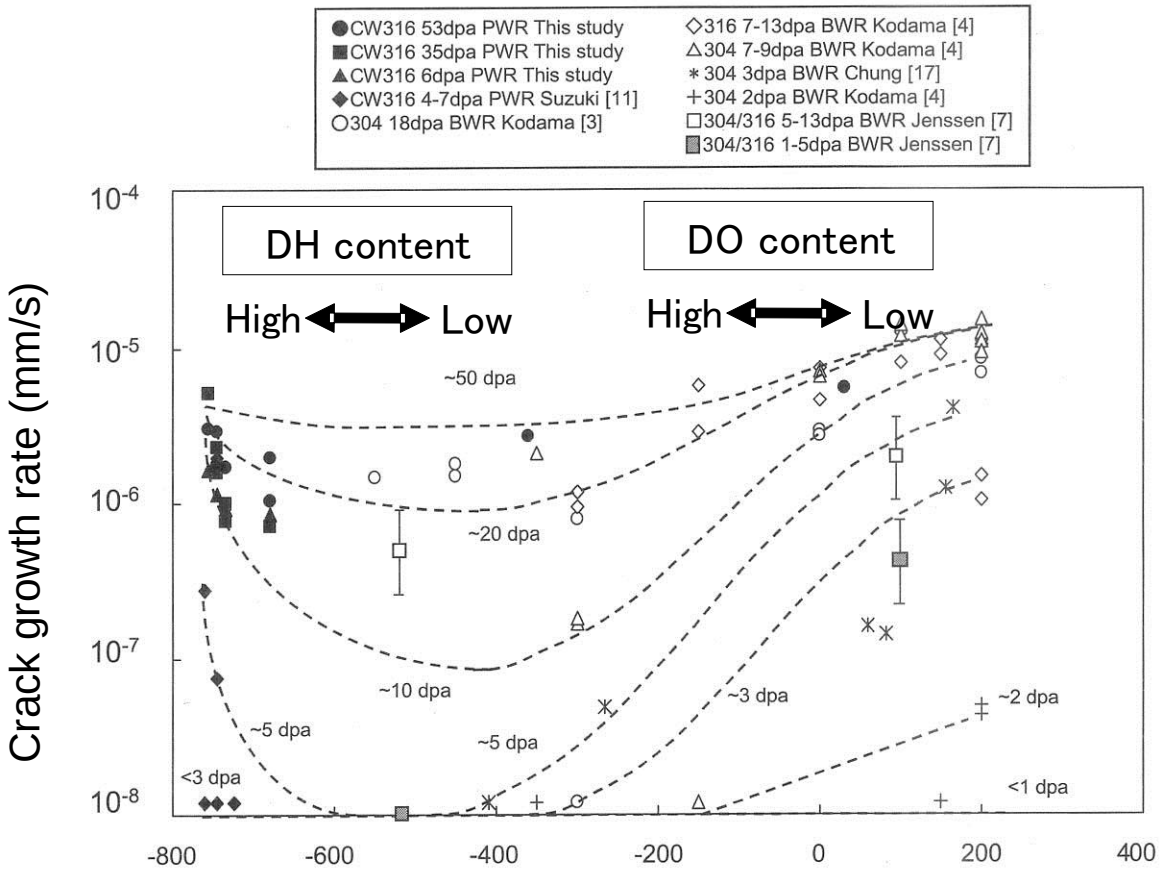

Fukuya et al.

Relationship between ECP in irradiated SS and crack growth rate

- IASCC susceptibility is high in high DO or DH environment.
- Influence of environment on CGR is small in high irradiated material.

2.5.4 IASCC of In-Core Materials

From production of neutron radiation damage to IASCC initiation

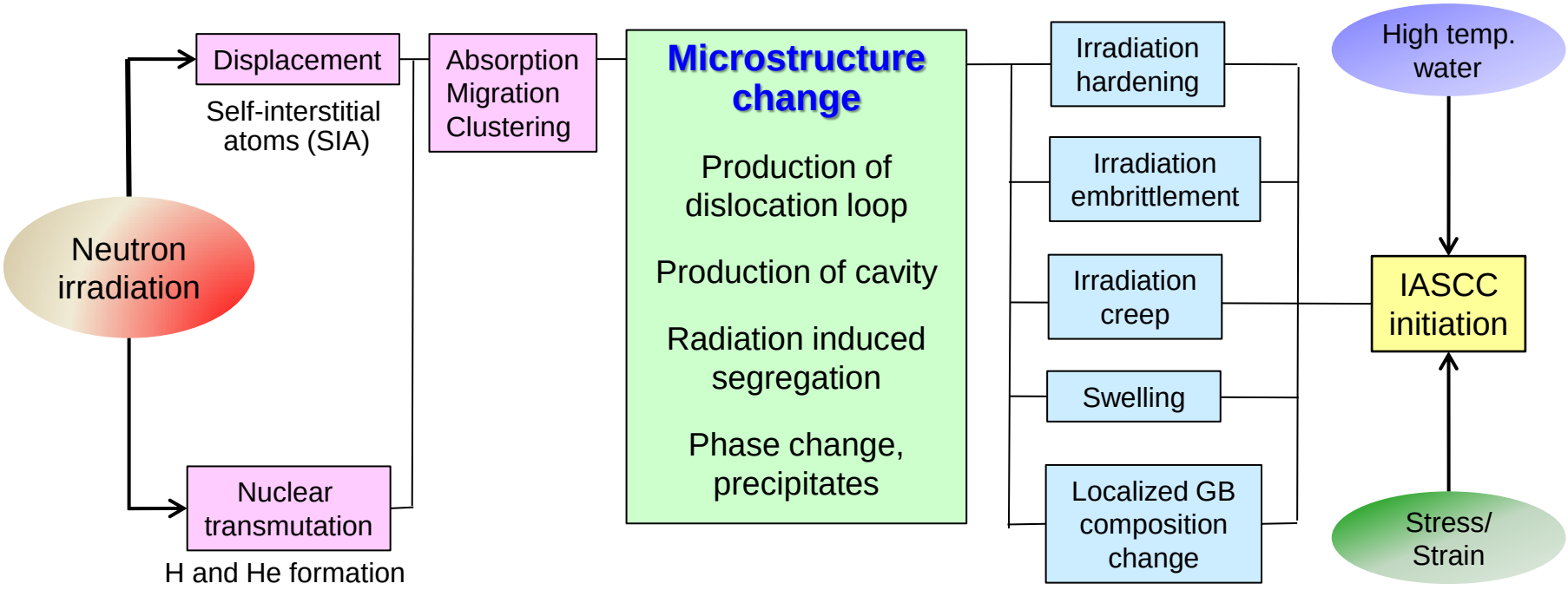

Mechanism of IASCC initiation have been already investigated above 20 years. It is found that radiation induced segregation and irradiation hardening are important factors, but several influences of irradiation on IASCC cannot be comprehensively explained.

2.5.4 IASCC of In-Core Materials

Mechanism of IASCC

Existing theories fall into five categories:

(1) Radiation-induced grain boundary chromium depletion

(2) Radiation hardening

(3) Localized deformation

(4) Selective internal oxidation

(5) Irradiation creep

Ref:“Fundamentals of Radiation Materials Science”, Gray S. Was, Springer, 2007.

The difficulty in determining the role of irradiation in SCC stems from the simultaneous occurrence of several effects. The attribution of one or a combination of effects to the observed increase in cracking is complicated.

2.5.4 IASCC of In-Core Materials

(1) Grain Boundary Chromium Depletion by Radiation Induced Segregation (RIS)

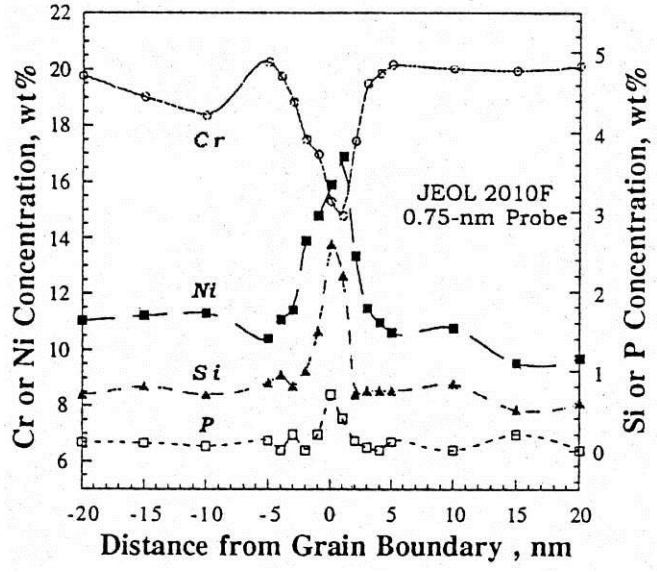

(Brummer, 1999)

Example of radiation induced segregation near the grain boundary

Difference between thermal and irradiation

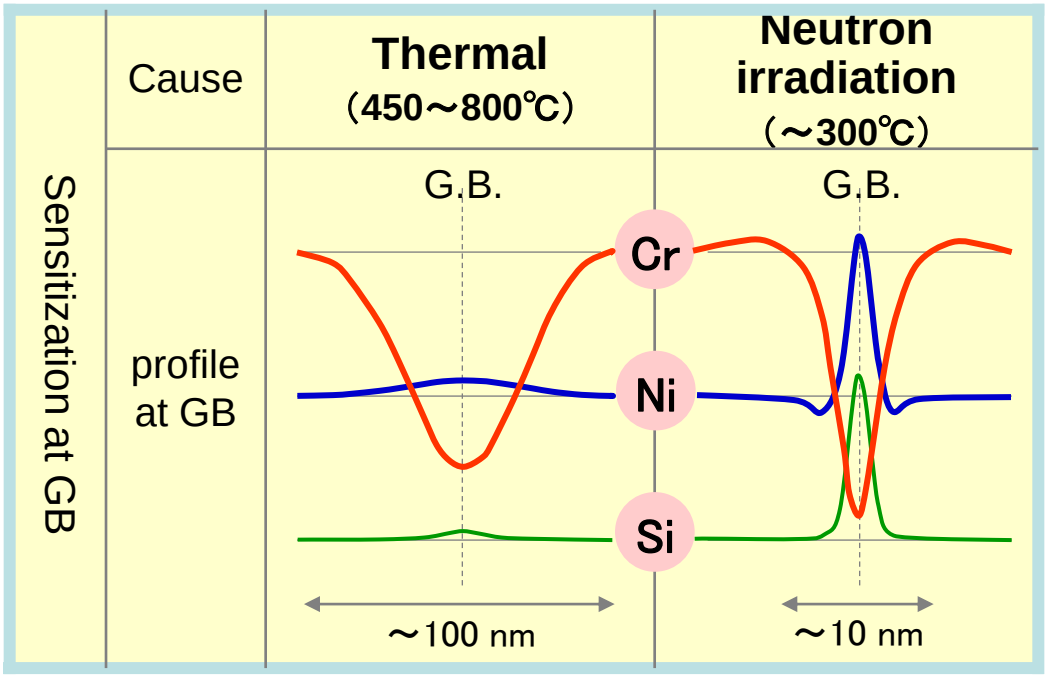

Plot of solute element profiles across a grain boundary

In the case of thermal non-sensitization, Cr depletion zone near grain boundary is made by neutron irradiation.

2.5.4 IASCC of In-Core Materials

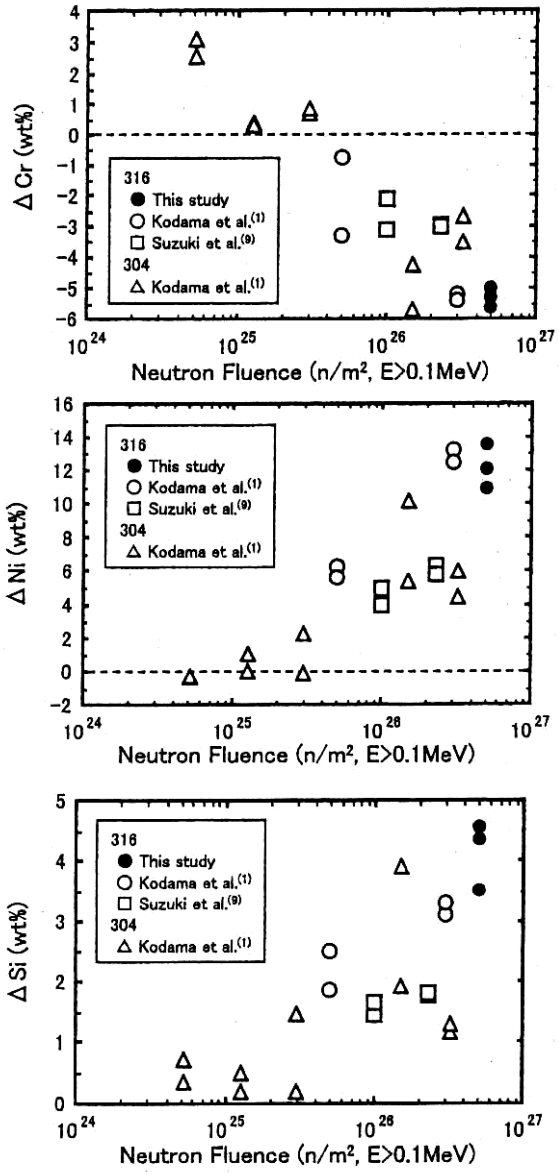

Fig. 7. Relationships between neutron fluence and changes in grain boundary chemistry.

(Furutani, 2001)

Mechanism of RIS

Inverse Kirkendall Segregation

Vacancy migration to boundaries prompts preferential depletion of fast diffusing solutes and enrichment of slow diffusing solutes

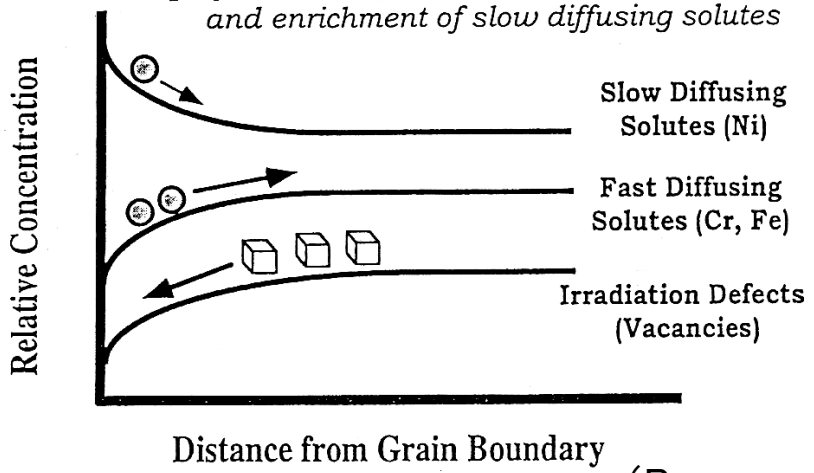

(Bruemmer,1999)

Interstitial Association Segregation

Self interstitials drag undersized solutes (Si, P) to boundaries causing uphill diffusion and enrichment

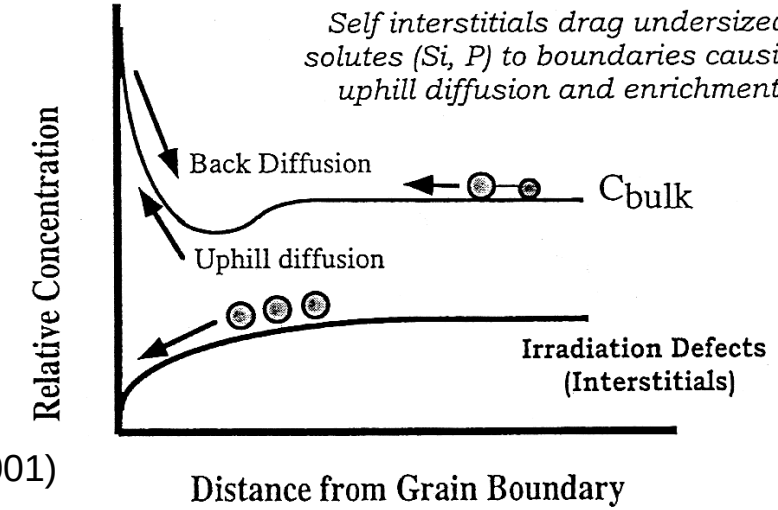

2.5.4 IASCC of In-Core Materials

Is it possible to explain IASCC phenomena by RIS ?

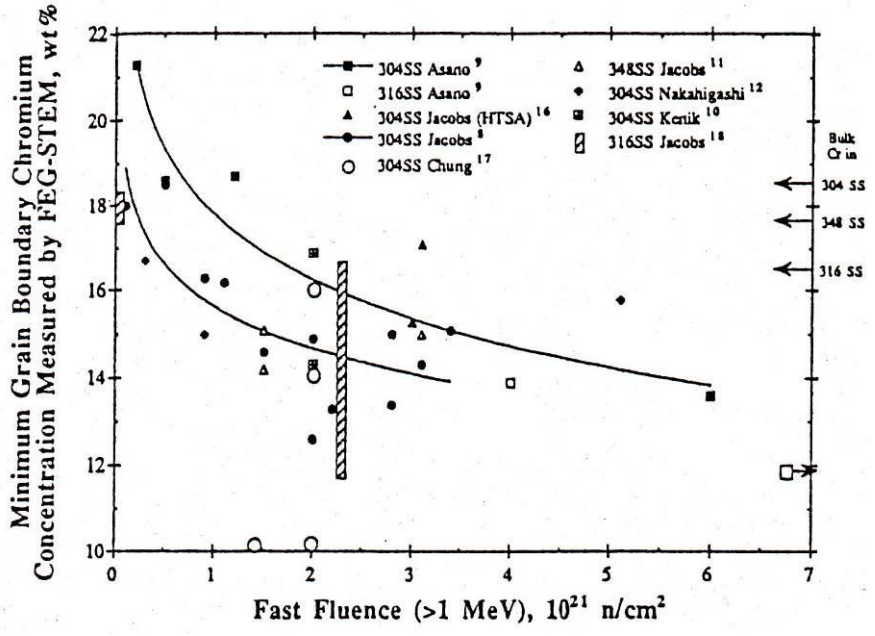

(Was, 1994)

Change of grain boundary Cr concentration as function of neutron fluence

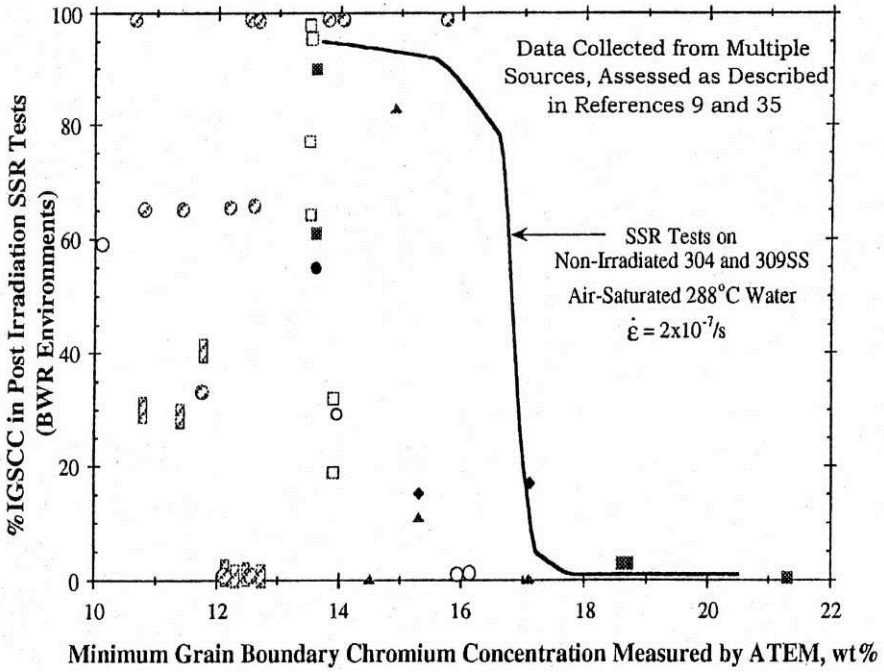

(Brummer, 1999)

Relationship between grain boundary Cr concentration and IASCC susceptibility

It is necessary to consider both local solute element change at grain boundary (RIS) and change of microstructure by formation of radiation defects at the same time.

2.5.4 IASCC of In-Core Materials

(2) Irradiation Hardening

- Influence of materials

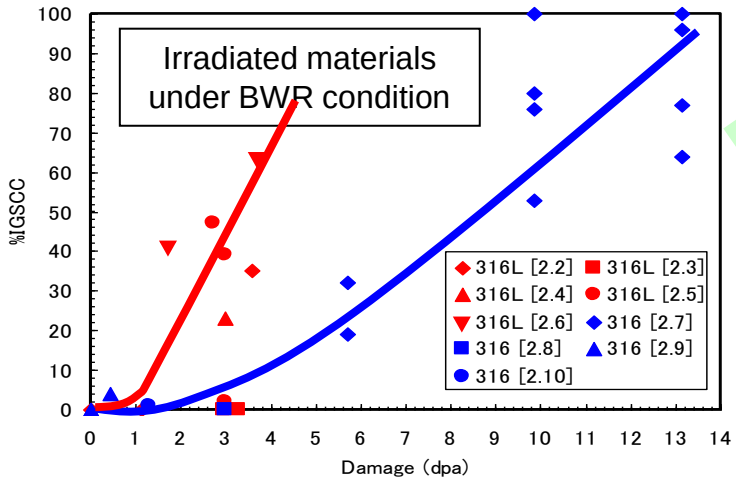

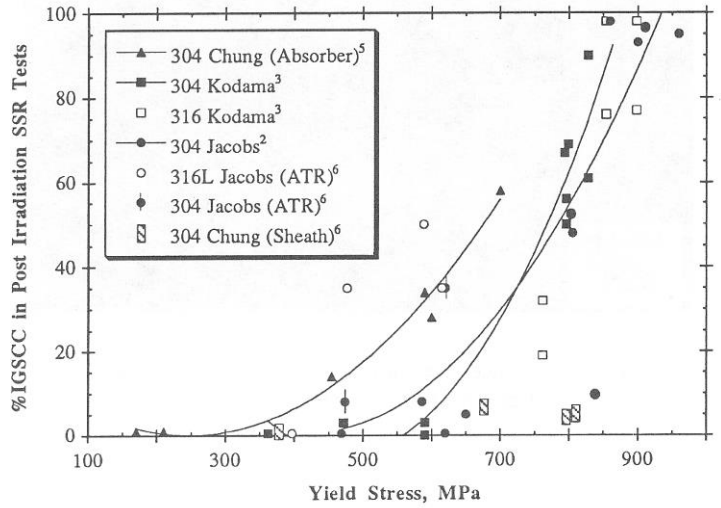

S. M. Bruemmer et al., Proc. 6th Int. Symp. Environmental Degradation of Materials In Nuclear Power System –Water Reactor-, TMS, 1993, p.537.

Effect of carbon addition on %IGSCC was able to explain by increase of yield stress.
But it is difficult to explain complicated effect of element addition by only increase of yield stress.

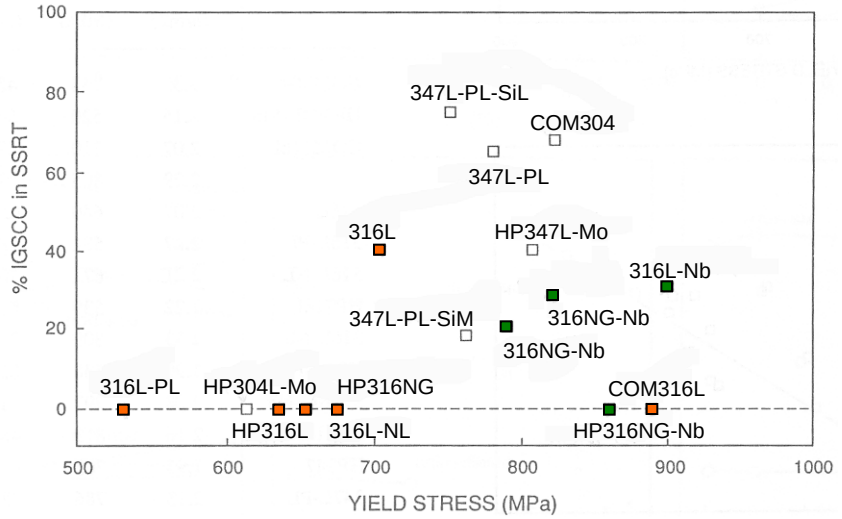

K. Fukuya et al., Proc. 6th Int. Symp. Environmental Degradation of Materials In Nuclear Power System –Water Reactor-, TMS, 1993, p.565.

2.5.4 IASCC of In-Core Materials

(3) Localized Deformation

Dislocation channels: Cause of localized deformation

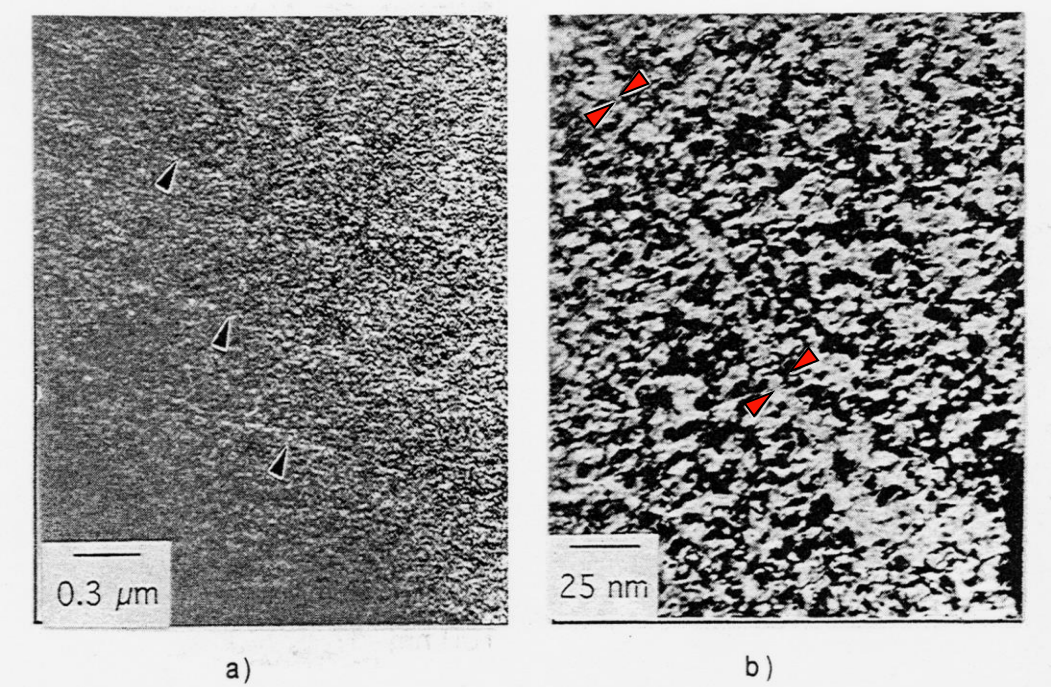

Fig. 5 Dislocation channels in 304L SS irradiated to 3 dpa and deformed at 288°C a) low magnification b) high magnification.

(Cole,1995)

Dislocation channel is portion in which point defect loop is absorbed and density of radiation defect is low by moving of dislocation.

Brittle fracture is occurred by small macroscopic deformation to concentrate localized deformation in dislocation channel area.

No empirical proof for relevance to SCC

2.5.4 IASCC of In-Core Materials

Formation of denuded zone near grain boundary
Neutron irradiation at 275℃

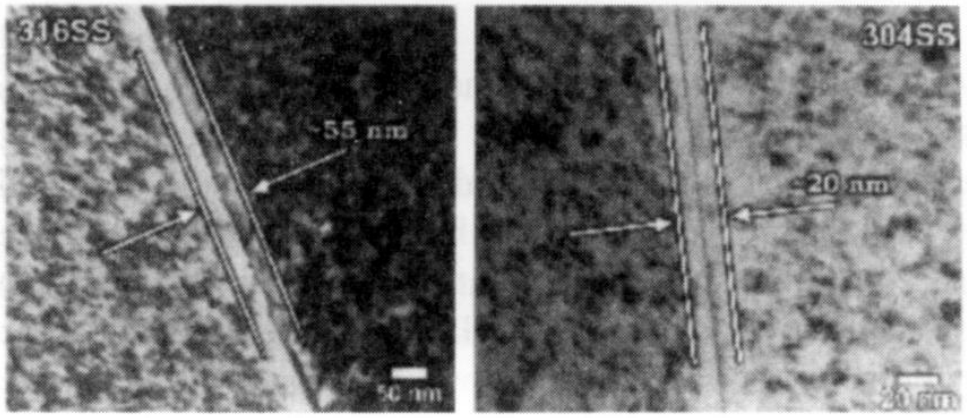

Figure 3. Observed denuded zones in 316SS and 304SS after LWR irradiation.

（Simonen, 1999)

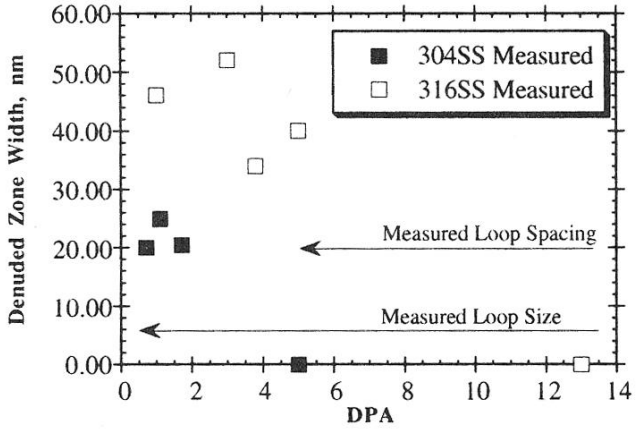

Figure 4 Measured denuded zone widths in 304SS and 316SS. Measured loop dimensions are also shown. Well-established denuded zones exist at low dpa but disappear at high dpa.

（Simonen, 1999)

Denuded zone near grain boundary　　Change of denuded zone width

Denuded zone with low density of radiation defects is formed near grain boundary of irradiated stainless steel. Even though denuded zone width is different with irradiation conditions, it is possible to be cause of concentration of deformation at grain boundary.

2.5.4 IASCC of In-Core Materials

(4) Selective Internal Oxidation

- Microstructure near crack tip
  - BWR : Top guide of Type 304 SS, 0.7dpa

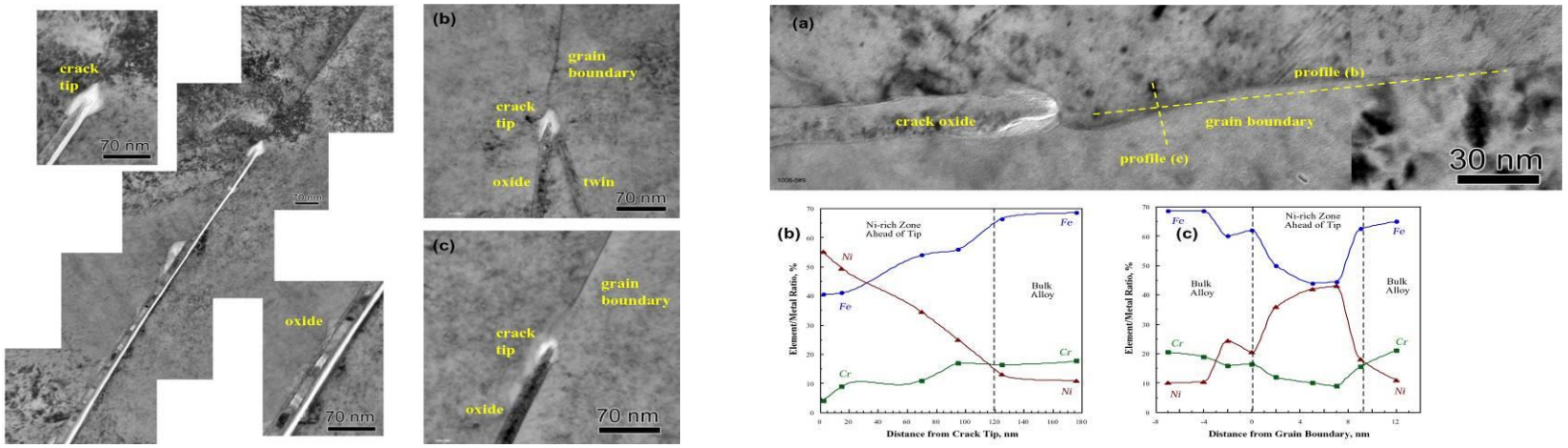

L.E. Thomas et al., proc. 11th Int. Conf. Environmental Degradation of Materials in Nuclear Power System-Water Reactors-, 2003, p.1049.

Oxide-filled cracks extended up to several tens of μm along all high-angle grain boundary. Oxides consisted of thin layers of epitaxial Cr-Fe-rich spinel next to metal grains, and Fe-rich spinel (magnetite) in middle. Grain boundaries appeared deflected by ～5 nm and returned to course of leading grain boundaries at ～60 nm past tips.

2.6 Remedies for Material Issues

2.6.1 Countermeasure of SCC

Countermeasure	Concrete Example
Improvement of materials	・Low carbon (Type 316L SS, etc.) ・Development/application of high SCC resistant alloy（Alloy 690, etc.）
Improvement of stress	・Improvement of surface worked method ・Surface peening treatment ・Improvement of welding method (reduction of residual stress)
Improvement of environment	・Injection of H2, NMCA, Zn and hydrazine ・Water chemistry management (degas operation in start-up) ・Development of monitoring technique (ECP sensor, etc.)
Advanced evaluation	・Improvement of SCC model and simulation method ・Improvement of nondestructive inspection technique ・Improvement of SCC test method ・In-pile SCC/water chemistry test in MTR
Preparation of standards	・Preparation of fitness-for-service standard and structural integrity evaluation guide ・Standardization of water chemistry control and SCC test ・Preparation of crack growth curve
Nurturing of talented people	・Persons who bear basic research for SCC

2.6.1 Countermeasure of SCC

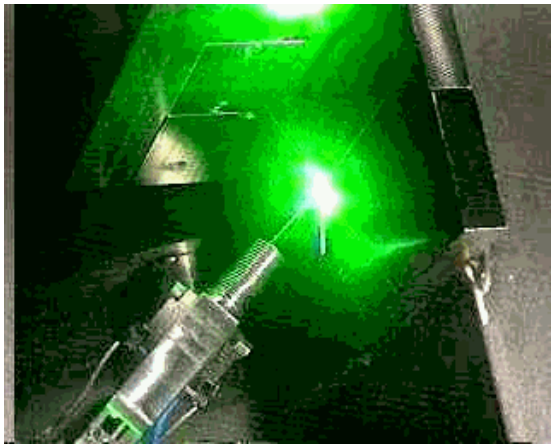

Laser peening (LP)

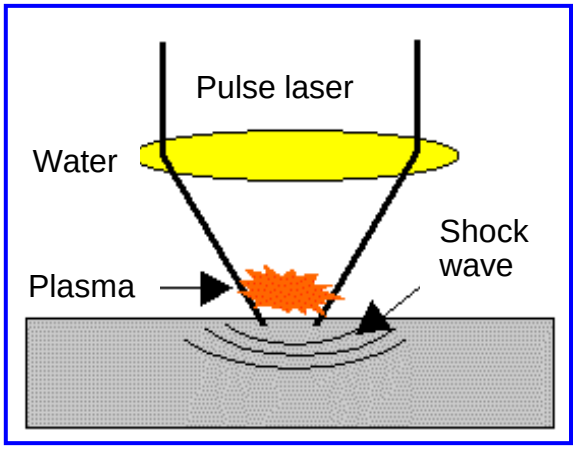

Principle of LP

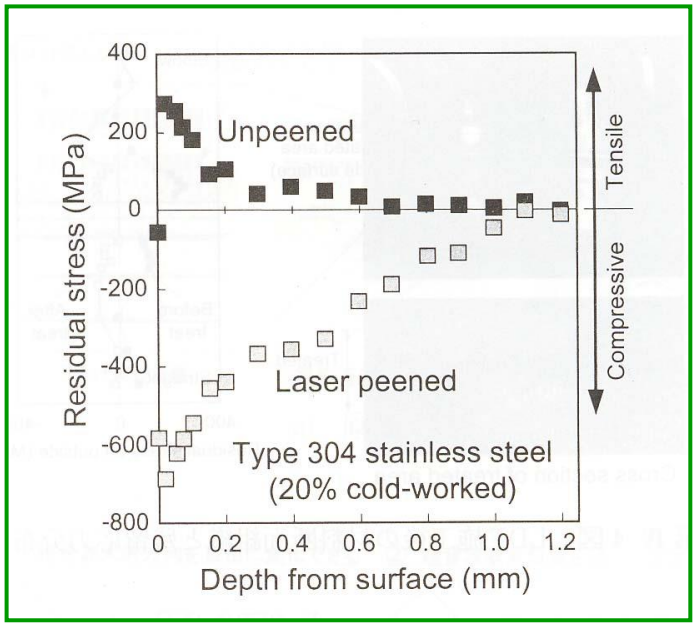

Improvement effect of residual stress by LP

Compression residual stress layer is formed due to impact force of plasma initiated in surface of material by pulse laser irradiation in water. Tensile residual stress near welding joint of core shroud is able to convert to compression stress until about 1 mm depth by laser peening treatment.

(Journal of the Atomic Energy Society of Japan, Vol. 44, No. 4 (2002))

2.6.1 Countermeasure of SCC

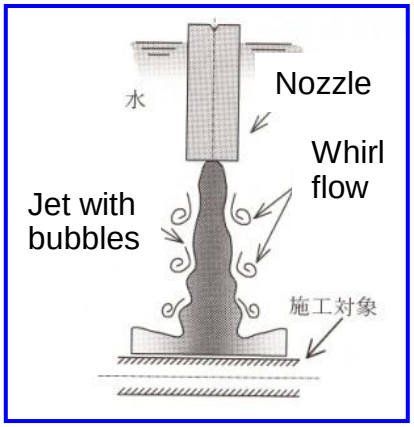

Principle of water jet peening (WJP)

When high pressure water jet out in water, whirl is initiated in boundary between jet water and surrounding stopped water. Since pressure in center of whirl is low, water in center of whirl is evaporated and many bubbles are formed. With reaching downstream, pressure of water is recovered and bubbles are crushed. And then big force of several tens thousand of pressure is formed and stress situation in surface of metal is improved by this force.

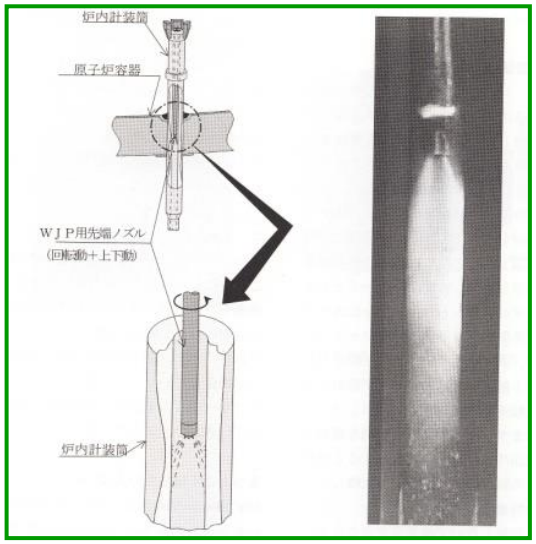

Example of application of WJP

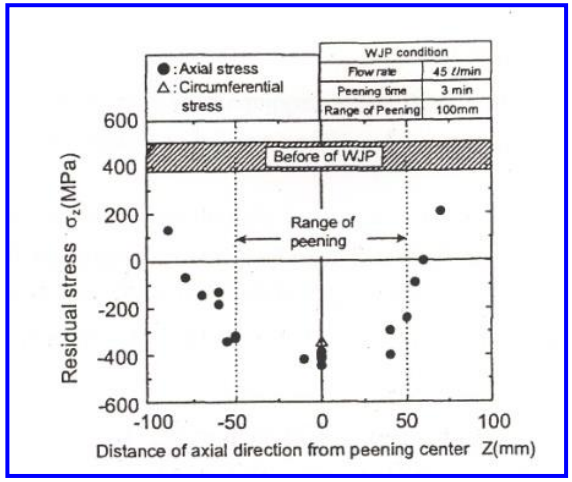

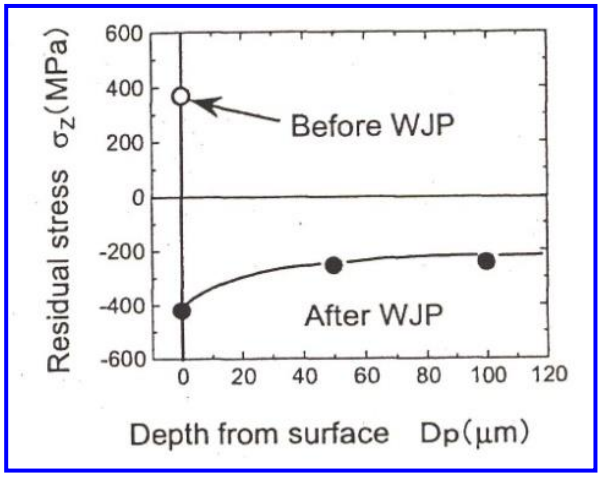

Improvement effect of residual stress by WJP

(Atomic Energy Society of Japan, Advanced Atomic Energy a la carte (2002))

2.6.1 Countermeasure of SCC

CRC: Corrosion Resistant Cladding

In the corrosion-resistant cladding technique, Type 308L weld metal is applied to the inside surface of the pipe at the pipe weld ends before making the final field weld. This duplex weld metal covers the region that will become sensitized during the final weld process, thus providing intergranular SCC resistance by maintaining low carbon and a sufficient ferrite level in the region that would normally be sensitized.

Numerous laboratory data generated on welded and furnace-sensitized Type 308 and Type 308L weld metal prompted the conclusion that a minimum amount of ferrite (7 %) must be present to provide a high degree of resistance to intergranular SCC in BWR environments. As with Type 304 stainless steel, reducing the carbon level is also beneficial as in the L-grade steels.

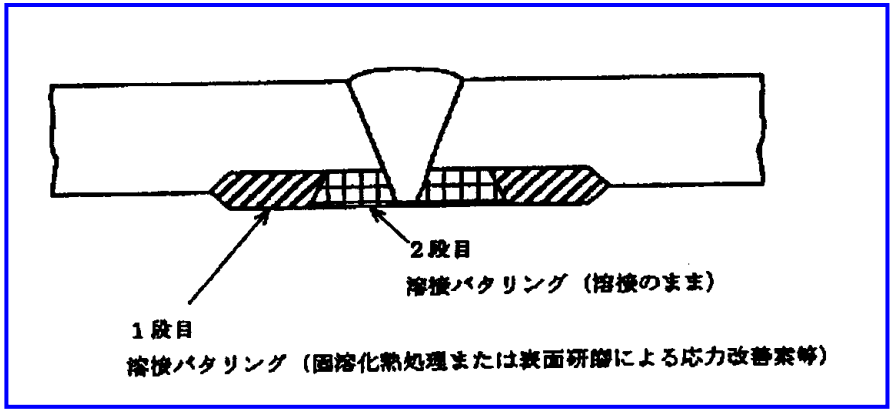

Illustration of corrosion-resistant cladding

2.6.1 Countermeasure of SCC

HSW: Heat Sink Welding

The heat sink welding procedure both reduces the sensitization produced on the inside surface of welded pipe and, changes the state of internal surface residual welding stresses from tension to compression. Heat sink welding involves water cooling the inside surface of the pipe during all weld passes subsequent to the root pass or first two layers.

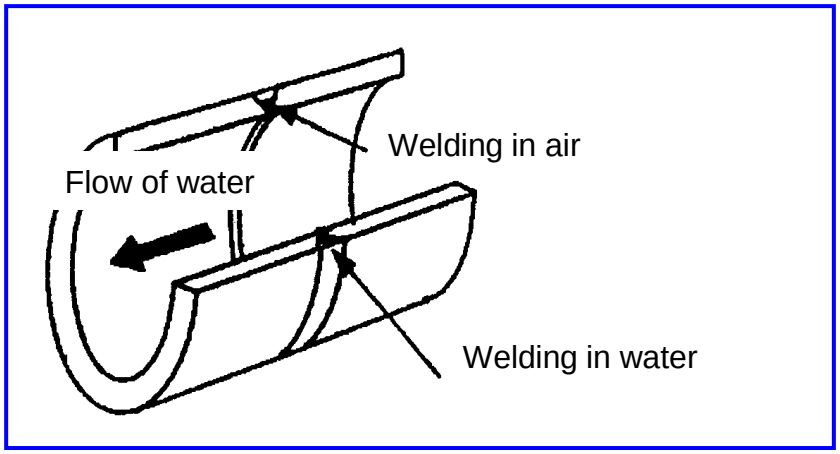

Illustration of heat sink welding process

IHSI: Induction Heating Stress Improvement

The process involves induction heating the outer pipe surface of completed girth welds to approximately 400°C while simultaneously cooling the inside surface, preferably with flowing water. Thermal expansion caused by the induction heating plastically yields the outside surface in compression, while the cool inside surface plastically yields in tension. After cooldown, contraction of the pipe outside surface causes the stress state to reverse, leaving the inner surface in compression and the outside surface in tension.

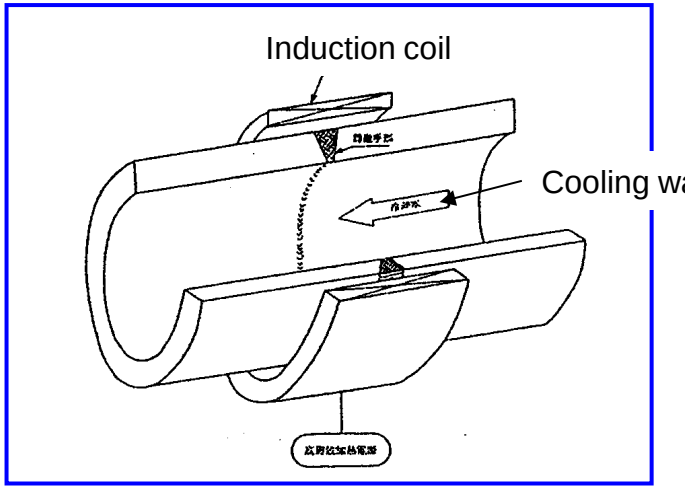

Illustration of heating and cooling process for induction heating stress improvement

2.6.1 Countermeasure of SCC

Hydrogen Injection（＋NMCA: Noble Metal Chemical Addition）

The hydrogen add to the primary coolant recombines with the radiolytically produced oxidizing products (primarily oxygen (O_2) and hydrogen peroxide (H_2O_2)), reducing the oxygen level in the coolant and the corrosion potential of the stainless steel piping.

The consequence of injecting amounts of hydrogen > 0.3 ppm into the feed-water is that volatile nitrogen species (N_2, NH_3) are formed, and the radiation levels in the main stream line and turbine may increase by a factor of X4 to X5 due to the formation of ^{16}N via an (n, p) reaction on O^{16}.

Few amount of hydrogen promote recombination between oxygen and hydrogen by utilizing catalytic effect of introducing a noble metal onto the material surface.

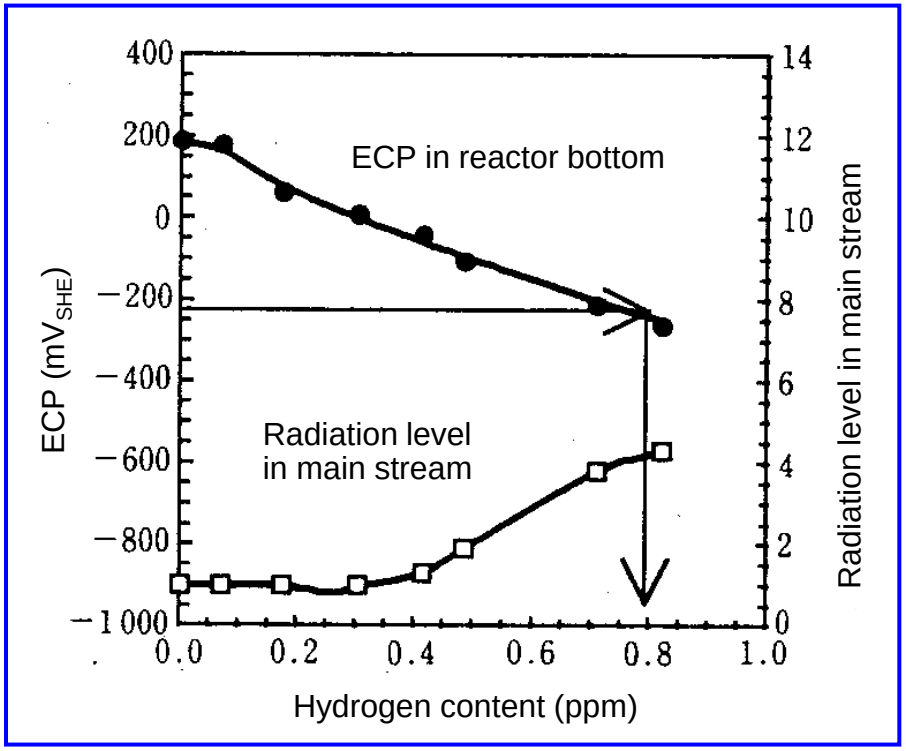

Reduction of ECP and increase of radiation level in main steam line by hydrogen injection

(Handbook of Water Chemistry of Nuclear Reactor System, Atomic Energy Society of Japan, 2000.)

References:

[1] S. Glasstone and A. Sesonske, *Nuclear Reactor Engineering – Reactor Design Basics*, fourth edition volume one, An international Thomson Publishing Company, 1994.

[2] J. T. A. Roberts, *Structural Materials in Nuclear Power Systems*, Plenum Press, 1981.

[3] R. W. Staehle, "Anatomy of Proactivity", Proceeding of the International Symposium on Research for Ageing Management of Light Water Reactors and Its Future Trend, Institute of Nuclear Safety System, Inc., October 2007.

[4] R. Jones, "EPRI's R&D Programs on Materials Degradation in LWR's", NRC Regulatory Information Conference (RIC) 2006 Session Th5BC Materials Degradation, March 9, 2006.

[5] G. E. Dieter, *Engineering Design – A Materials and Processing Approach*, McGraw-Hill Book Company, 1983.

[6] IAEA-TECDOC-1557, "Assessment and management of ageing of major nuclear power plant components important to safety: PWR pressure vessel internals", IAEA, 2007.

References:

[7] B. M. Ma, *Nuclear Reactor Materials and Applications*, Van Nostrand Reihold Company Inc., 1983.

[8] A. J. Sedriks, *Corrosion of Stainless Steels*, Second edition, A Wiley-Interscience Publication John Wiley & Sons, Inc., 1996.

References in 1.3-1.5 & 2

1. *Materials Science and Technology Vol.10 A&B*, Eds. R.W. Cahn, P. Haasen, E.J. Kramer, 1994, VCH.
2. *Aging and life extension of major light water reactor components*, Eds. V. N. Shah and P. E. MacDonald, 1993, Elsevier.
3. G. S. Was, *Fundamentals of Radiation Materials Science*, 2007, Springer.
4. B. M. Ma, *Nuclear Reactor Materials and Applications*, 1983, Van Nostrand Reinhold Company Inc.
5. S. Glasstone and A. Sesonske, *Nuclear Reactor Engineering*, 1994, Chapman & Hall, Inc.
6. 薄田寛、損傷防止技術を中心とした軽水炉構造材料、1988、アイピーシー.
7. Proceedings of the 2nd International Seminar on "*Structural Intergrity of Light Water Reactor Components*", Eds. L. E. Steele, K. E. Stahlkopf, L. H. Larsson, 1981, Applied Science Publisher.
8. Proc. 3rd Int. Conf. on *Mechanical Behaviour of Materials*, ICM3, Cambridge, England, Aug. 1979,
9. *Irradiation Effects in Cladding and Structural Materials*, ed. S. H. Bush, ASM, Rowman and Littlefield, Inc.
10. *Residual Stresses in Welded Construction and their Effects*, Ed. R. W. Nichols, 1978.
11. Proc. Conf. on *Maintenance welding in Nuclear Power Plants*, Eds. P.D. Flenner and R. G. Dermott, 1978, Welding Technology Series, American Welding Society, Inc.

If you have some questions or comments, please contact

kaji.yoshiyuki@jaea.go.jp